ACOUSTIC MEASUREMENT STUDY

40 x 80 FOOT

SUBSONIC WIND TUNNEL

PREPARED FOR

NATIONAL AERONAUTICS & SPACE ADMINISTRATION

AMES RESEARCH CENTER

MOFFETT FIELD, CALIFORNIA

CONTRACT NAS2-7759

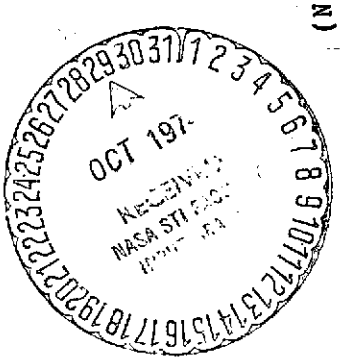

Robin M. Towne and Associates, Inc.
Consultants in Sound and Vibration

228 MOHAWK BUILDING • PORTLAND, OREGON 97204 • TELEPHONE (503) 221-0210
105 N. E. 56TH STREET • SEATTLE, WASHINGTON 98105 • TELEPHONE (206) 523-3330

ACOUSTIC MEASUREMENT STUDY
FINAL REPORT, CONTRACT NAS2-7759

SUBMITTED TO

NATIONAL AERONAUTICS & SPACE ADMINISTRATION
AMES RESEARCH CENTER
MOFFETT FIELD, CALIFORNIA

SUBMITTED BY

ROBIN M. TOWNE & ASSOCIATES, INC.
CONSULTANTS IN SOUND & VIBRATION
SEATTLE, WASHINGTON

APRIL 1974

TABLE OF CONTENTS

LIST OF FIGURES

LIST OF FIGURES

LIST OF FIGURES

LIST OF FIGURES

LIST OF FIGURES

LIST OF FIGURES

LIST OF FIGURES

LIST OF FIGURES

LIST OF TABLES

1.0 ABSTRACT

This is a report of an acoustical study conducted during the period from September 1, 1973 to April 30, 1974 in and around the 40 x 80 foot subsonic wind tunnel located at the NASA Ames Research Center. Sound pressure levels and vibration amplitudes were measured inside and outside of the tunnel and on the tunnel structure.

This report contains a discussion of the technical aspects of the study, the field measurement and data reduction procedures and results, and provides conclusions resulting from the study which bear upon near field and far field tunnel noise, upon the tunnel as an acoustical enclosure, and upon the sources of noise within the tunnel drive system,

2.0 INTRODUCTION AND PURPOSE

The National Aeronautics and Space Administration, Ames Research Center, desires to evaluate the acoustical impact of their 40 foot by 80 foot wind tunnel upon the far field areas surrounding the center, upon the near field areas at the center, to quantitatively define the primary noise sources within the tunnel and to make an analysis of the acoustical characteristics of the tunnel enclosure. For these purposes, Robin M. Towne and Associates, Inc., were retained under Contract NAS2-7759 to perform the following tasks:

1. Examine the noise sources at Ames and quantitatively establish the impact of the 40 x 80 foot wind tunnel upon the far field. The noise sources to be considered in this study included the Bayshore Freeway, Moffett Field Airport, the 40 x 80 foot wind tunnel, and other sources at Ames. The significance of wind and of temperature inversions were considered.

2. Examine the major noise sources at Ames and vicinity and evaluate the impact of the 40 x 80 foot wind tunnel upon the near field.

3. Make measurements necessary to identify and evaluate the noise produced by the primary noise sources within the tunnel. These sources are identified as the fan blade tips, the inlet and outlet diffusers, the fan blade/nacelle strut interaction and the arrangement of the six fans.

4. Analyze the tunnel as an acoustical enclosure and evaluate the structural system and materials for

their acoustical control properties and effectiveness. Substantiate the analyses with sound transmission and vibration measurements.

The above tasks were performed with the tunnel operating at 75% and 100% power. The data and analyses were developed with a view to providing information which would be useful for the design of future large subsonic wind tunnels so that the tunnels will be more appropriate for applications which require minimal acoustic interference with model test data.

The results of Robin M. Towne & Associates' investigations are given in this report.

3.0 TECHNICAL DISCUSSION

3.1 Wind Tunnel

The 40 x 80 foot wind tunnel is a closed-circuit tunnel shown in Figure 3.1. The air is driven by six fans, each 40 feet in diameter and having six blades. The fans are arranged in two rows of three fans in each row. The fans are powered by six electric motors of 6000 horsepower (4.476×10^6 watts) each. The maximum dynamic pressure delivered to the test section by these fans is about 130 lbs. per square foot (6224.43 Newtons per square meter). Fan speed and required power as a function of test section dynamic pressure are shown in Figure 3.2.

The walls of the wind tunnel, with the exception of the test section and the fan section, are corrugated asbestos cement (transite) which is 3/8 inches (.0095 meters) thick, installed with about 4 inches (.102 meters) side lap and 6 inches (.152 meters) end lap. The test section and fan section are steel plate with varying thickness as shown on Figure 3.1. Adjacent to the test section is a work area. The exterior of the wind tunnel is reinforced as shown in Figure 3.3, and the tunnel is oriented on the Ames site as shown in Figure 3.4.

3.1.1 Noise Sources

Within the wind tunnel described above, the primary noise sources exist in the drive train. These sources are identified as follows:

a. Blade tip clearance
b. Blade/strut interaction
c. Fan arrangement and lift noise
d. Number of blades
e. Proximity of structural surfaces to the fans.

Blade tip clearance can be a significant parameter in noise produced by the drive train configuration. Hubbard (Reference 27) reports data for shrouded propellers which show that as the ratio of tip clearance to diameter is increased, and during conditions of unseparated flow at the shroud surface, the sound pressure does not significantly change as long as the clearance ratio does not exceed about 1 percent. Greater tip clearance ratios and separated flow provide increasing sound pressures. Hubbard & Regier report tests (Reference 9) which show that the presence of circular walls increase the pressures about 1.5 over and above that of free space pressures. These curves are reproduced for convenience in Figure 3.6. The fan/shroud configuration in the 40x80 foot tunnel are considered to relate closely to the unseparated flow configuration tested and reported in Reference 27.

Useful data relative to fan directivity is provided in reference 8. Fan torque principally determines the acoustic directivity of a fan. Torque and thrust components are in phase behind the plane of rotation and out of phase in front of this plane. The maximum directivity strength lies at an angle of 15^{0} to 30^{0} behind the plane of rotation. As tip speed decreases and the number of harmonics decrease, the ratio of thrust force to torque force normally decreases. This tends to shift maximum directivity farther from the plane of rotation.

The interaction which takes place between the fan blades and the struts is complex. The noise which is produced by this interaction is viewed as predominantly a combination of the effect of the blades passing in and out of the strut wake, the struts as a reflecting surface near to the blades, and the noise produced by the vibrating struts. The struts are caused to vibrate by the acoustic pressures produced by the rotating blades and by the mechanical vibration of the engine assemblies.

In considering the acoustic effects of the six fan arrangement, it is simplest to start with the acoustics of a single fan. Three components of noise are present: vortex noise, thickness noise, and lift noise. The mechanism by which each component is generated is given in Appendix 2. The nature of the vortex noise described in Appendix 2 suggests a very high frequency noise having an inefficient mechanism of generation. This source probably has little effect, therefore, and can be disregarded. Thickness noise does not become significant until tip Mach numbers approach one (Reference 10). The tip Mach number at maximum q_u (105) operation during this experimental program was about 0.47. Hence, we disregard the thickness noise component. Lift noise is representable by a dipole distribution (Appendix 2), and the maximum of its directivity pattern lies at an angle of about 30^0 behind the plane of rotation (Ref. 8). For low subsonic tip speeds, the fundamental is the most important component. As speed increases, the higher harmonics become more important until they may even exceed the fundamental. Hubbard and Regier attribute significance to the first one-half dozen or so harmonics at high subsonic tip speeds. In assessing the acoustic effects of the six-fan arrangement we have, therefore, considered the lift noise component only

for a single fan as defined in Appendix 2, and corrected for the six fans, and for the acoustic characteristics of the tunnel enclosure. These results are then compared to the measured noise and any differences are attributed to the fan arrangement.

Each time a fan blade passes an element of area in the fan disc, the air receives an impulse. The impulse may be Fourier analyzed into a steady component and a series of oscillating components whose frequencies are integral multiples of the blade passage frequency. The effect of the number of blades is to increase the impulse frequency, and to cancel out all harmonics except those that are integral multiples of the number of blades. For a given power, the addition of more blades reduces the noise. The magnitude of the noise reduction is a function of the strength of the cancelled harmonics. This is shown for a given fan in Figure 3.7, taken from Reference 8. In general, the higher the tip speed, the less reduction in noise level. Reducing tip speed in combination with increasing the number of blades provides the most substantial noise reduction.

3.1.2 Tunnel Enclosure Acoustics

The evaluation of the tunnel as an acoustical enclosure includes the evaluation of its sound transmission, its structural system, and materials.

The sound transmission of the tunnel walls is directly related to the forced vibration response of the walls to the internal acoustic pressures, and the rate of transmission determines in part the magnitude of the stabilized sound pressure level of the semi-reverberant sound field in the tunnel. The second factor which determines the magnitude

of this semireverberant sound field is the rate of dissipation - dissipation consisting of air absorption, losses in the moving structure and losses due to any sound absorption by materials internal to the tunnel. Dissipation in the wall structure is normally small and there are no significant absorbing materials in the tunnel. This leaves air absorption and wall transmission as the principal enclosure controls for interior sound levels in the steady state tunnel condition. Panel response and noise radiation are discussed in Appendix 1. Air absorption at given humidity and temperature values is documented in the literature. At the low frequencies which predominate in the tunnel, air absorption is small.

The effects of the structural system upon tunnel enclosure acoustics is related to the above paragraph. In addition the tunnel geometry is important. If the diffusers and guide vanes provide steady turbulent flow, there will not be appreciable increases in sound level in their vicinity. If unsteady turbulent flow exists, the increased velocity through the diffusers will tend toward the creation of quadropole sound sources. In this event, the sound pressures in their vicinity will be random and will increase by approximately the eighth power of velocity (V^8). Large quadruples generating low frequencies would exist close to the exit/inlet planes of the diffusers and small guadruples with their higher frequencies would exist farther away from these planes.

The measurement of absorption within an enclosure is usually made by a determination of the rate of decrease in level of sound after a source within the enclosure is shut off. The period of time during which the level falls uniformly to 60 dB below that which existed at the time of shut off is called the reverberation time. Reverberation

times are usually determined in the preferred octave bands and for moderately sized enclosures can be related to the mean absorption coefficients of the room surfaces, their areas, and the room volume.

The most familiar equation used to compute absorption from reverberation time measurements is that due to Sabine (Ref. 15).

$$T = \frac{60V}{1.086\ c\ \Sigma\ S_i\ (\alpha_{sab})_i}$$

Where T = reverberation time (seconds)
V = total room volume (cubic feet)
c = the speed of sound in air (feet per second)
S_i = the surface area of material "i" (square feet)
$(\alpha_{sab})_i$ = the absorption coefficient, or fraction of the energy absorbed, of material "i" (dimensionless).

Implied in the Sabine Equation and other reverberation time expressions is the assumption that all the sound energy in the enclosure is incident on all surfaces in proportion to their area during the time of decay.

3.1.3 Noise Source Identification

The principal noise sources in the wind tunnel are associated with the drive system. It is therefore not possible to measure the spectrum of each separate source at some point of interest by the technique of activating only one source at a time. These individual source spectra must be measured in the presence of the total noise field and somehow isolated in the data analysis. The coherence function is well suited to this task, being analogous to a filtering technique which filters out only that noise associated with a given source.

The coherence technology is discussed in Appendix 3. The Hewlett-Packard Fourier Analyzer has been used to effect Appendix 3. There are many noise sources other than drive train sources in the tunnel which add to the total noise field. These sources are principally due to structural looseness and reverberation and hence only appear when the drive train is active. Wall panel sizes vary somewhat, and the panel attachments vary considerably in effectiveness. Hence, there is considerable panel and door rattle noise. The frequencies and amplitudes produced by this structural vibration are unknown, as certainly is phase information. Because of the variation in structure, there would be a considerable variation in noise spectra from one of these sources to the next. A random variation would mean that the average of several such spectra would tend toward zero. The more spectra used in the averaging, the closer to zero will be the average value. Averaging of the power spectra of the total noise field in the tunnel over many samples of this noise field would then tend to leave only drive train noise to deal with when determining noise sources. The task required of the coherence analysis is then simplified, and the resulting coherence functions are more accurate.

3.2 Near Field

For purposes of this measurement study, the near field of the 40 x 80 foot wind tunnel was taken to be the Ames facility itself. This facility contains many noise sources in addition to the 40 x 80 foot tunnel, most of them being other wind tunnels. One purpose of the near field acoustic measurements was to determine the impact of the 40 x 80 foot tunnel on the Ames site. Measurements were therefore taken at several locations with this tunnel operative and

again with this tunnel inoperative. A second purpose of the near field measurements was to determine where the inverse square law became effective.

The classical theory of propagation is usually modeled on radiation from relatively simple sources such as a sphere or piston in a free field. Studies show that for these simple sources, two zones of propagation exist. At relatively short distances from the source, the intensity undergoes a series of maxima and minima which are a result of phase addition of waves from different parts of the vibrating surface of the source. At considerably greater distances, these phase differences become negligible and the intensity decays in a uniform manner in conformance with a freely propagating spherical or cylindrical wave. These zones are known as the near field and far field, respectively, and are analogous to the Fresnel and Fraunhofer regions of propagation of electromagnetic waves.

There is no fixed point at which the near field changes to the far field, although in the case of a circular piston source, it is generally accepted that far field propagation can be approximated to within 4% beyond a minimum distance such that

$$r > \frac{ka}{2\pi}$$

and $r >> a$

Where a = the largest radius or one-half length of the source

r = distance from source to field point

$k = 2\pi/\lambda$

λ = wavelength of sound

The theoretical treatment of radiation from a large rectangular source is complicated. We would expect that

fluctuations of intensity in the near field would occur, but feel that the criteria for defining the approximation for far field would be somewhat different.

It should be emphasized that the differences between any classical theory and the practical situations at the tunnel are substantial. Surrounding buildings reflect and channel the radiation down avenues. Phase differences due to different propagation path lengths to points in the source are compounded by reflections from adjacent buildings. The tunnel wall cannot logically be considered as a source where all points on the surface move in phase with one another.

These factors make it difficult to predict the propagation losses theoretically, although the results of classical propagation theory may be used in a broad sense to interpret the results of measurement.

3.3 Far Field

For purposes of this measurement study, the far field begins at the borders of the Ames site and continues outward until the noise from the 40 x 80 foot tunnel, in any frequency band, can no longer be measured. The purpose of these far field measurements was again to determine the impact of the tunnel. The technique of de-activating the source of interest to determine its impact was useful. Far field ambient noise includes freeway noise, airport noise (Moffett Field, primarily) and other Ames sources. The freeway and the airport sources generated high frequency noise which confused or overpowered 40 x 80 foot tunnel noise in these same frequencies. The only impact expected was in the fundamental of the tunnel and its first few harmonics.

4.0 MEASUREMENTS AND DATA ACQUISITION PROCEDURES

Test procedures were devised to optimize the quantity of data obtained in order to realize the goals of the investigation while keeping tunnel operating time to a minimum. For this reason, detailed on-site data reduction was rejected in favor of magnetic tape recording with frequent calibration of the recorder and instrumentation to ensure reliability. Data reduction was accomplished in Seattle.

4.1 Instrumentation and Data Recording Within the Tunnel

Data acquisition within the tunnel was accomplished in a series of six tests with each test being performed at two power settings corresponding to approximately q_μ = 60 and 105 (75% and 100% power).

Vibration data were acquired using Columbia piezo-accelerometers type 302-6 with a nominal sensitivity of 100 mv/g while airborne noise data were recorded through Bruel & Kjaer condenser microphones type 4145 (1") and type 4136 (1/4") with nominal sensitivities of -120 dB re 1v/μ bar and -152 dB re 1v/μ bar respectively. All microphones in the wind stream were equipped with nose cones.

A schematic diagram of instrumentation following microphones and accelerometers is shown in Figure 4.1.

Frequency modulation (FM) magnetic tape recordings were made for a period of ten minutes during each of the six test series. A four-channel Hewlett-Packard model 3960A, FM tape recorder was employed for this purpose. In all cases, recordings of the signals received simultaneously from four probes were made at 15"/sec to permit subsequent

analysis over a frequency range of 5 Hz. to 8000 Hz.

The disposition of probes (microphones and accelerometers) is shown in Figures 4.2 through 4.7. Reasons for their placement in these positions and their relationship to the overall task are summarized in Table 4.1.

In general, particular locations were chosen for simultaneous data acquisition to enable time-locked data for use in coherence analyses.

It will be noted in Table 4.1 that every test series included a microphone located at bent 74. This position was considered to provide a base spectrum to which data taken in different test series could be referred.

Precautions were taken during the installation of the microphones to avoid the generation of signals in the system through vibration of the microphone stands and housings. This was considered particularly important in view of the low frequency components of the spectrum expected from the propellers. Figure 4.8 shows a photograph of a typical microphone stand used during the tests with a sectional sketch of the interior of the housing with a sleeve of sponge neoprene.

Some difficulty was anticipated in mounting accelerometers to the transite walls of the tunnel. The type of accelerometers employed for the tests are normally mounted directly to test surfaces by using a short threaded stud. Transite, being an asbestos material, cannot be conveniently threaded to take these studs, and it was decided to fix triangular mild steel plates to the walls with self-tapping screws and attach the accelerometers to them. The dimensions of the plates (6" x 6" x 9" nominal 1/2" thick) were such

that no undue restraints were imposed on the structure to interfere with the first few orders of vibrational modes of the wall panels. The resonant frequency of these plates was well beyond the test frequencies of interest.

All microphones and accelerometers were calibrated at the start and termination of each test series. Calibrations were made of the microphones by using a Bruel & Kjaer pistonphone type 4220 (250 Hz.) at the microphone with the signal passing through all associated cabling and electronics to the tape recorder. Accelerometers were calibrated using a Bruel & Kjaer vibration pick-up preamplifier type 1606 which incorporates a vibrating table generating a calibration level of 1g at 60 Hz. Here again, the signal passed through the cable chain to the recorder. Additional calibrations were made each time tape reels were changed on the recorder by inserting a 1v RMS 250 Hz. signal on each track of the tape by means of a signal generator.

4.2 Instrumentation and Data Recording in the Near Field

Data collection in the near field was directed towards two separate studies. The first of these was a determination of the relationship between propagation loss and distance from the tunnel, while the second concerned the impact of the tunnel on the ambient noise within the Ames facility. Instrumentation used in the near field duplicated that used in airborn noise recording within the tunnel.

Bearing in mind that in the near field the sound intensity can vary quite markedly over short distances, a measurement technique was devised which would provide a continuous record of sound pressure level and distance from the source rather than a multiplicity of discreet points.

One microphone was set at a fixed distance from the tunnel wall, while a second microphone was held by a person walking away from the tunnel in directions which provided line-of-sight sound propagation down avenues that were approximately perpendicular to the tunnel walls.

Tape recordings were made both for the outward transit (away from the tunnel) and for the return. Distance markers were relayed by using a key on a radio held by the walker and recorded as distance markers on the recording tape. These marks were relayed every ten paces. Recordings were repeated for a total of three directions shown on Figure 4.9. The techniques could not be used for transits to the west of the tunnel since heavier traffic along the frontage road could have resulted in damage to the microphone cables. Instead, recordings west of the tunnel were made at fixed intervals of 25 feet.

In addition to the continuous recording of sound pressure level and distance, single records were made for a period of five minutes from several spot locations within the facility. Most of these recordings were made on the roofs of buildings where a relatively unobstructed propagation path existed from the tunnel to the observation point. These locations are also noted on Figure 4.9.

Reverberation time was measured in the section of the tunnel just downwind from the fans. The volume of this enclosure bordered by the fans and turning vanes was approximately nine million cubic feet. An adequate sound system was not available for the tests. Impulse noise was generated by popping balloons and by slamming large metal door.

4.3 Instrumentation and Data Recording in the Far Field

Figure 4.10 shows the instrumentation which was used to document far field data. All equipment was battery driven for operation from an automobile.

Sound was monitored by a Bruel & Kjaer type 2203 Precision Sound Level Meter (SLM) through a windscreen. The SLM had ten-dB step attenuators which were set for optimum output signal-to-noise ratio. The SLM output was then split with one channel going directly to a Sony TC 770 tape recorder and the other being frequency modulated and recorded on another track of the same recorder. All field recordings were calibrated periodically using a B&K 4220 pistonphone calibrator. The reason for this procedure was to obtain valid data from 4 Hz. to 20 kHz. The direct channel of the Sony TC 770 recorded the range from 20 Hz. to 20 kHz. and the FM data was carried on a Vetter Model 2D, 3200 Hz carrier, to record the range from 4 Hz. (dictated by the SLM follower) to 375 Hz.

Figure 4.11 shows the far field data reduction system. All far field data were reduced in discreet one-third octaves using the B&K 2130 Real Time Analyzer (RTA), B&K 401 Digital Coupler and computer time-sharing software. Data reduction from the direct channel of the Sony 770 was effected by playing the desired information into the RTA and digitizing the one-third octaves from 25 Hz. to 20 kHz. together with the A-weighted values. In all cases, the lowest recorded overall value was digitized for the tunnel-on condition because it was assumed the tunnel output was steady-state noise, and any increase during a recording sample would be due to a non-tunnel event. There was little fluctuation during recording periods. To obtain one-third

octave information down to 6.25 Hz. in this manner, it was necessary to demodulate the FM data from the second channel of the Sony 770 and record it at 3-3/4 inches per second onto an FM channel of the Hewlett-Packard (HP) recorder. The HP-recorded information was then played into the RTA at 15 inches per second (or four times the recording speed). This procedure frequency shifted the information upward by four without affecting levels, and permitted the acquisition of the desired one-third octave data.

The tape dub procedure described above deteriorates the signal-to-noise ratio of the original recording. However, care was taken in making the dub, and optimum S/N was maintained by monitoring the signal on an oscilloscope. Additionally spot checks were performed on the original recorded data using a General Radio 1564A one-third to one-tenth octave analyzer. Checks were also made between the AM and FM channels in the overlapping frequency range of 20 Hz. to 375 Hz. and found to be in good agreement.

4.3.1 Permanent Monitoring

In an effort to measure the fluctuation in far field level as a function of variations in weather, a continuous monitoring station was located atop the clubhouse in the trailer park on Space Park Way. This station ran continuously for several days during both our December, 1973 and March, 1974 measurement periods. To obtain tunnel noise and a minimum of noise from other sources in the far field, only the 31.5 Hz. octave band was monitored.

Sound was monitored by a B&K 4145 one-inch condenser microphone covered by a windscreen. The signal was amplified

by a General Radio P-42 microphone follower, fed into a Hewlett-Packard 8052A SLM, then into an HP 8055A octave filter set. The output was then amplified again by an HP 966A post amplifier and passed to a B&K 2304 graphic level recorder (see Figure 4.12).

The level recorder has an accurate paper speed enabling continuous determination of time for all 31.5 Hz. octave records. The system was calibrated periodically using a B&K 4230 calibrator, and the time base was verified from tunnel time records and graphic level signature.

4.4 Near Field Measurement Results

In order to discriminate between noise produced by the tunnel and noise arising from sources adjacent to a microphone located at some distance from the tunnel, and to define the propagation losses in terms of frequency, an analysis was made of the data in 1/10 octave bands centered at two frequencies which are consistent with the tunnel noise as well as the all-pass band, 5 Hz, to 8000 Hz. These frequencies were 26 Hz., the tunnel fundamental, and 78 Hz, the second harmonic. This harmonic was chosen in preference to the first harmonic at 52 Hz. since it provided a greater separation in the wavelength for estimating the onset of far field propagation.

Results of the tests using a moving microphone are presented in Figure 4.13 through 4.19. In these charts, the zero position corresponds to that point at which the fixed and moving microphones were approximately five feet apart in a plane parallel with the tunnel walls and at a vertical distance from the wall given by the fixed microphone position. The end point of the transit is noted as

the distance in feet from the fixed microphone. The records preceeding and following these end points correspond to the period of time spent in and around the end points and cannot be referred to the distance markers. The symmetry between the records walking away from the tunnel and back towards it should be noted.

An average value of the attenuation to points on the outgoing and return paths was calculated in the 26 Hz. 1/10 octave band and the 80 Hz. 1/10 octave band.

Figures 4.26 and 4.27 show the result of obtaining the difference in sound pressure level at a location above the concrete wall on the west side of the tunnel and a microphone at successive points 25 feet to the west.

These results illustrate the complexity of the radiation from the tunnel walls. Although the averaging of the data from the original records has smoothed the rapid oscillations in amplitude which occur over small changes in distance, large amplitude variations are present over considerable distances from the tunnel.

It is believed that the proximity of buildings in the area over which transits were made is the major factor in the production of these large amplitude variations. This belief is founded on the assumption that the tunnel wall cannot be considered as a radiator which moves so that each element on it has the same phase of displacement. This is a necessary condition for periodic phase components to arise in the individual paths from points on the source to the

receiver. These periodic phase components result in variations in intensity in the near field. If the radiator has spatially distributed random phase displacements, the near field will have randomly distributed phase components from points on the radiator surface. This will not produce regular variations of intensity with increments in distance from the source. Reflections from buildings at fixed distances from the source would, however, locally increase the sound pressure levels. This is apparent in the symmetry of the records from the moving microphone. The data presented in Figures 4.20 through 4.27 can only be interpreted as showing a general trend in attenuation with distance from the tunnel. It is believed that if the source were located remote from other buildings, the sound pressure levels would decay in a more regular manner than is depicted in these figures.

Using the records of the overall sound pressure level vs. distance shown in Figures 4.13 through 4.19, we have estimated the average slope of the attenuation vs. distance. Three of these curves give values of 2 dB attenuation for doubling distance, one gives approximately 3 dB, while the other two give 5 dB for doubling distance. On the average, this shows an attenuation of 3 dB for doubling of distance. These values are in agreement with spreading from a line source, which is a fair approximation to the configuration of the tunnel for the near field.

Since the source is of finite extent, it should be expected that at great distances from the source the propagation losses of 10 log r would increase until the source may be regarded as a point radiator with losses of approximately 20 log r.

Data from roof-top microphones and locations G & H which were relatively remote from high buildings were analyzed to provide all pass levels in the range 25 to 8000 Hz. and 1/3 octave levels in the same range. The data corresponding to these locations are shown in Figures 4.28 through 4.35. Supplementing these data with that gathered in the far field (distances greater than 1000 feet from the tunnel) and looking only at the 1/3 octaves containing the principal tunnel frequency components, i.e., 25 Hz. to 80 Hz., a plot of level vs. distance was obtained. This is shown in Figure 4.36. The sope of this curve does indeed increase with distance from the source. To distances of 200 feet the slope is 3 dB; between 200' and 400' it approximates 6 dB; while for distances greater than 400', it approaches 8 dB.

A similar result has been reported by Lyon (Ref. 24) quoting the work of Delaney (Ref. 25) although those results pertain to A scale levels. It is apparent that a mechanism other than geometric spreading is causing additional attenuation.

Differences in the results obtained from the data gathered by transits along the avenues and those obtained at rooftop level indicate that less attenuation occurs at street level. This might be attributable to sound being channeled along the avenues, an occurrence which would tend to restrict losses through geometric spreading.

Sound levels within the Ames facility while the tunnel is in operation show significant energy in the low frequency end of the audible spectrum. Although this energy is included in levels measured on the A-scale, its contribution to the background noise perceived by a listener is not fully emphasized by A-scale readings. For this reason

measurements of the levels within the facility, while the tunnel was shut down, are presented in 1/3 octave levels, so that a comparison might be made with 1/3 octave levels recorded with the tunnel in operation. The corresponding A scale level is included in the analysis for comparison with data gathered prior to these measurements.

Ambient daytime levels in the facility were recorded on March 22, 1974 at the locations shown in Figure 4.37. These records were made over the time period 1500 hrs. to 1700 hrs., a time which had activity corresponding approximately to the activity within the facility for the near field tunnel noise measurements made in December, 1973. One-third octave sound levels for the ambient noise measurements at these locations are shown in Figures 4.38 through 4.45.

It should be noted that one significant noise source was present during both these time periods. This was reported to be a cooling tower in the vicinity of the Fluid Dynamics Laboratory to the northwest of the 40 x 80 foot tunnel. The noise spectrum of this source was rich in high frequency components and could be described as similar to a high pressure air valve venting to atmosphere. The source is readily detectable in the spectra of ambient noise measured at locations F, G & H (Figure 3.4).

For the purpose of this investigation, the 1/3 octave levels of the ambient noise measurements have been averaged to provide a mean ambient noise spectrum. This averaging was made of the levels in the 1/3 octaves in dB rather than conversion to pressure amplitude before averaging. Averaging of levels in dB is a common practice for statistical evaluation of noise levels. The mean ambient spectrum is presented in Figure 4.46. The presence of the cooling tower

noise can be detected in this spectrum and emphasizes the fact that at a location such as Ames ambient is a relative term and is dependent on the presence or absence of sources other than the 40 x 80 foot tunnel.

In order to evaluate the impact that the tunnel noise has on the working environment within the facility, an estimate has been made of the intrusion that the sound levels outside a building would have on the interior working spaces.

For the purpose of judging the acceptability of the noise within a building, it is usual practice to refer to the series of criteria of octave band sound levels known as Noise Criterion (NC) or Preferred Noise Criterion (PNC). The latter of these two criteria, developed in Reference 15, provides a useful measure of the acoustical comfort provided to the occupant of spaces within a building while taking into account the intended use of the space. In general, office spaces might be assigned a PNC 35 criterion. This curve is reproduced in Figure 4.47.

To meet this criterion, structural walls are designed to provide sufficient attenuation to limit the intrusion of external noise sources.

The noise reduction provided by typical concrete walls with non-operable windows is of the order of 8 dB at 31.5 Hz., 14 dB at 63 Hz., and 20 dB at 125 Hz. If the levels outside the building are in excess of the sum of the PNC level desired and the noise reduction, then the impact on the inside environment can be judged in the light of the magnitude of this excess. This analysis can only be applied to occupied spaces on the side of the building with a reasonably unobstructed propagation path to the tunnel, and

those spaces used for activities other than office functions may allow a significantly higher background level than PNC 35. In addition, estimates of PNC levels at frequencies which have been shown to have anomalous propagation properties can only be interpreted as gross approximations. Despite this, it is believed that an estimate of near field impact derived in this manner will be useful. Attention has been directed only to these frequency bands where the tunnel noise has excessive magnitude and where coincidentally the structural attenuation of buildings is minimum.

Levels in the 31.5, 63 and 120 Hz. bands for records obtained from the eight fixed near field sites are given in Table 4.2, together with their distances from the tunnel wall. The levels in excess of PNC 35 after subtraction of the noise reduction loss given above are also tabulated in Table 4.2. Values of this excess are plotted vs. distance from the source in Figure 4.48.

Within the three frequency bands of interest, the interiors of structures on the Ames site could be impacted by as much as 5 to 25 dB by the 40 x 80 foot wind tunnel.

The balloon tests gave large variations in reverberation results. It is suspected that the balloon source failed to adequately energize the dominant room modes. Better results were obtained for low frequencies by slamming the door. Here reverberation time was shown to be 18.6 seconds (standard deviation = 3.40 seconds) at 500 Hz.

Average reverberation results are given in Table 4.3. For the door slamming energy source there was up to 30 dB of measureable decay for low frequencies. For the balloon source there was only 15 dB of measureable decay for the higher frequencies. This accounts for the greater variation

in results at the higher frequencies where, ordinarily, more stable results would be expected.

A final note of interest regarding the interior tunnel reverberation characteristics is the high reflectivity around 1.6 kHz. This phenomenon is noticeable when one walks on the tunnel floor in soft-soled shoes and hears a high frequency ricochet sound. This ricochet sound is caused by a diffraction grating effect on the corrugated wall surfaces which reinforces the sound at this particular frequency.

4.5 Far Field Measurement Results

Figure 4.49 shows the measurement results and far field contours for the 31.5 Hz. and 63 Hz. octave bands. The figure is presented without weighting networks or psychological criteria applied. One third octave band far field measurement results are shown in Appendix 5.

It is evident here that the tunnel does not radiate omnidirectionally but produces the greatest sound pressure levels to the north by northwest. This phenomenon is not attributable to wind, since the wind was between three and six knots from the NNW during measurement periods. It is suspected that local barriers such as buildings are the strongest influence on far field impact.

The theory that local structures control tunnel impact to the far field is supportable on two counts. One mechanism is the attenuation of sound by barriers and the other is reflection by the local structures east of the tunnel (Ref. 22). Other factors affecting the general contour pattern are the stronger source (i.e., the fans) on the west side of the tunnel, and the louver intakes on the

north side downwind of the fans.

Figures 4.50, 4.51 and 4.52 show the far field contours for the 26 Hz, 52 Hz., and 78 Hz., one-third octaves, respectively. These contours become lower in level and represent more omnidirectional characteristics with increased frequency. The only appreciable impact to the far field is the 26 Hz. pure tone. Due to the relatively low level and frequency proximity to other community noise sources, the 80 Hz. contours show the least impact and present the greatest variation in results. The greater impact to the north-by-northwest of the lower frequencies probably is due to the reflection characteristics of local structures at the particular frequencies.

The basic assumption in assessing far field impact is that noise will be considered a nuisance when it inspires any fear reactions from residents (e.g., sleep, TV viewing, speech, etc.). Several descriptors are available which describe the spectral and temporal characteristics of noise with regard to annoyance. All of these consider the decreased sensitivity of the ear to low frequencies. Unfortunately, some do not consider sources with components below 50 Hz. and those that do have generally just extended the spectral weighting lower to accommodate filter design. No recognized noise impact scheme has yet been designed and psychoacoustically tested for steady state low frequency sound. However, psychoacoustic results used in developing Steven's Loudness Level MK VII (in units of PLdB) show that it is reasonable to extend typical low frequency weighting to the 25 Hz range (Ref. 17). Additionally, Kryter has shown that merely summing weighted energy is not sufficient to describe annoyance. It is necessary to consider the presence of pure tones in the spectrum (Ref. 18).

The most commonly employed community noise descriptor is dBA which is measured by applying a single weighting network to all sounds. A-weighting de-emphasizes low frequencies (-44.7 dB at 25 Hz.) and slightly pre-emphasizes the ear's most critical range (+ 1.3 dB at 2500 Hz.).

As A-weighting generally approximates the Perceived Level (PLdB) weighting (Ref. 26) for low frequencies at low levels and is generally understood, it is used here in describing far field impact. Figure 4.53 depicts the far field dBA contours based upon our measurements. Due to the strong pure-tone component at 26 Hz., however, it would be reasonable to assess a three to five dBA penalty increase in the measured levels to describe far field impact.

Results from this measurement program have not enabled us to adequately document the desired weather effects. During our measurement periods in December, 1973 and March, 1974, there were no significant alterations in the weather.

Temperature inversions are measured from "soundings" performed only every six hours and only from the Oakland area weather facility. This information furnished to the Moffett Field weather facility and, in turn, supplied to us, revealed the typical Bay Area condition of a moderate inversion around 2000 ft. MSL. Classical models of noise propagation reveal that the sound path up to two miles away rarely attains a height greater than 100 feet over flat terrain and under normal light wind conditions (Ref.21). Thus, it would be difficult to conclude that temperature inversions around 2000 feet would have any appreciable effect on our measurements.

Weather information revealed that the wind consistently was at three to six knots from the north-by-northwest. The wind information comes from an anemometer located atop the Moffett Field operations building on the west side of the field. There will probably be some wind gradient from the surface to the estimated anemometer altitude of 120 feet. Additionally, the presence of alternate mud, fields, pavement, buildings and other ground material will cause low level up and down drafts, which would considerably upset any simplified wind assumption (Ref.23).

Variations of six dB in level at the permanent monitoring station were recorded for ostensibly steady state tunnel operation and wind conditions (speed and direction). It is probable that surface wind variations unavailable from standard aviation weather facilities are the cause of these level fluctuations.

Contours shown are representative of full tunnel power which is only used a small percent of the time. Measurements for partial power revealed considerably less impact. Additionally, tunnel startup to full power takes several minutes indicating that there should be no startling effect or fear syndrome associated with the tunnel noise as there often is with aircraft noise.

Ambient sound level measurements made during the day and on weekends are shown in Figures 4.54 to 4.69, and were generally from 45 dBA to 50 dBA. Throughout most communities, it is reasonable to assume that ambient levels will be at least 60 dBA one percent of the time. As the tunnel runs at full power approximately one percent of the time, it may be concluded that there is no impact outside of the 55 dBA contour (55 dBA + dBA for pure tone component).

The area encompassed by this contour is largely uninhabited except for the Navy housing immediately to the west of the tunnel (in the near field) and to the southwest on Stevens and Orange Avenues.

For most far field measurement locations, a short sample of the ambient level was also recorded for the tunnel-off condition. Data obtained in this manner were not of sufficient duration to typify the statistical distribution of sound for the 24-hour day. To properly describe the far field noise environment, much longer recordings would be required throughout the area. It is suspected that ambient levels measured are lower than typical because they were made on week-ends when other local sources were minimal.

Ambient levels to the east of the tunnel vary with automobile traffic, other tunnel operations and surface aircraft activity around the large hangar. To the north of the tunnel, there is minimal human activity making ambient levels quite low with occasional large peak levels from aircraft. To the west of the tunnel, background levels are dictated by traffic on the Bayshore Freeway and by Moffett Field and NASA-Ames activities. To the south of the tunnel are the Bayshore and Stevens Creek Freeways. These completely dominate the entire ambient noise environment and render the tunnel itself completely inaudible. Here, recorded ambients in the densely populated areas varied typically between 20 dBA and 60 dBA.

In summary, the acoustical impact to residents in the far field is considered to be minimal. Much of the area within the 55 dBA contour is directly beneath the downwind leg of a Moffett Field flight path. With wind predominately from the NNW, this RW 32L circular pattern is used heavily. Most operations are from P-3 aircraft which also produce

low frequency sound (63 Hz.).

Perhaps the greatest impact to the far field is not the low frequency noise itself, but rather the low frequency vibration which it could excite in individual structures.

Two approaches were undertaken to investigate wind and temperature inversion effects upon far field noise propagation: 1) continuous monitoring of the 31.5 Hz. octave data in parallel with accurate and comprehensive hourly weather data from the Moffett Field weather facility, and 2) selection of far field measurement positions at discrete distances of 2000, 4000, 6000 and 8000 feet in various directions on discreet radials from the tunnel which were measured at two times four months apart. Typical continuous monitoring results are shown in Figure 4.70.

To adequately measure wind effects on noise propagation, it is deemed necessary to monitor low elevation wind gradients at several points along the propagation path (Ref.20).

4.6 Measurement Results Within the Tunnel

Data recorded from the microphone locations within the tunnel were initially analyzed into 1/3 octave bands using a Bruel & Kjaer type 3347 real time analyzer. This equipment was used in conjunction with a time shared IBM 370 computer through a teletype with a telephone coupler. Data in the form of 1/3 octave levels in the range 25 Hz. to 8000 Hz. were stored temporarily on punched paper tape and then passed to the computer.

The analysis of airborne signals which were made in this manner are presented in Figures 4.71 through 4.100.

for the two operational modes of the tunnel corresponding to 60 q_u and 105 q_u. The four 1/3 octave levels above 8000 Hz. should be ignored in the interpretation of these plots since they are in excess of the flat frequency response of the FM tape recorder system.

The majority of the energy in the airborne data is below 400 Hz. This is to be expected since the fundamental frequency of the drive system is in the region of 26 Hz. For this reason, a digital analysis of representative data to define the spectrum with a 1 Hz. band width at low frequencies was made using the Hewlett Packard Fourier Analyzer. The narrow band acoustic data are shown in Figures 4.101 to 4.105. Two primary concerns of this study were:

1. The evaluation of the tunnel as an acoustical enclosure, and
2. A definition of drive train acoustic sources.

For these purposes, the narrow band data were useful. To assist these evaluations, the coherence functions were calculated for several pairs of acoustic signals (see Appendix 3), and are shown in Figures 4.106 to 4.111. These coherence functions were re-plotted to show the percentages of sound pressure level in the fundamental frequency and its harmonics which traveled downstream of the fans. Figure 4.112 shows that the fundamental and the first two harmonics of blade tip noise are highly coherent, indicating that these frequencies travel directly from the fan blades to Bent 74. The remaining frequencies are less coherent, indicating arrival at Bent 74 from other sources. Figure 4.113 shows the fundamental and the first three harmonics to be highly coherent. The guide vanes apparently do little to alter the path of these frequencies, but tend to cause higher frequencies to disperse. Figure 4.114 indicates that only the first harmonic travels directly from Bent 74 to the test section.

Figures 4.115 to 4.134 trace sound pressure level around the tunnel by frequency. The significance of these plots is that the turning vanes tend to increase the amplitude of some frequencies and that in general, frequencies of 250 Hz. and higher are well attenuated through to the test section. Frequencies up to 100 Hz. remain high in amplitude through the test section.

The averaging of only 30 data samples effectively eliminated random data from the narrow band plots. This would indicate the absence of significant turbulence through the diffusers.

VIBRATION

Strictly speaking, transmission loss (TL) is a physical quantity which is attributable to a structure which has been subjected to a precise acoustical test procedure defined by the American Society for Testing and Materials (ASTM). The method adopted for this measurement program consisted of a measure in one-third octaves of the levels within the tunnel, and subtracting from them the levels from similar measurements made outside the tunnel at approximately ten feet from the weall. It is assumed that at the locations used for the internal measurements, a diffuse acoustical field existed. The procedure might more appropriately be called a measurement of the Field Insertion Loss (FIL) of the wall.

Measurements were made at two locations which correspond to the pairs of airborne measurements of test points 2 and 11 (Bent 74), and test points 14 and 15 (Bent 91). The results of these measurements are presented in Figures 4.135 through 4.138. Figure 4.139 shows the average FIL for both positions and tunnel operating conditions. At low fre-

quencies the curve follows a 6 dB/octave slope in correspondence with mass law control. At 250 Hz., stiffness control takes over and the curve follows a -6 dB/octave slope to a resonant control region around 1000 Hz.

Data gathered from each of the accelerometer positions within the tunnel were digitally analyzed in the frequency range 0 to 400 Hz. so as to avoid aliasing and to enable a 1 Hz. resolution of the spectrum. Acceleration amplitude in units of g was plotted on a digital plotter against a frequency abcissa. The results of these analyses are presented in Figures 4.410 through 4.155. Figure 4.160 shows a narrow band insertion loss of 23 dB, in the frequency range 26 to 130 Hz. which is the second harmonic of blade tip noise. This frequency approaches an anti-resonance of the wall panels. Figure 4.111 shows about 60% common energy between the panel motion at this frequency and sound measured at the same frequency by the microphone located outside of the tunnel. This would imply that about 40% of the acoustic pressure outside the tunnel was due to sources other than motion of the particular panel tested.

Figure 4.107 shows coherence between blade tip noise and strut vibration to be high in the blade tip noise fundamental and in the first, second and seventh harmonics. We do not attribute strut vibration in the fundamental and the noted harmonics to acoustic pressures in spite of the high coherence. The mechanical design of the motor/fan system could well be transmitting mechanical vibration to the struts in these modes and hence show the apparent high relationship to acoustic pressures. Multiple coherence methods would be required to separate these multiple sources.

5.0 ANALYSIS RESULTS

5.1 Fan Noise

The fan noise analysis consisted of calculating the sound pressure levels that were expected at two positions; one in the near field, and one in the far field of the fans. For the purpose of this analysis, the far field is considered to exist at distances greater than two fan diameters away from the fan.

5.1.1 Near Field

The sound pressure level in the near field of the tunnel was calculated using equation (9) in Appendix 2. The equation is repeated here for convenience.

$$P_{rms} = \frac{1}{4\pi^2\sqrt{2}} \int_0^{2\pi} \frac{1}{S_\varepsilon} \left(T X + \frac{Q Y}{R_o} \operatorname{Sin}\Theta \right) \left(\frac{1}{S_\varepsilon^2} + \frac{iK}{S_\varepsilon} \right) e^{i(mB\Theta + KS)} \, d\Theta \qquad (5.1)$$

The above equation predicts the lift noise for a propeller with parameters as defined in Appendix 2. As stated in the technical discussion, the near field sound pressure level was considered to be due entirely to lift noise. This is confirmed in the frequency spectrum analysis of the near field noise because higher frequencies are not significant.

Harmonic sound pressure levels were calculated for blade tip noise in the vicinity of Position 1, which was located approximately one foot downstream from the lower center fan, and approximately six inches off the floor. The equation above predicts the near field lift noise for a propeller in a free field condition, so that the pressure calculated from that equation was therefore corrected for tunnel effects.

These tunnel effects are (1) tunnel reverberation, (2) the sound pressure level increase due to the fan shroud, and (3) the increase of sound pressure level due to the location of the microphone near the floor. The tunnel reverberation effect at this near field position was assumed to be negligible because of the magnitude of the direct component of the sound. Hubbard and Reiger (Ref.9) show that the increase in sound pressure level due to the fan shroud is about 4 dB. The location of the microphone near the floor will also add about 6 dB due to pressure doubling near the surface.

Taking these tunnel effects into account, the sound pressure level is given by

$$L_p = 20 \log \frac{P_{rms}}{P_o} + 10 \text{ dB} \qquad (5.2)$$

Where P_{rms} is given by equation (5.1)
$P_o = 2 \times 10^{-4}$ dynes/cm^2 = 2×10^{-5} N/m^2

The calculated values of sound pressure level at Position 1 are compared to the measured sound pressure level spectrum at the same location in Figure 5.1. The difference between the calculated and measured values may be a result of several factors; however, none conclusively. The wind tunnel fans were modeled by a propeller with a twenty-foot long blade. It is considered that this was the best model, but since it was not an exact representation of the fans, some error may have been introduced. Another source of error may be the close spacing of the fan's blades, since the equation model's typical propellers, and most propellers do not have six blades.

5.1.2 Far Field

The far field sound pressure level at Position 2 (Bent 74) was calculated using NTIS distributed report #N73-31945, entitled, "Aircraft Noise Source and Contour Estimation", by D. G. Dunn. The methodology used to calculate the sound levels at Position 2 is given in Appendix 4.

The calculated values of sound pressure level at Position 2 are compared to the measured sound pressure level spectrum of the same location in Figure 5.2. The reasons that were stated for the differences between measured and calculated sound pressure levels in the near field apply here also.

5.2 Wall Vibration Response and Field Insertion Loss

The tunnel wall response was calculated for a panel located near Bent 74, using Equation (7) of Appendix 1. Equation (7) is repeated here for convenience.

$$\overline{\xi^2}_s = \frac{A^2 PSD_N(\omega_s) j^2(\omega_s) \pi}{4\delta_s m_s^2 \omega_s^3}$$

The calculations were made for the first three modes of the panel using excitation by the measured acoustic pressures inside the tunnel. These are compared with the measured panel response (at the same position) in Figure 5.3.

The sound pressure level outside the tunnel was then calculated for the same three modes, using Equation (11)

of Appendix 1. Equation (11) is repeated below.

$$P = \rho_o CV \cos(\omega t - Kr)$$

The calculated sound pressure level ten feet outside the tunnel, at Bent 74, is compared to the portion of the measured sound pressure level due to the panel vibration in Figure 5.4. The portion of the sound pressure level due to the panel vibration was found by multiplying the measured outside sound pressure level by the coherence between the tunnel wall vibration and the measured outside microphone response.

The field insertion loss (FIL) of the tunnel wall was calculated by subtracting the calculated sound pressure level outside the tunnel from the measured sound pressure level inside the tunnel. The measured pressure level inside was used because it was also used as the forcing function for the panel vibration. The calculated and measured values of the FIL of the tunnel wall are compared in Figure 5.5.

The difference between the measured and calculated FIL might be attributed to two factors. The first factor is the assumptions that were involved in the calculations. The second factor is the fact that the measured transmission loss takes into account the acoustical "leaks" that exist in the tunnel walls; i.e., doors and windows. In addition, the measured values consist of the contributions from all of the panels, whereas the analytical approach included these panels only indirectly through the coherence function.

6.0 CONCLUSIONS

The following conclusions are based upon the foregoing study results.

1. A reduction in tip speed of 25 percent would reduce tip noise approximately 6 dB. A 25 percent reduction in tip speed, however, would place the fundamental acoustic frequency of the tunnel at about 20 Hz. which is about the threshold of audibility. This lower frequency would increase tunnel wall noise trnsmission problems and would still be in a frequency region audible to persons external to the tunnel. It therefore would probably be advisable to increase the number of fan blades together with tip speed reduction. This change would increase the fundamental acoustic frequency of the tunnel, thereby reducing the noise transmission task of the tunnel walls. Simultaneously, the blade tip noise level would be reduced because of the increased number of blades.

2. The existing tunnel contains virtually no absorption. Particularly effective locations for absorption would be in an area 15° to 30° behind the plane of blade rotation, on the guide vanes, and on the tunnel walls, particularly around the bends.

3. The interaction between the fan blades and the nacelle struts has not been satisfactorily determined. The coherence between blade tip noise and strut vibration is high in the fundamental and three harmonics, indicating a strongrelationship. However, it is considered

highly probable that a strong relationship might also exist between strut vibration and mechanical vibration within the motor assembly. This determination would require coherence measurements that have not been made.

4. The guide vanes are ineffective in dispersing frequencies close to the blade tip fundamental, but scatter the higher frequencies. The sound pressure levels of most frequencies show some amplification through the guide vanes, probably because of reflection.

5. Using the usual working space criteria applied to office buildings, the near field of the 40 x 80 foot wind tunnel provides a considerable acoustic impact - from 5 dB to 25 dB depending upon the frequency examined and the building location (300 to 1000 feet from the tunnel).

6. The far field (one-quarter mile or greater distant from the tunnel) of the 40 x 80 foot wind tunnel does not appear to significantly impact the community in an acoustic sense. The possibility of an induced vibration impact, however, does exist.

7. Considerating the complexity of the wall panels and the associated difficulty of calculating sound radiated from corrugated panels, it is our opinion that we have presented an adequate method for predicting wall vibration response and panel noise radiation. We also are of the opinion that an adequate method has been presented for predicting the near field and far field

noise within the tunnel. Calculated and measured data adequately support each other.

8. Calculations of fan noise within the tunnel have been based upon the assumption of incoherent sources for the six fans. These calculations agree reasonably well with measured values. The fans are therefore concluded to act as incoherent sources, and the fan arrangement to not have negative acoustic effects.

9. The transite walls of the tunnel do not have an adequate insertion loss in the low frequency region to protect near field buildings from noise intrusion. If a powered model were tested, this condition would be expected to be even more severe. The design of tunnel alterations or new tunnels should consider other wall constructions; perhaps a septum in front of the transite walls with an air space between the two and/or the use of panels of varied dimensions which are farther removed from blade passage frequency than are the existing panels. The existing tunnel has too much structural looseness and too many openings that are not provided with sound traps to be considered a good acoustical enclosure.

10. A fan system which produces a higher fundamental frequency would not be expected to impact the test section as severely as does the existing system.

11. The coherence technique presented here is considered to be a good method for estimating reverberation effects in a structure like the tunnel.

7.0 RECOMMENDATIONS

Based upon these study results, the following recommendations are offered:

1. A multiple coherence study of the drive train/strut system would assist the results of this program to define the blade noise/strut interaction.

2. A study which places microphones along the struts and which protrude into the strut boundry layer to varying depths is recommended in order to document sound pressure levels as a function of boundry layer.

3. If further far field weather impact data are desired, it is recommended that low level wind gradients be measured.

REFERENCES

1. Franken, P.A., "Sound Induced Vibrations in Cylindrical Vehicles", J.A.S.A. 34, 1962

2. Sutherland, L. C., "Sonic and Vibration Environment for Ground Facilities - A Design Manual", Report to NASA Marshall Space Flight Center, Contract NAS58-11217, March, 1968.

3. Soderman, P. T., "Sound Levels Generated by the NASA Ames 40- by 80 Foot Wind Tunnel", FSA Technical Memorandum No. 3, July 16, 1973.

4. Lee, Y. W., "Statistical Theory of Communication", John Wiley & Sons, Inc., 1960.

5. Powell, A., "On Structural Vibrations Excited by Random Noise Pressures", Douglas Aircraft Company Report S.M.22795.

6. Crandall, S. H., "Random Vibrations", M.I.T., 1958, Chapter 8.

7. Rayleigh, "The Theory of Sound", Volume 2.

8. Richards, E. J.and Mead, D.J., "Noise and Acoustic Fatigue in Aeronautics", John Wiley and Sons, 1968.

9. Hubbard & Regier, "Free Space Oscillating Pressures Near Propellers", NACA Report 996.

10. Diprose, "Some Propeller Noise Calculations Showing the Effect of Thickness and Planform", Technical Note M.S.19 (M.O.S.)

11. Dunn, D. G., "Aircraft Noise Source and Contour Estimation", July 1973, NTIS#N73-31945.

12. Beranek, Leo L., Noise and Vibration Control, Chapter 9, pp. 226-230, 240-243, McGraw-Hill, 1971.

13. Beranek, Leo L., Acoustics, Chapter 10, pp. 307-311, McGraw-Hill, 1954.

14. Cremer, L., "Calculation of Sound Propagation in Structures", Acoustica, Vol. 3, No. 5, 1953.

15. Beranek, Leo. L., "Noise and Vibration Control", 1971, p. 237.

16. R. M. Towne & Associates, Inc., "Aircraft Noise Study, Naval Air Station, Moffet Field, California", 1973.

17. The Journal of Acoustical Society of America (JASA), "Perceived Level of Noise by Mark VII and Decibels (E)", Vol. 51, No. 2 (Part 2), February 1972, p. 597.

18. "Federal Aviation Regulations, Part 36: Noise Standards, Aircraft Type Certification", Federal Register, Vol. 34, No. 226, pp. 18,815-18,878, November 25, 1969.

19. Aviation Weather Reports (historical), Moffett Field Naval Air Station Weather Facility, December 1973 and March 1974.

20. Rothwell, P., "Sound Propagation in the Lower Atmosphere", JASA, Vol. 28, No. 4, 1956.

21. Ingard, Uno, "Review of the Influence of Meteorological Conditions of Sound Propagation", JASA, Vol. 25, No. 3, May 1953.

22. Kurze, U. and Anderson, G. S., "Sound Attenuation by Barriers", Applied Acoustics, Vol. 4, No. 1, 1971.

23. Wiener, Francis M. and Keast, David N., "Experimental Study of the Propagation of Sound over Ground", JASA, Vol. 31, No. 6, 1959.

24. Lyon, R. H., "Role of Multiple Reflections and Reverberation in Urban Noise Propagation", Journal of the Acoustical Society of America, Vol. 55, No. 3, March 1974.

25. Delaney, M. E., Copeland, W. E., and Payne, R. S., "Propagation of Traffic Noise in Typical Urban Situation", National Physical Lab Report, Ac 54, October 1971.

26. Stevens, S. S., "Perceived Level of Noise by Mark VII and Decibels (E)", JASA, Vol. 51, No. 2, Part 2, February 1972, pp. 575-601.

27. Hubbard, H.H., "Sound Measurements for Five Shrouded Propellers at Static Conditions", NACA TN 2024, April 1950.

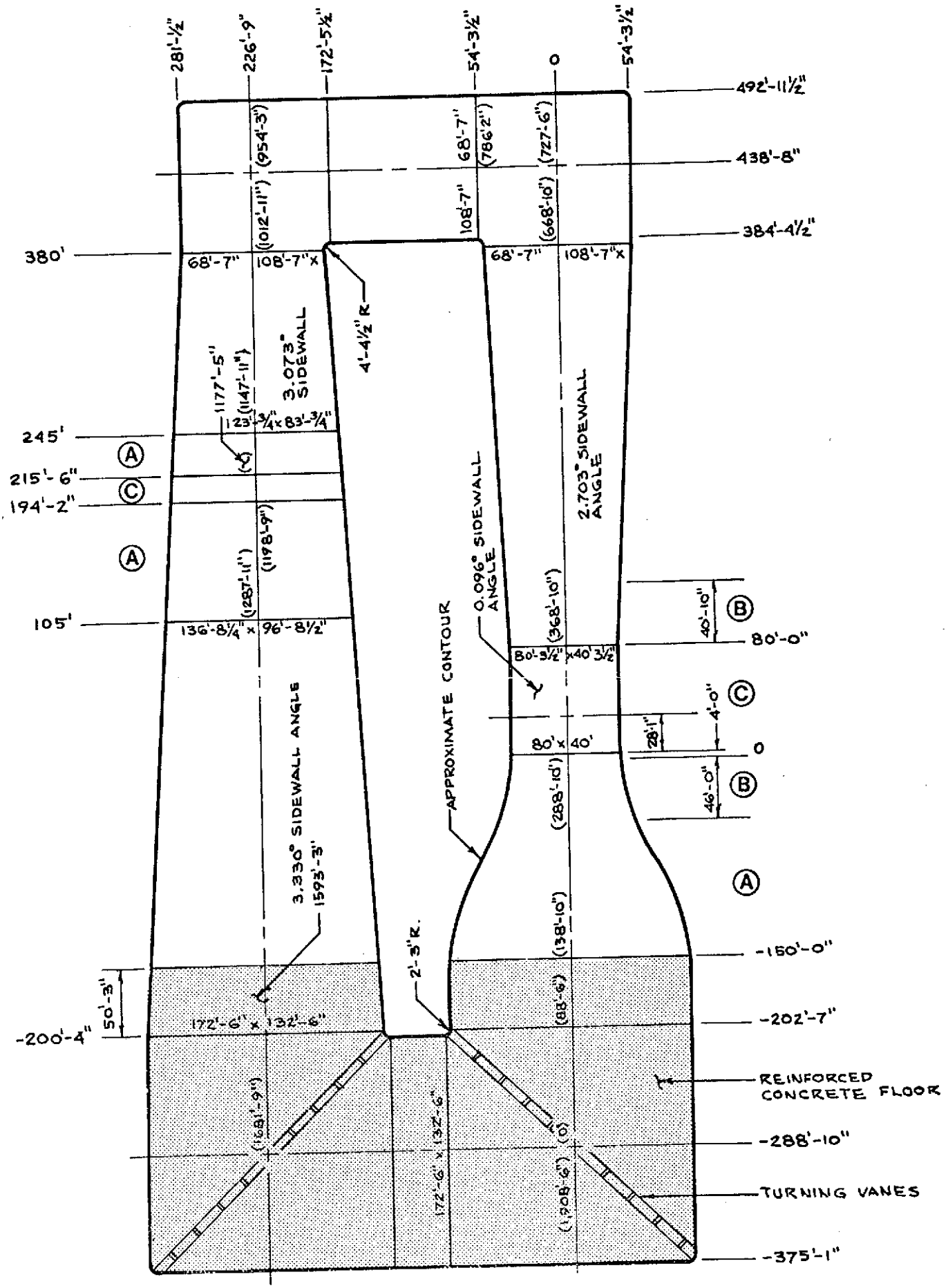

ROBIN M. TOWNE AND ASSOCIATES, INC.

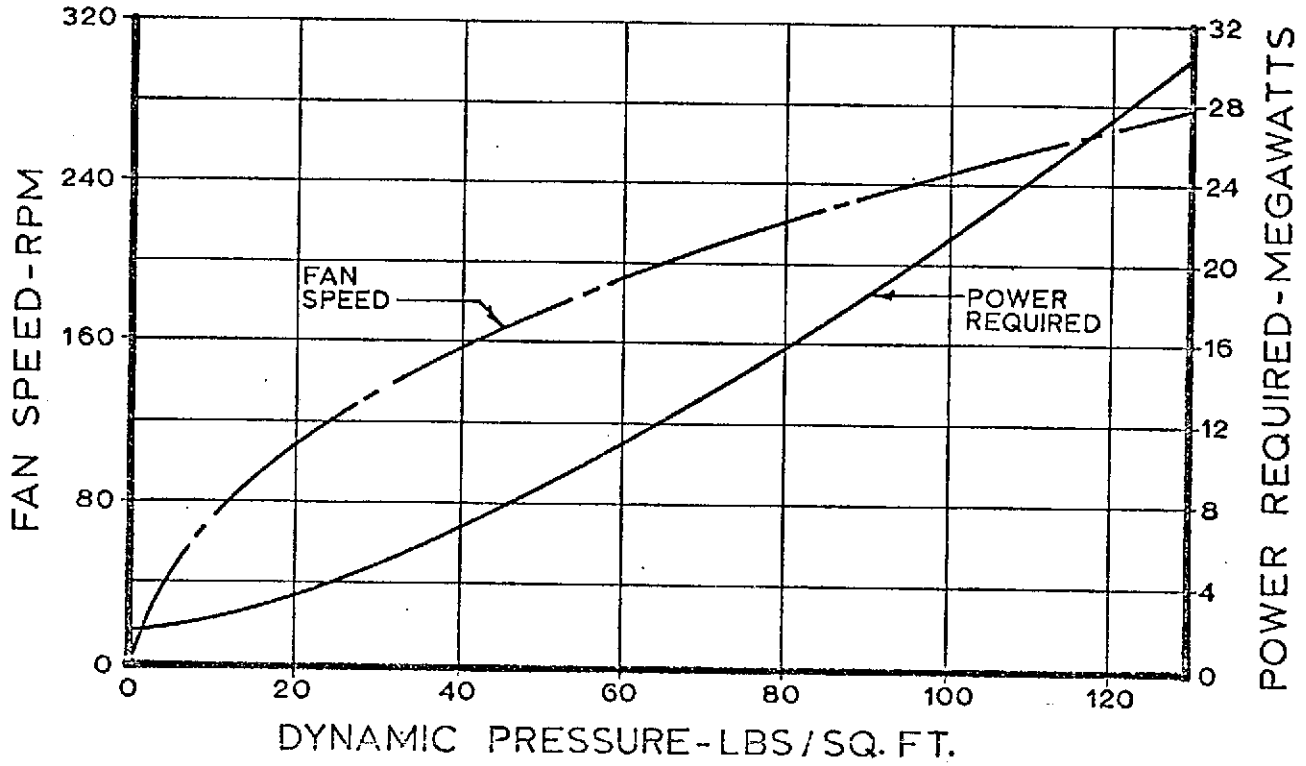

FAN ROTATIONAL SPEED AND POWER REQUIRED VERSUS TEST SECTION DYNAMIC PRESSURE

FIGURE 3·2

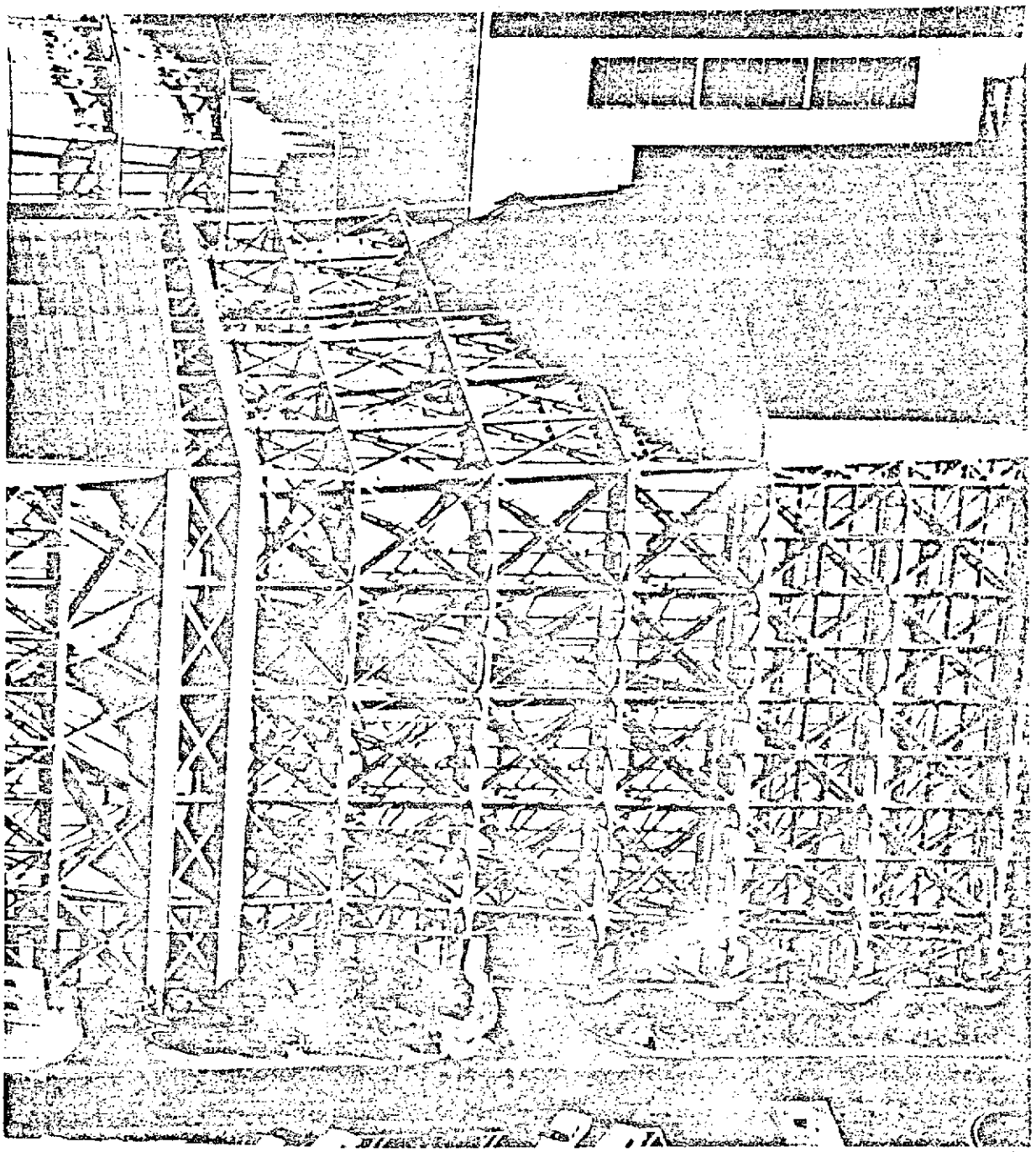

40 X 80 WIND TUNNEL EXTERIOR STRUCTURE

FIGURE 3-3

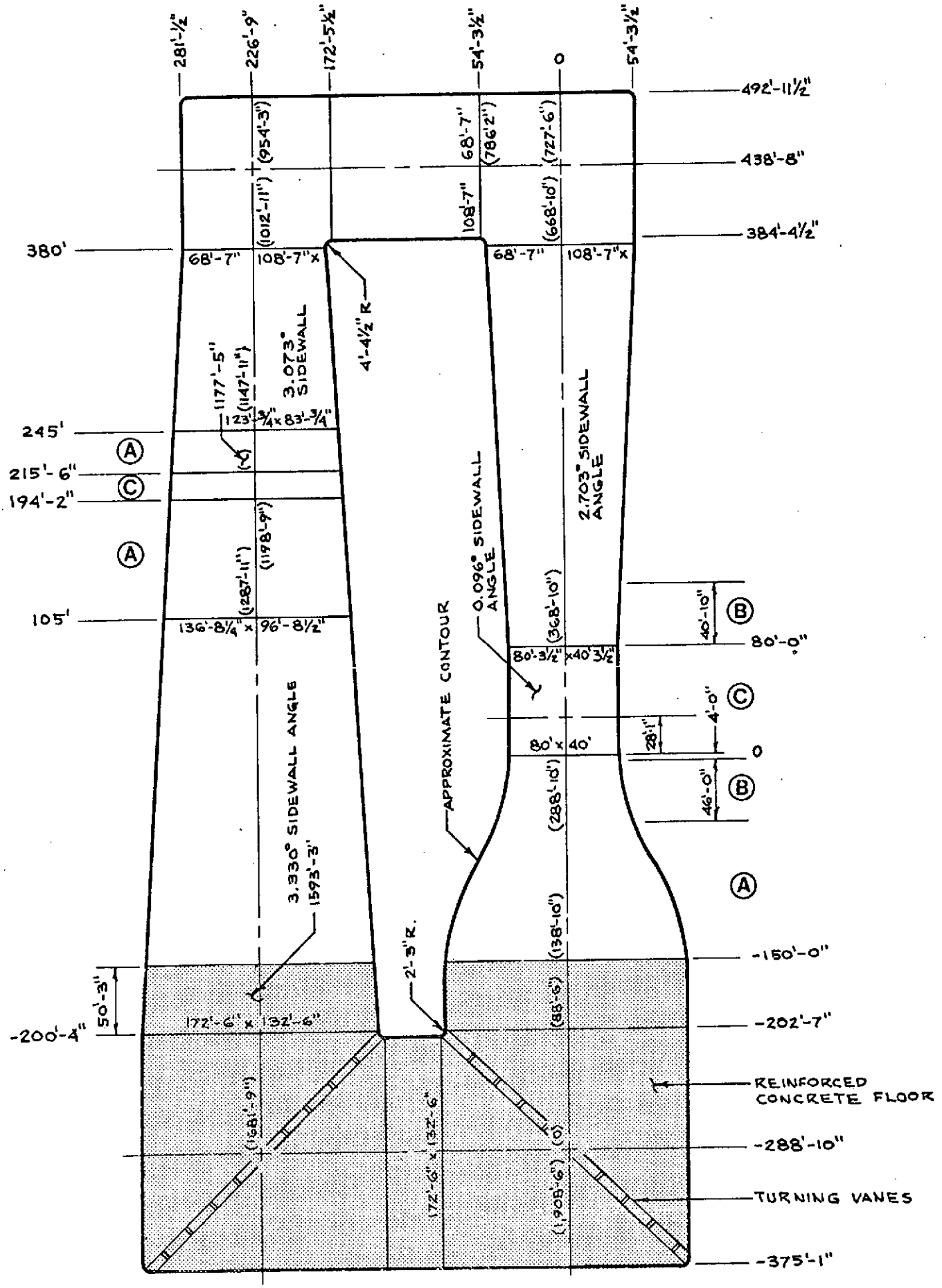

ROBIN M. TOWNE AND ASSOCIATES, INC.

NOTES

1. COVERING FOR CEILING AND FLOOR OF PASSAGE WAYS IS TAR COATED 16 GAUGE (1/16") CORRUGATED IRON EXCEPT AS NOTED OTHERWISE.
2. COVERING FOR ENTRANCE, EXIT AND DRIVE MOTOR TRANSITION SECTIONS IS 1/4" THICK STEEL PLATE AS NOTED.
3. TEST SECTION AND DRIVE MOTOR COVERING IS 3/8" PLATE AS NOTED.
4. ALL OTHER COVERING IS 3/8" THICK CORRUGATED ASBESTOS CEMENT. THIS COVERING HAS 4.2" PITCH AND IS INSTALLED WITH 4.2" (ONE CORRUGATION) SIDE LAP AND 6" MINIMUM END LAP

SCALE

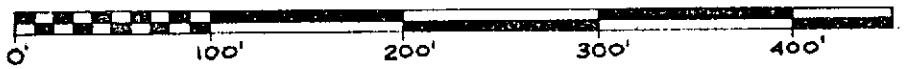

LEGEND

CODE	DESCRIPTION
(A)	1/4" THICK STEEL PLATE
(B)	5/16" THICK STEEL PLATE
(C)	3/8" THICK STEEL PLATE

40 x 80 WIND TUNNEL

FIGURE 1

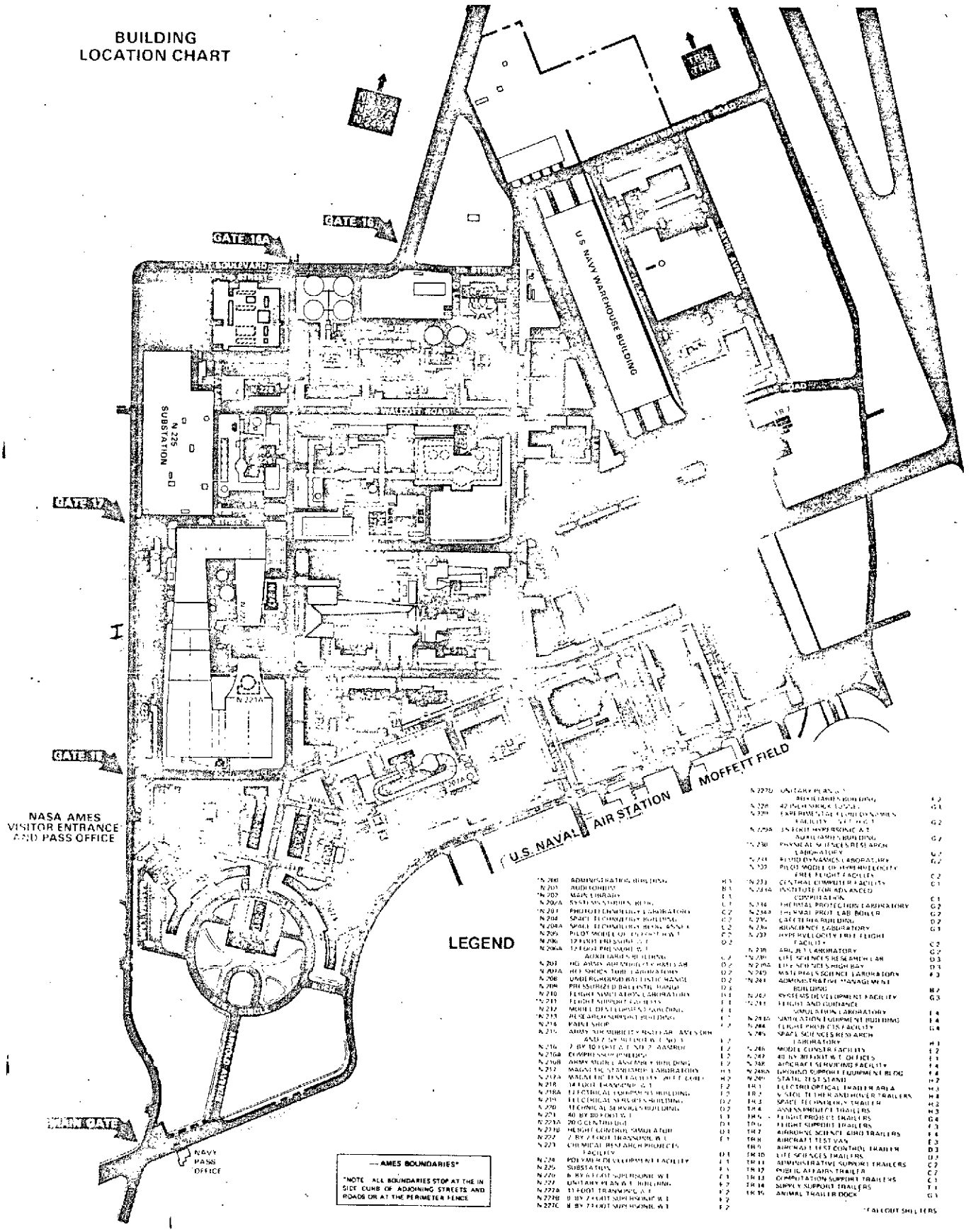

REPRODUCIBILITY OF THE ORIGINAL PAGE IS POOR

FIGURE 3-4

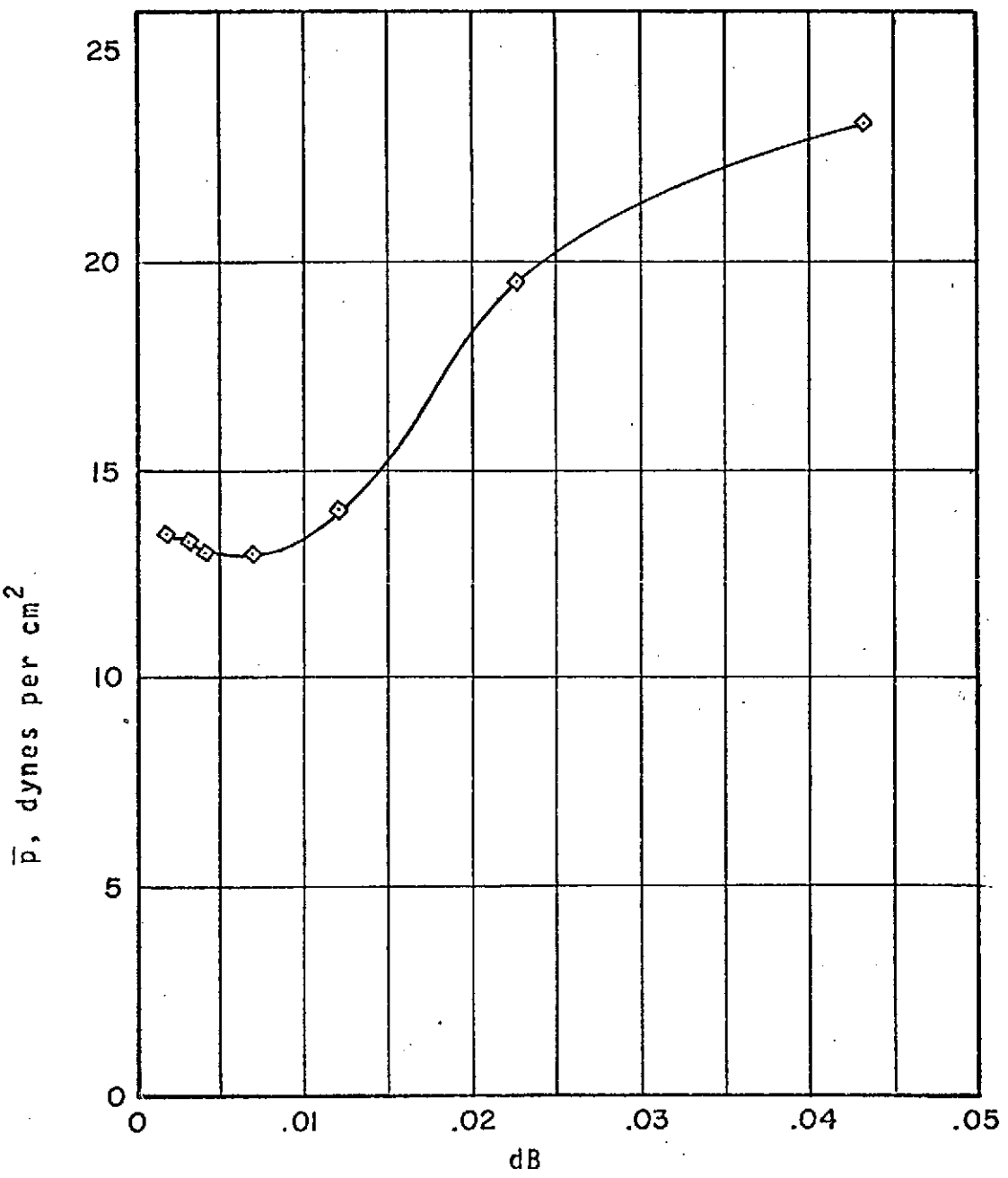

EFFECT OF TIP CLEARANCE RATIO ON TOTAL SOUND EMISSION OF A SHROUDED PROPELLER

Figure 3.5

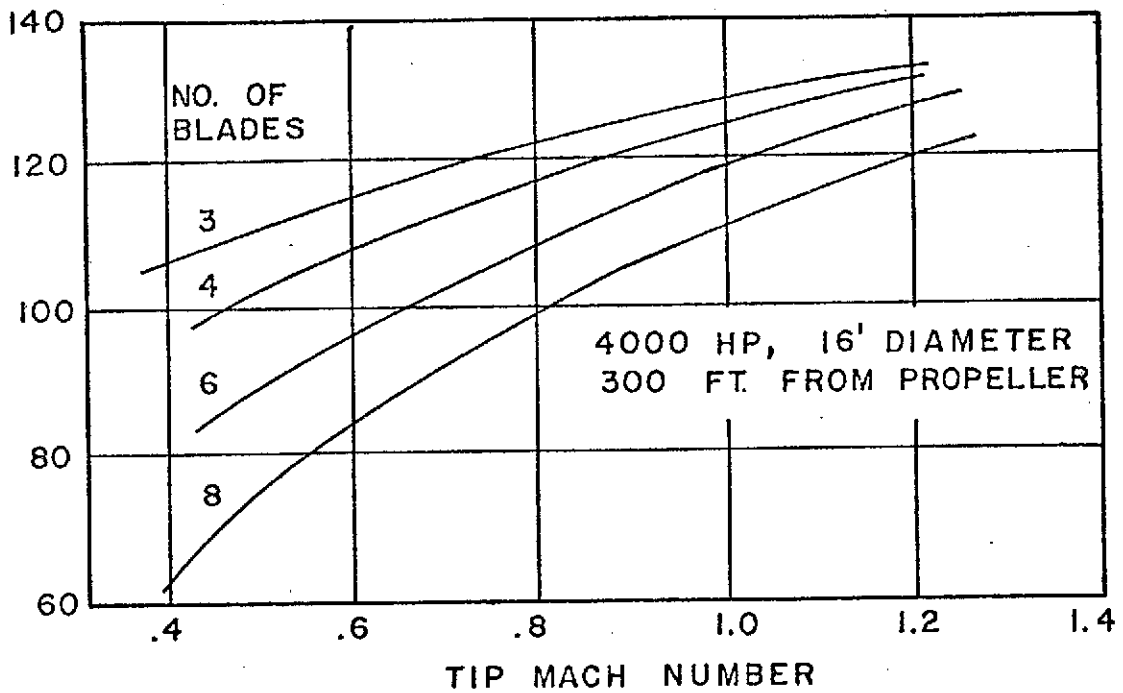

FIGURE 3.7- Effect of Number of Blades and Tip Mach Number on Noise Level, Constant Power

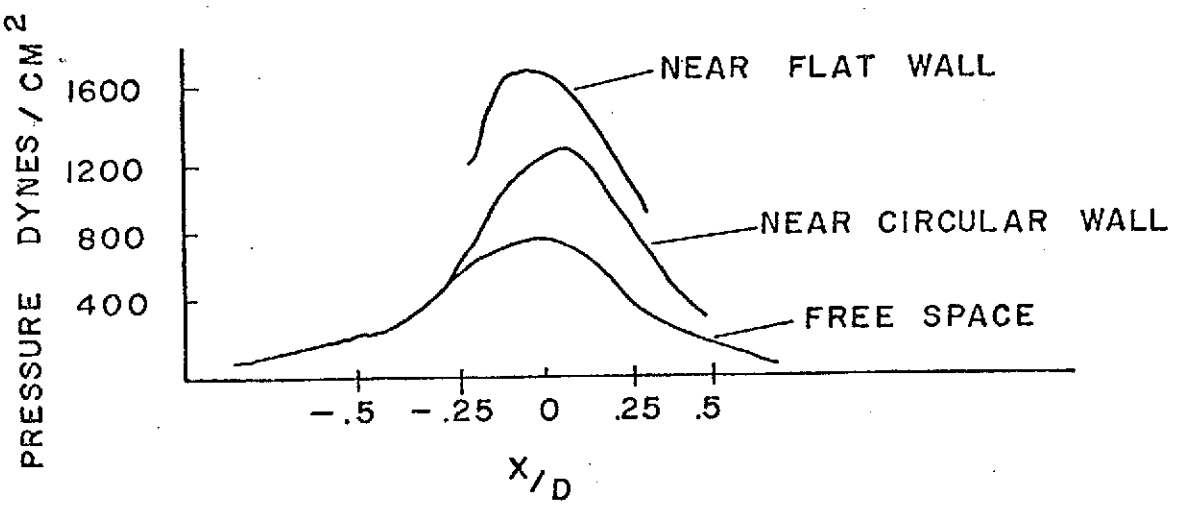

- EFFECT OF REFLECTING SURFACES ON FREE SPACE TIP CLEARANCE NOISE

FIGURE 3.6

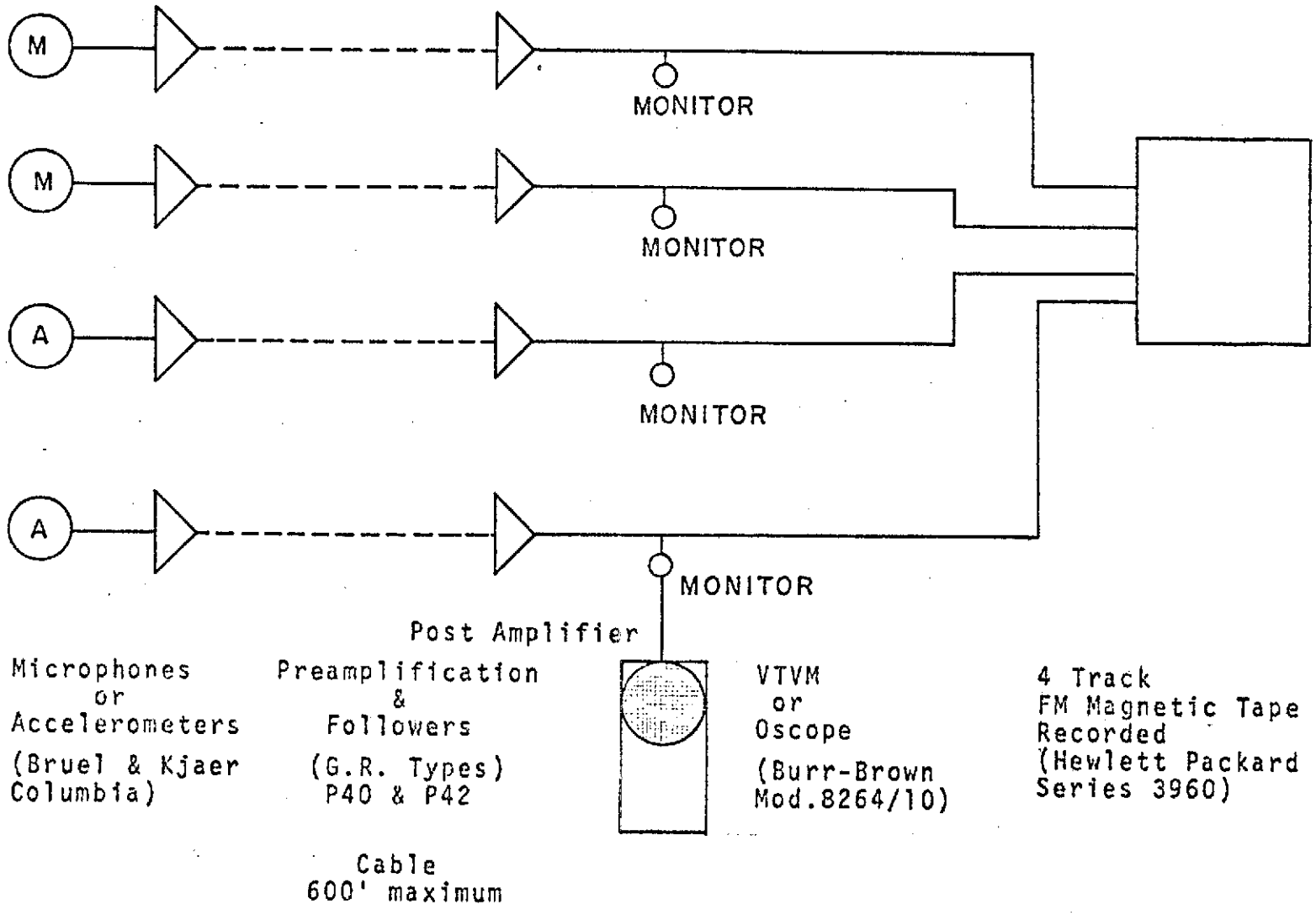

FIGURE 4.1
SCHEMATIC DIAGRAM OF INSTRUMENTATION
FOR MEASUREMENTS INSIDE THE TUNNEL

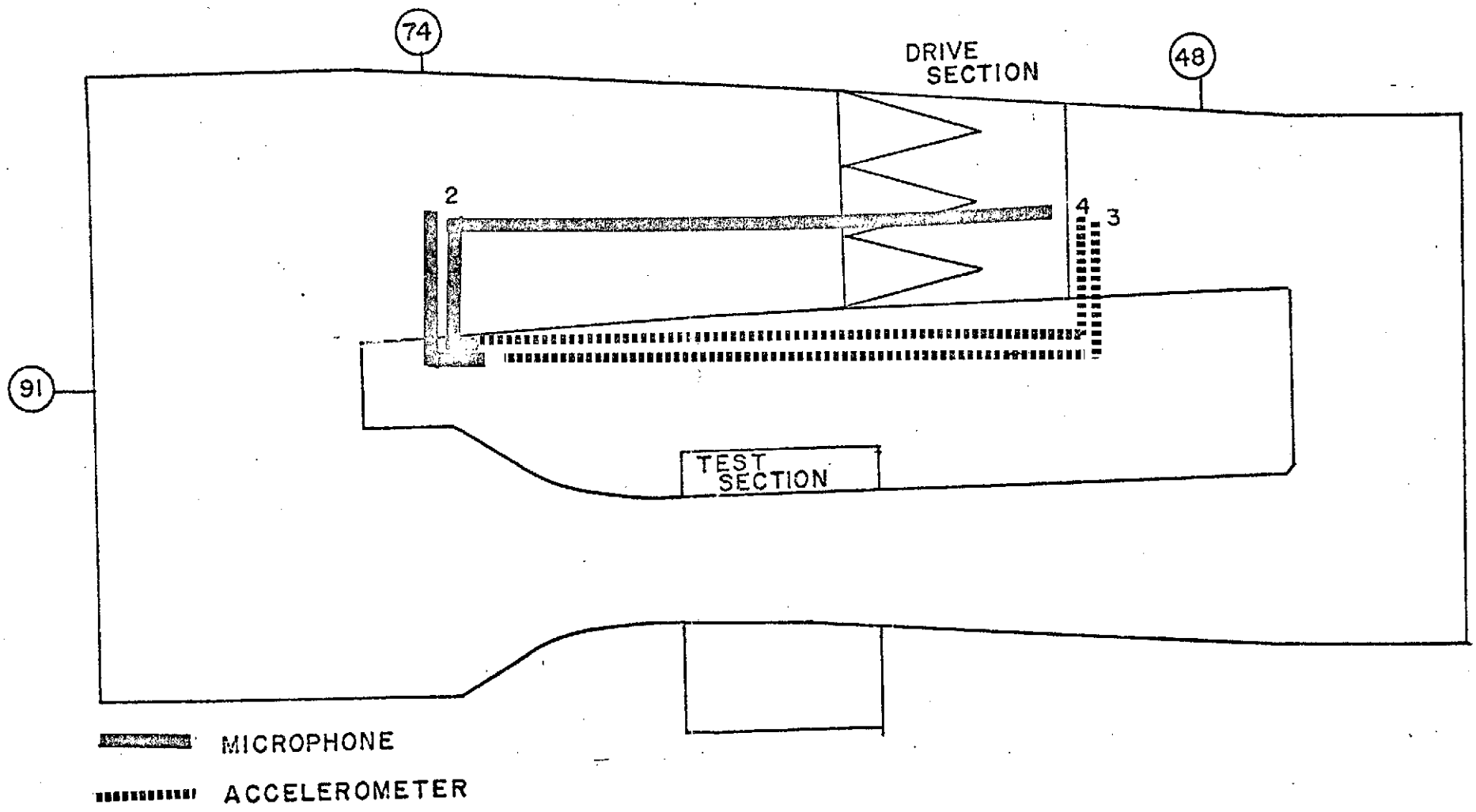

PROBE LOCATIONS
TEST SERIES #1

Figure 4-2

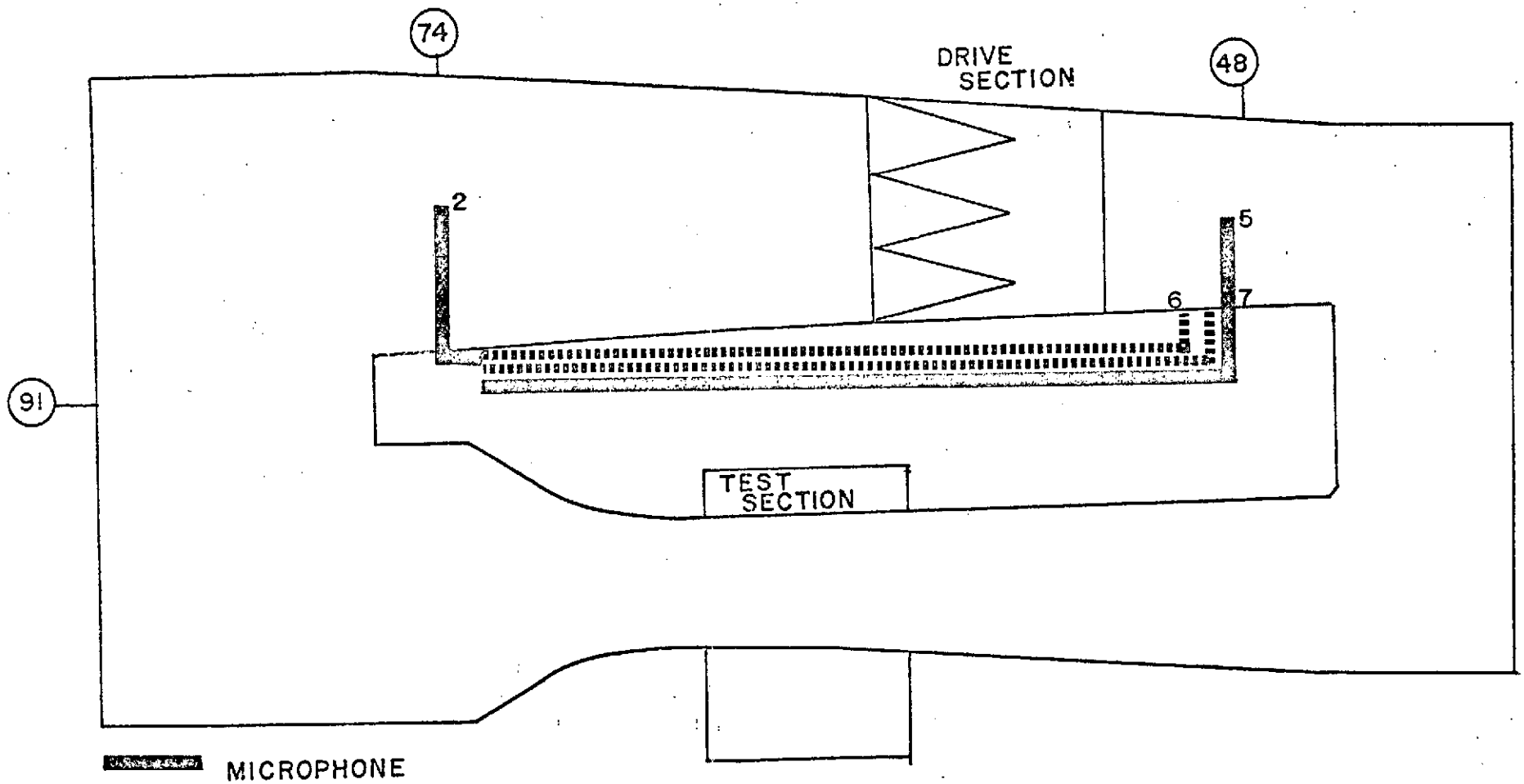

PROBE LOCATIONS
TEST SERIES #2

Figure 4-3

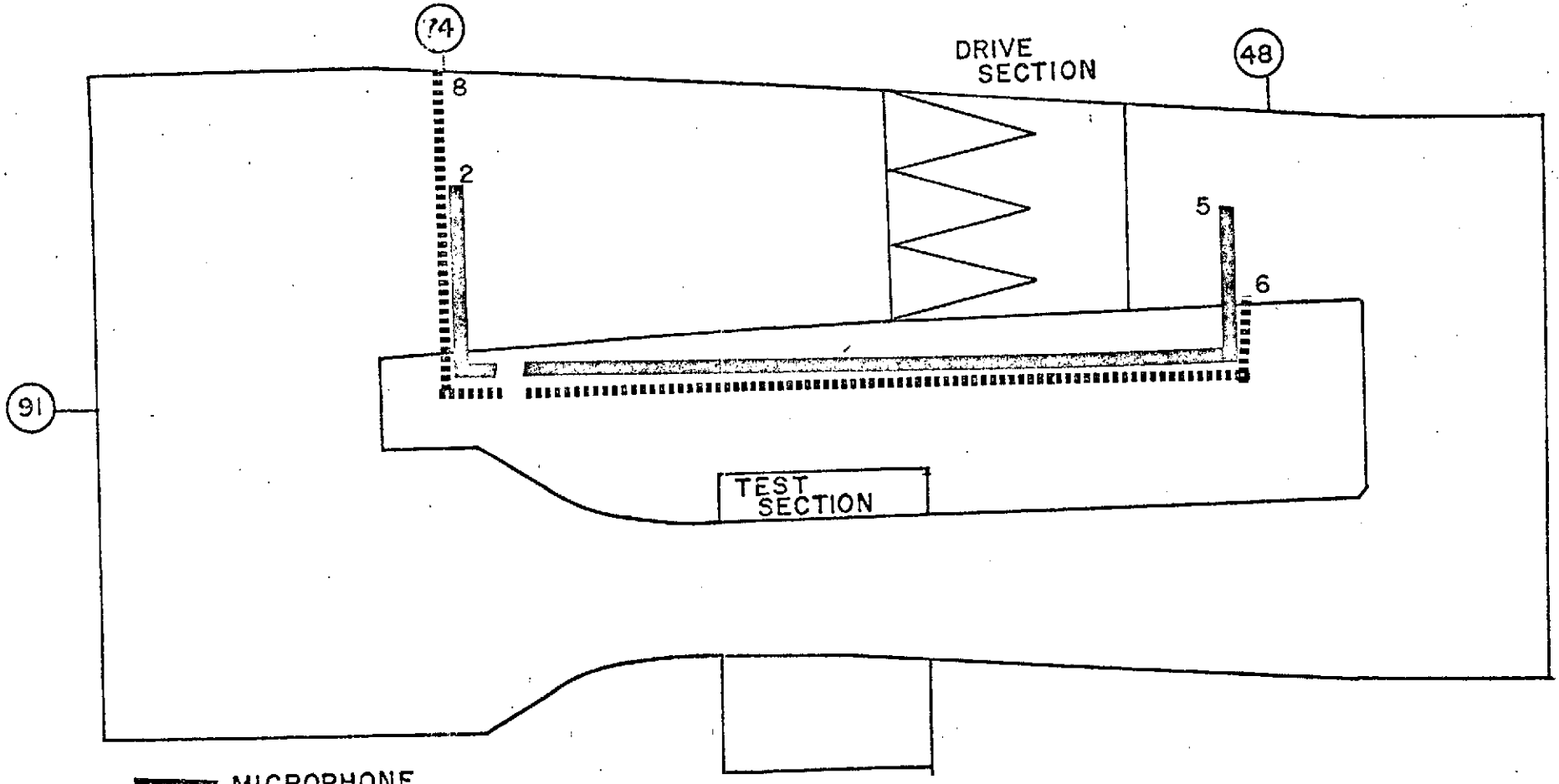

PROBE LOCATIONS
TEST SERIES #3

Figure 4-4

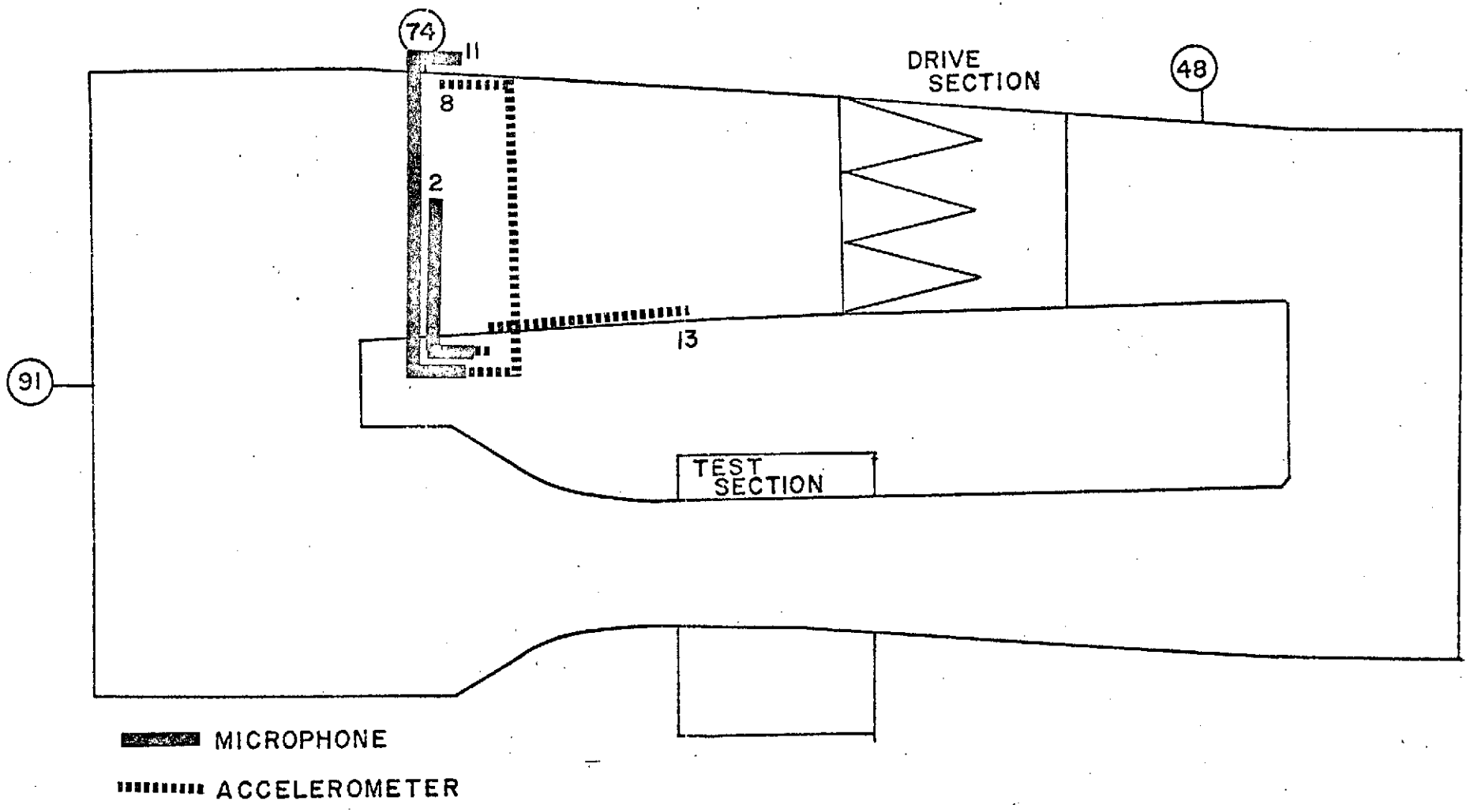

PROBE LOCATIONS
TEST SERIES #4

Figure 4-5

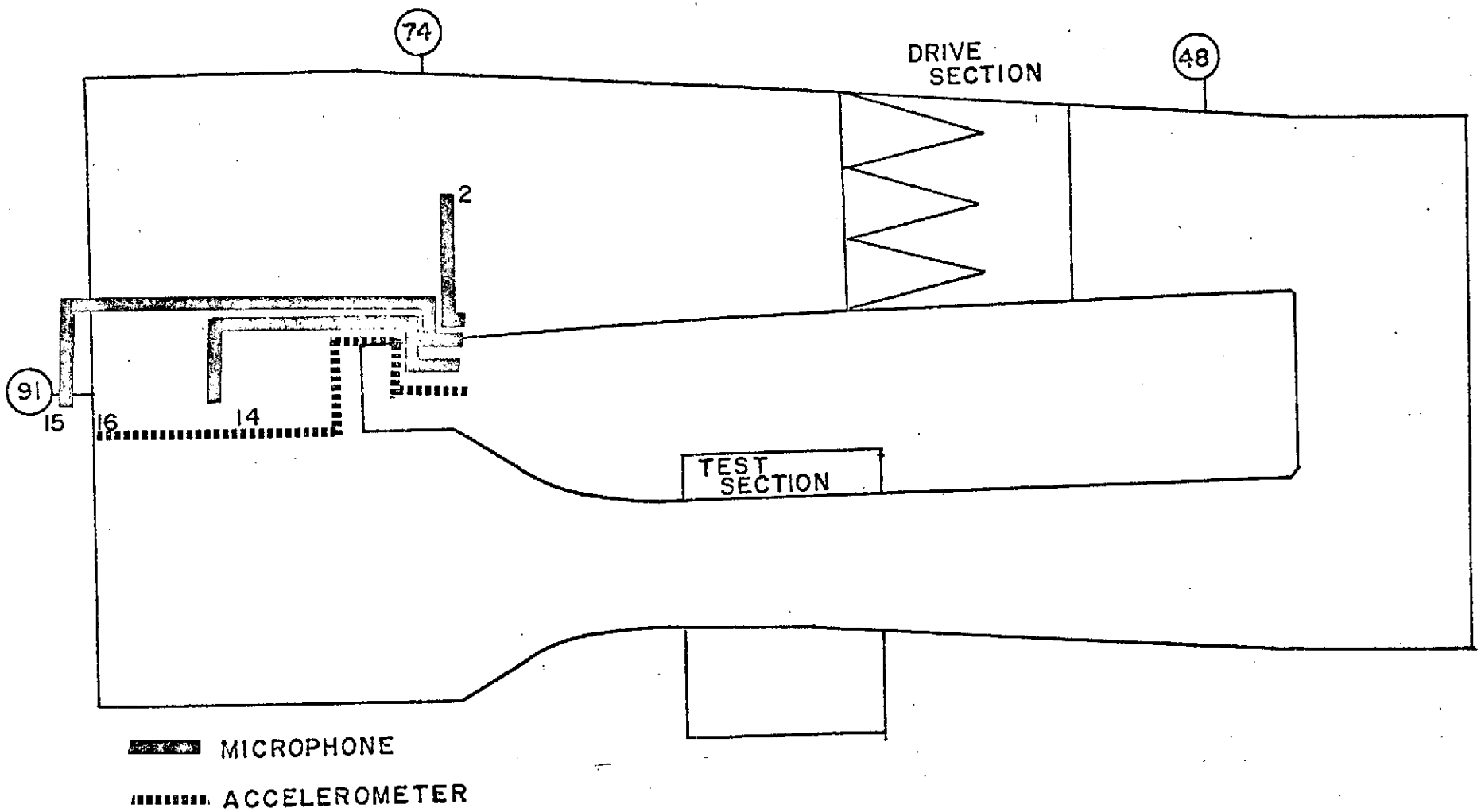

PROBE LOCATIONS
TEST SERIES #5

Figure 4-6

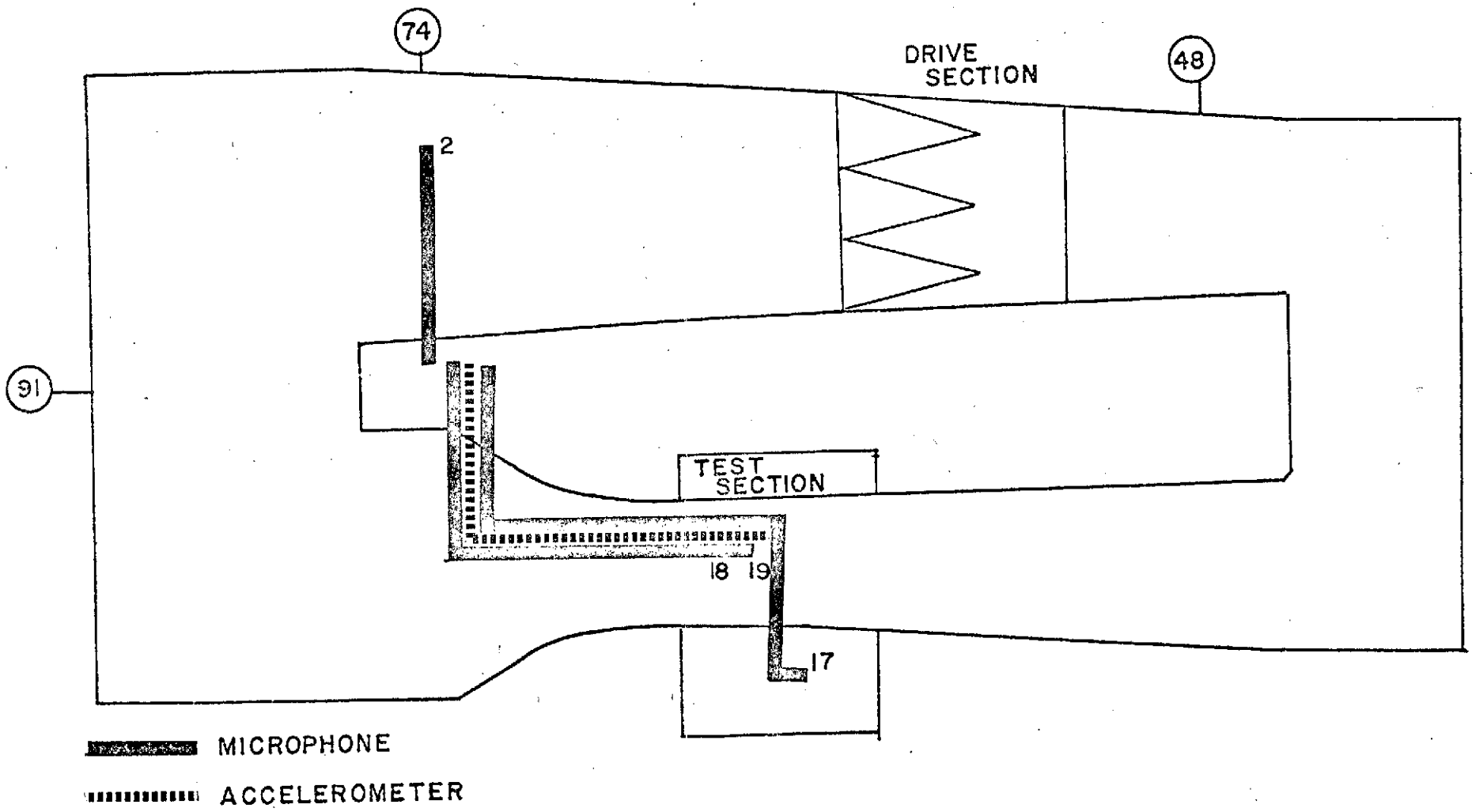

PROBE LOCATIONS
TEST SERIES #6

Figure 4-7

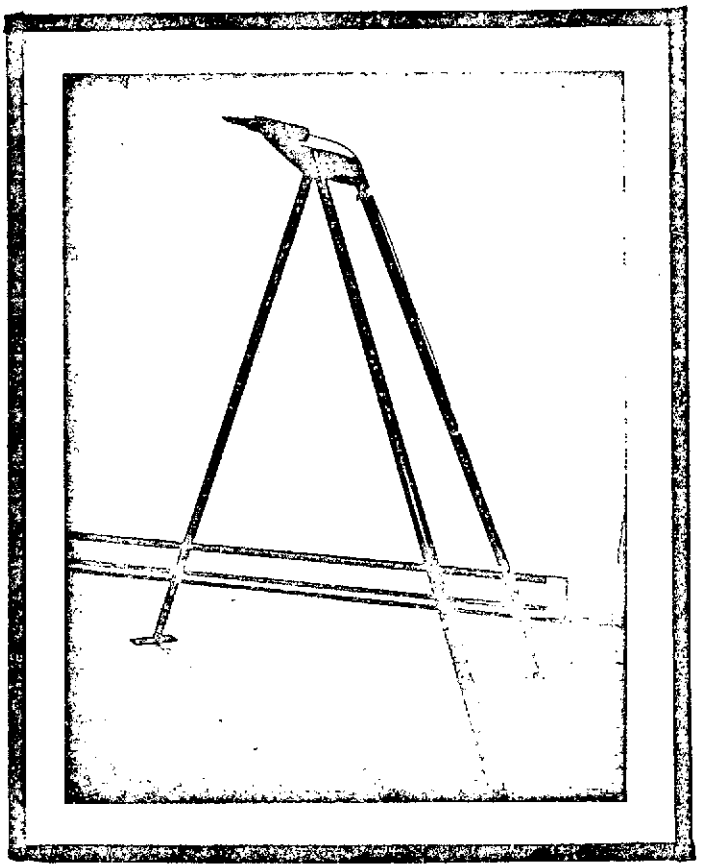

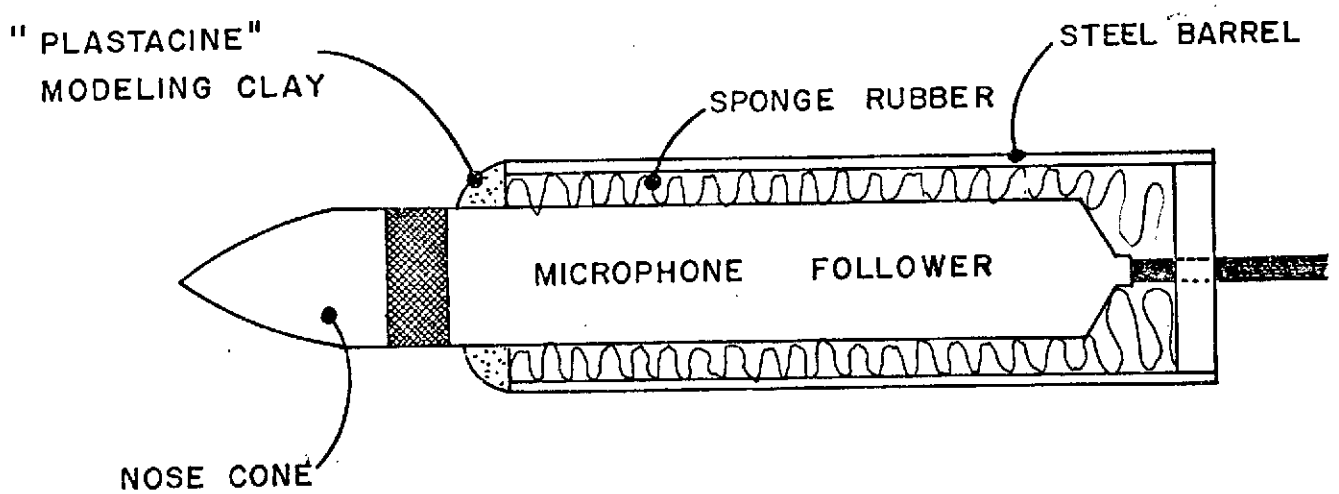
" PLASTACINE"
MODELING CLAY
STEEL BARREL
SPONGE RUBBER
MICROPHONE FOLLOWER
NOSE CONE

Figure 4-8

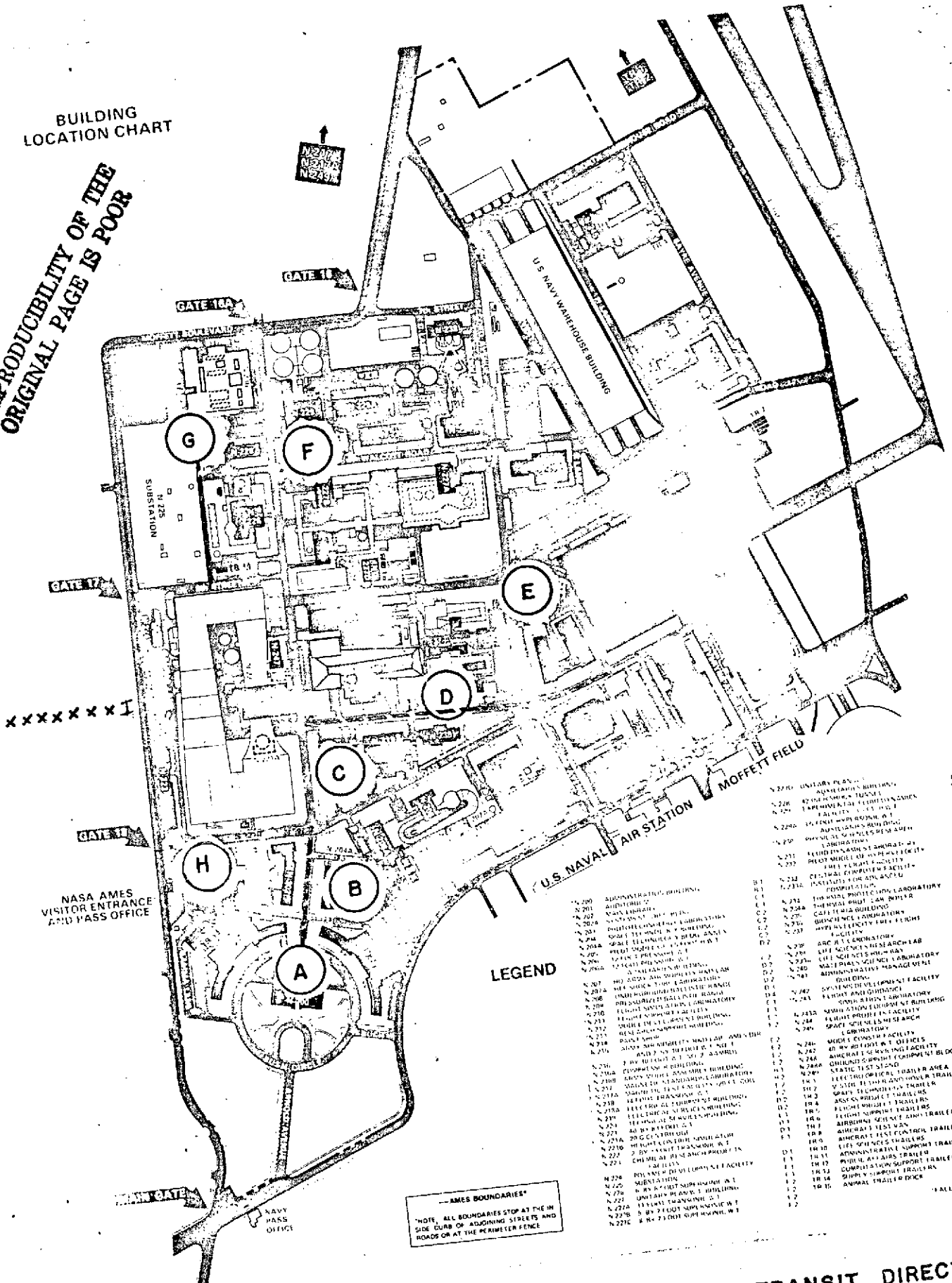

MEASUREMENT LOCATIONS AND TRANSIT DIRECTIONS USED TO OBTAIN NEARFIELD DATA WITH TUNNEL OPERATING

———— TRANSIT DIRECTION

× × × × DISCRETE POSITIONS

FIGURE 4-9

FARFIELD PORTABLE RECORDING SYSTEM

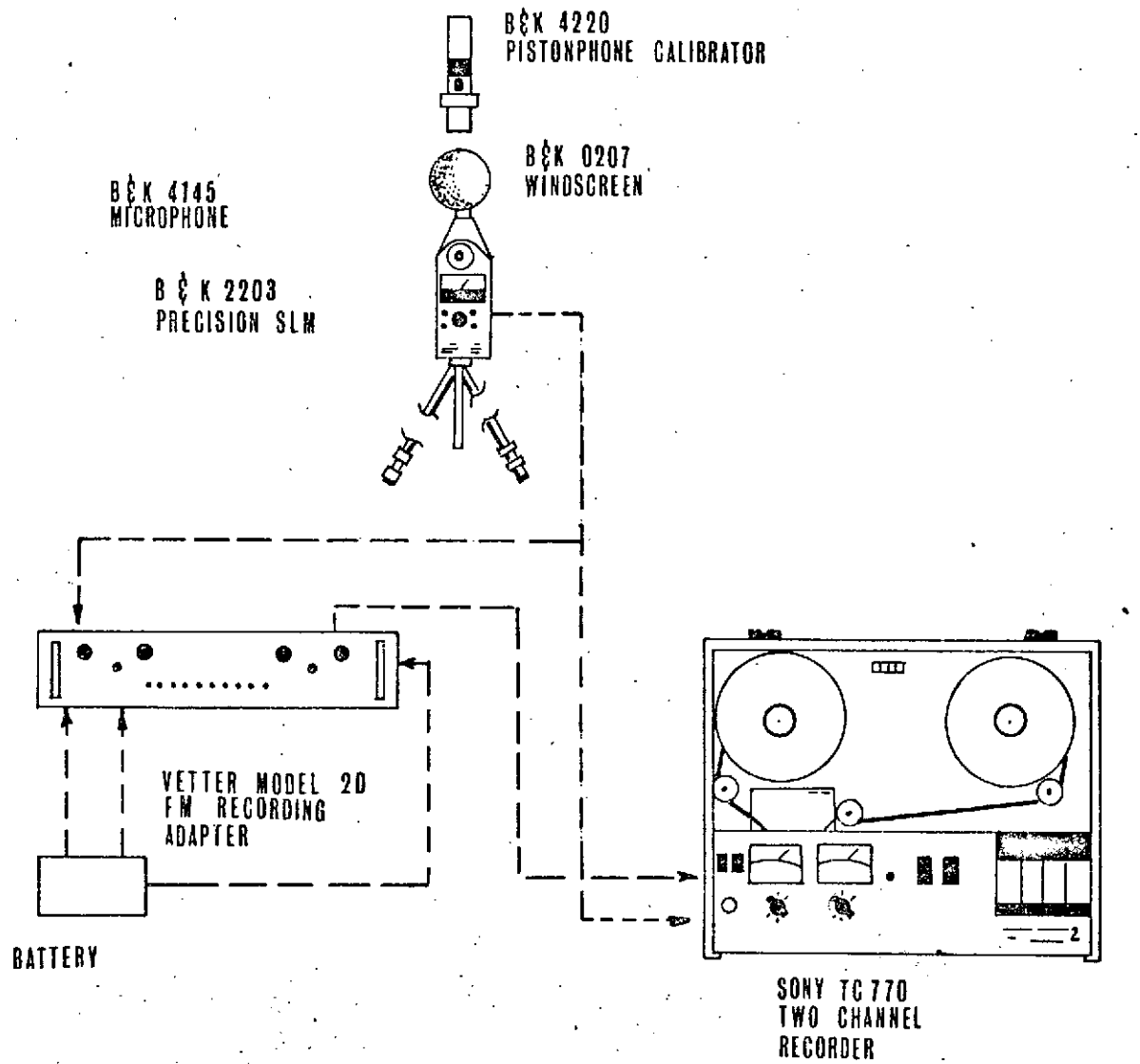

FIGURE 4-10

ROBIN M. TOWNE AND ASSOCIATES *Consultants in Acoustics*

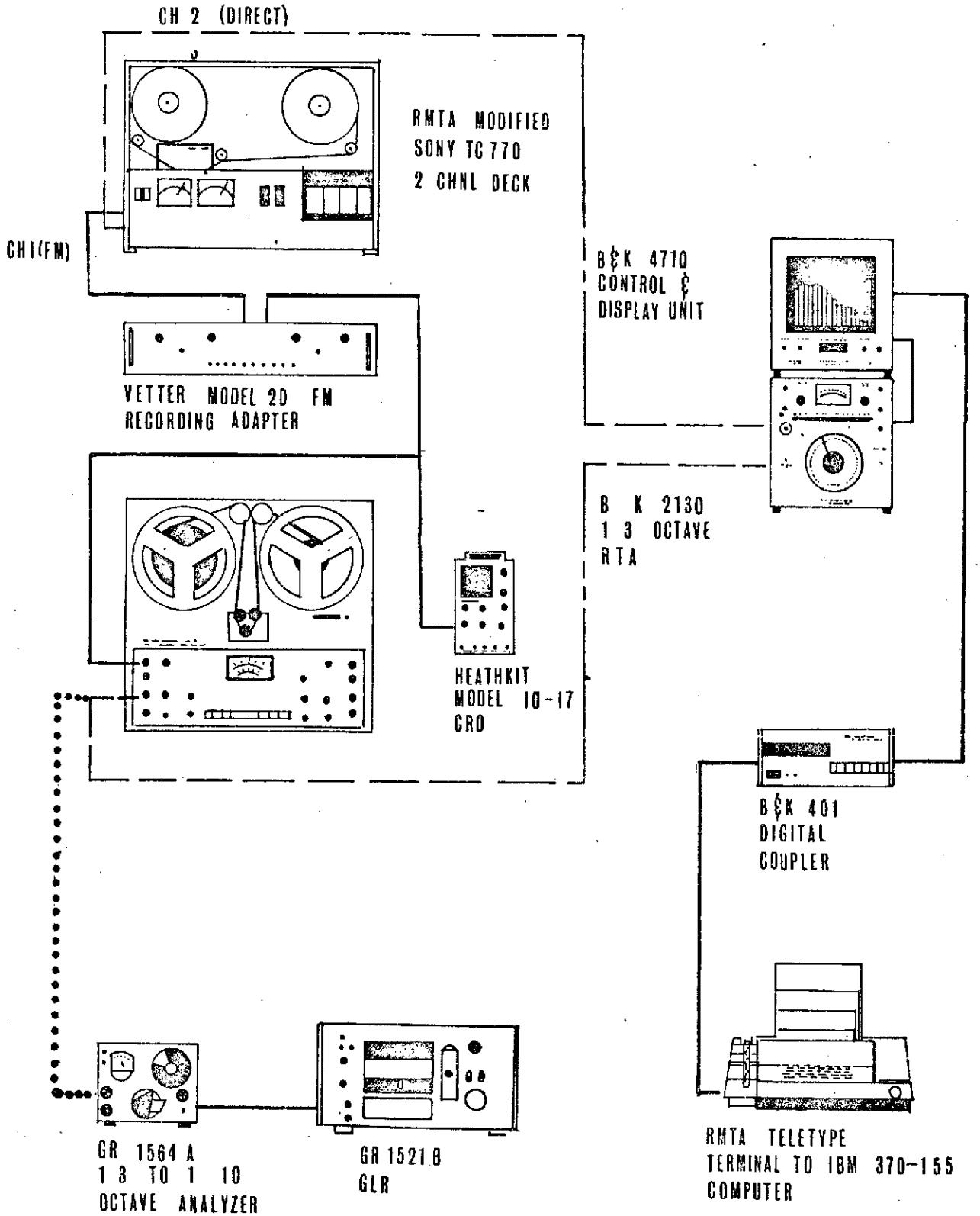

FAR FIELD DATA REDUCTION SYSTEM

ROBIN M. TOWNE AND ASSOCIATES *Consultants in Acoustics*

FIGURE 4-11

FAR FIELD PERMANENT MONITORING STATION

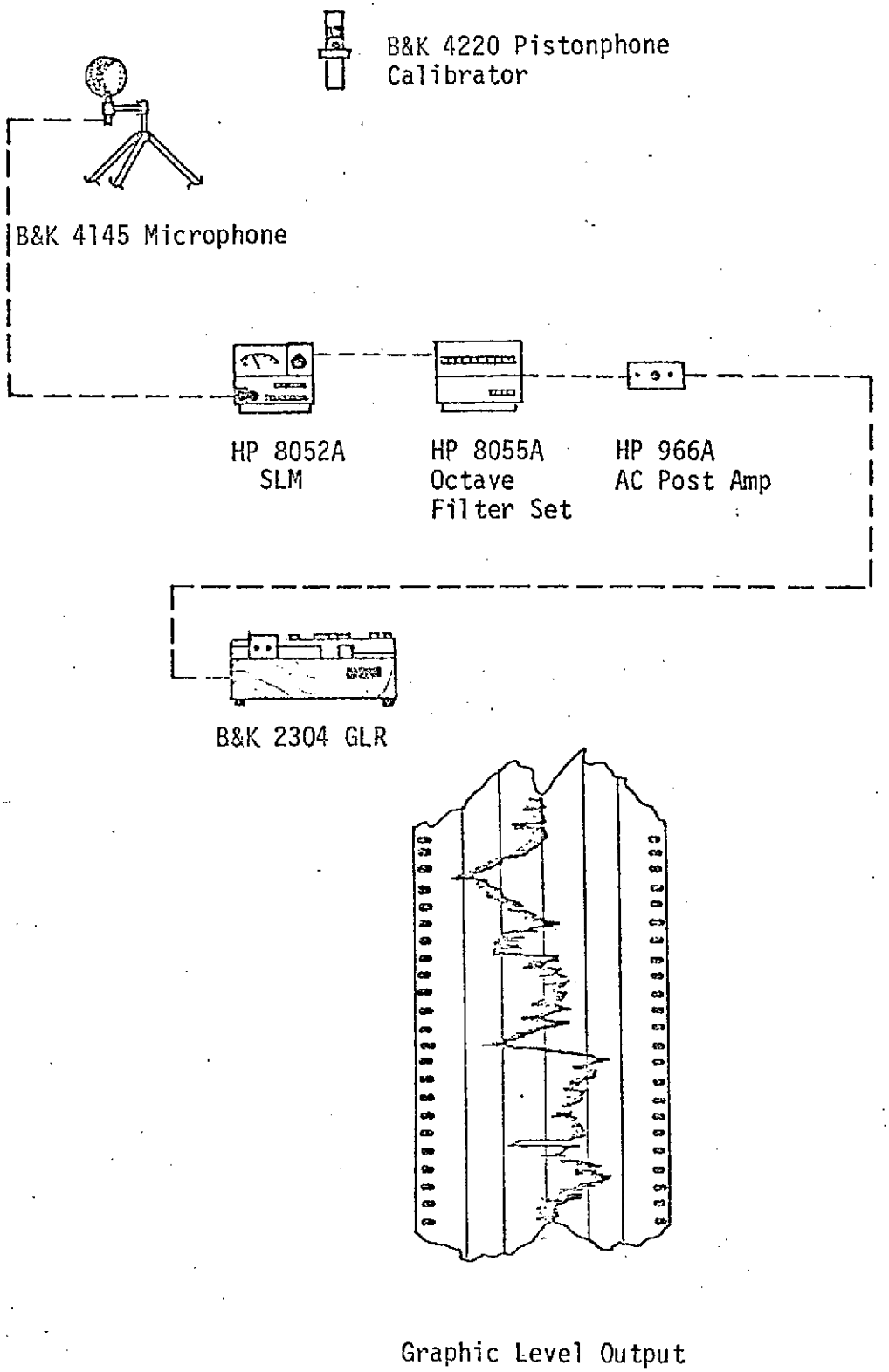

Figure 4-12

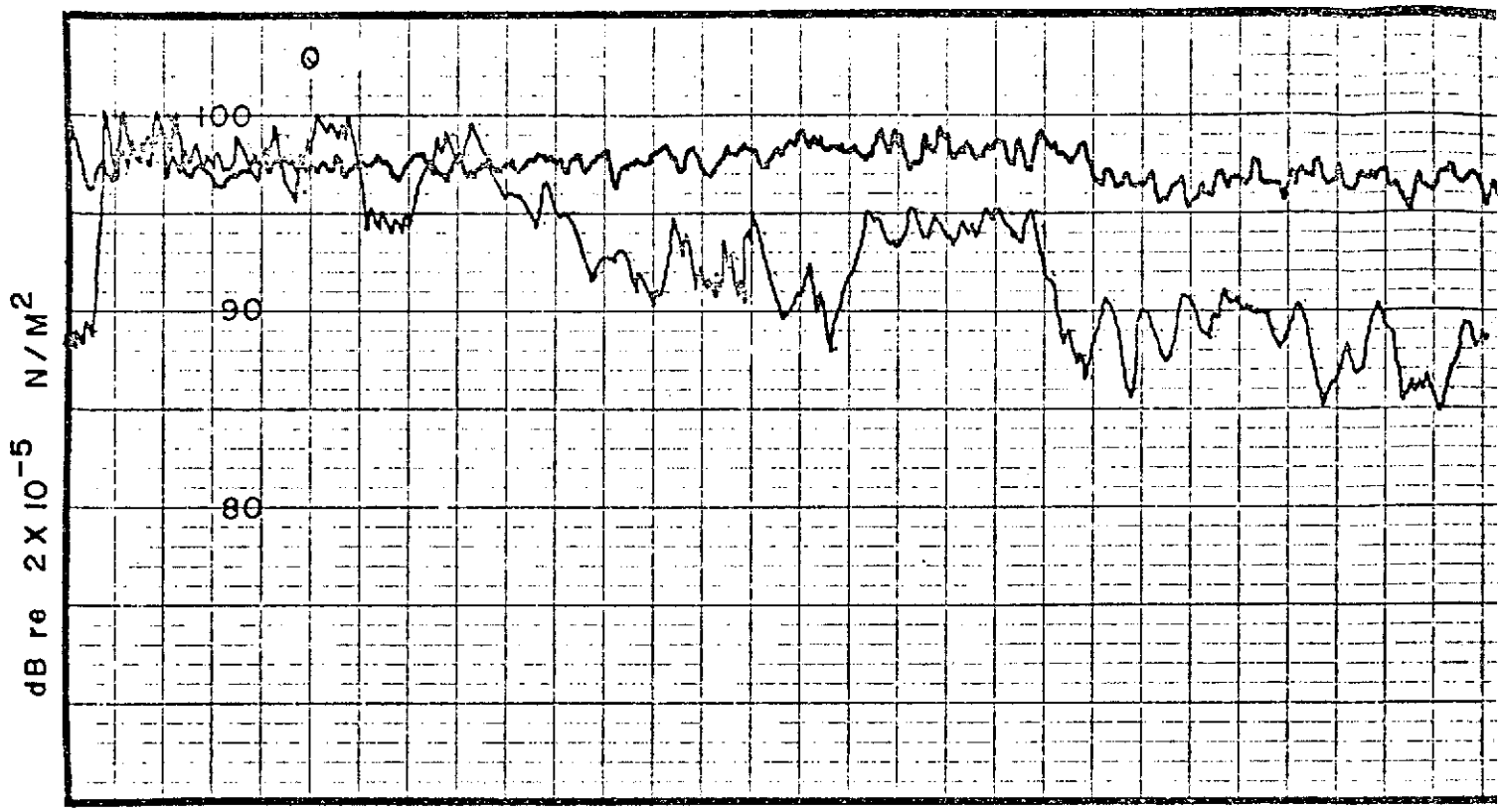

OVERALL LEVELS OF FIXED (
MICROPHONES AT INTERSECTION OF A
UPPER PLOT : MICROPHONE MC
LOWER PLOT : MICROPHONE M
ABCISSA 25 FT/ DIV

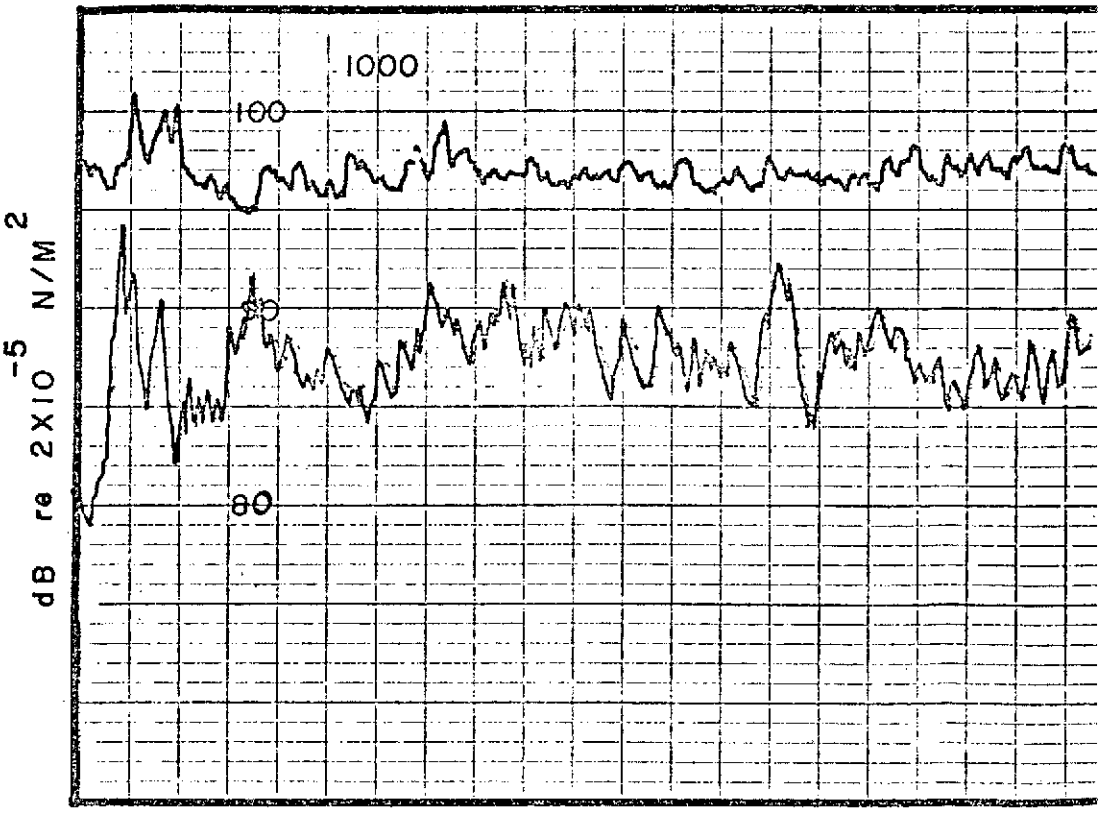

FIGURE 4·13

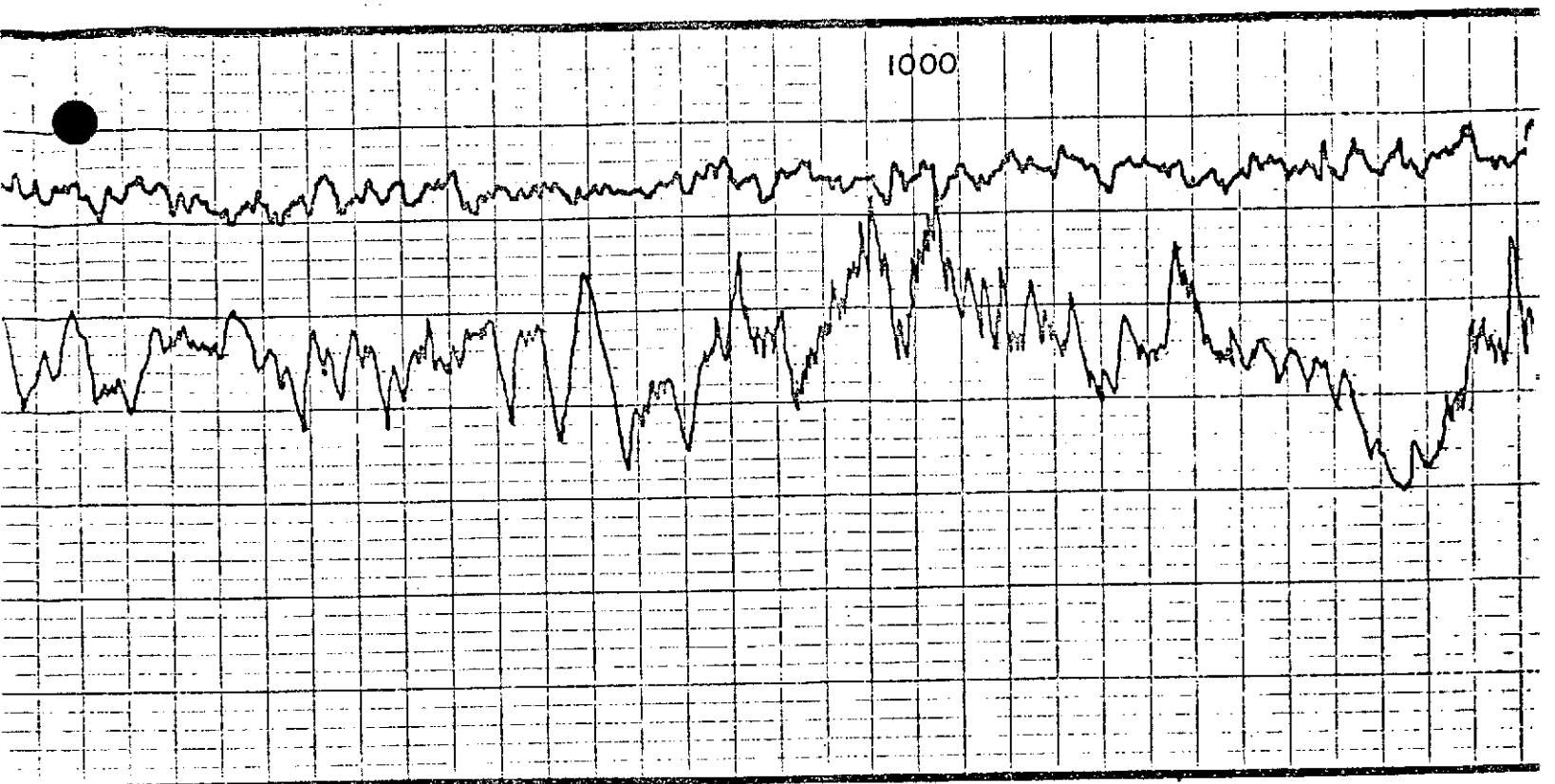

FIXED (BLK) & MOVING (RED)
TION OF ARNOLD & DURAND
PHONE MOVING EAST
PHONE MOVING WEST

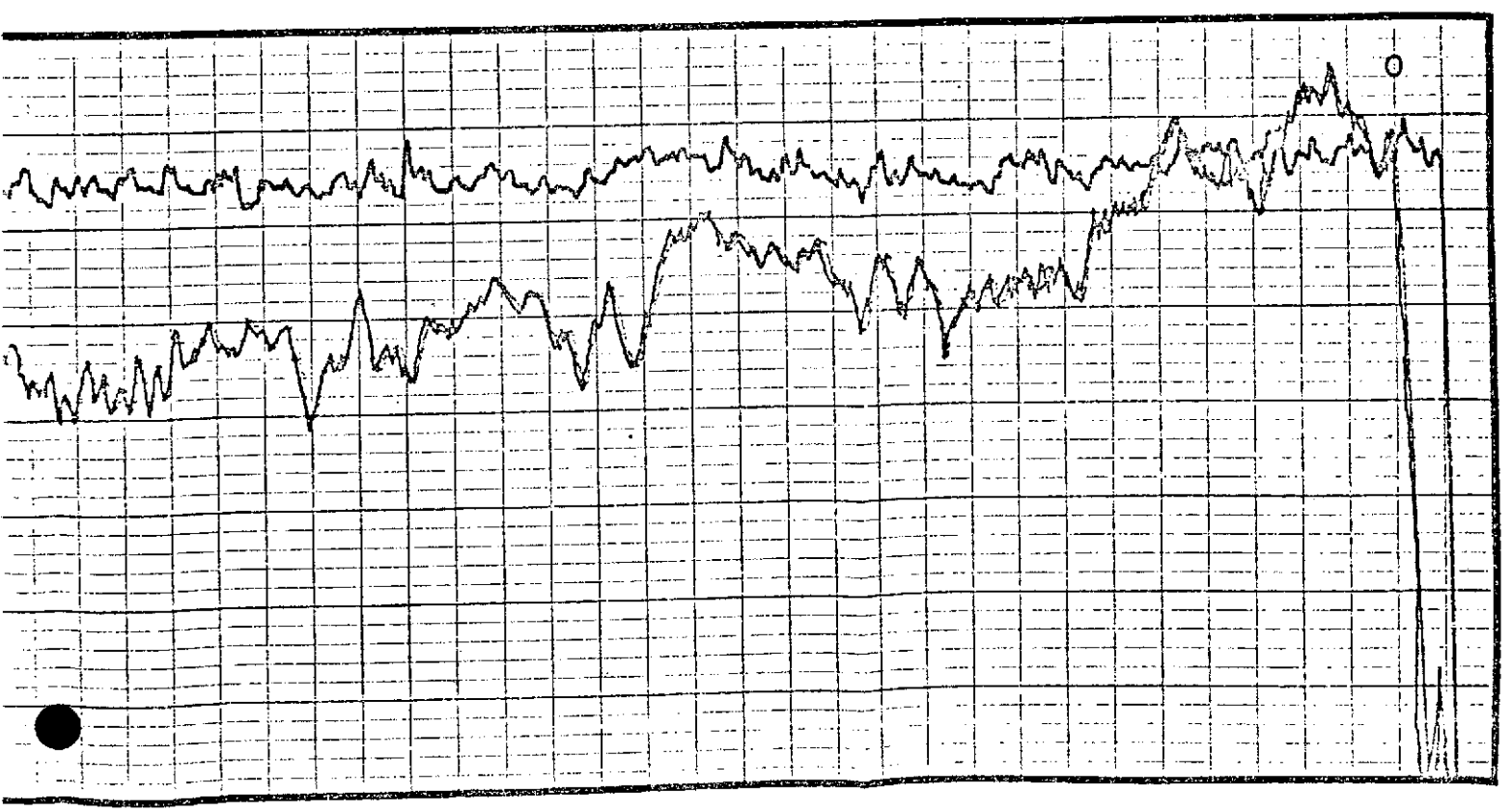

E 4·13

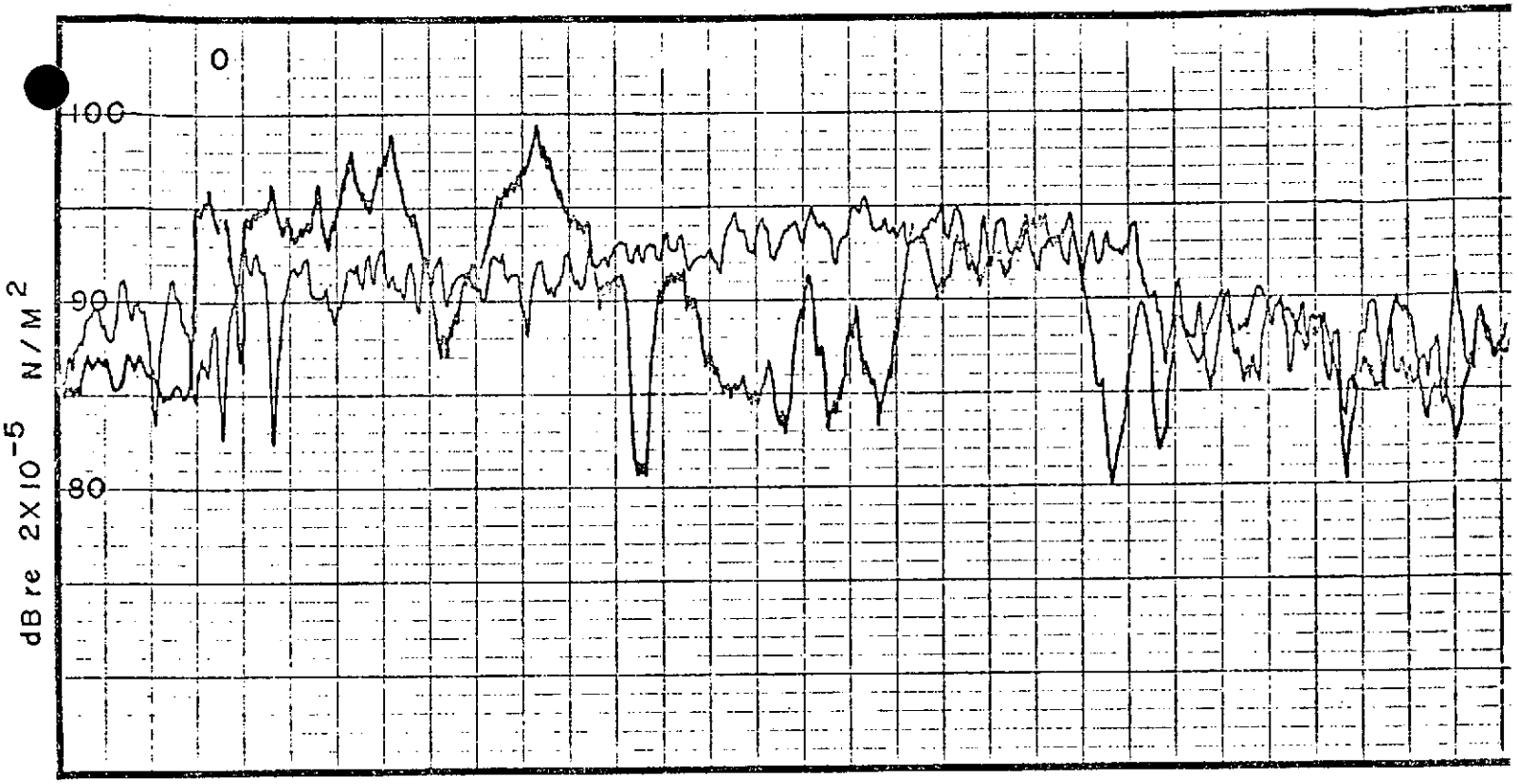

1/10 OCTAVE LEVELS CENTERED AT 26Hz OF
FIXED MICROPHONE AT INTERSECTI
UPPER PLOT: MICROPHONE
LOWER PLOT: MICROPHON
ABCISSA 25 FT/DIV

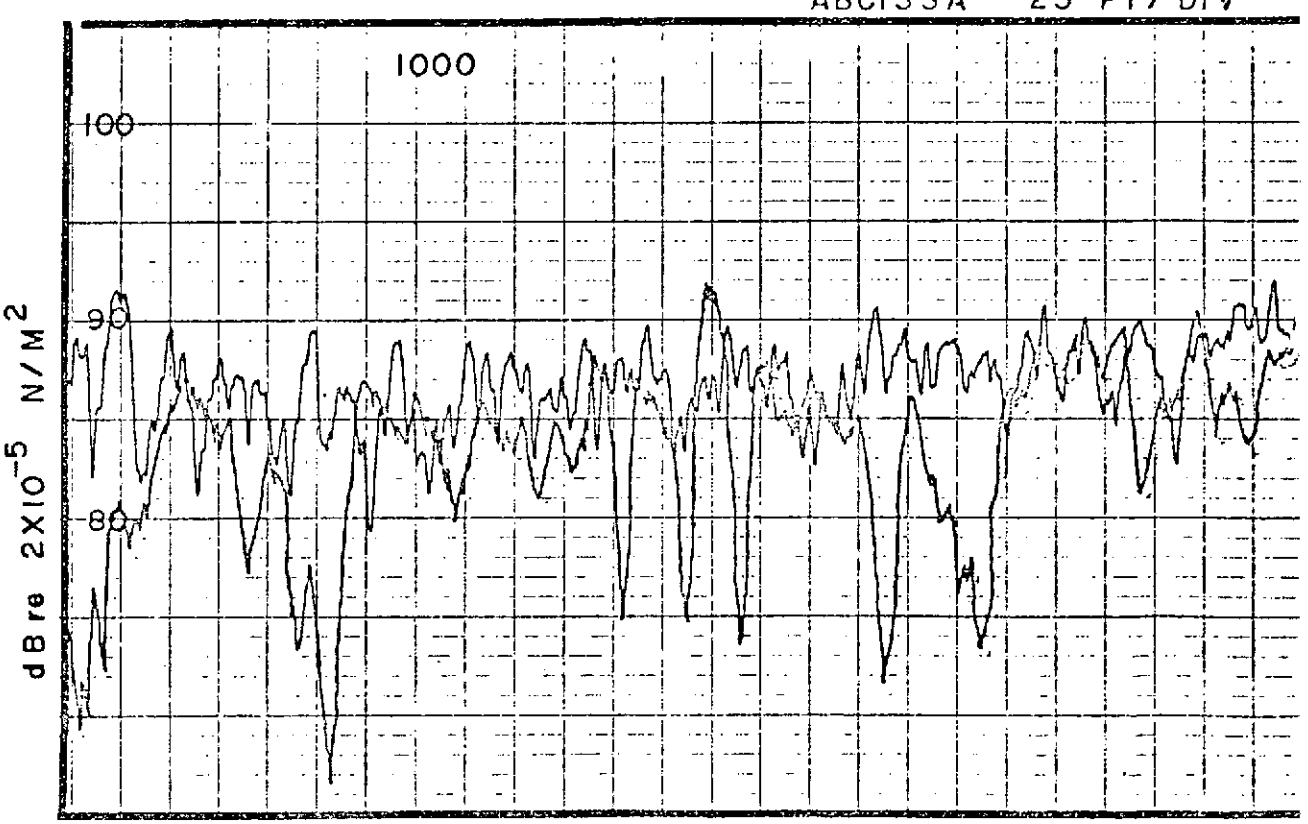

FIGURE 4-14

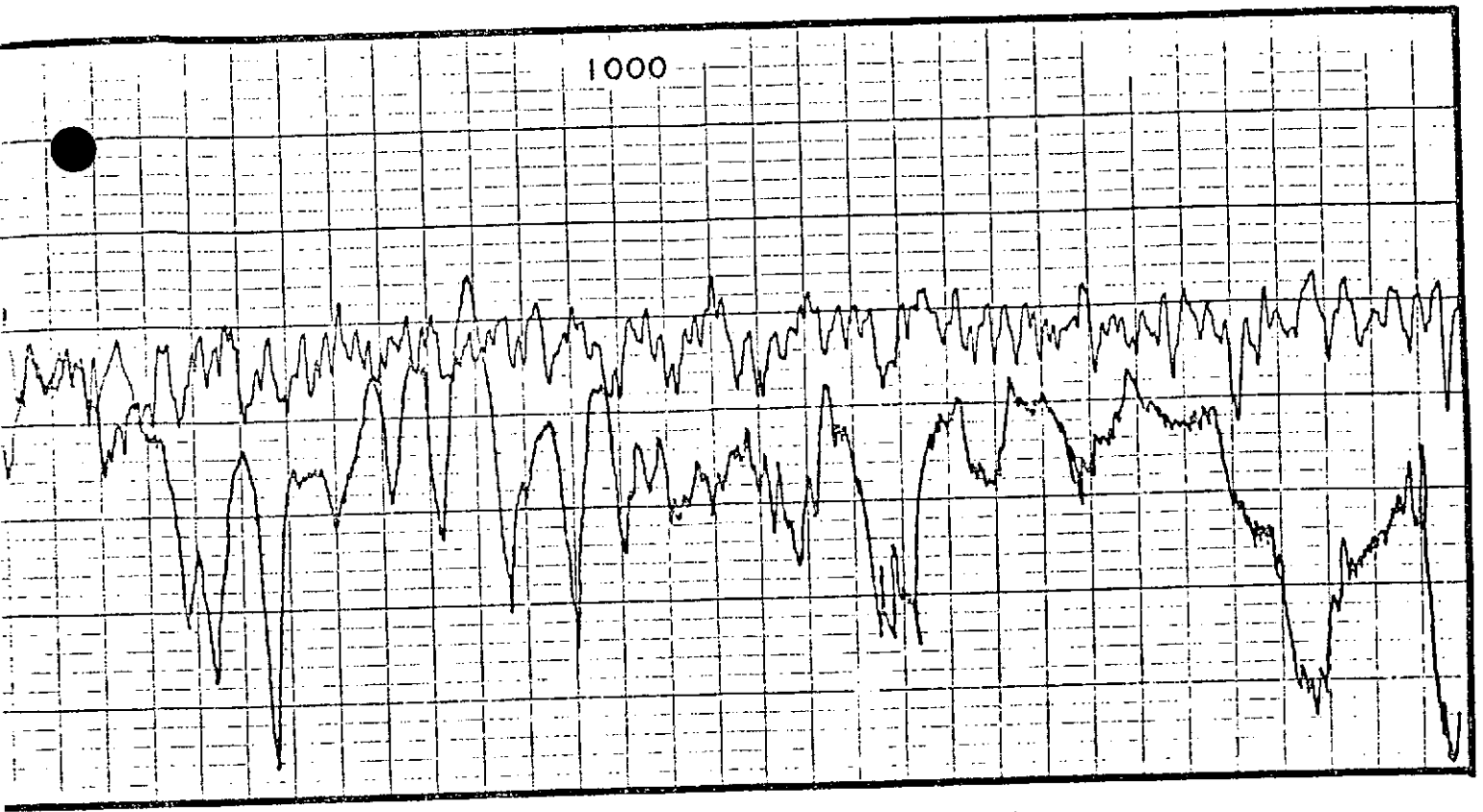

F FIXED (BLK) AND MOVING (RED) MICROPHONES
CTION OF ARNOLD AND DURAND
HOME MOVING EAST
HOME MOVING WEST

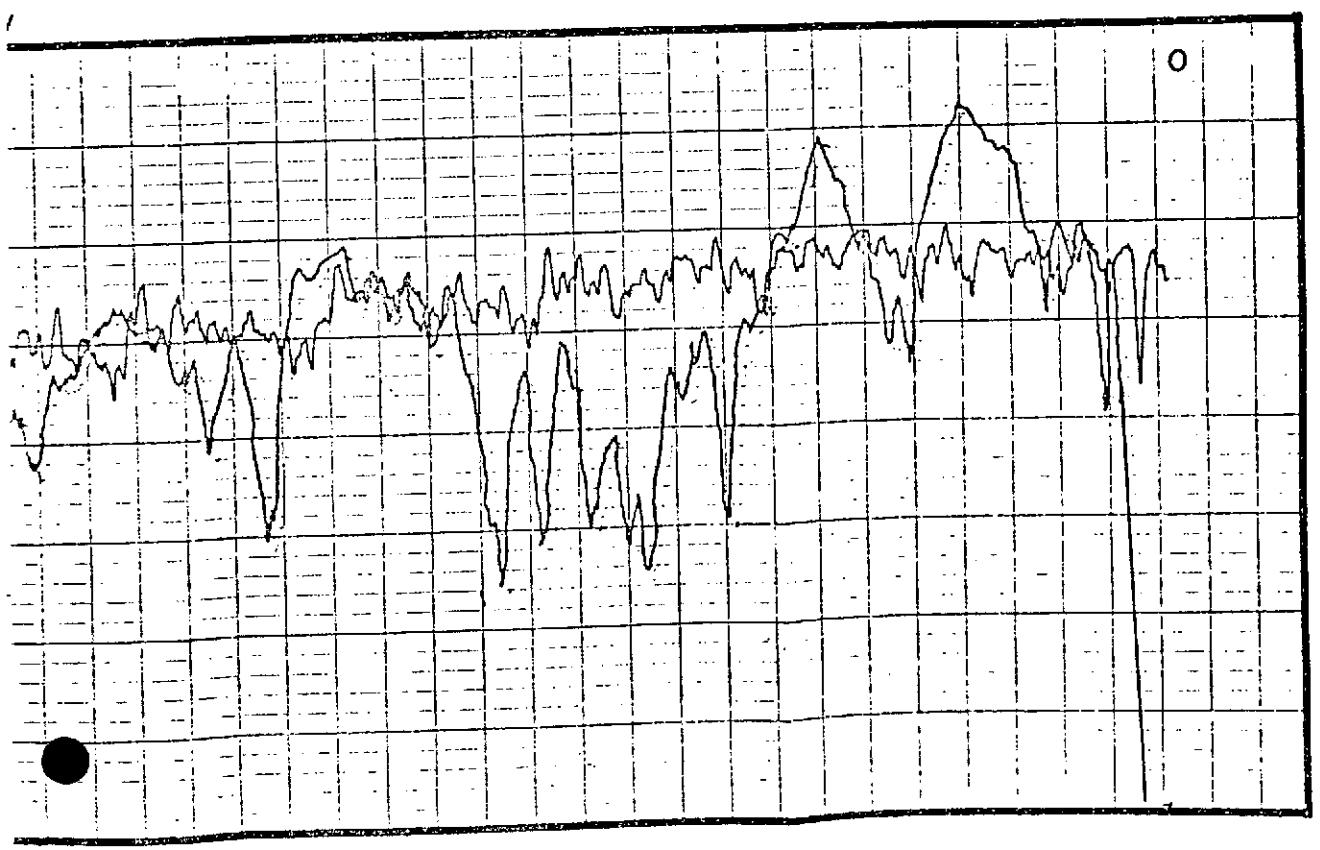

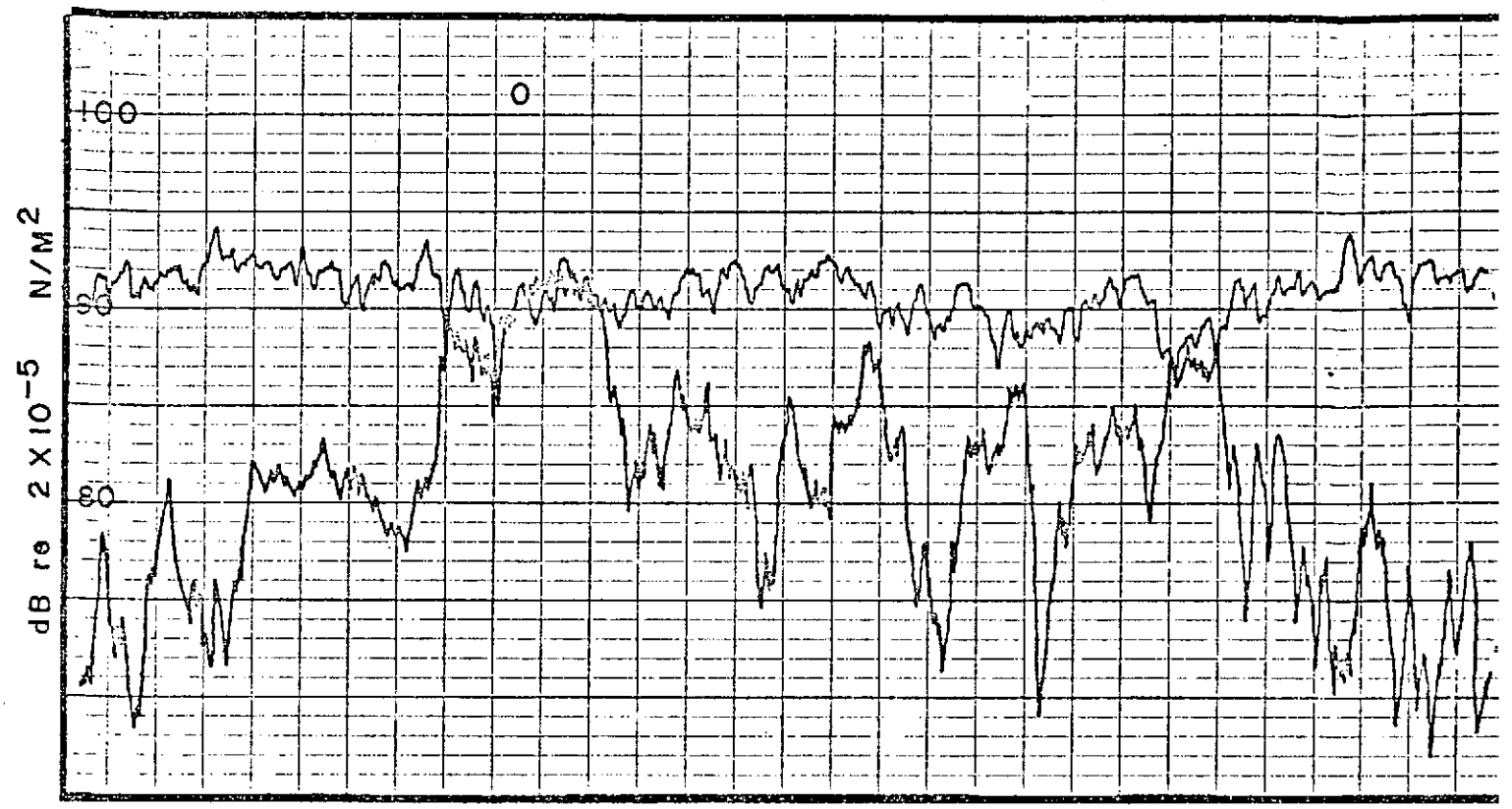

1/10 OCTAVE LEVELS CENTERED AT 80 Hz
FIXED MICROPHONE AT INTERSECTION
UPPER PLOT : MICROPH
LOWER PLOT : MICROPH
ABCISSA 25 FT/DIV

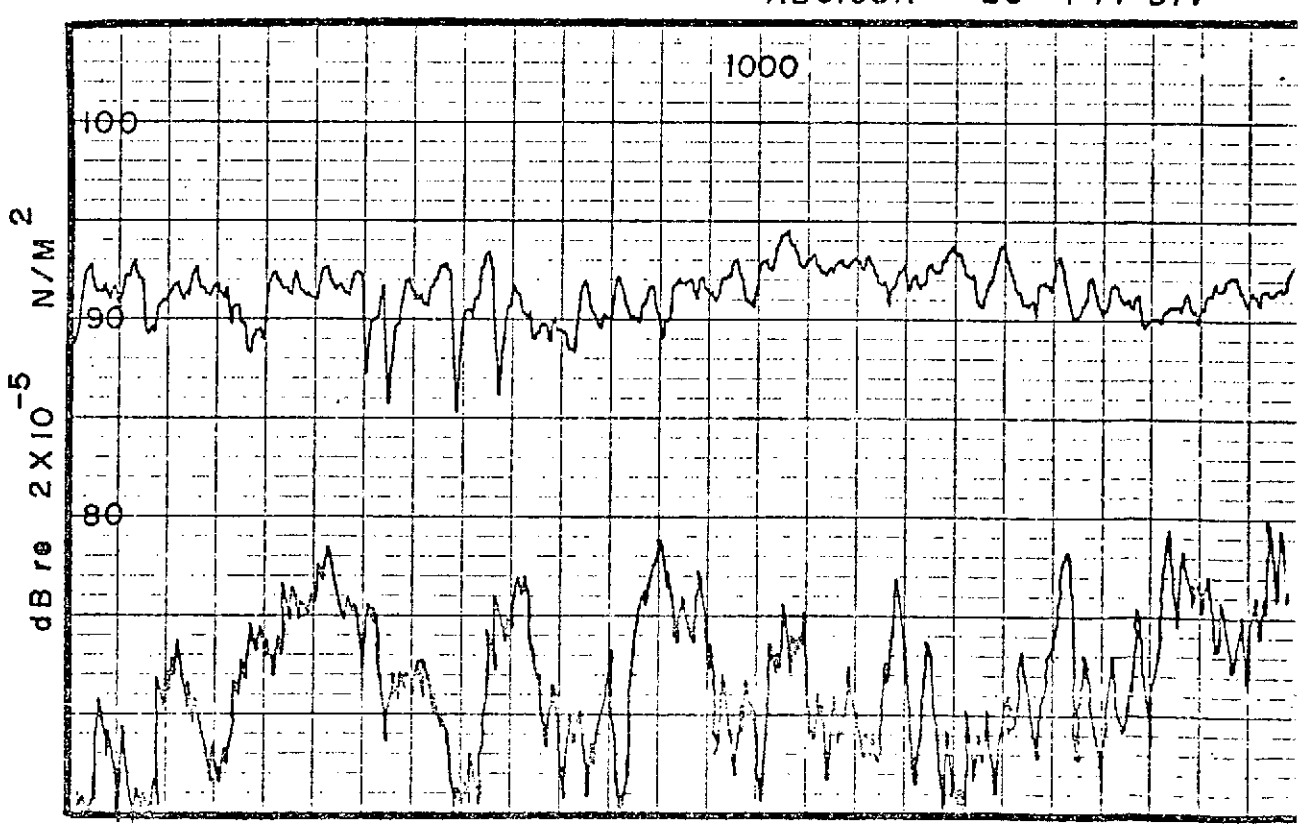

FIGURE 4·15

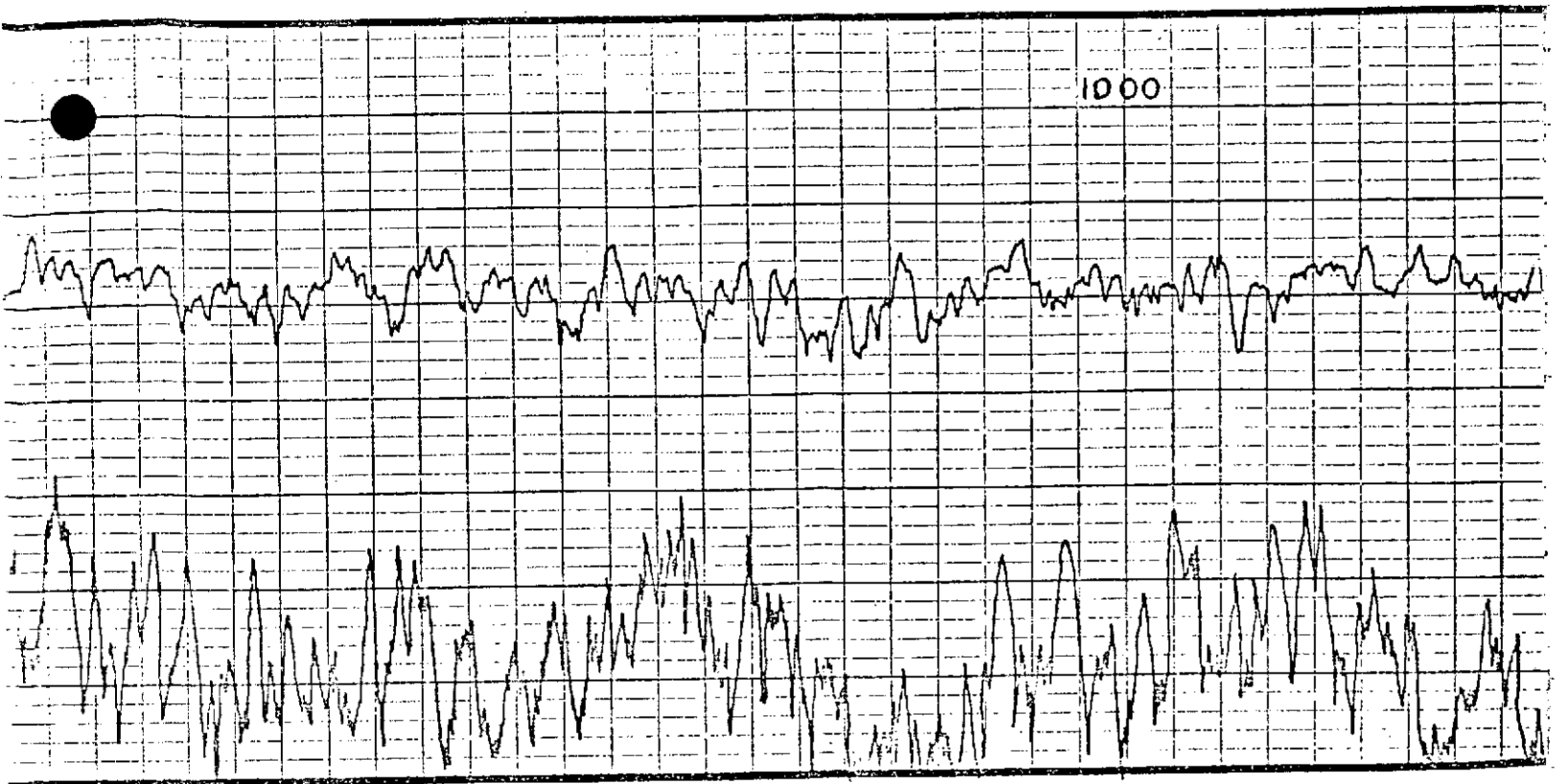

80 Hz OF FIXED (BLK) AND MOVING (RED) MICROPHONES

SECTION OF ARNOLD AND DURAND

ROPHONE MOVING EAST
MICROPHONE MOVING WEST

/ DIV

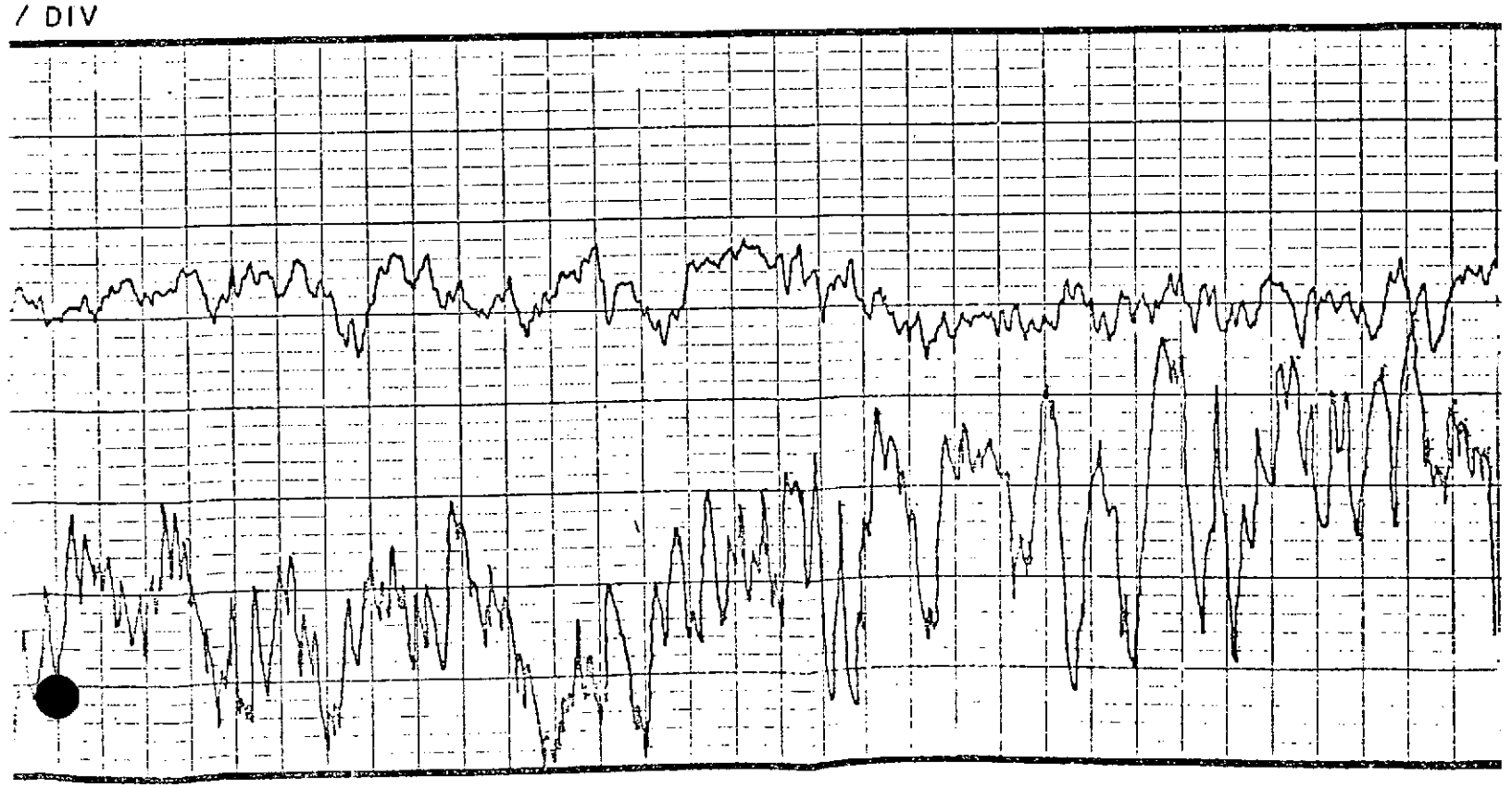

RE 4·15

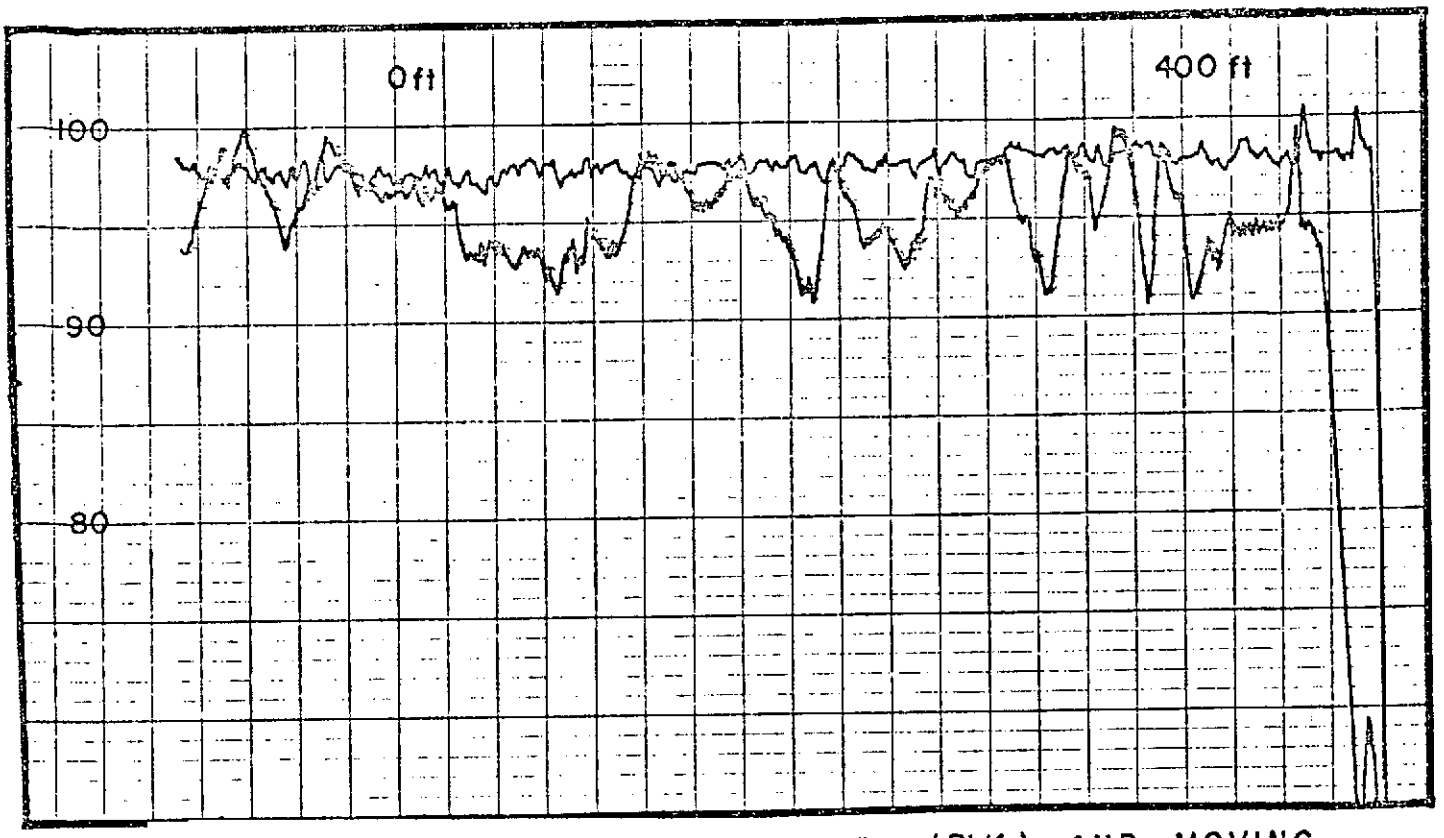

OVERALL LEVELS OF FIXED (BLK) AND MOVING (RED) MICROPHONES.

FIXED MICROPHONE AT INTESECTION OF ARNOLD AND KING.
UPPER PLOT MICROPHONE MOVING SOUTH. ABCISSA 25 FT / DIV
LOWER PLOT MICROPHONE MOVING NORTH ABCISSA 28 FT / DIV.

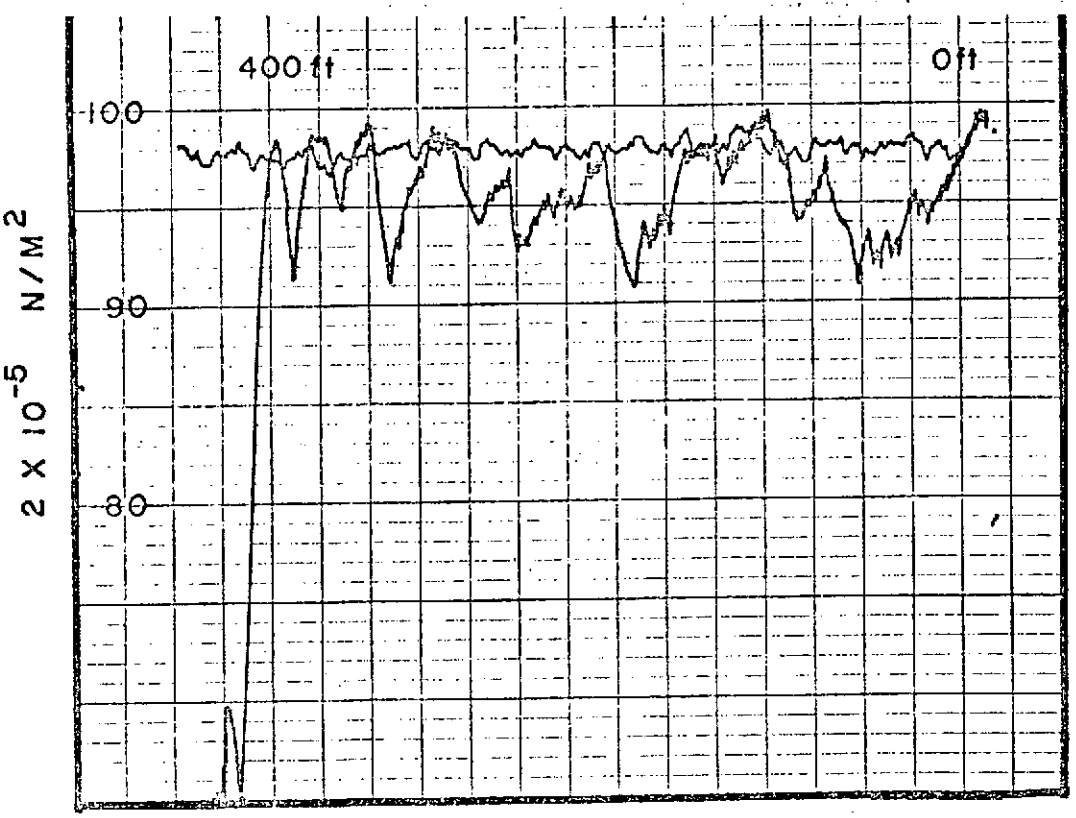

FIGURE 4·16

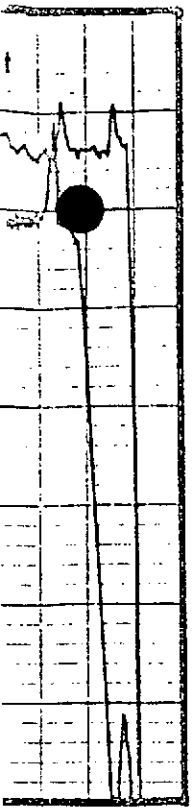

ING

ND

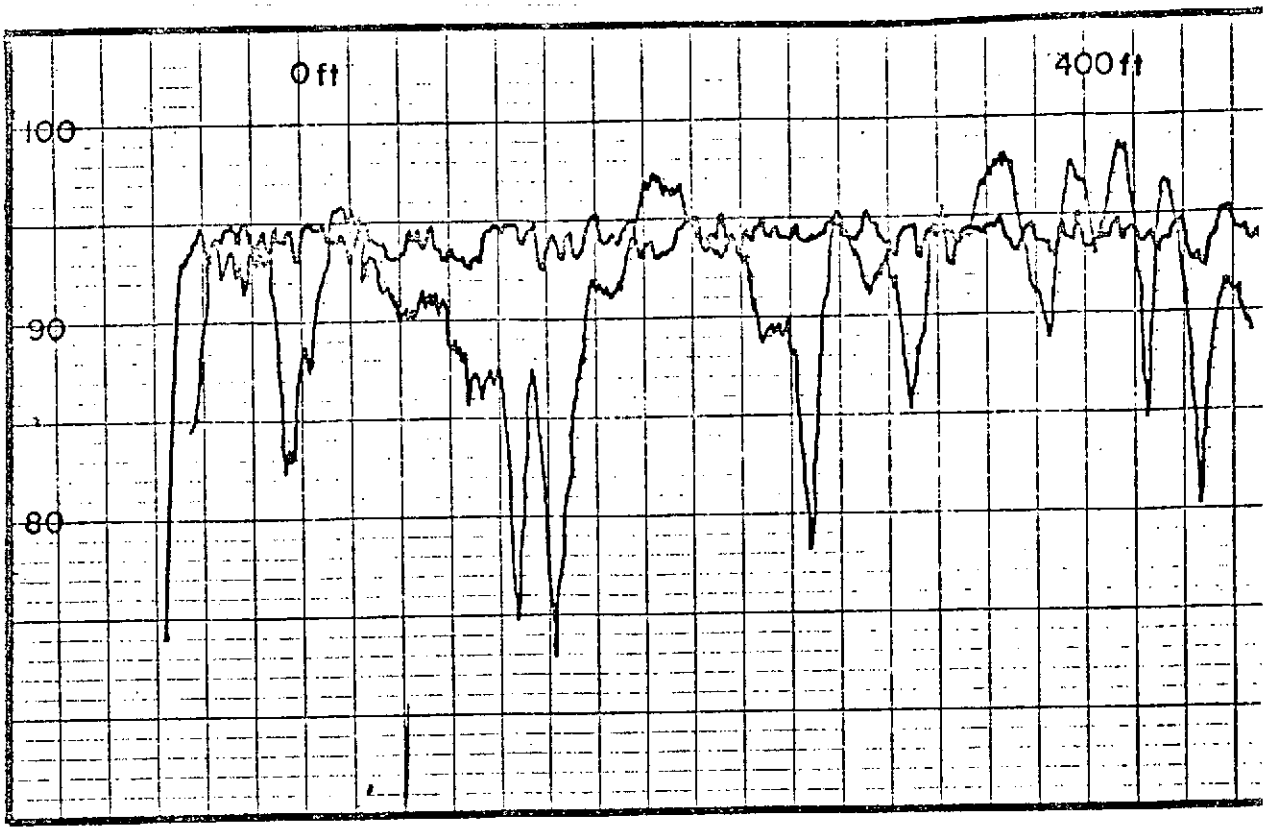

1/10 OCTAVE LEVELS CENTERED AT 26 Hz OF FIXED MICROPHONES

FIXED MICROPHONE AT INTERSECTION OF ARNOLD AND KING

UPPER PLOT MICROPHONE MOVING SOUTH. ABCISSA 25 FT / DIV

LOWER PLOT MICROPHONE MOVING NORTH ABCISSA 28 FT / DIV

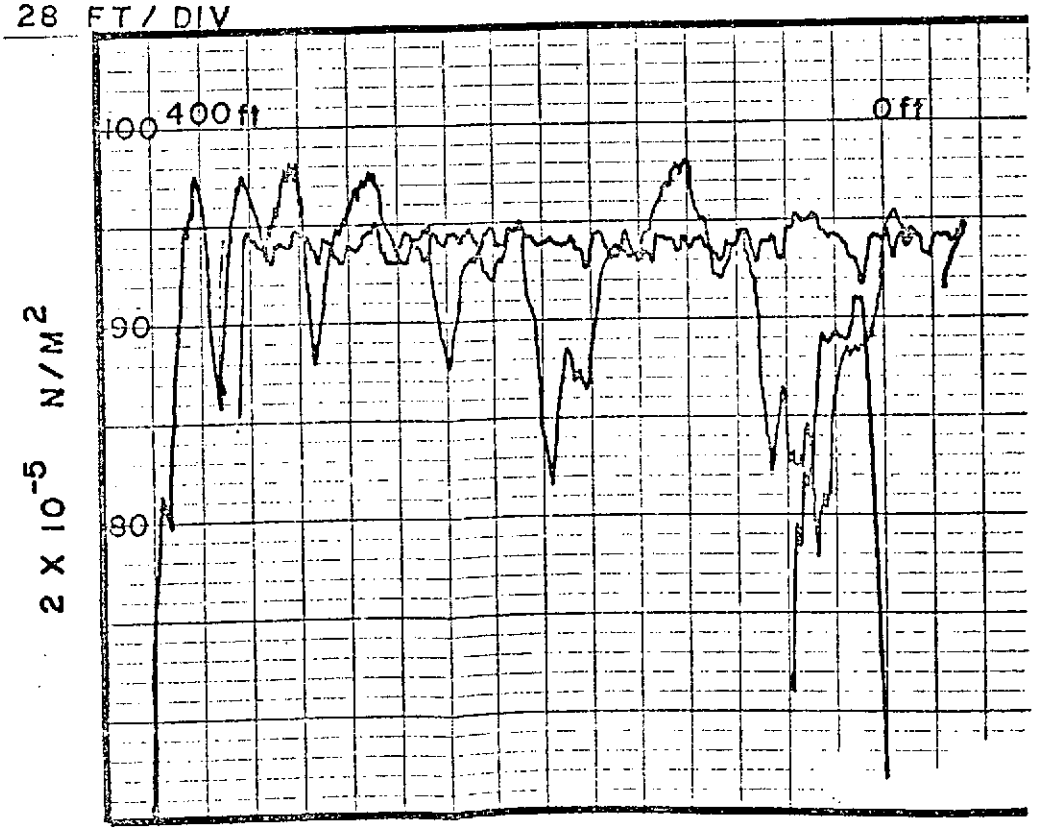

IGURE 4·16

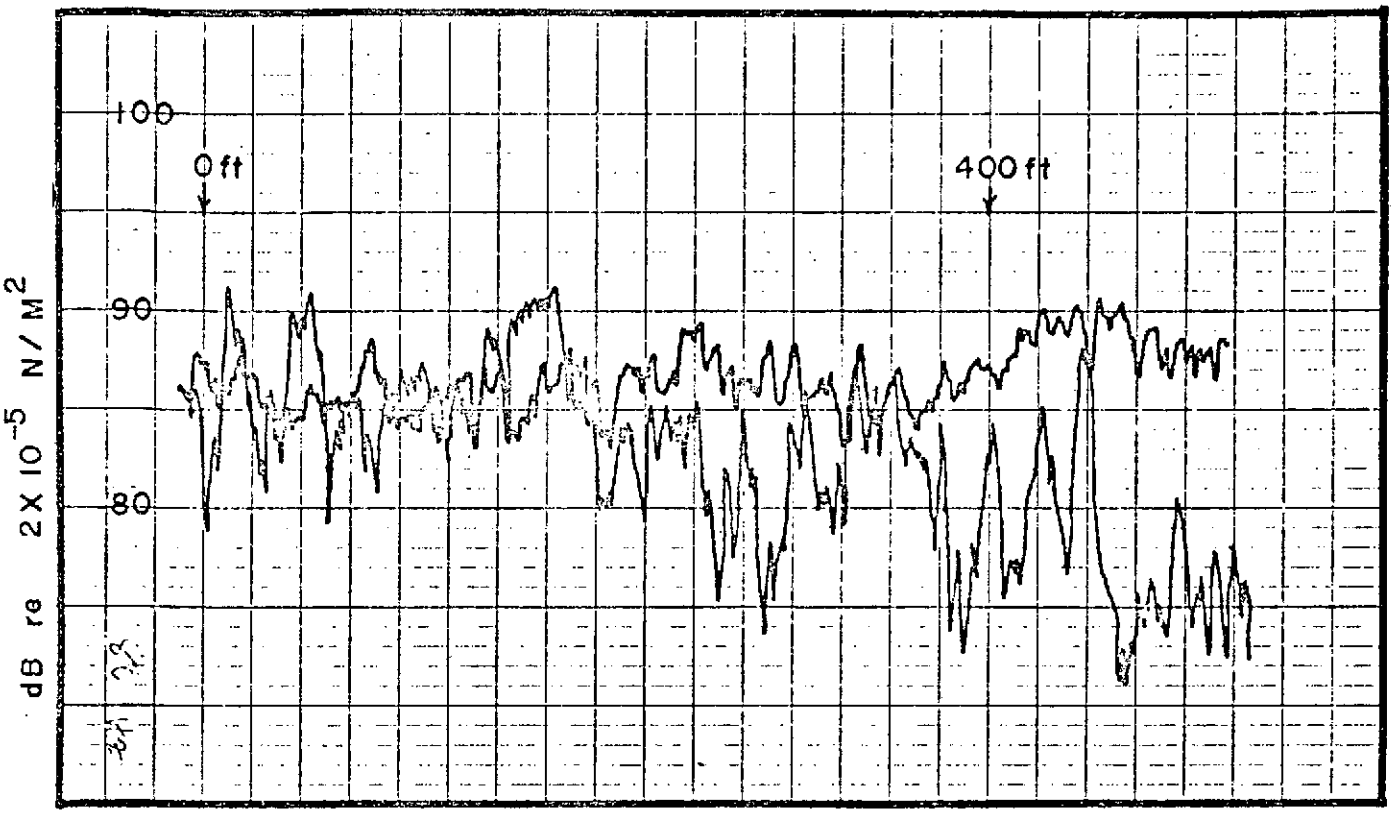

1/10 OCTAVE LEVELS CENTERED AT 80 Hz OF FIXED MICROPHONES

FIXED MICROPHONE AT INTERSECTION OF ARNOLD AND KING

UPPER PLOT MICROPHONE MOVING SOUTH. ABCISSA 25 FT / DIV

LOWER PLOT MICROPHONE MOVING NORTH ABCISSA 28 FT / DIV

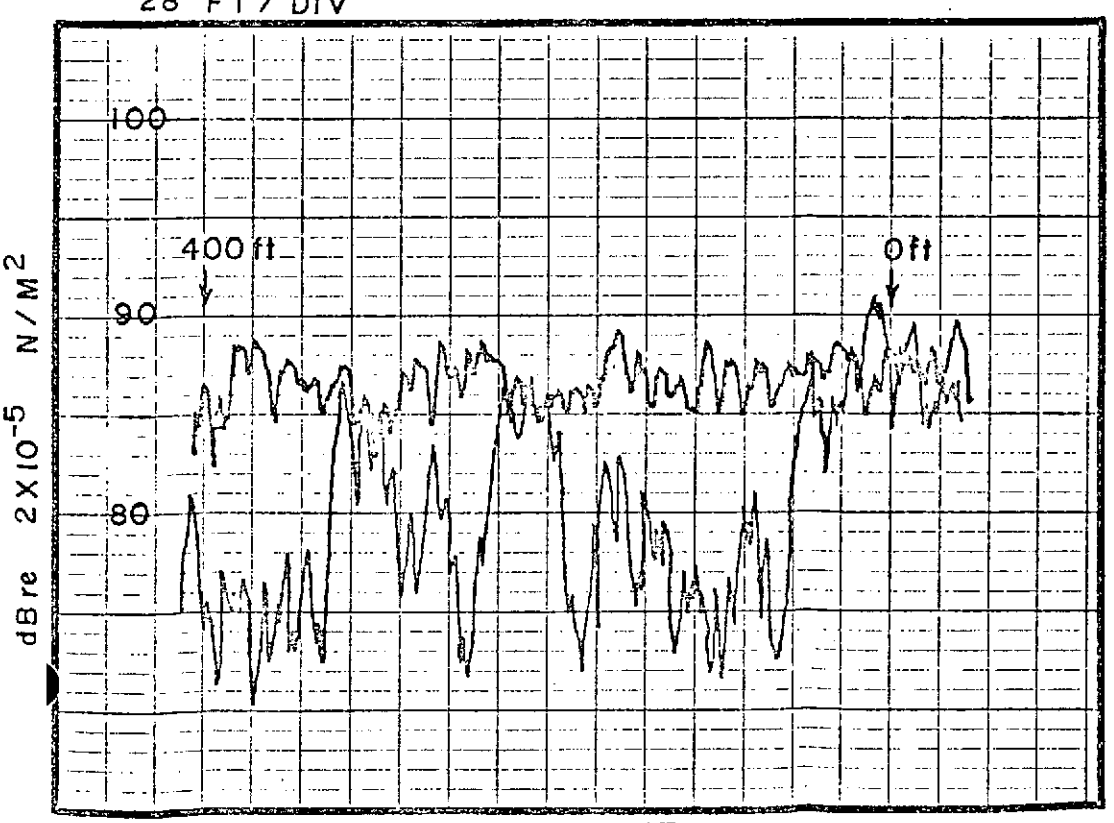

FIGURE 4-17

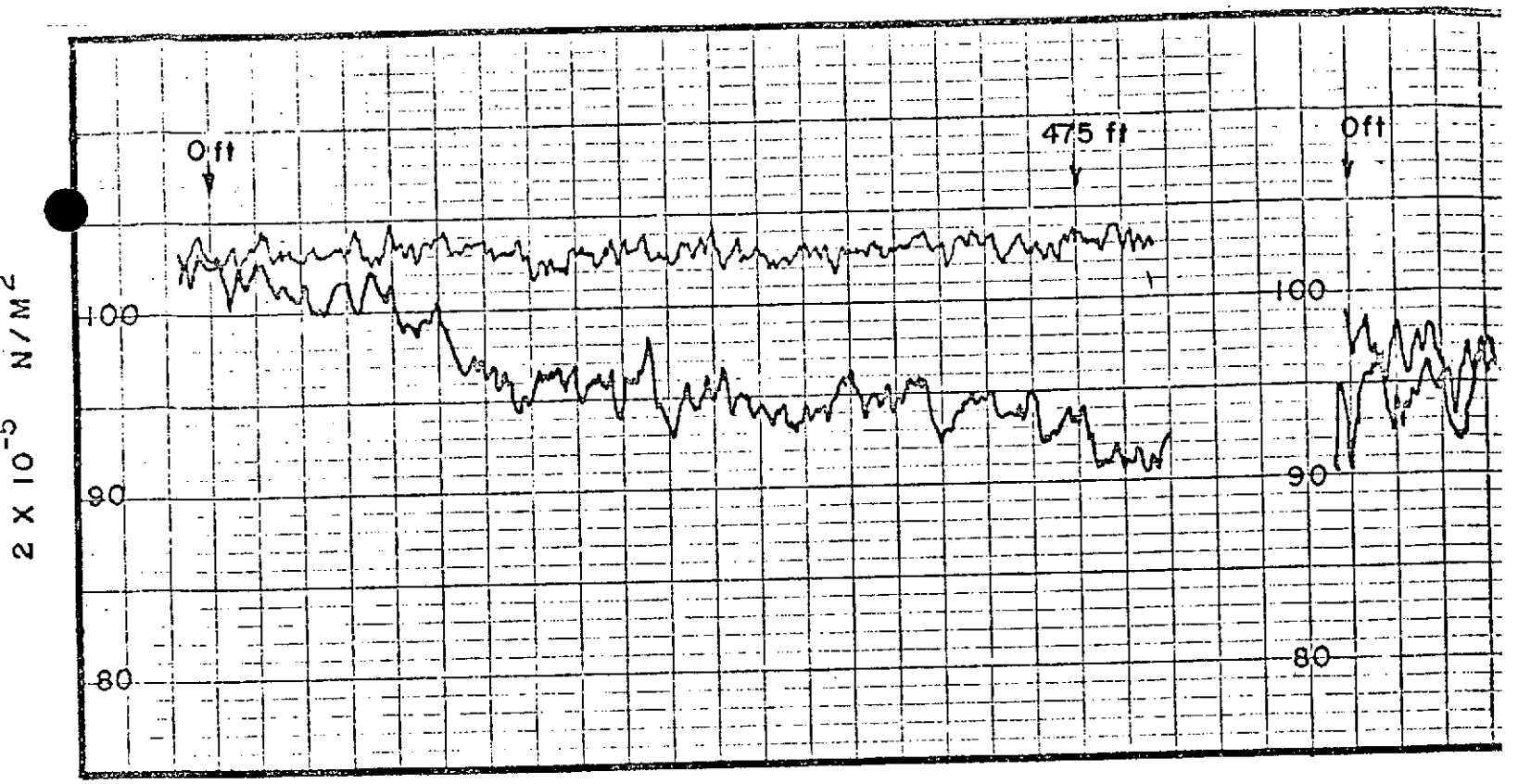

OVERALL LEVELS OF FIXED (BLK) AND MOVING (RED) MICROPHONES

FIXED MICROPHONE AT INTERSECTION OF 5TH AND BETA.

UPPER PLOT MICROPHONE MOVING NORTH

LOWER PLOT MICROPHONE MOVING SOUTH

ABCISSA 25 FT/ DIV

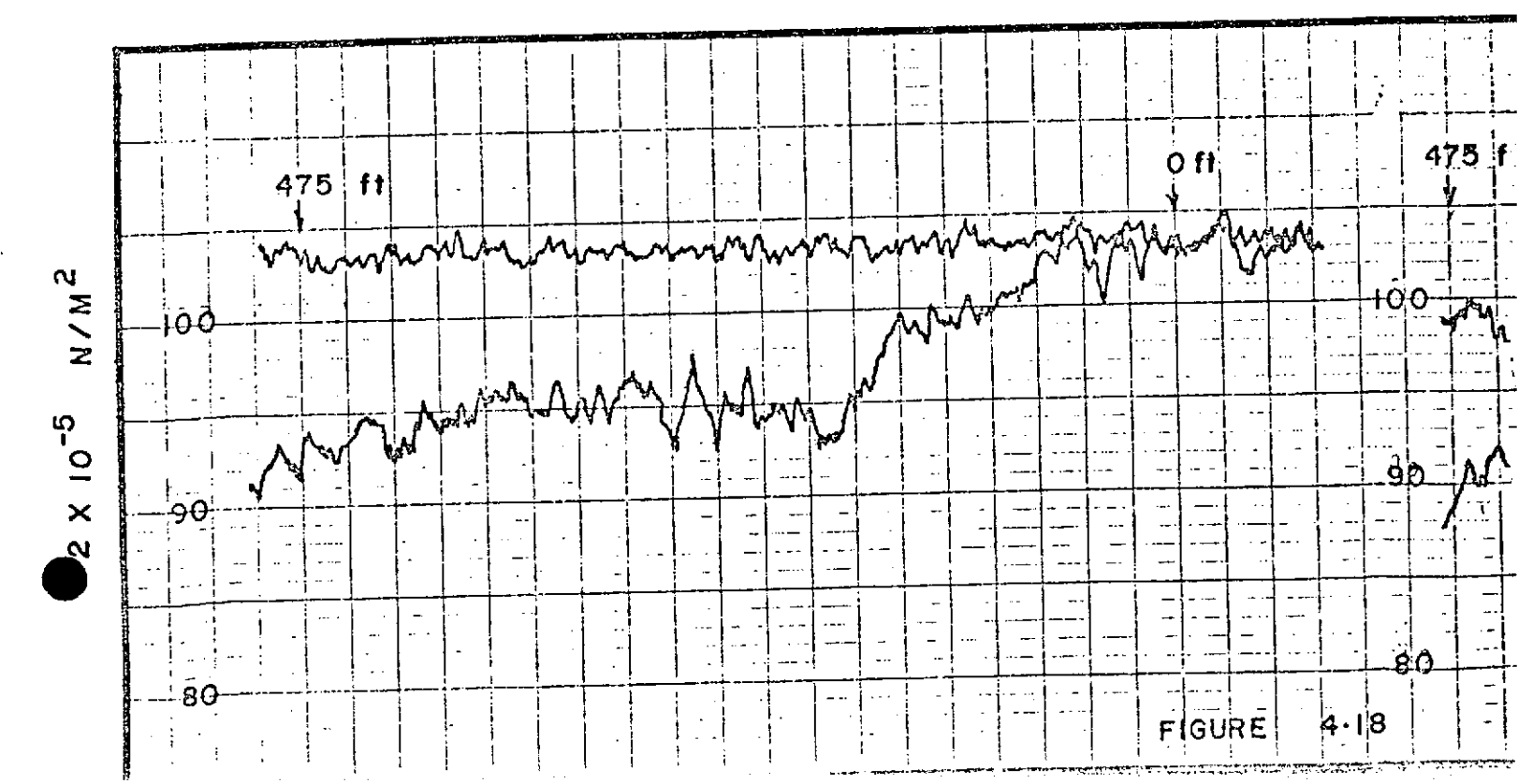

FIGURE 4·18

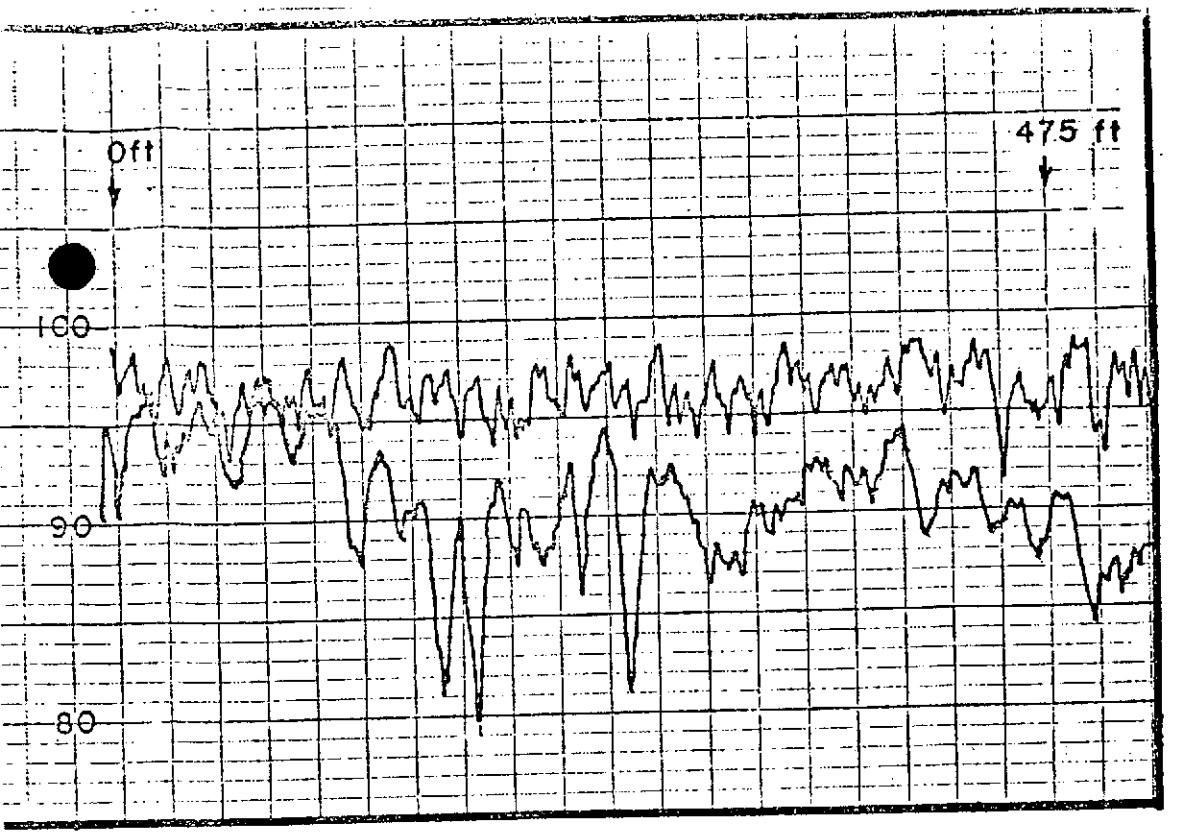

1/10 OCTAVE LEVELS CENTERED AT 26 Hz OF FIXED (BLK) AND MOVING (RED) MICROPHONES.

FIXED MICROPHONE AT INTERSECTION OF 5TH AND BETA.

UPPER PLOT MICROPHONE MOVING NORTH

LOWER PLOT MICROPHONE MOVING SOUTH

ABCISSA 25 FT / DIV

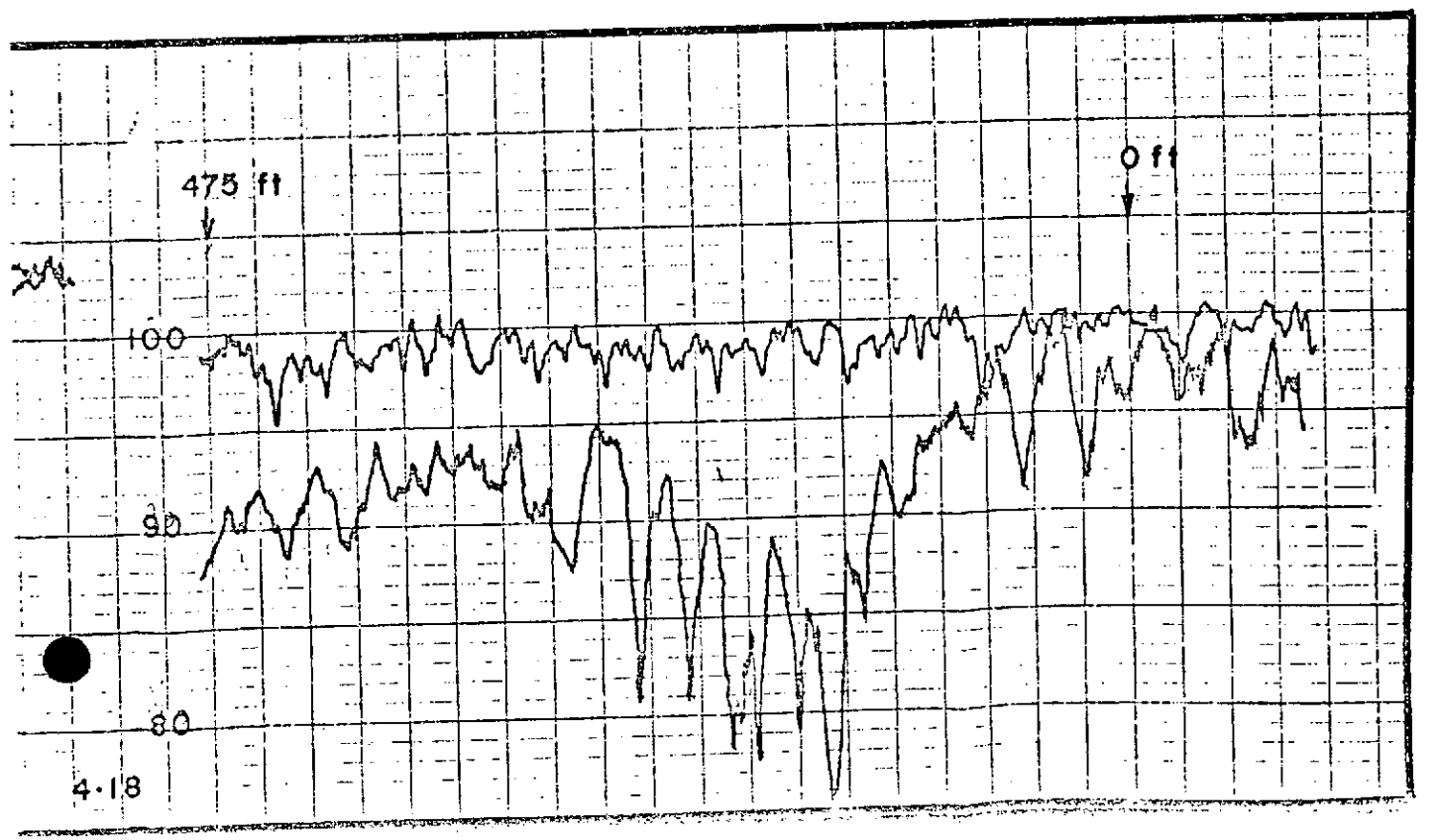

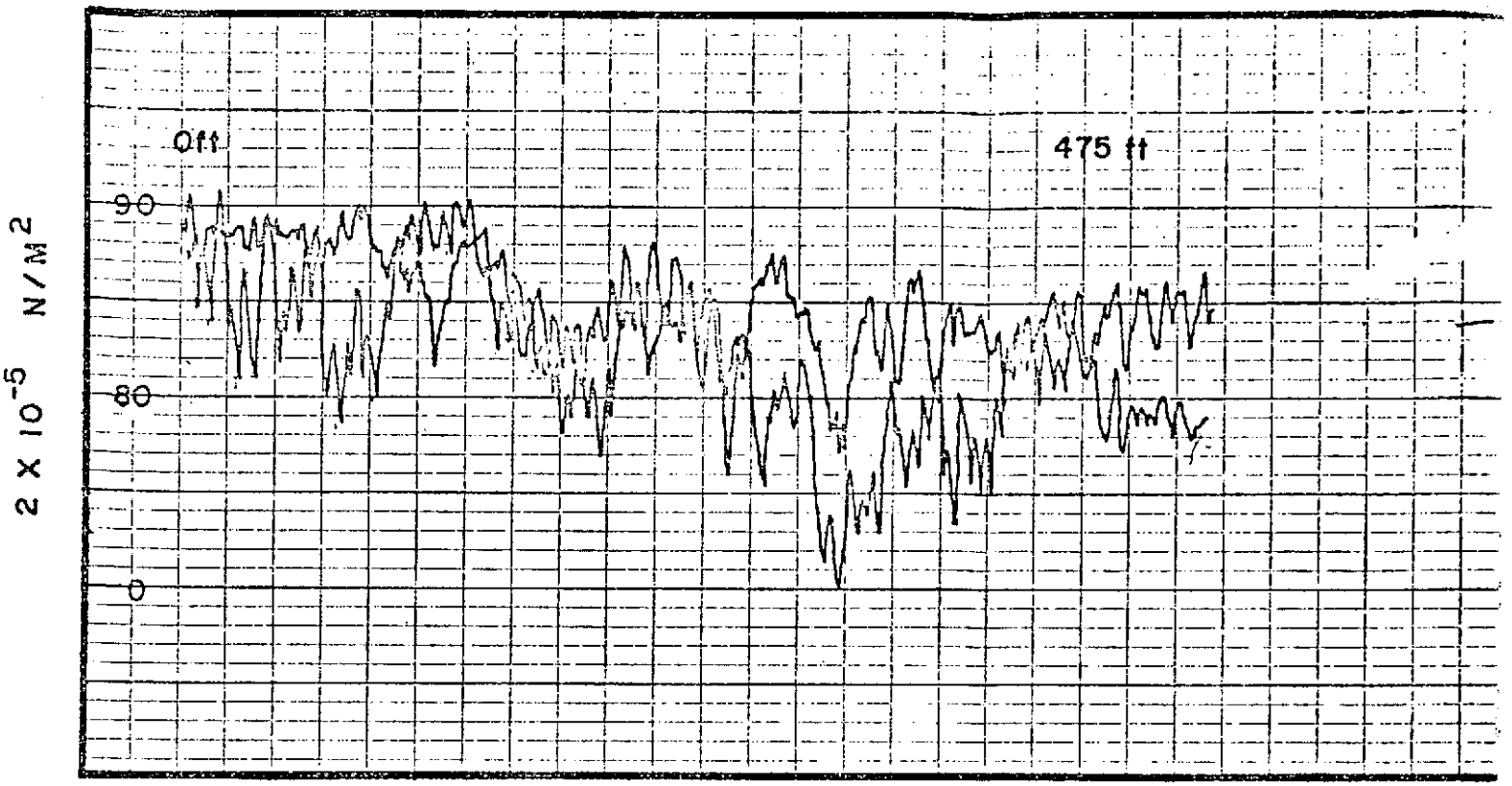

1/10 OCTAVE LEVELS CENTERED AT 80 Hz. OF FIXED (BLK) AND MOVING (RED) MICROPHONES.

FIXED MICROPHONE AT INTERSECTION OF 5TH AND BETA.

UPPER PLOT MICROPHONE MOVING NORTH

LOWER PLOT MICROPHONE MOVING SOUTH

ABCISSA 25 FT / DIV

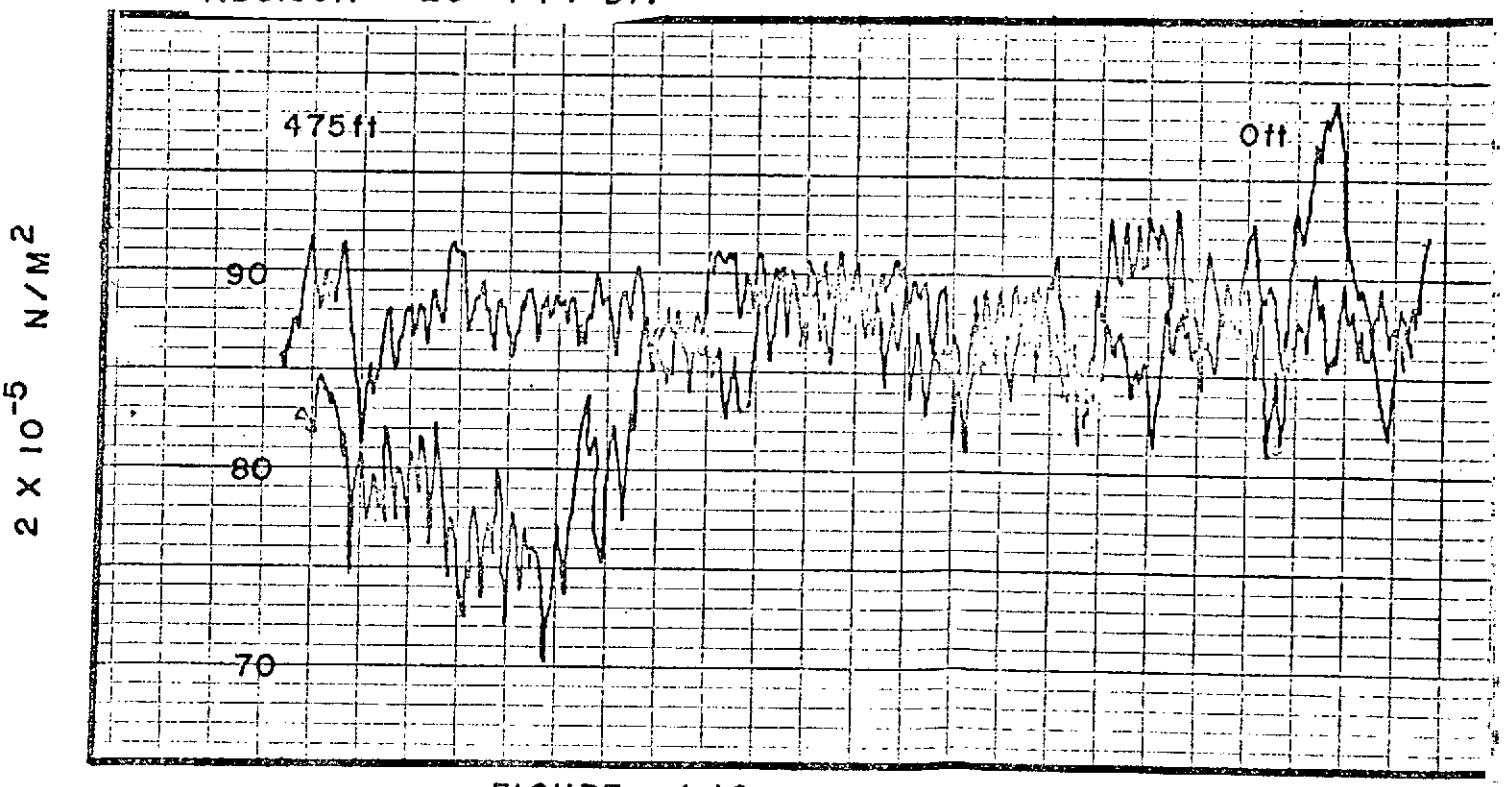

FIGURE 4·19

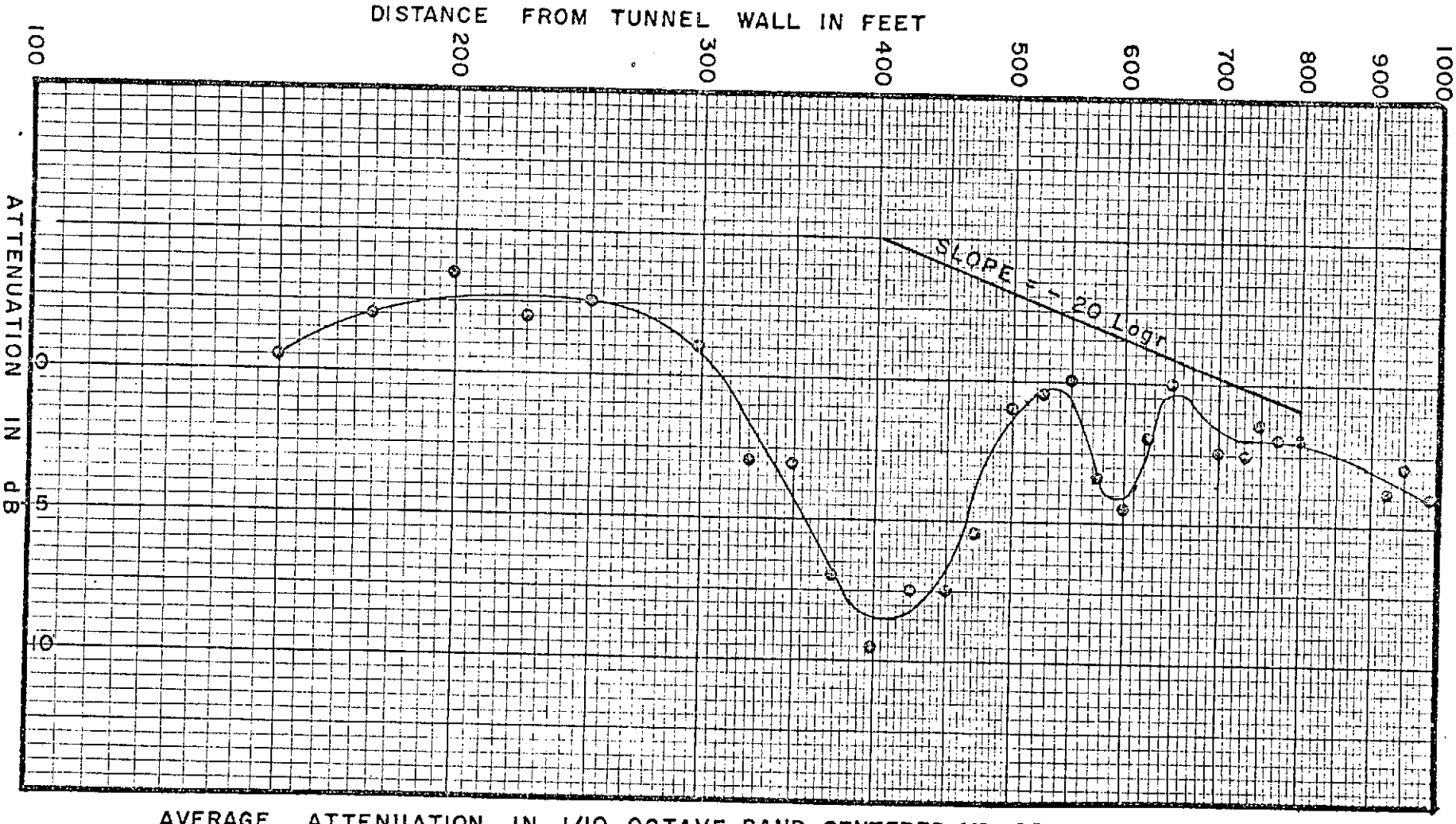

AVERAGE ATTENUATION IN 1/10 OCTAVE BAND CENTERED AT 26 Hz FOR TRANSIT ALONG DURAND ROAD FROM ARNOLD AVENUE

Figure 4-20

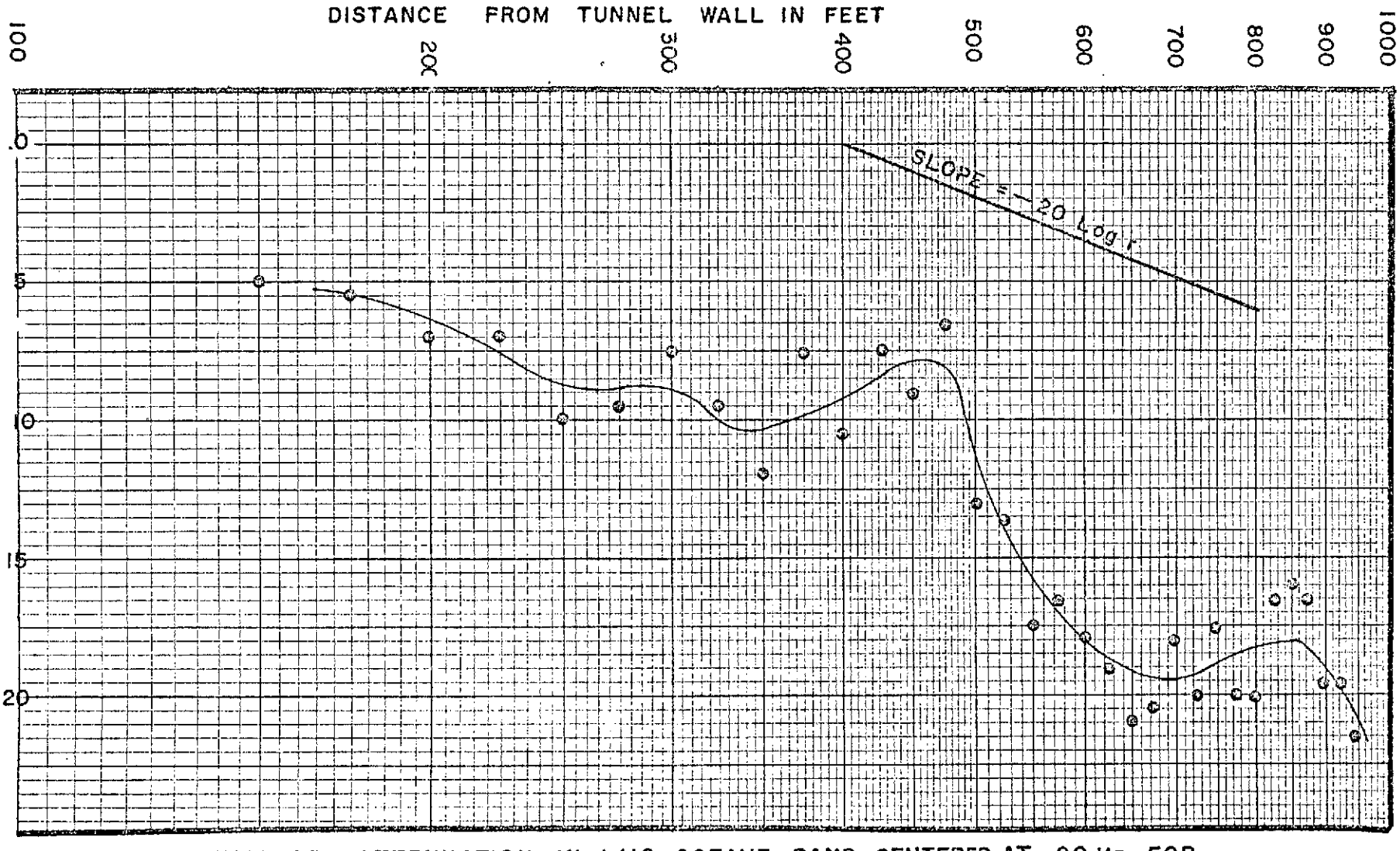

AVERAGE ATTENUATION IN 1/10 OCTAVE BAND CENTERED AT 80 Hz FOR TRANSIT ALONG DURAND ROAD FROM ARNOLD AVENUE

Figure 4-21

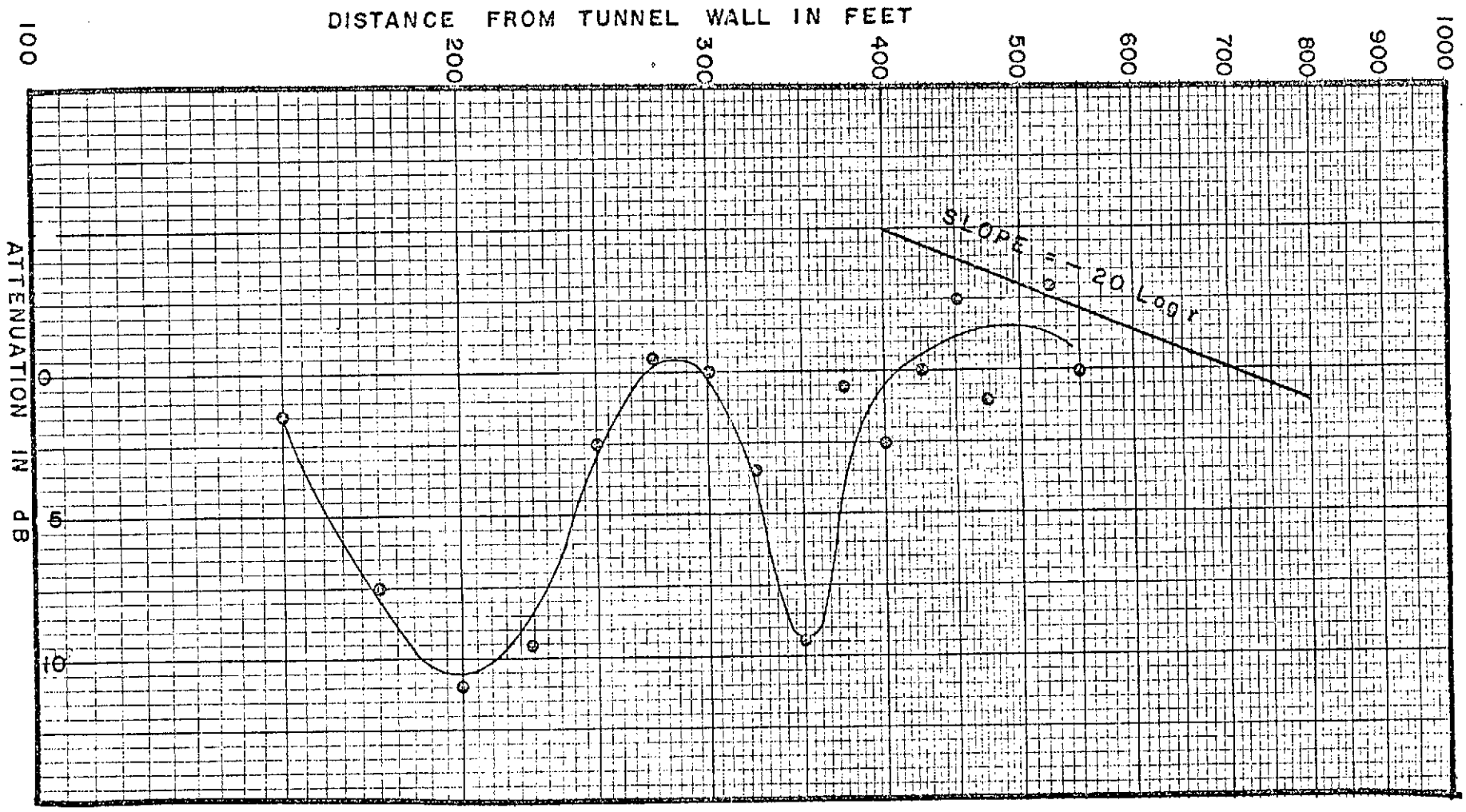

AVERAGE ATTENUATION IN 1/10 OCTAVE BAND CENTERED AT 26 Hz FOR TRANSIT ALONG ARNOLD AVENUE FROM KING ROAD

Figure 4-22

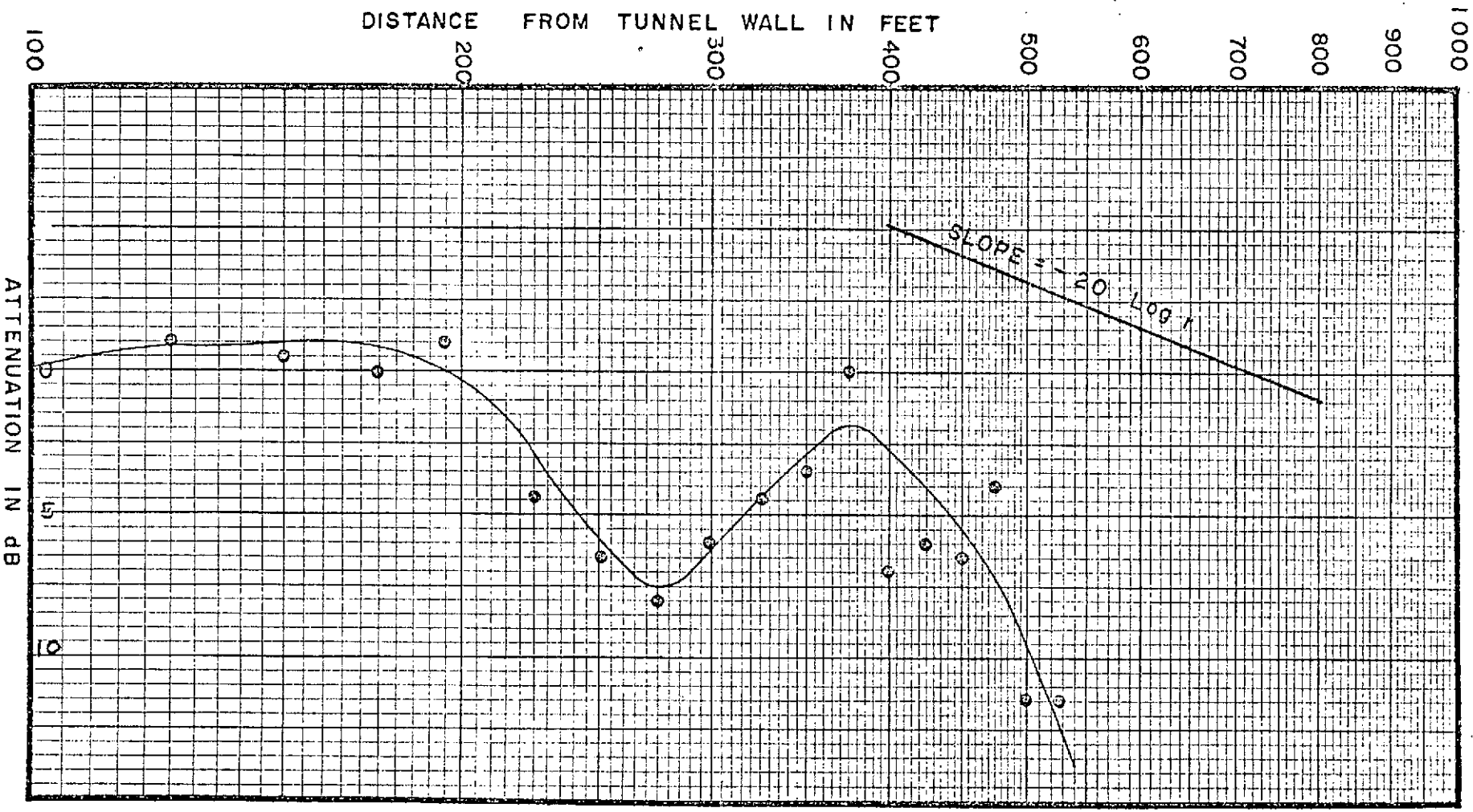

AVERAGE ATTENUATION IN 1/10 OCTAVE BAND CENTERED AT 80. Hz FOR TRANSIT ALONG ARNOLD AVENUE FROM KING ROAD

Figure 4-23

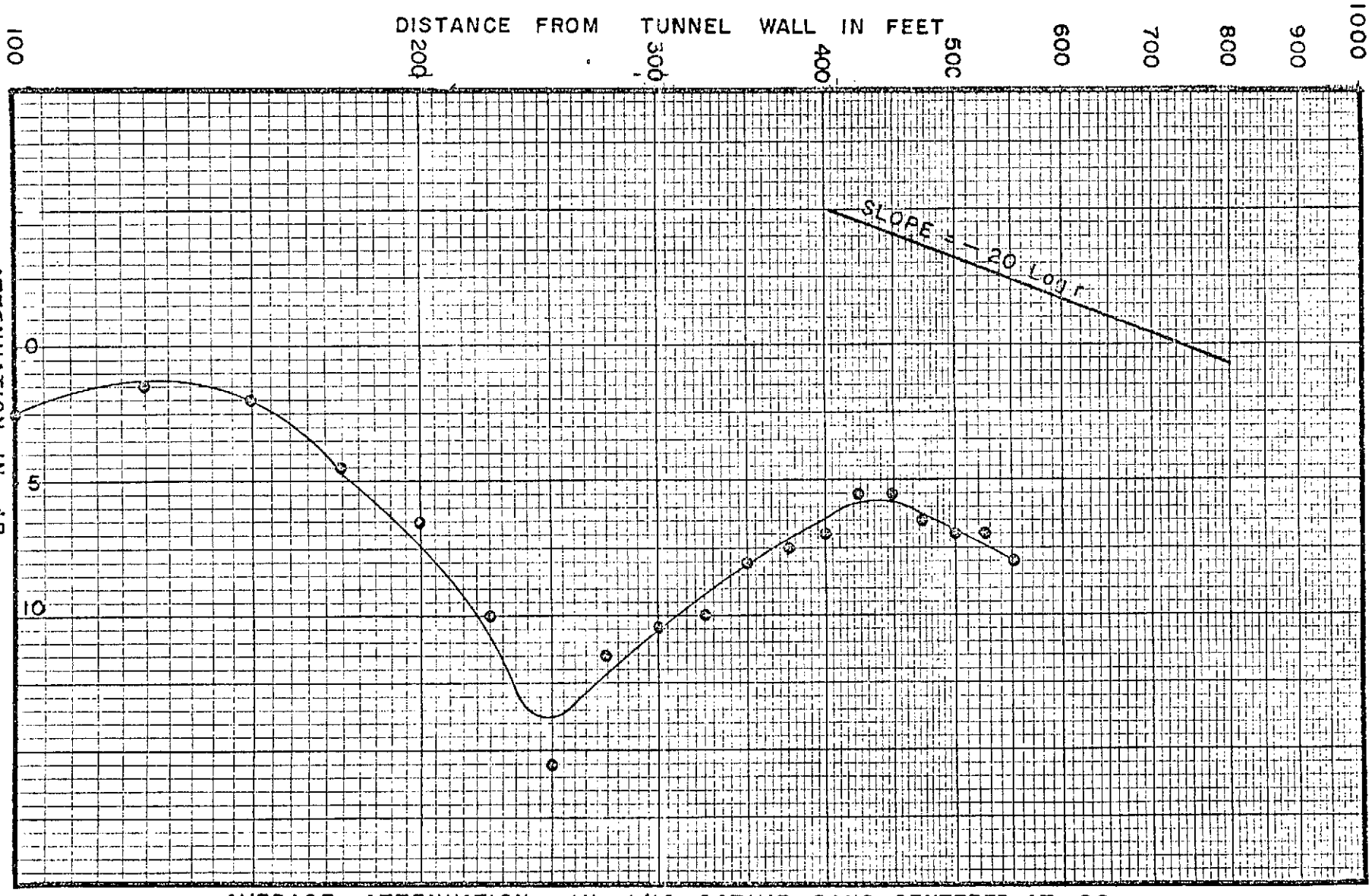

AVERAGE ATTENUATION IN 1/10 OCTAVE BAND CENTERED AT 26 Hz FOR TRANSIT ALONG BETA LANE FROM 5TH STREET

Figure 4-24

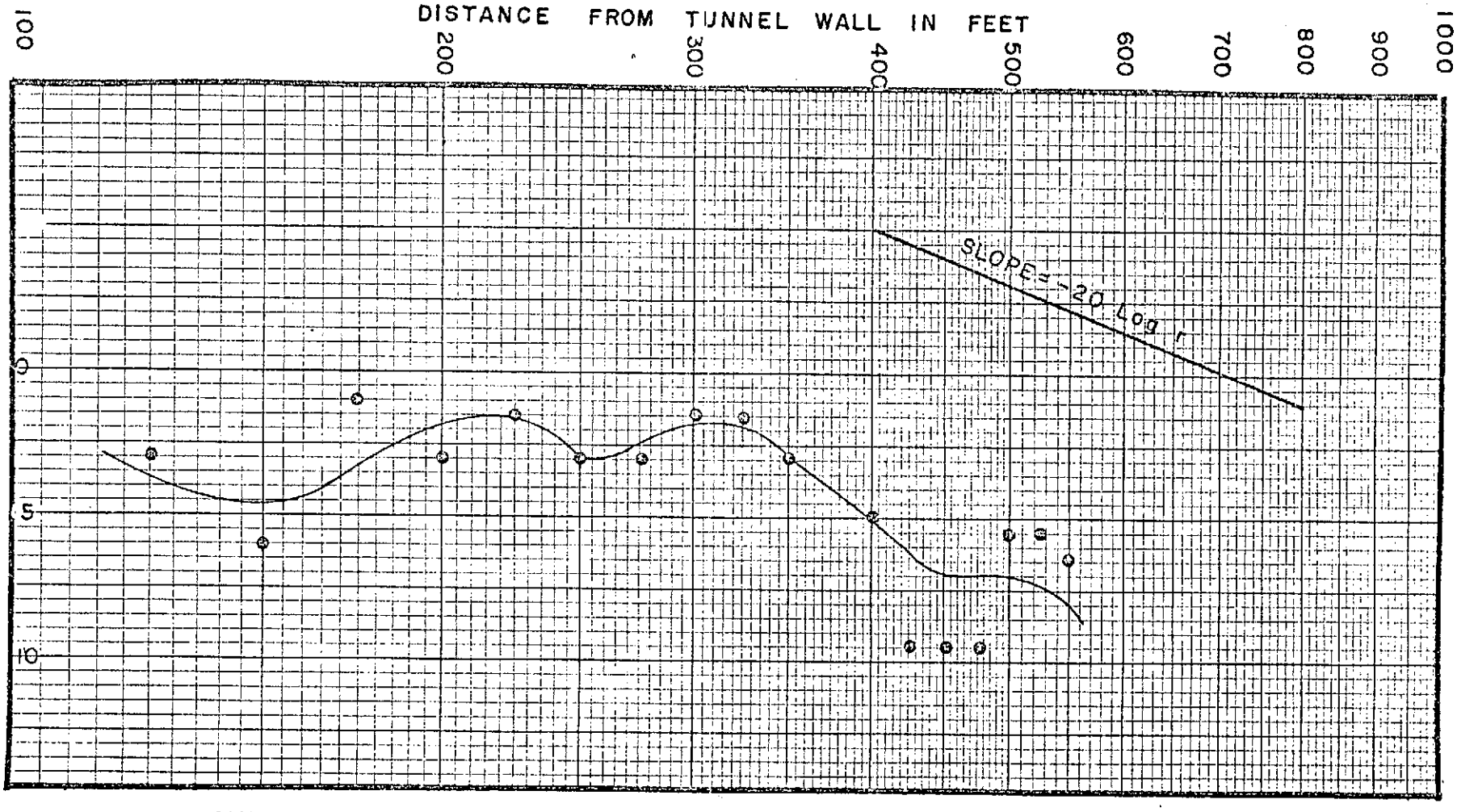

AVERAGE ATTENUATION IN 1/10 OCTAVE BAND CENTERED AT 80 Hz FOR TRANSIT ALONG BETA LANE FROM 5TH STREET

Figure 4-25

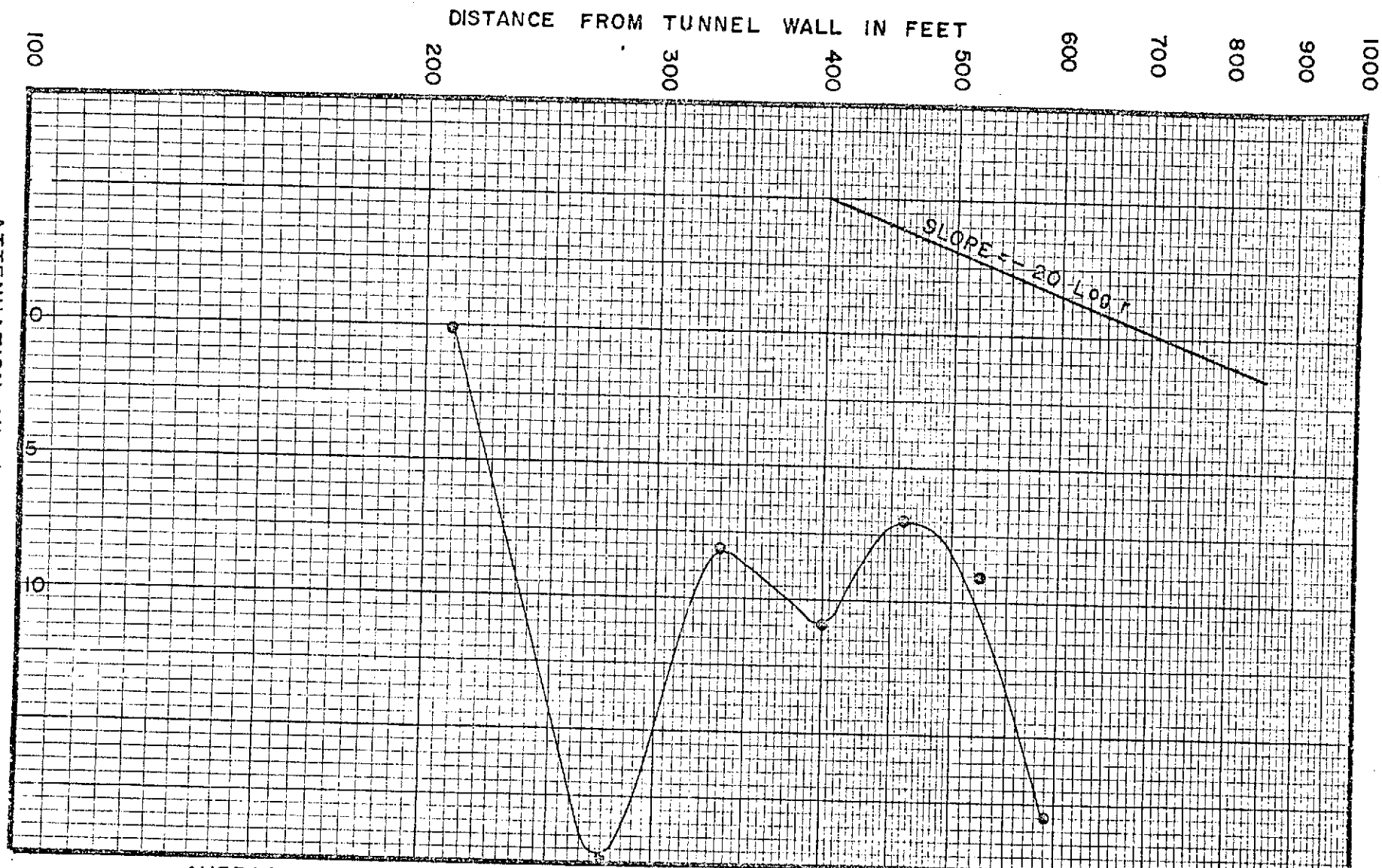

AVERAGE ATTENUATION IN 1/10 OCTAVE BAND CENTERED AT 26 Hz FOR DISCRETE LOCATIONS WEST OF THE TUNNEL

Figure 4-26

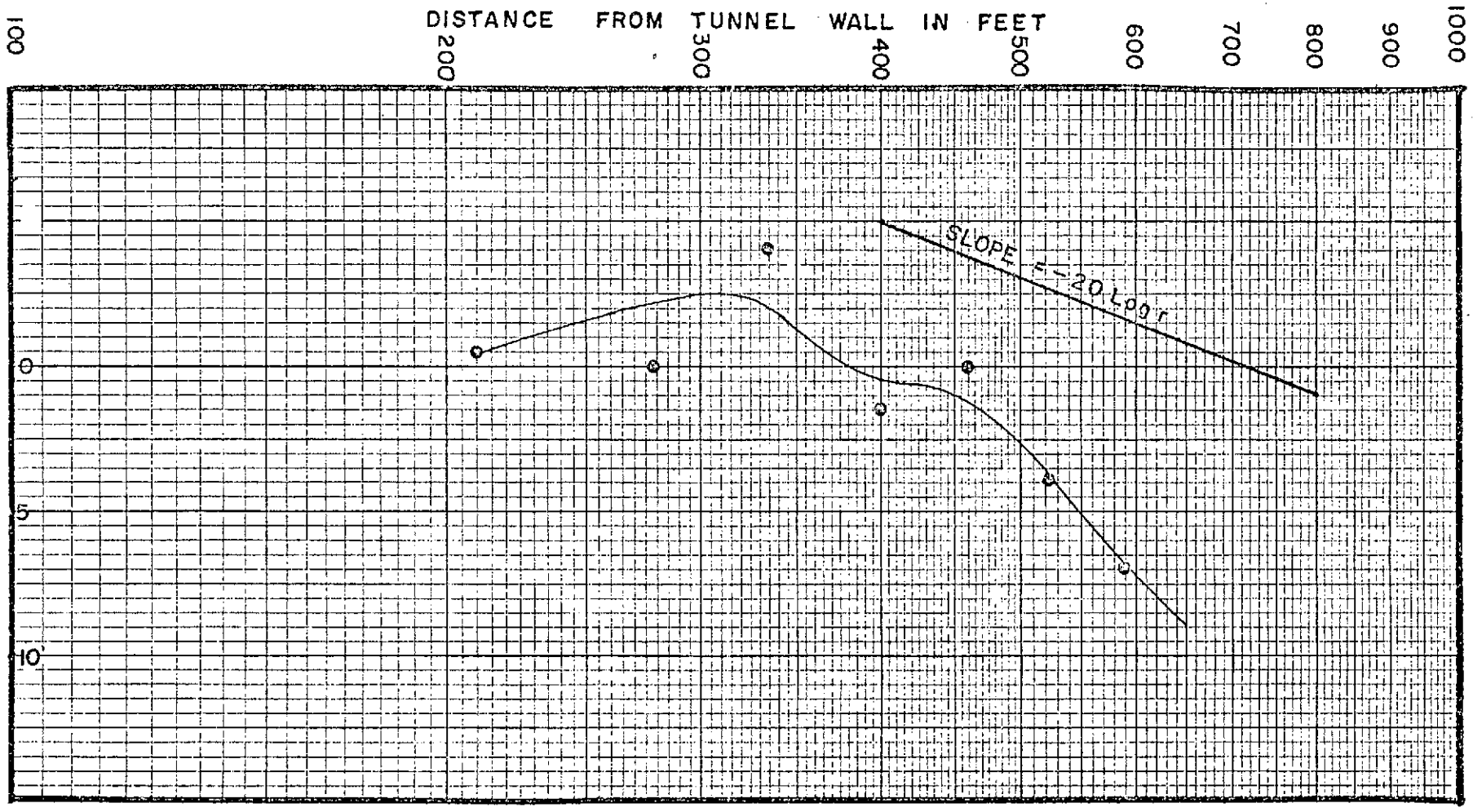

AVERAGE ATTENUATION IN 1/10 OCTAVE BAND CENTERED AT 80 Hz FOR TRANSIT DISCRETE LOCATIONS WEST OF THE TUNNEL

Figure 4-27

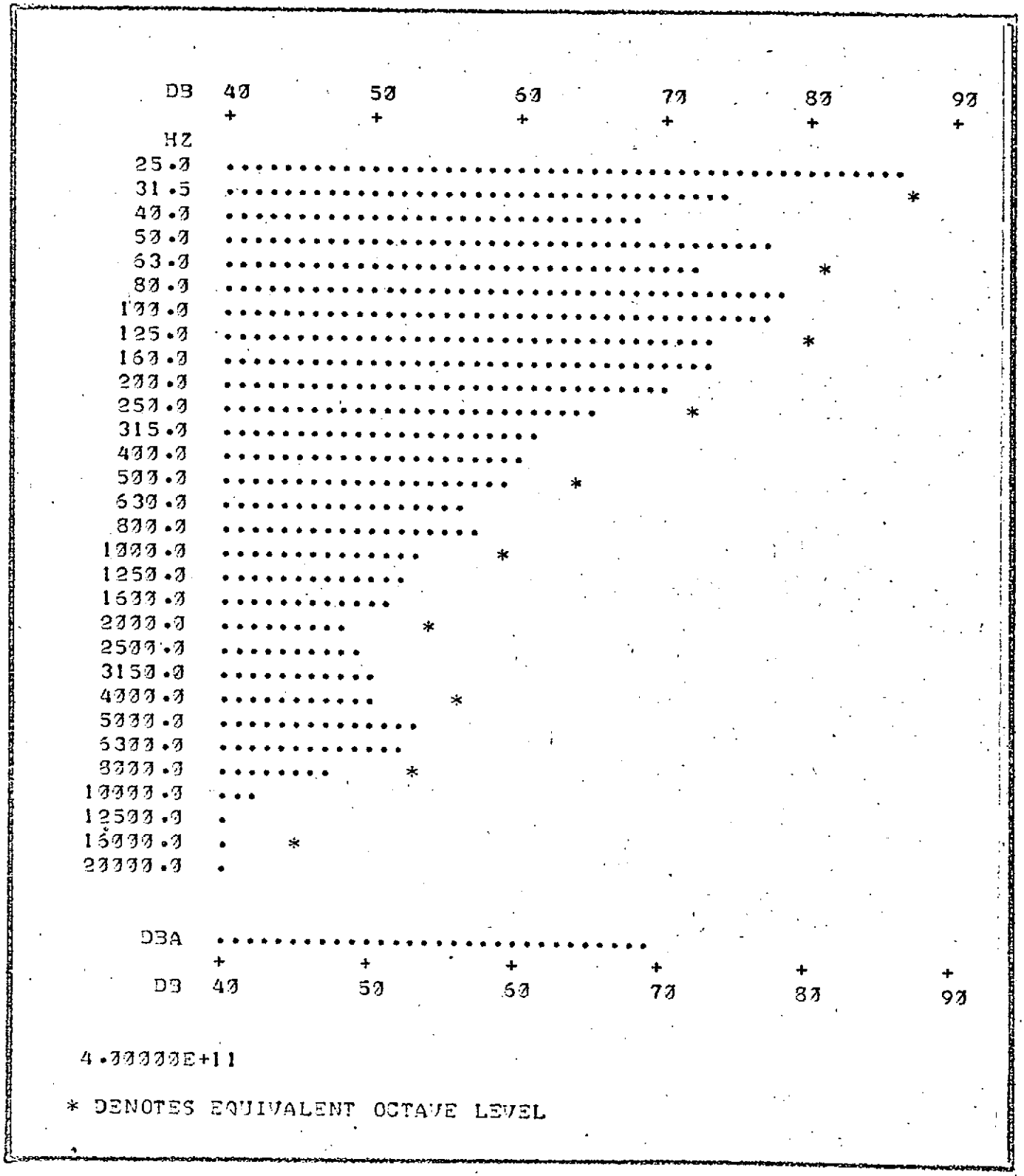

1/3 OCTAVE BAND LEVELS OBTAINED AT NEAR FIELD POINT A (FIGURE 4.9) WITH TUNNEL OPERATING, q_u = 105 p.s.f.

Figure 4-28

C-2

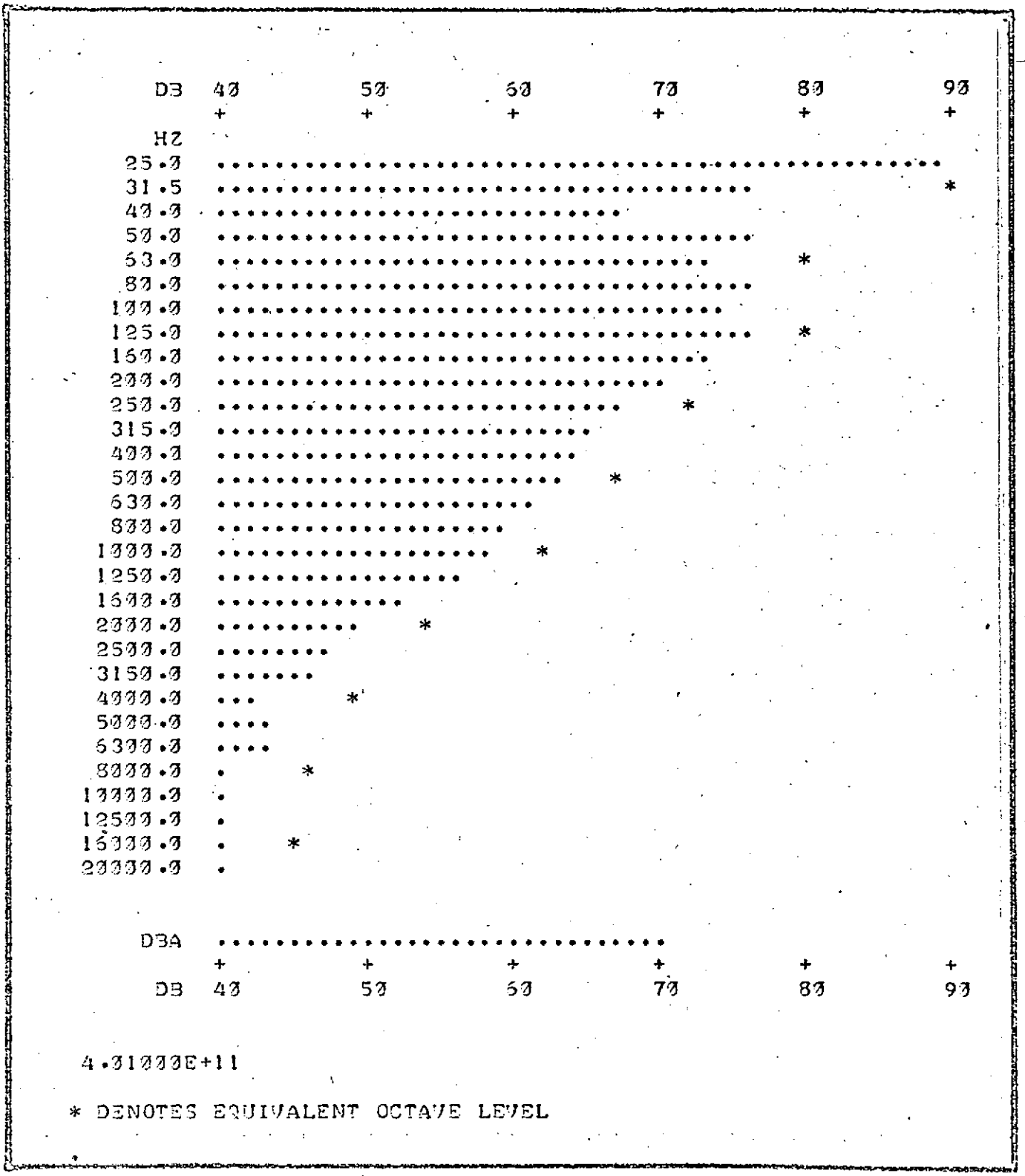

1/3 OCTAVE BAND LEVELS OBTAINED AT NEAR FIELD POINT B (FIGURE 4.9) WITH TUNNEL OPERATING, q_u = 105 p.s.f.

FIGURE 4-29

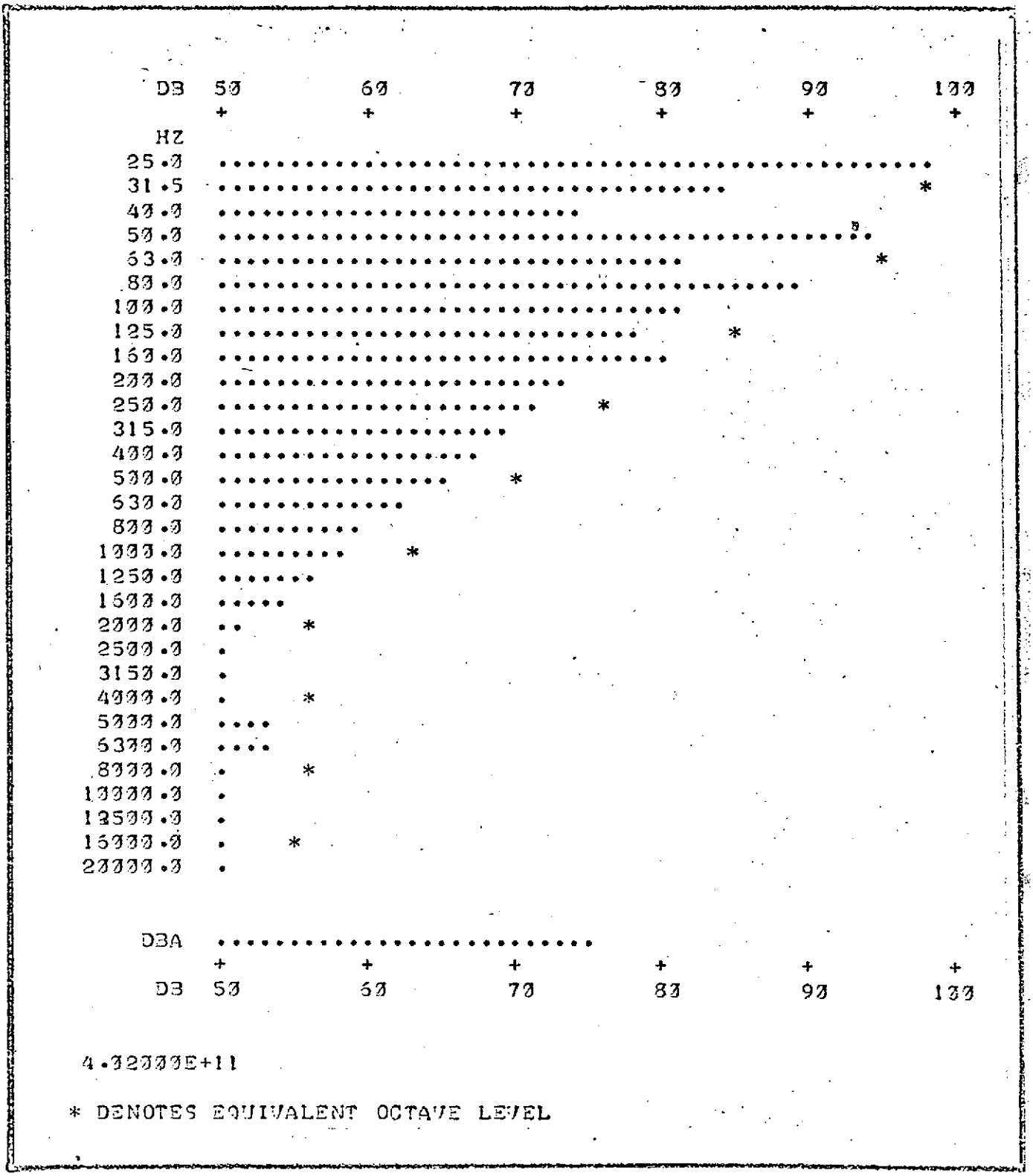

1/3 OCTAVE BAND LEVELS OBTAINED AT NEAR FIELD POINT C (FIGURE 4.9) WITH TUNNEL OPERATING, q_u = 105 p.s.f.

Figure 4.30

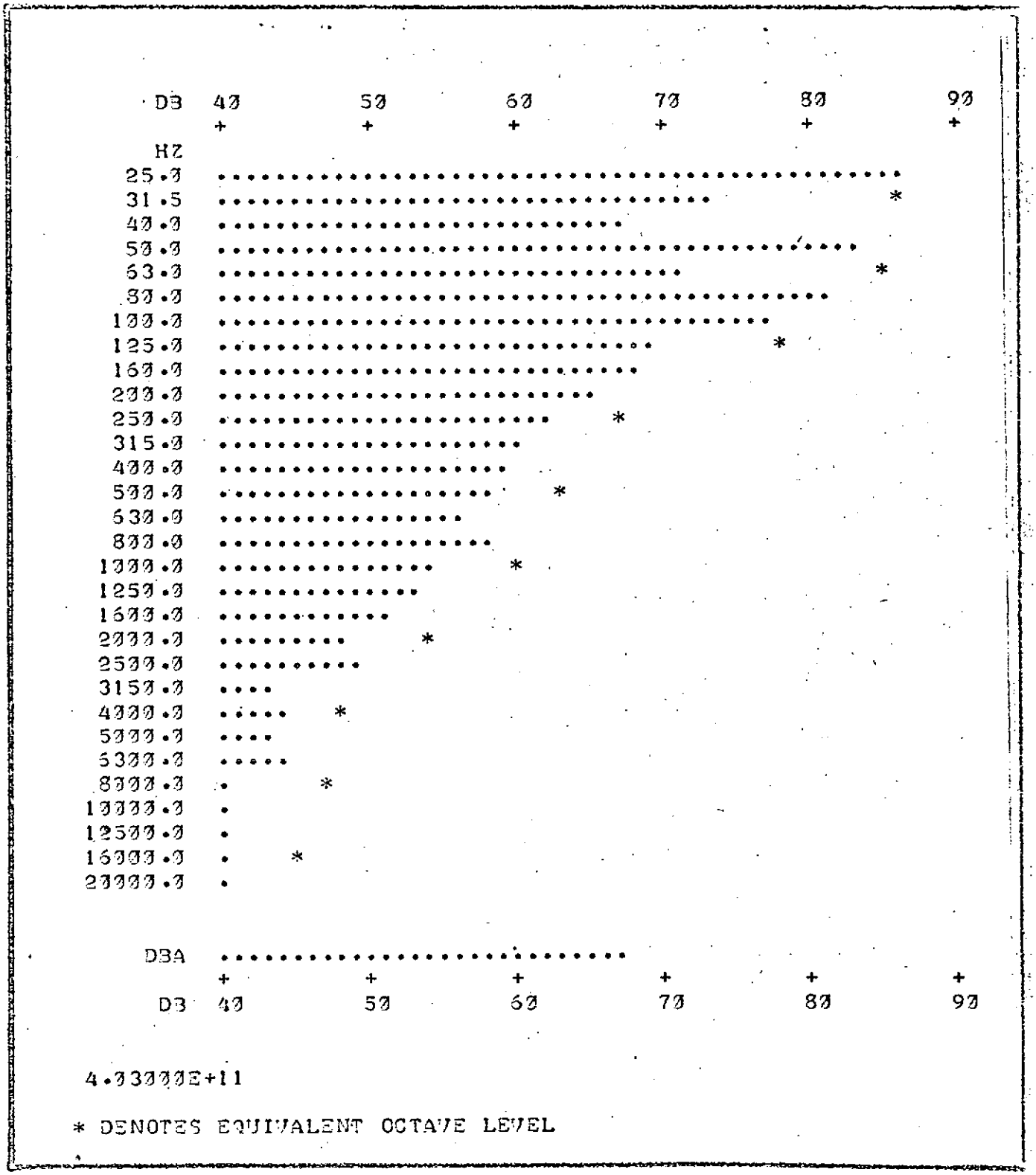

1/3 OCTAVE BAND LEVELS OBTAINED AT NEAR FIELD POINT D (FIGURE 4.9) WITH TUNNEL OPERATING, q_u = 105 p.s.f.

Figure 4-31

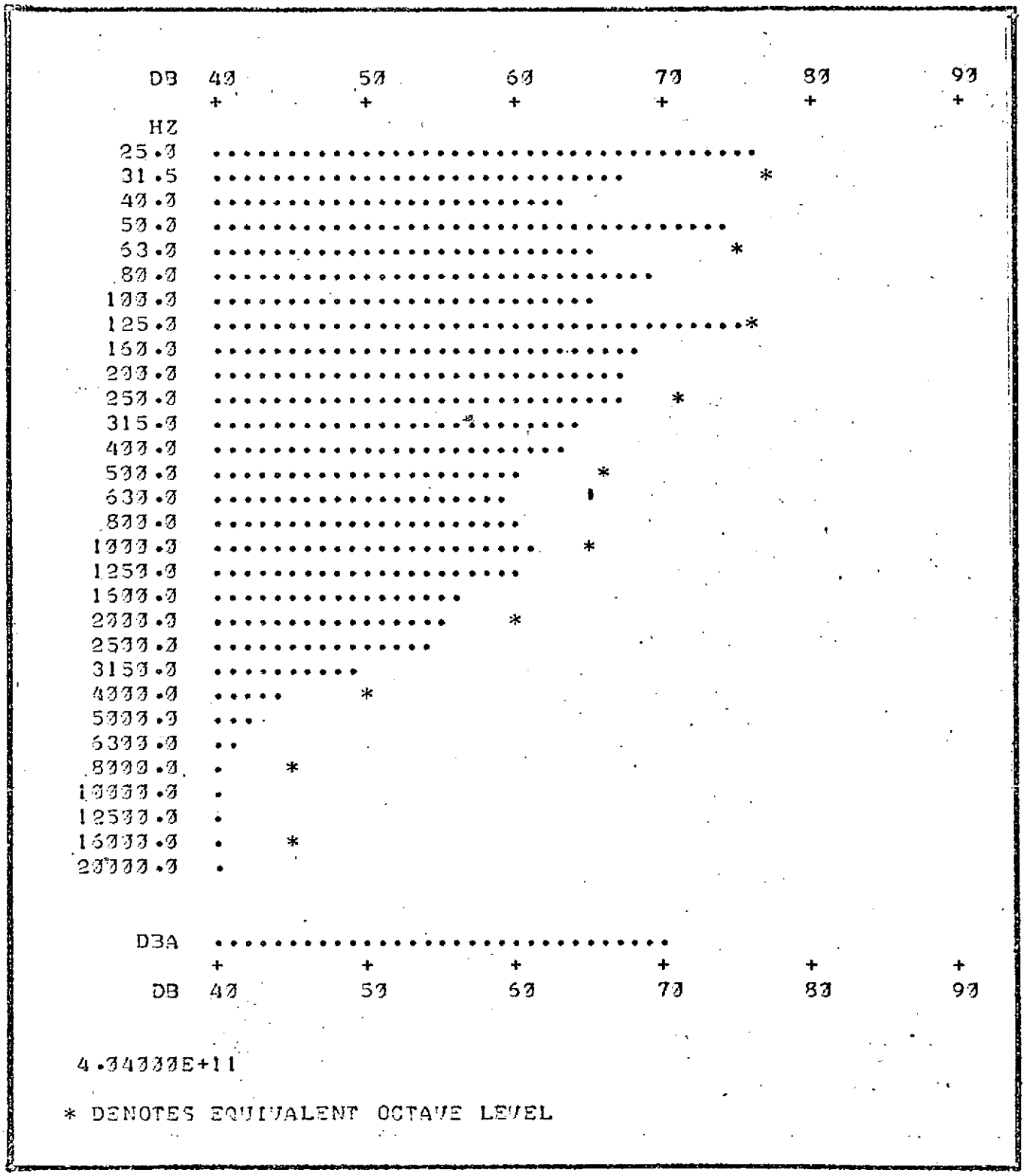

1/3 OCTAVE BAND LEVELS OBTAINED AT NEAR FIELD POINT E (FIGURE 4.9) WITH TUNNEL OPERATING, q_u = 105 p.s.f.

Figure 4.32

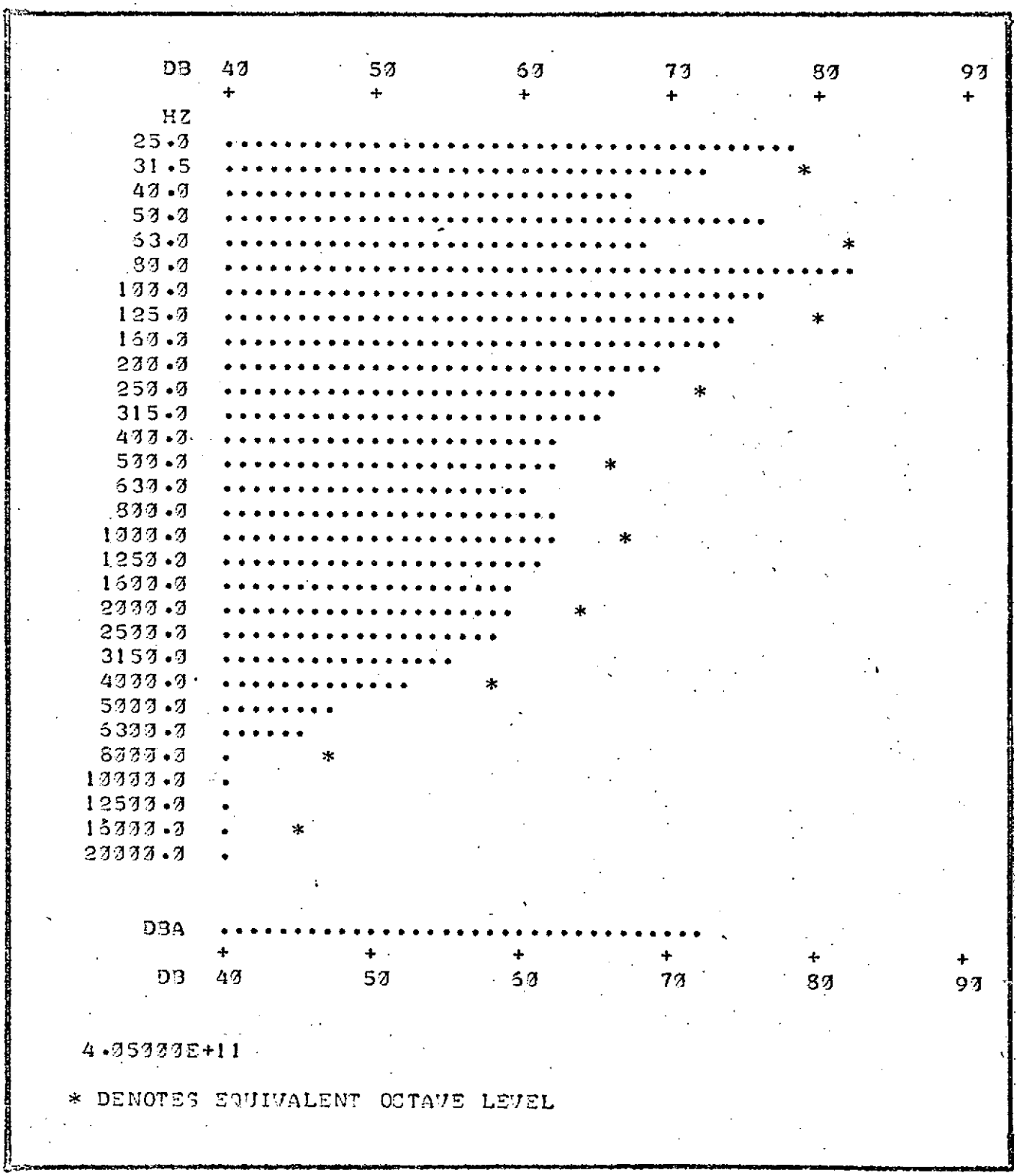

1/3 OCTAVE BAND LEVELS OBTAINED AT NEAR FIELD POINT F (FIGURE 4.9)WITH TUNNEL OPERATING, q_u = 105 p.s.f.

Figure 4-33

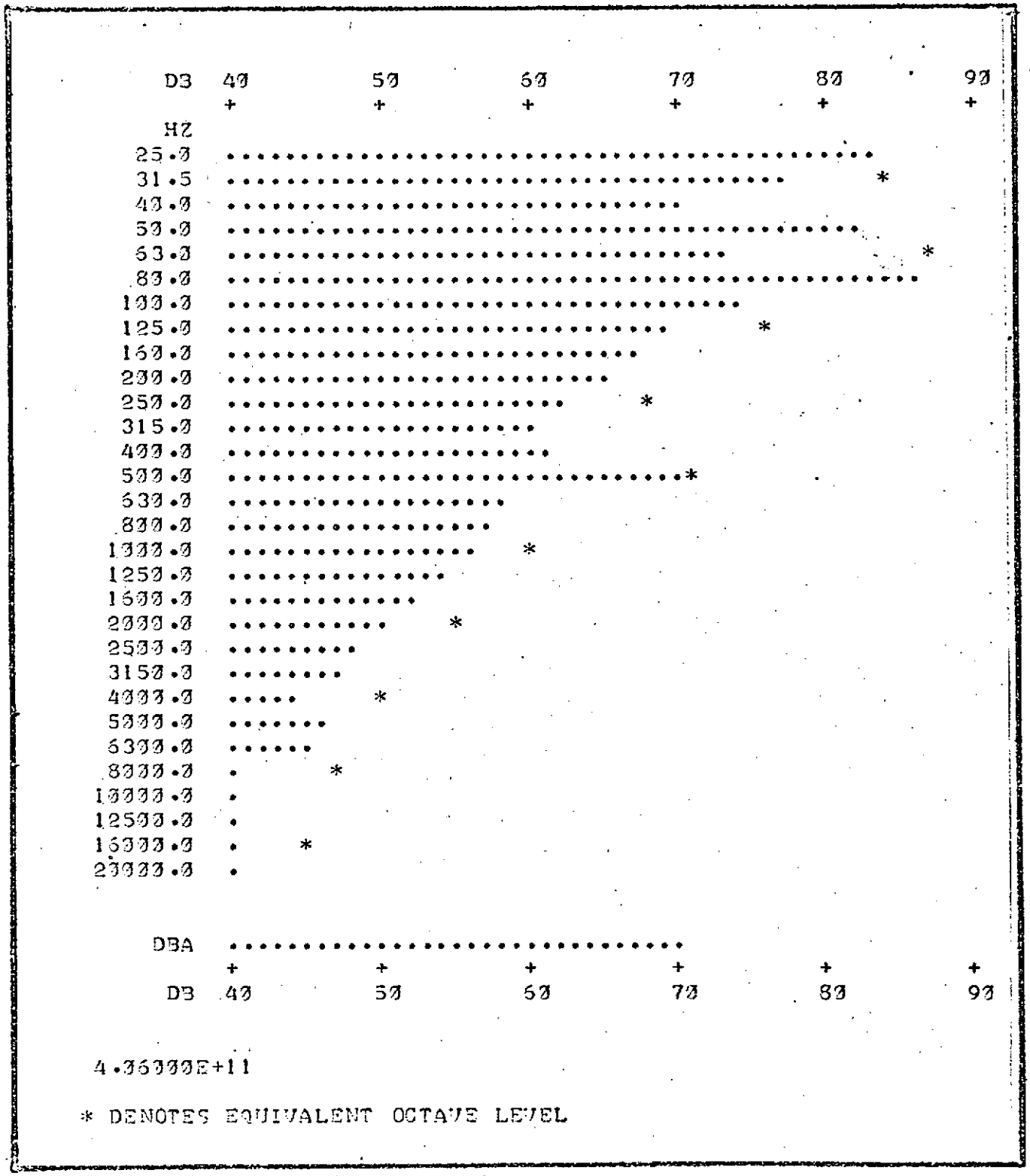

1/3 OCTAVE BAND LEVELS OBTAINED AT NEAR FIELD POINT G (FIGURE 4.9) WITH TUNNEL OPERATING, q_u= 105 p.s.f.

Figure 4-34

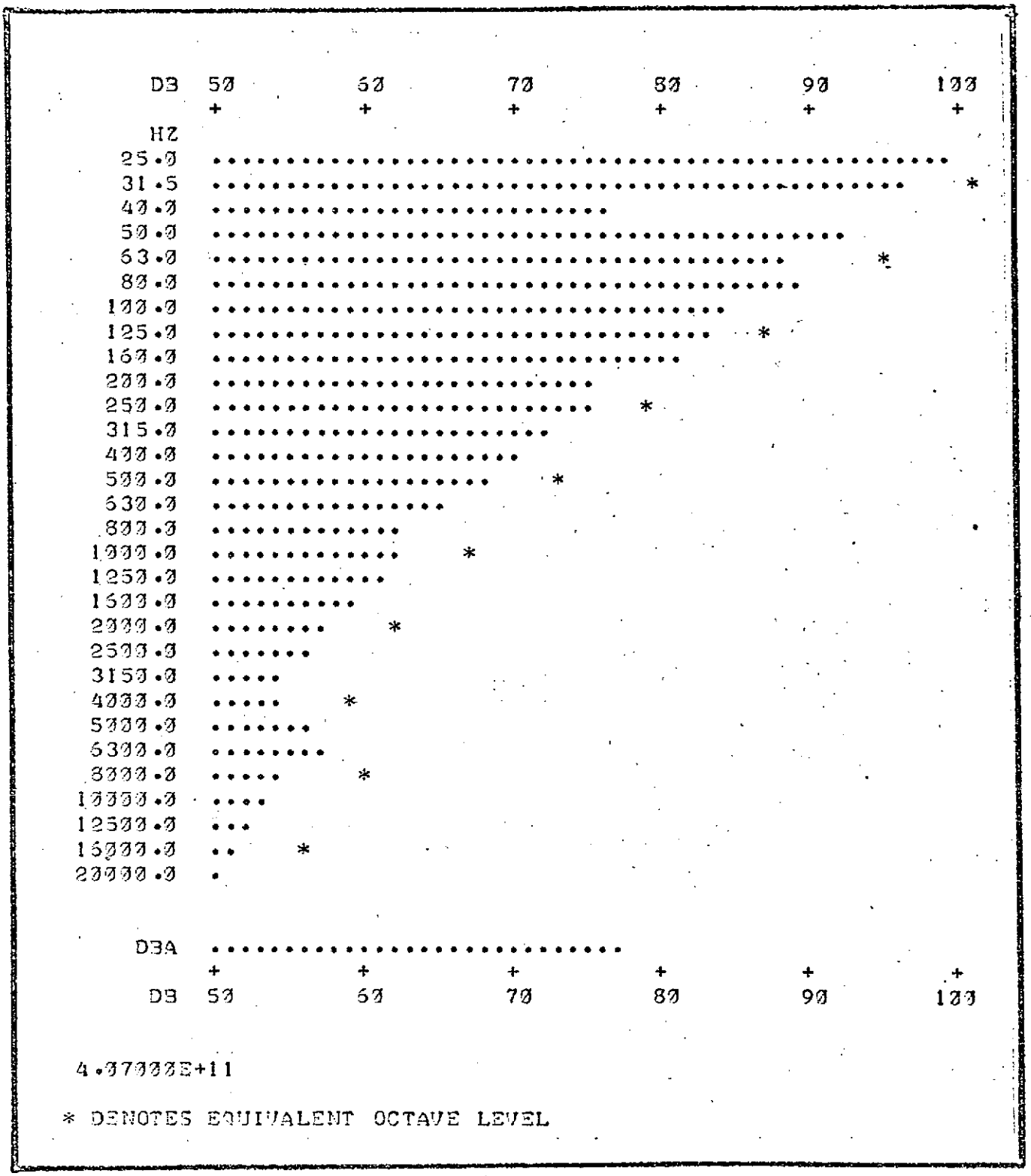

1/3 OCTAVE BAND LEVELS OBTAINED AT NEAR FIELD POINT H (FIGURE 4.9) WITH TUNNEL OPERATING, q_u = 105 p.s.f.

Figure 4-35

Figure 4-36

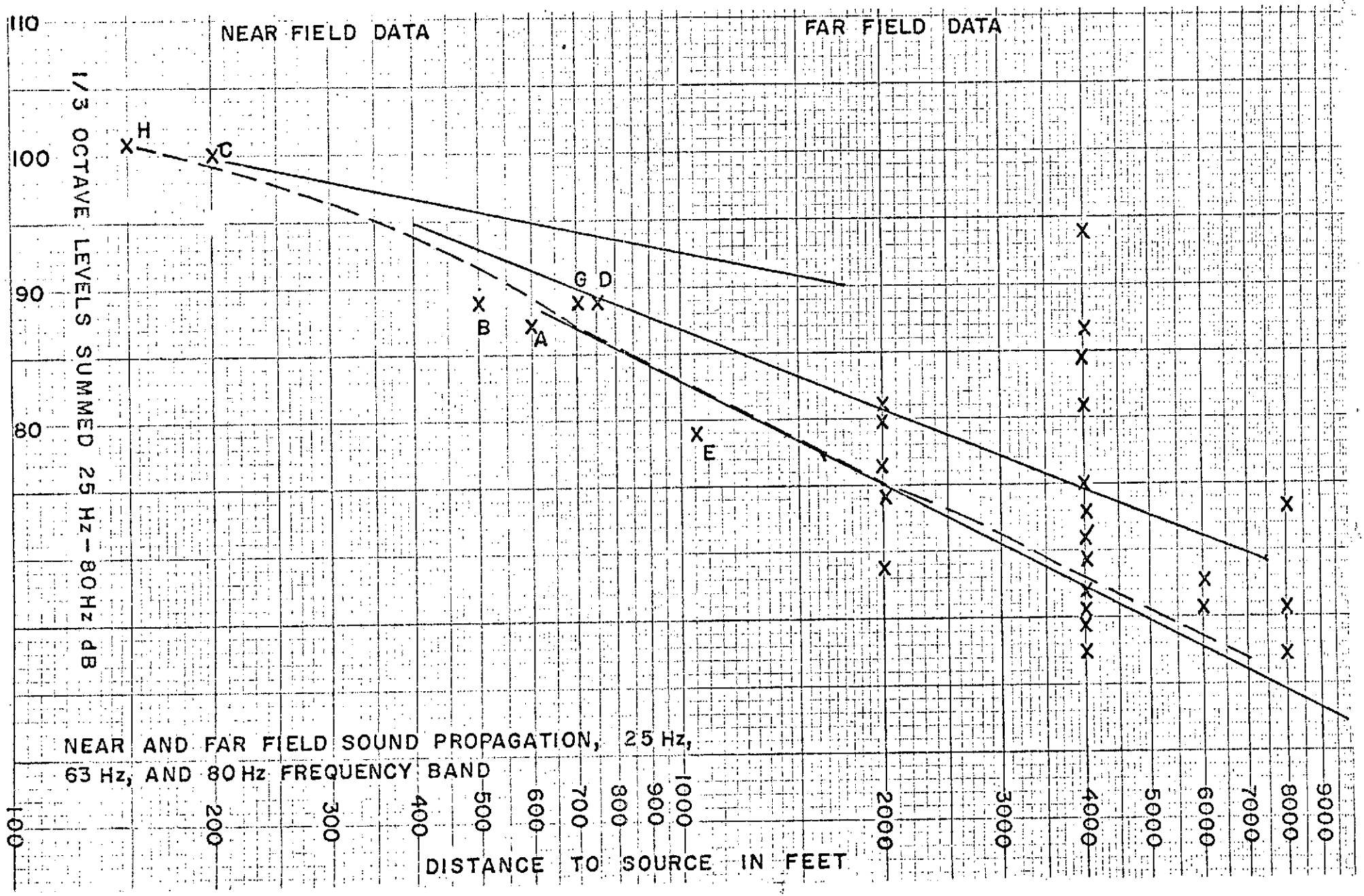
NEAR FIELD DATA
FAR FIELD DATA
1/3 OCTAVE LEVELS SUMMED 25 Hz - 80 Hz dB
110
100
90
80
H
C
G
D
B
A
E
NEAR AND FAR FIELD SOUND PROPAGATION, 25 Hz,
63 Hz, AND 80 Hz FREQUENCY BAND
100
200
300
400
500
600
700
800
900
1000
2000
3000
4000
5000
6000
7000
8000
9000
DISTANCE TO SOURCE IN FEET

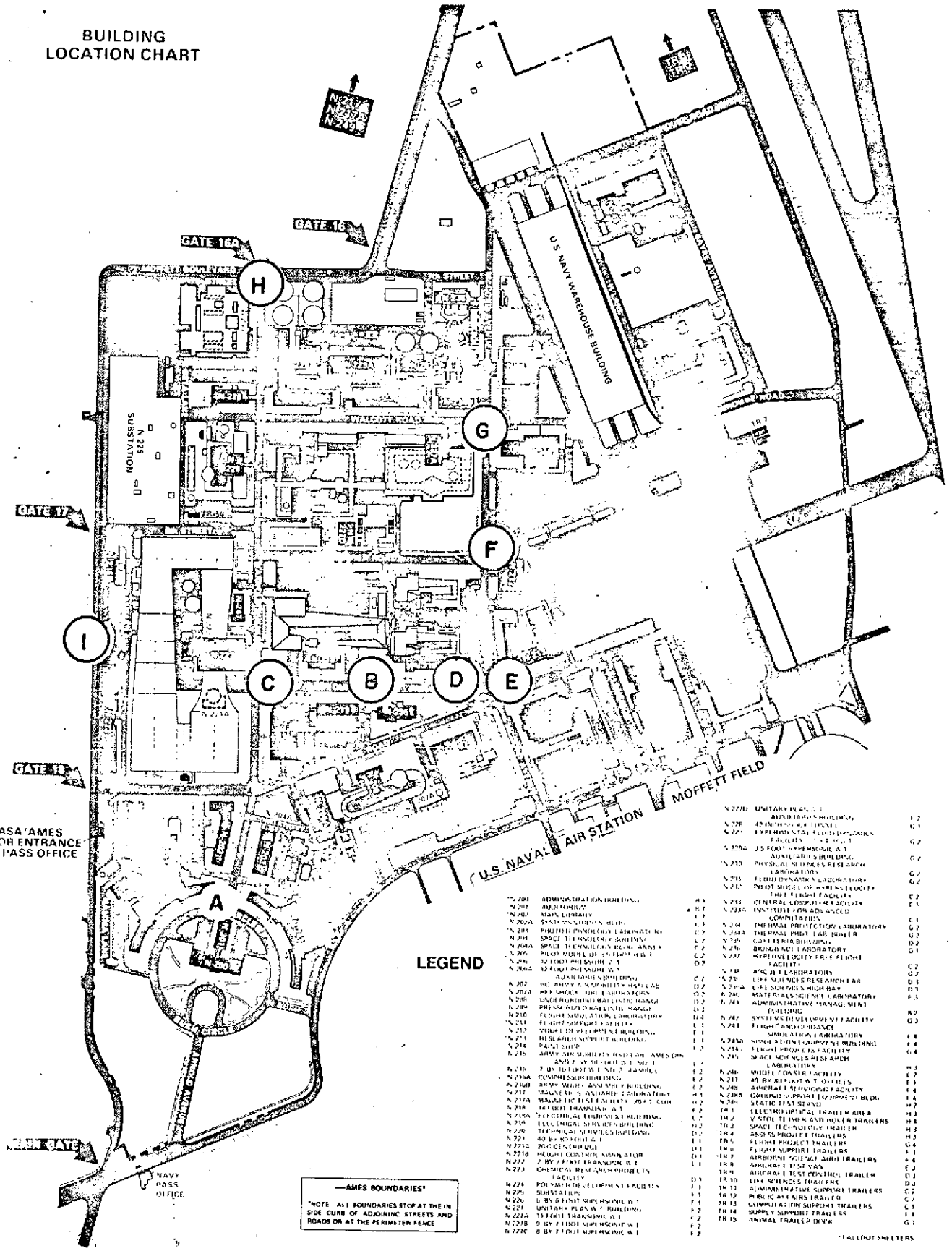

MEASUREMENT LOCATIONS USED FOR THE DETERMINATION OF AMBIENT LEVELS WITHIN THE AMES FACILITY

FIGURE 4-37

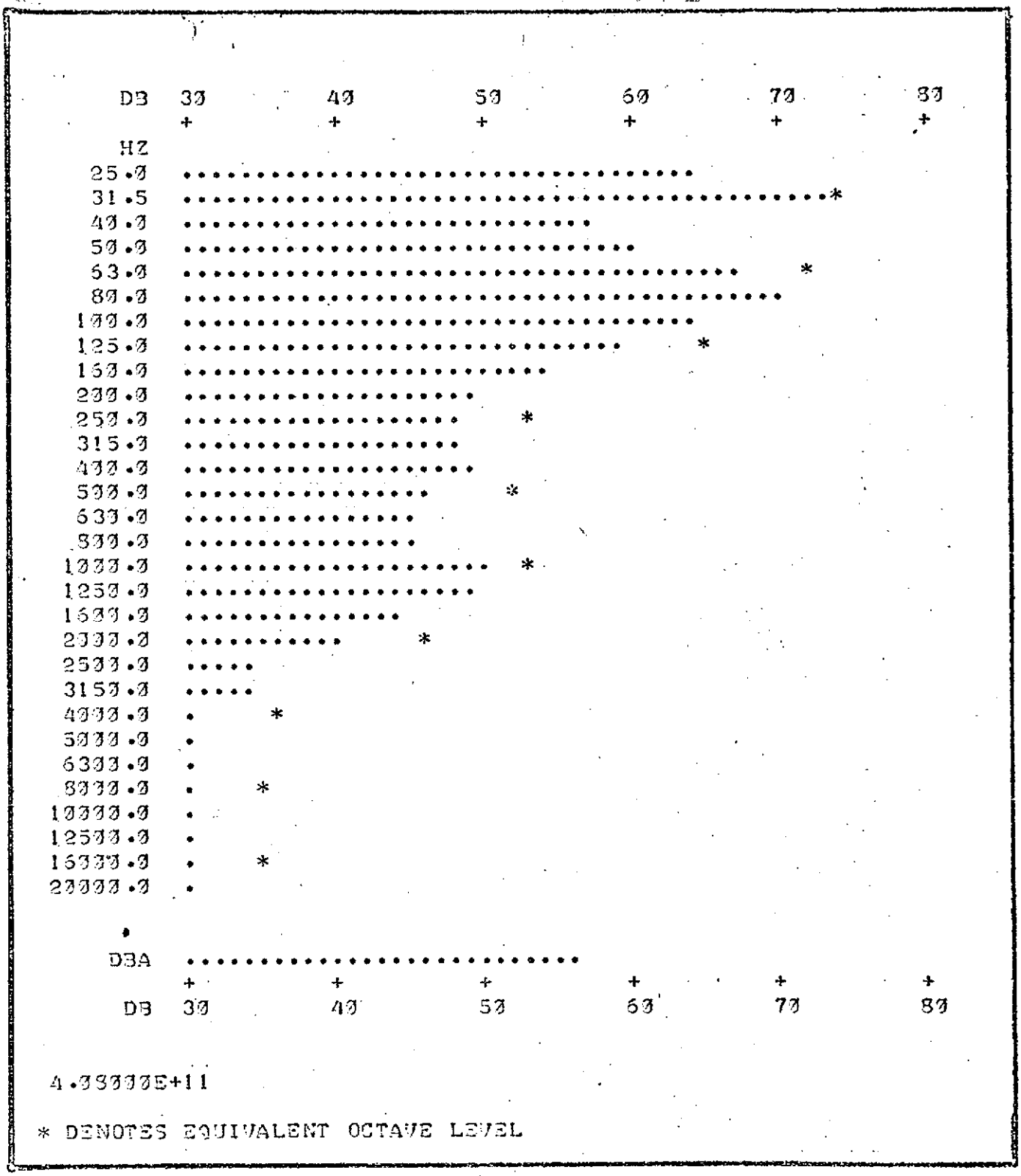

1/3 OCTAVE BAND AMBIENT LEVELS OBTAINED
AT NEAR FIELD POINT A (Fig. 4-37)

FIGURE 4-38

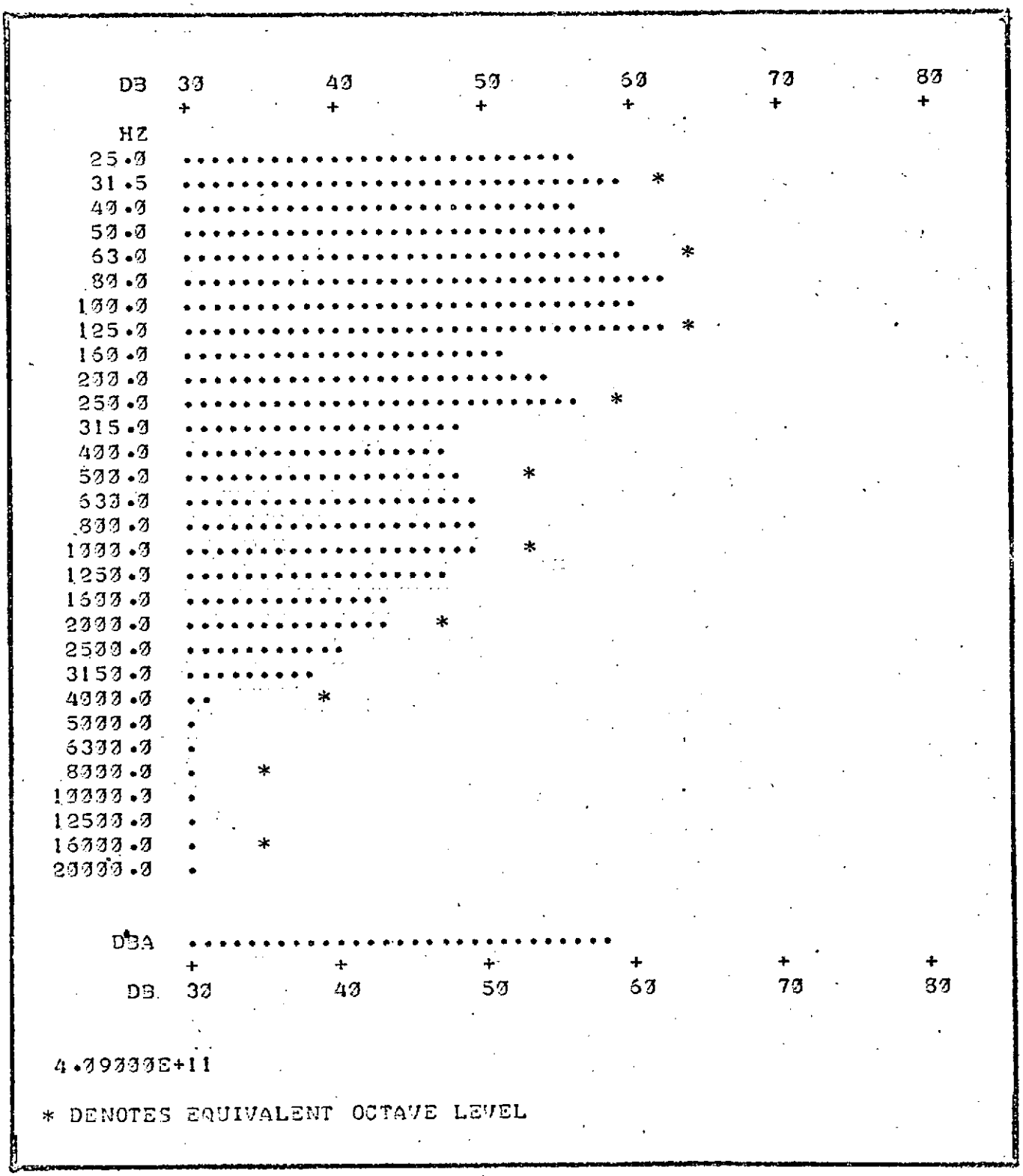

1/3 OCTAVE BAND AMBIENT LEVELS OBTAINED
AT NEAR FIELD POINT B (Fig. 4-37)

FIGURE 4-39

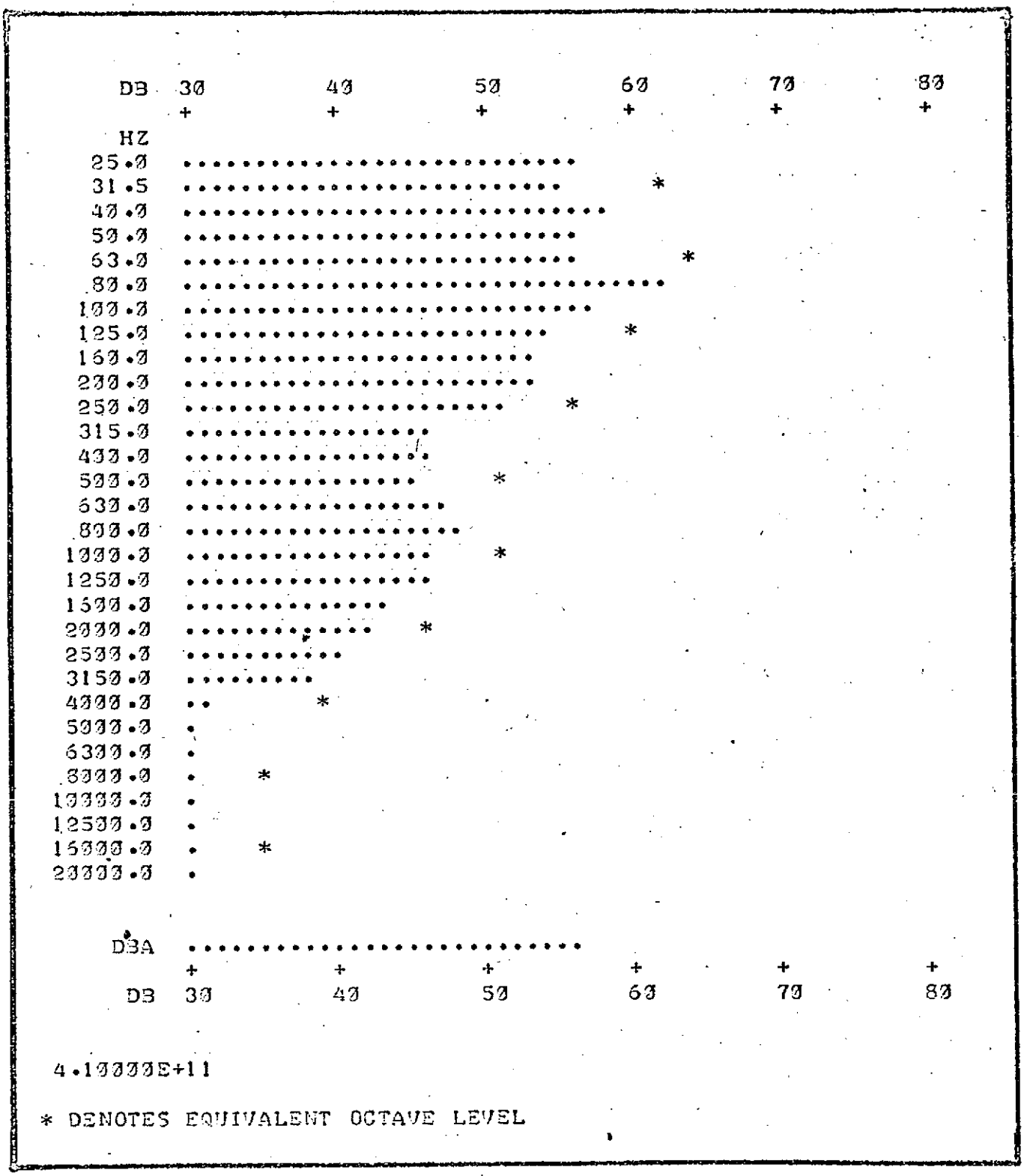

1/3 OCTAVE BAND AMBIENT LEVELS OBTAINED
AT NEAR FIELD POINT C (Fig. 4-37)

Figure 4-40

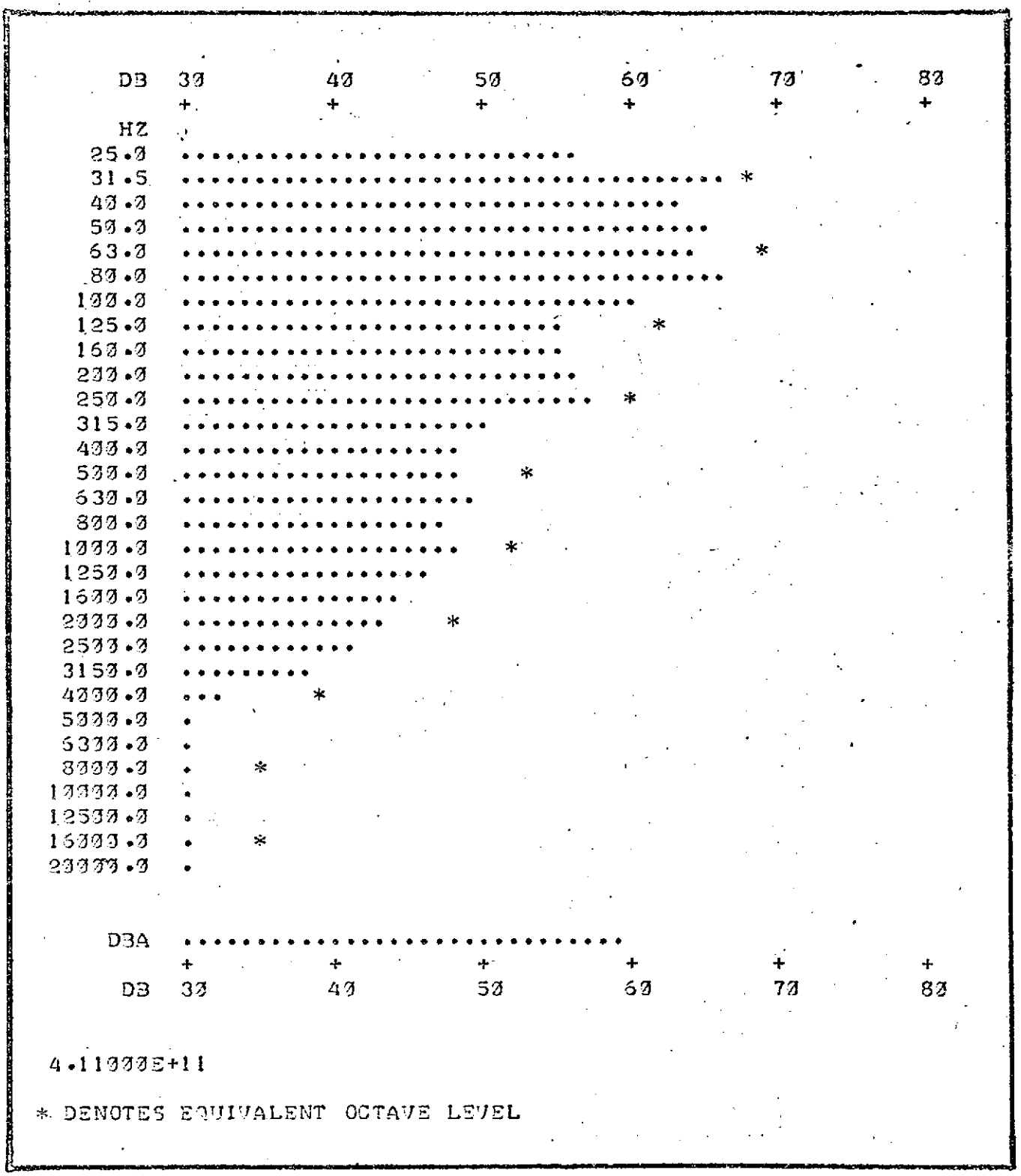

1/3 OCTAVE BAND AMBIENT LEVELS OBTAINED
AT NEAR FIELD POINT D (Fig. 4-37)

Figure 4-41

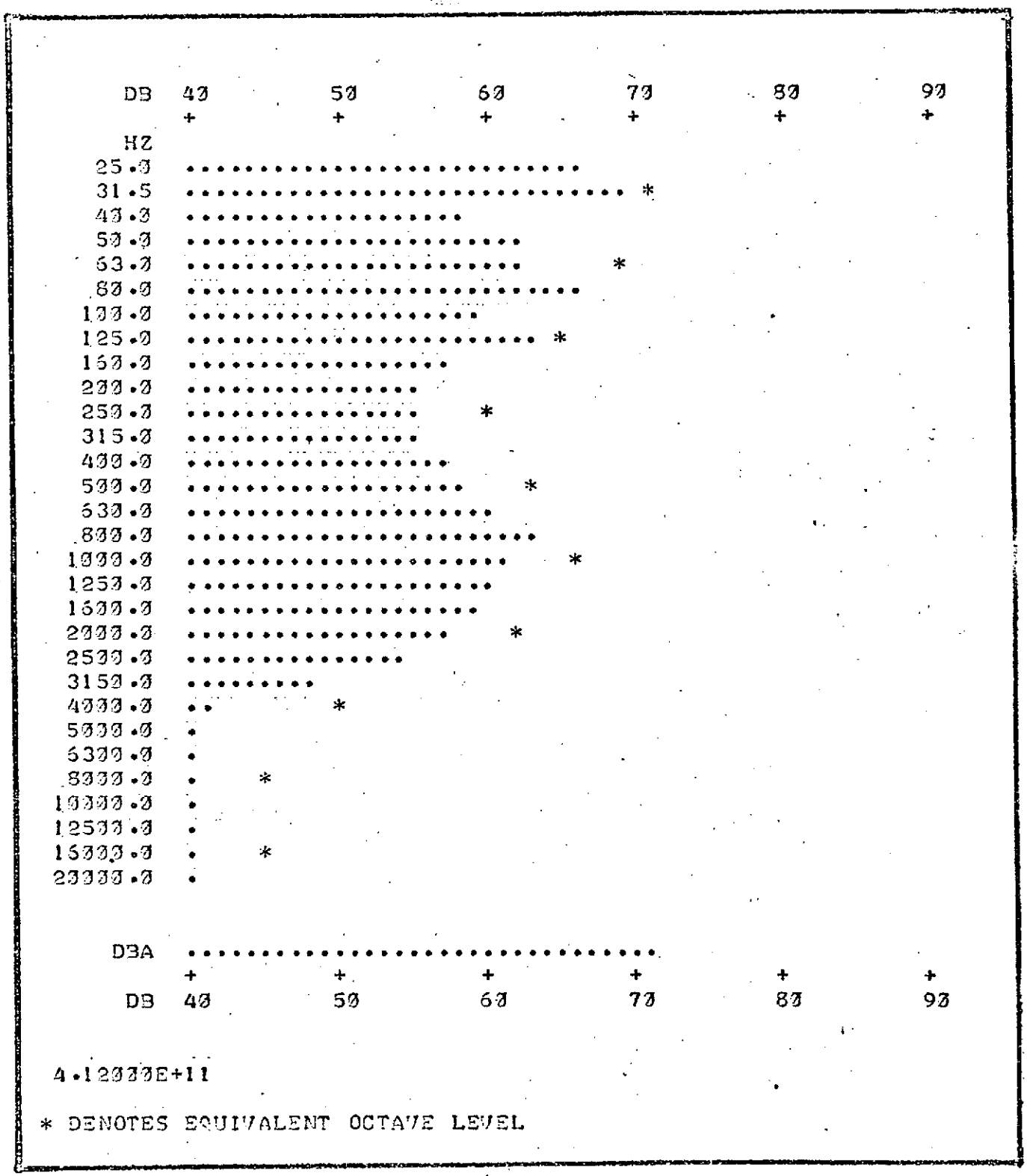

1/3 OCTAVE BAND AMBIENT LEVELS OBTAINED
AT NEAR FIELD POINTS E & F (Fig. 4-37)

Figure 4-42

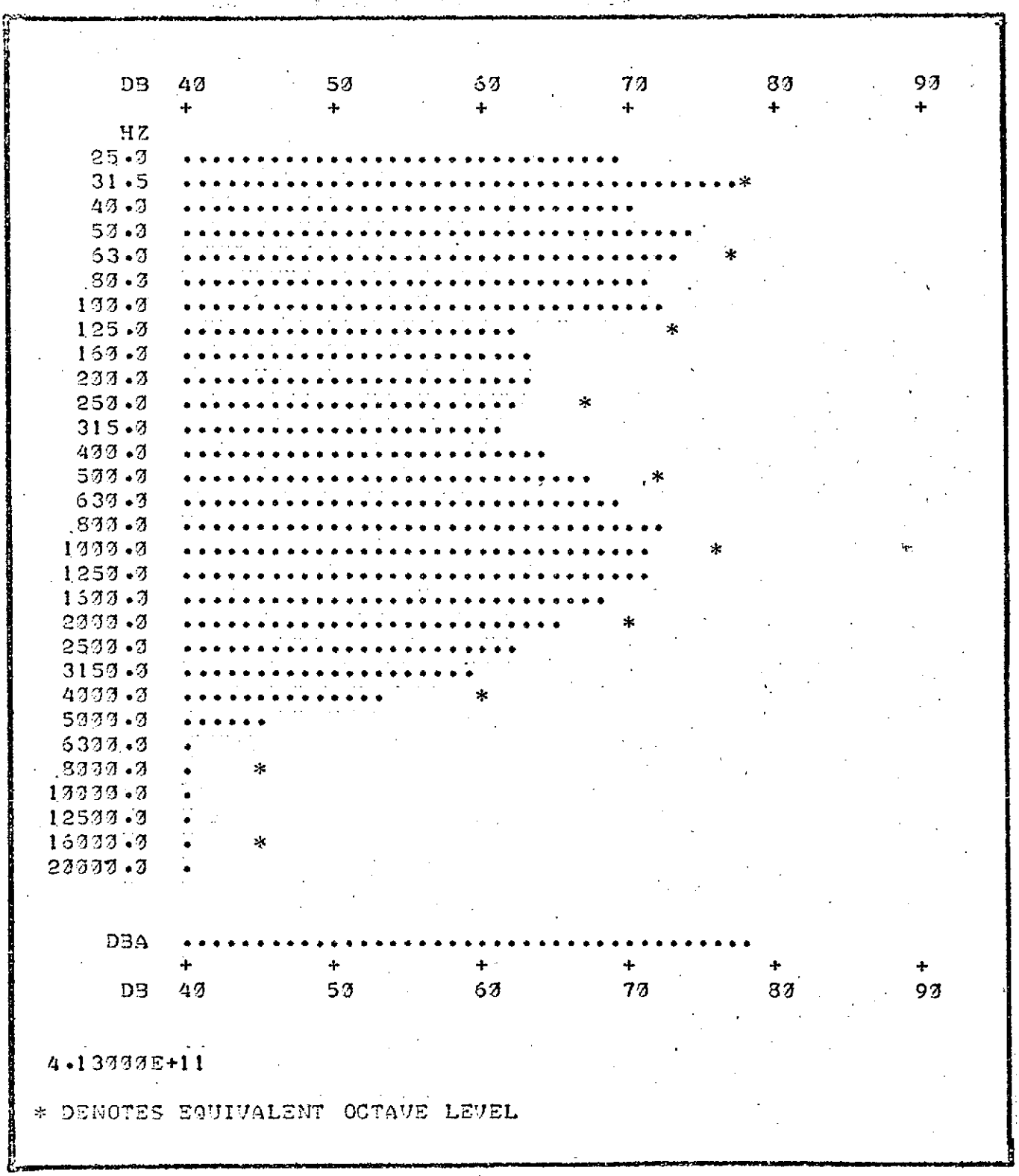

1/3 OCTAVE BAND AMBIENT LEVELS OBTAINED
AT NEAR FIELD POINT G (Fig. 4-37)

Figure 4-43

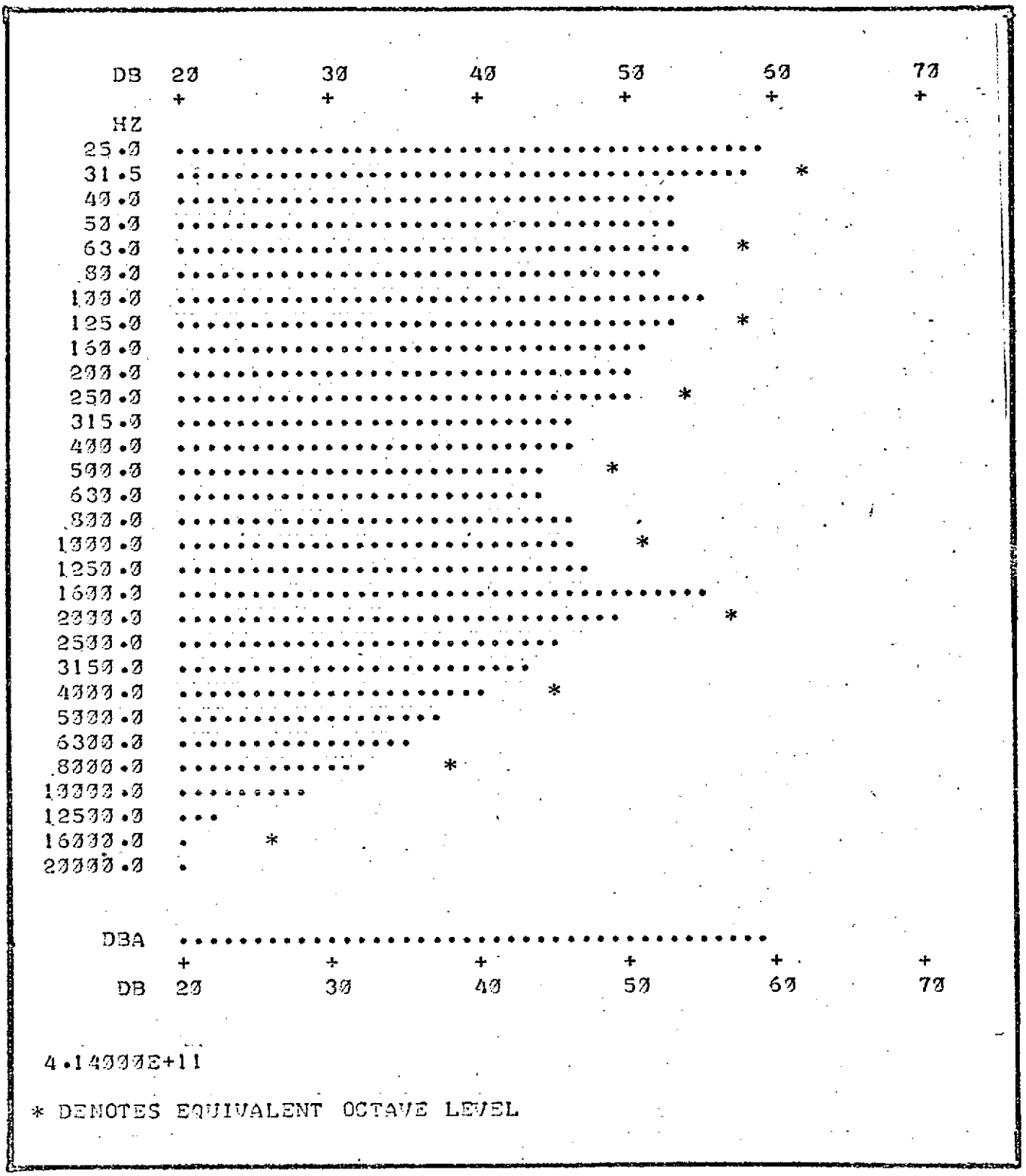

1/3 OCTAVE BAND AMBIENT LEVELS OBTAINED
AT NEAR FIELD POINT H (Fig. 4-37)

FIGURE 4-44

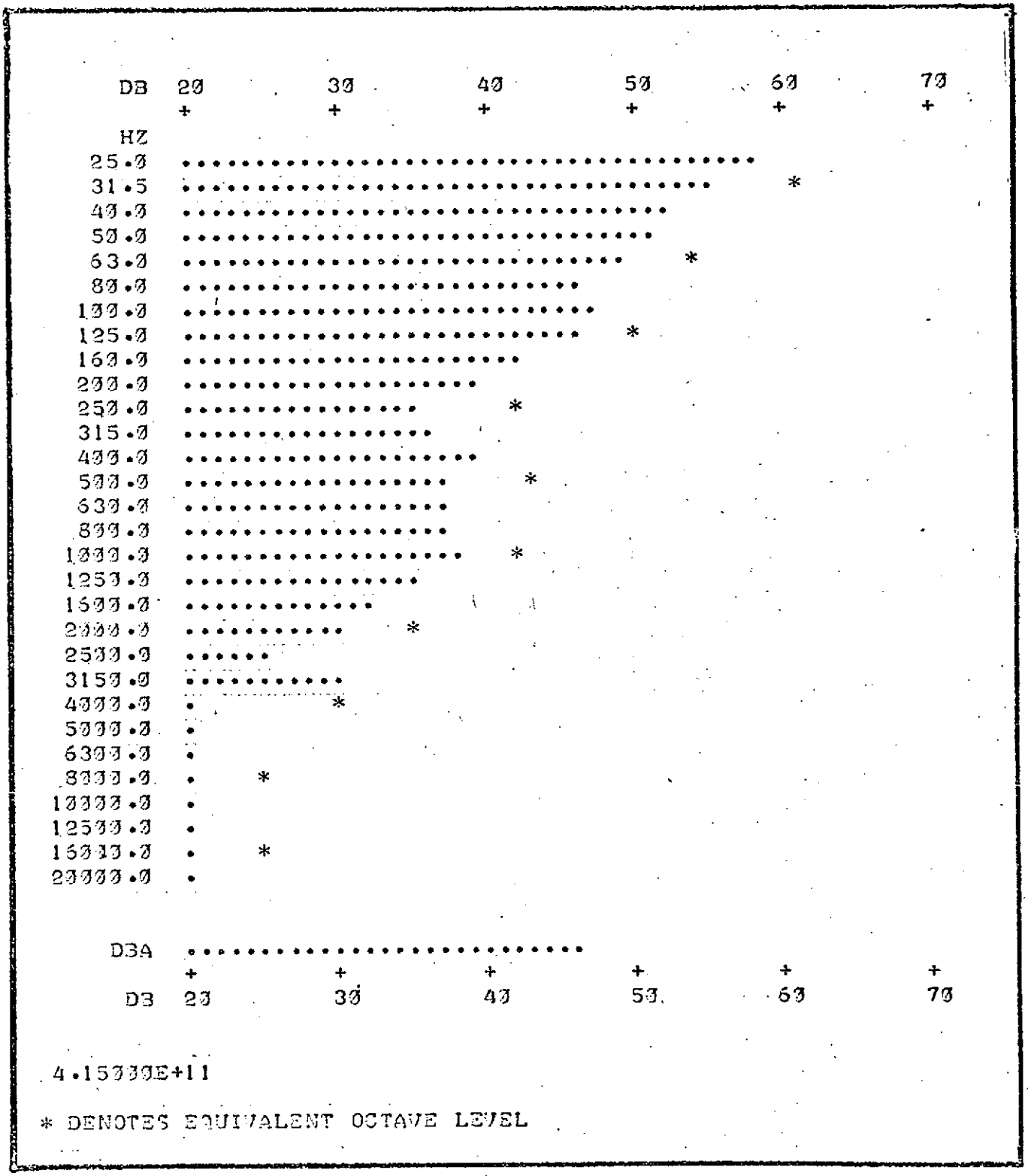

1/3 CTAVE BAND AMBIENT LEVELS OBTAINED
AT NEAR FIELD POINT I (Fig. 4-37)

Figure 4-45

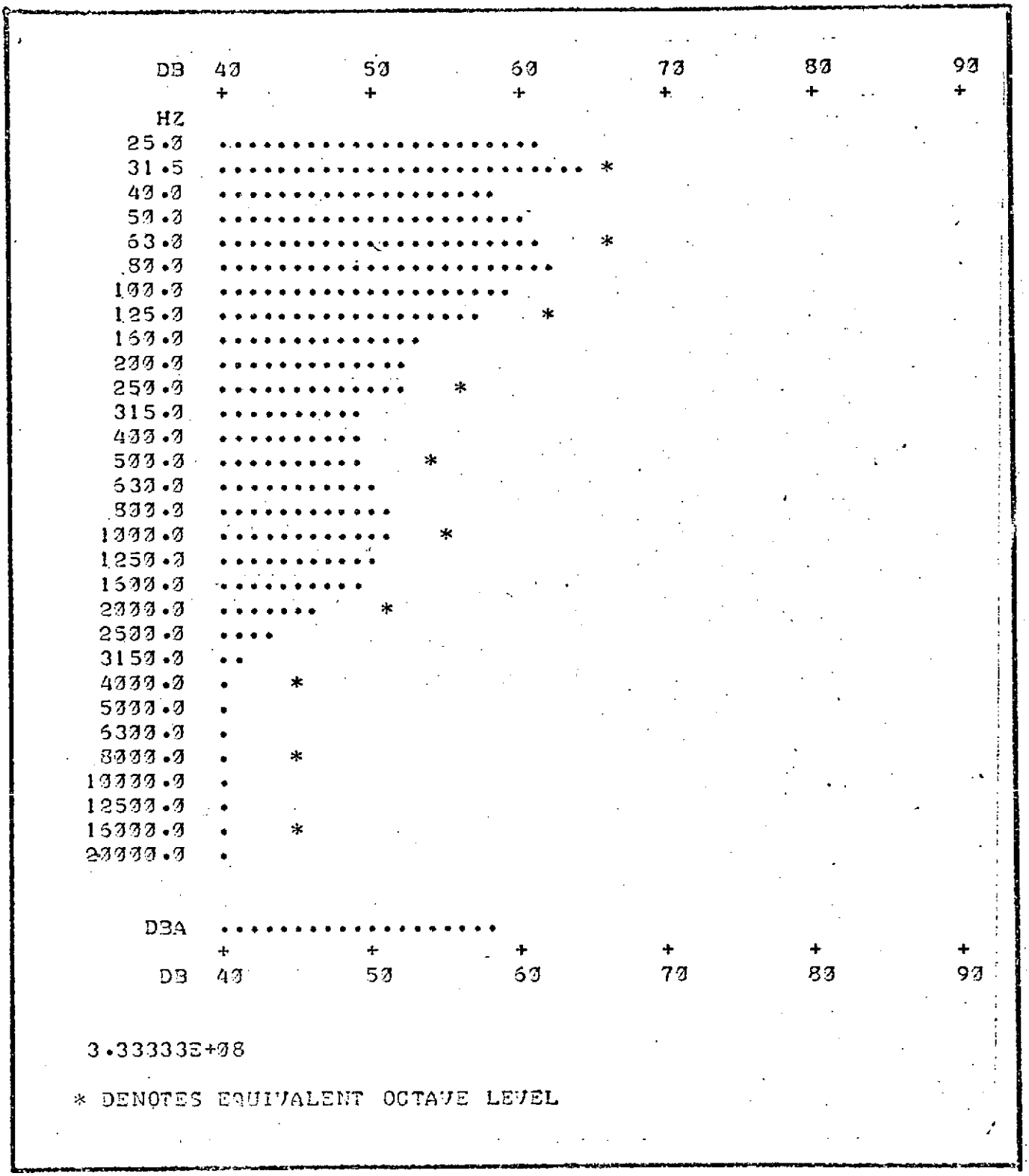

MEAN AMBIENT LEVEL NEAR FIELD

FIGURE 4-46

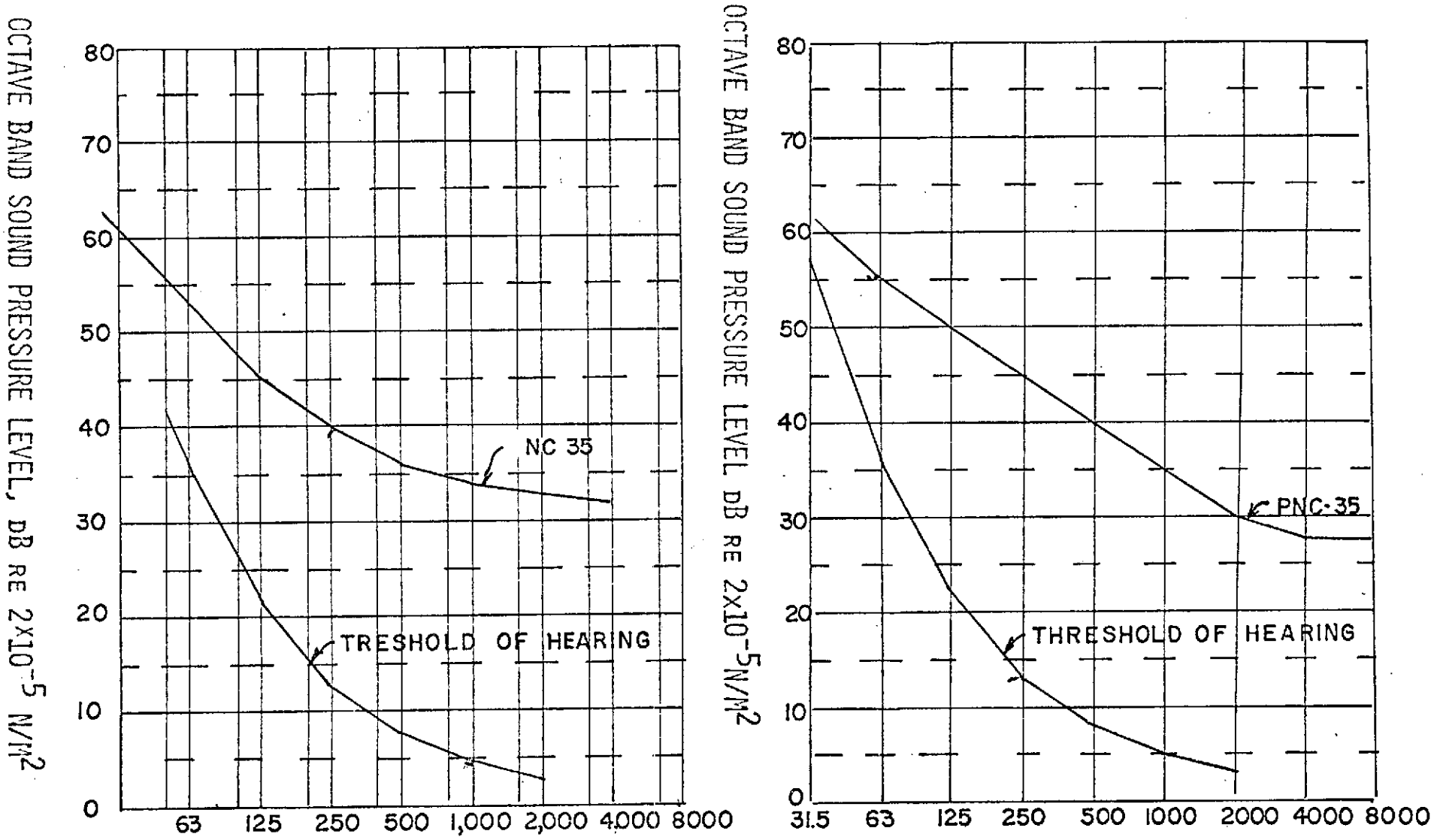

PERFERRED NOISE CRITERIA

FIGURE 4-47

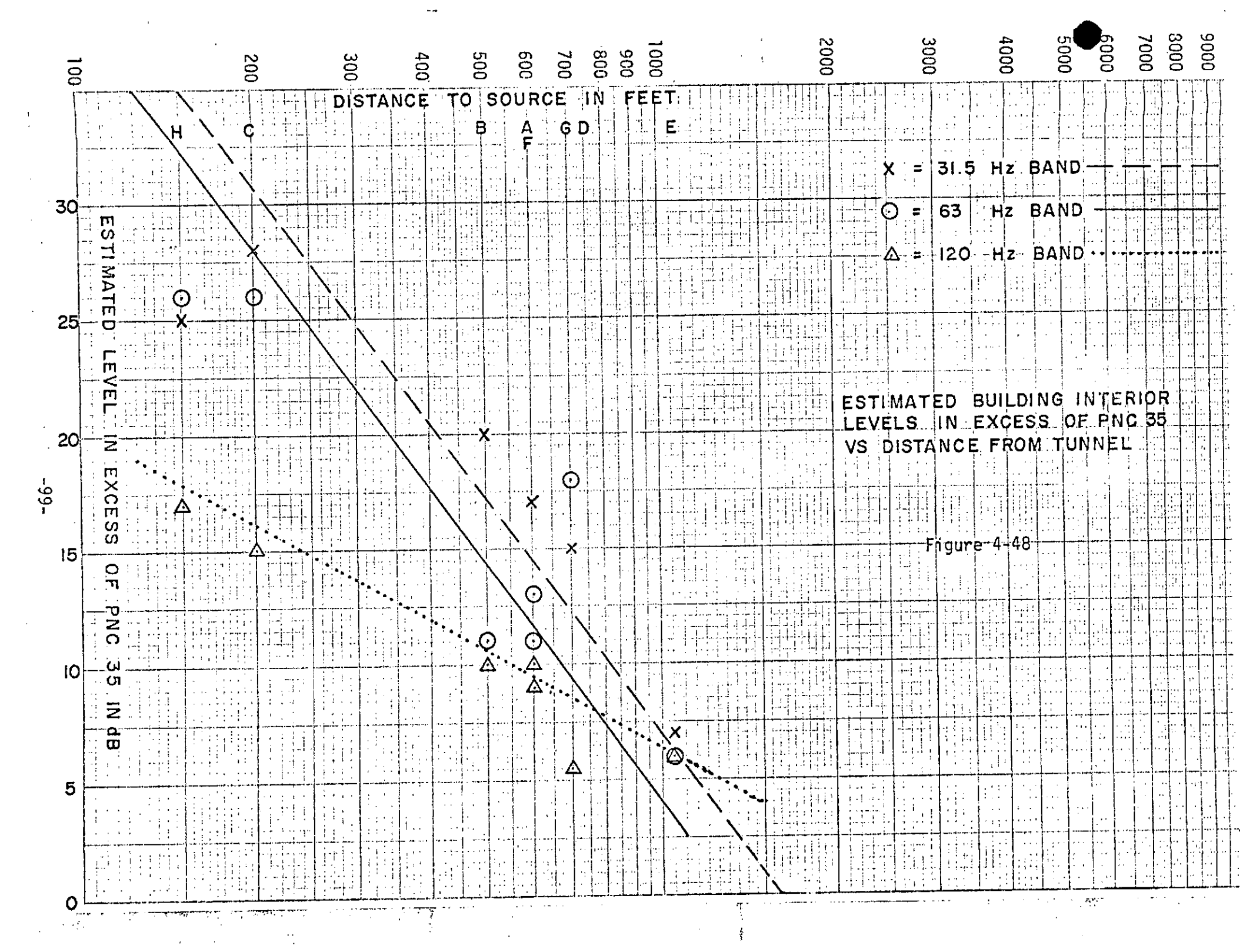
DISTANCE TO SOURCE IN FEET
100
200
300
400
500
600
700
800
900
1000
2000
3000
4000
5000
6000
7000
8000
9000
H
C
B
A
F
G
D
E
X = 31.5 Hz BAND
⊙ = 63 Hz BAND
△ = 120 Hz BAND
ESTIMATED BUILDING INTERIOR LEVELS IN EXCESS OF PNC 35 VS DISTANCE FROM TUNNEL
ESTIMATED LEVEL IN EXCESS OF PNC 35 IN dB
0
5
10
15
20
25
30

Figure 4-48

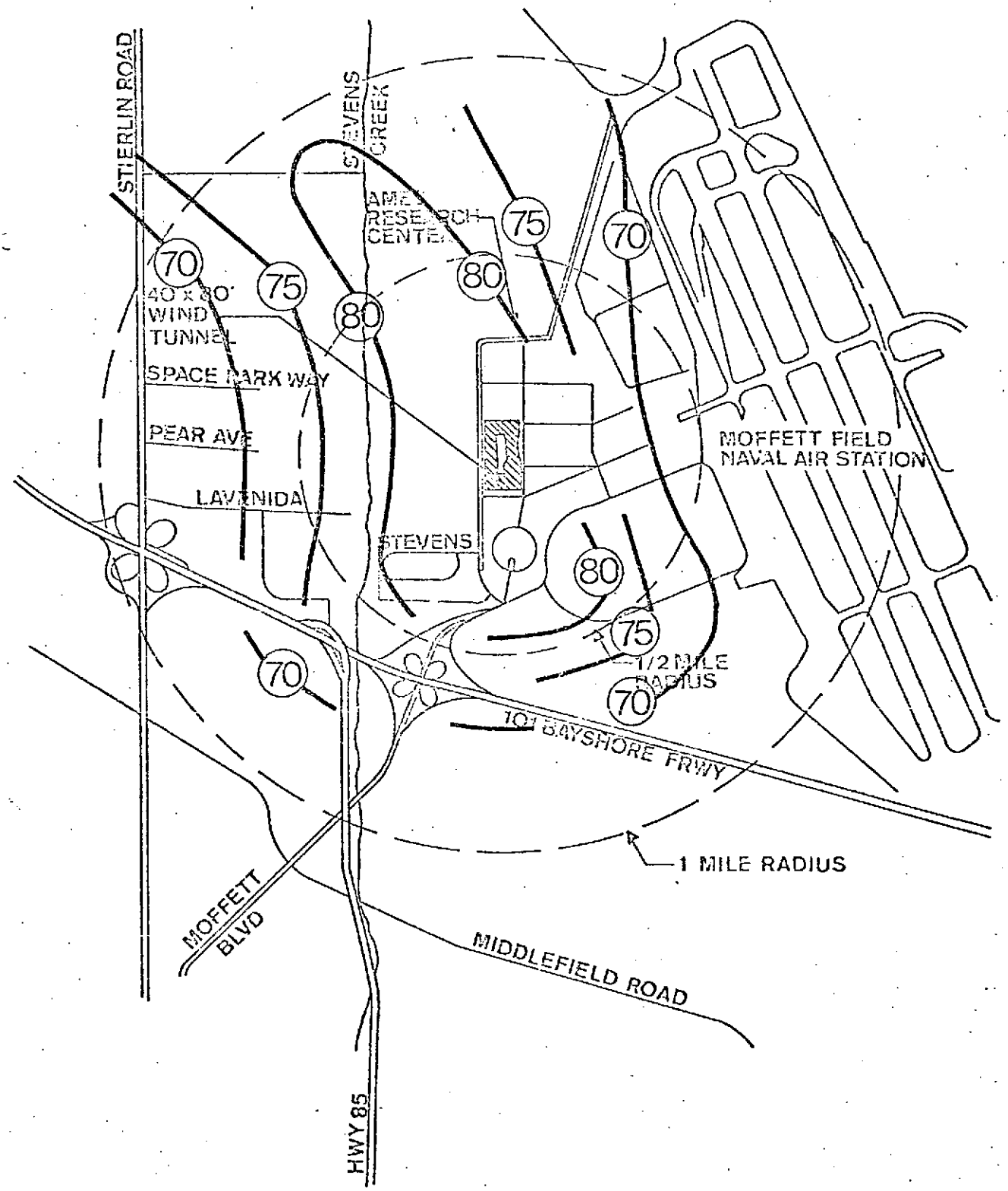

FAR FIELD NOISE CONTOURS

31.5 Hz AND 63 Hz OCTAVE BANDS

q_u=105

FIGURE 4-49

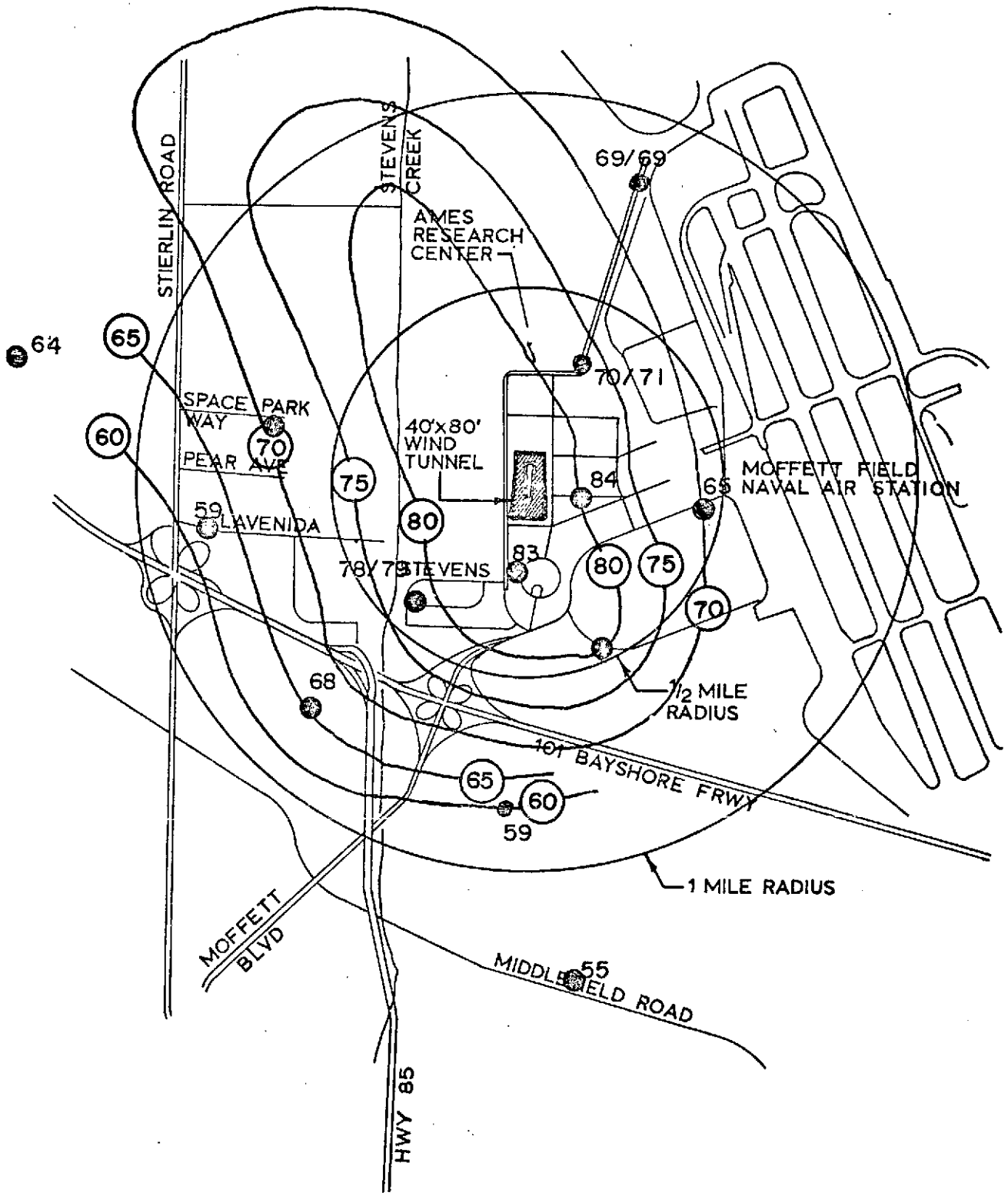

FAR FIELD NOISE CONTOURS
25 Hz OCTAVE BAND
q_u = 105 p.s.f.

Figure 4-50

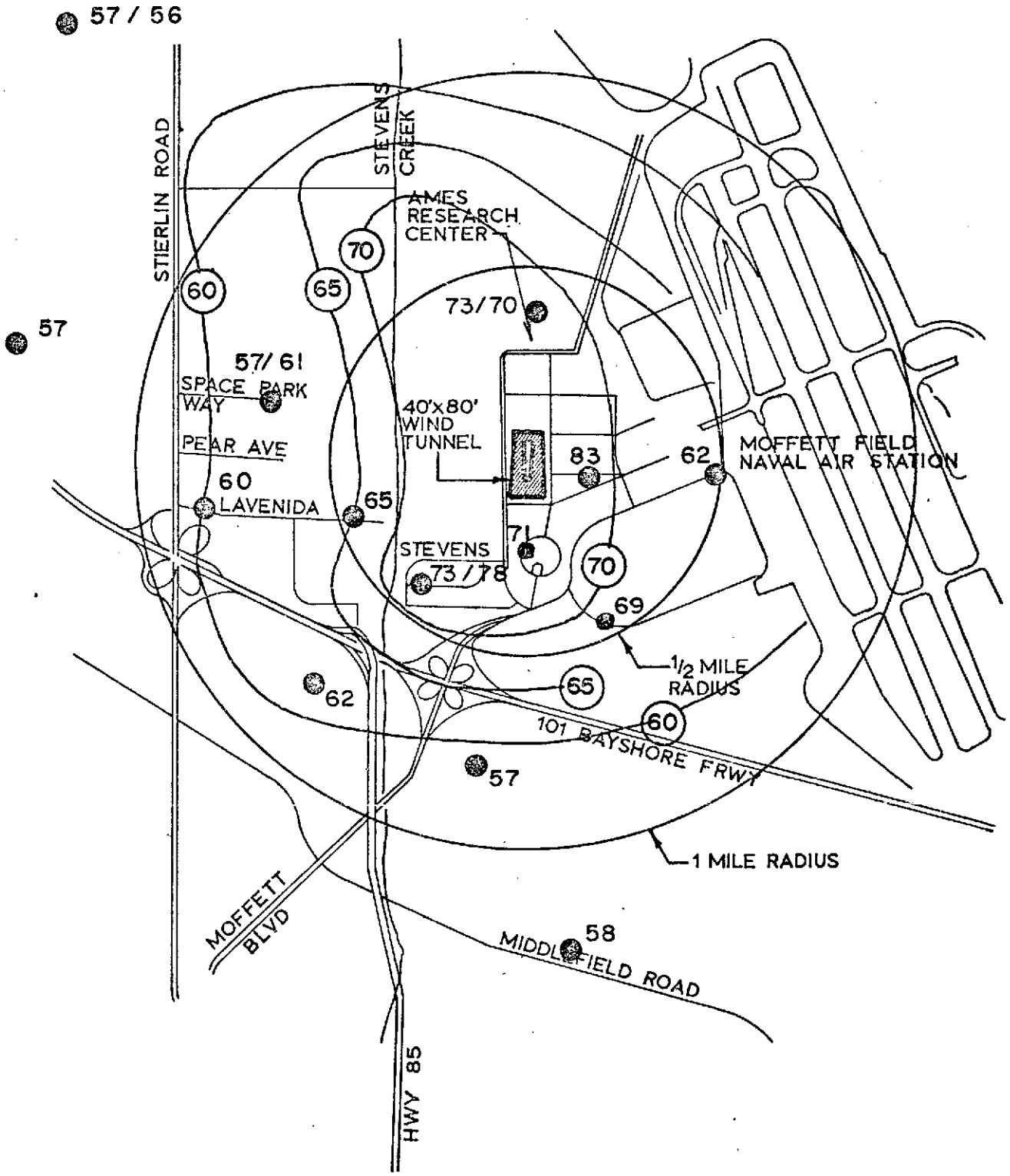

FAR FIELD NOISE CONTOURS
50 Hz 1/3 OCTAVE BAND

q_u = 105 p.s.f.

Figure 4-51

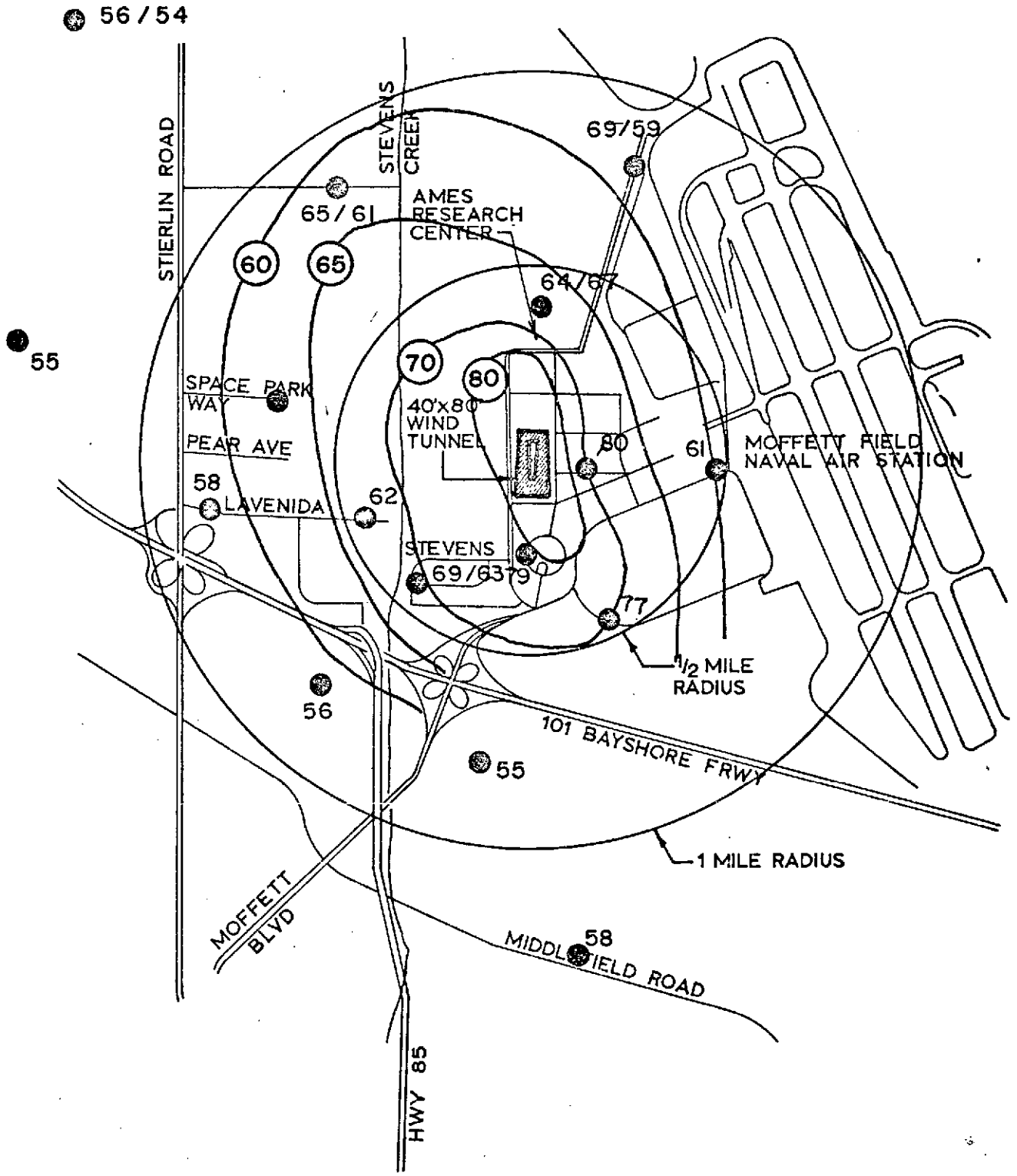

FAR FIELD NOISE CONTOURS
80 Hz 1/3 OCTAVE BAND
q_u = 105 p.s.f.

Figure 4-52

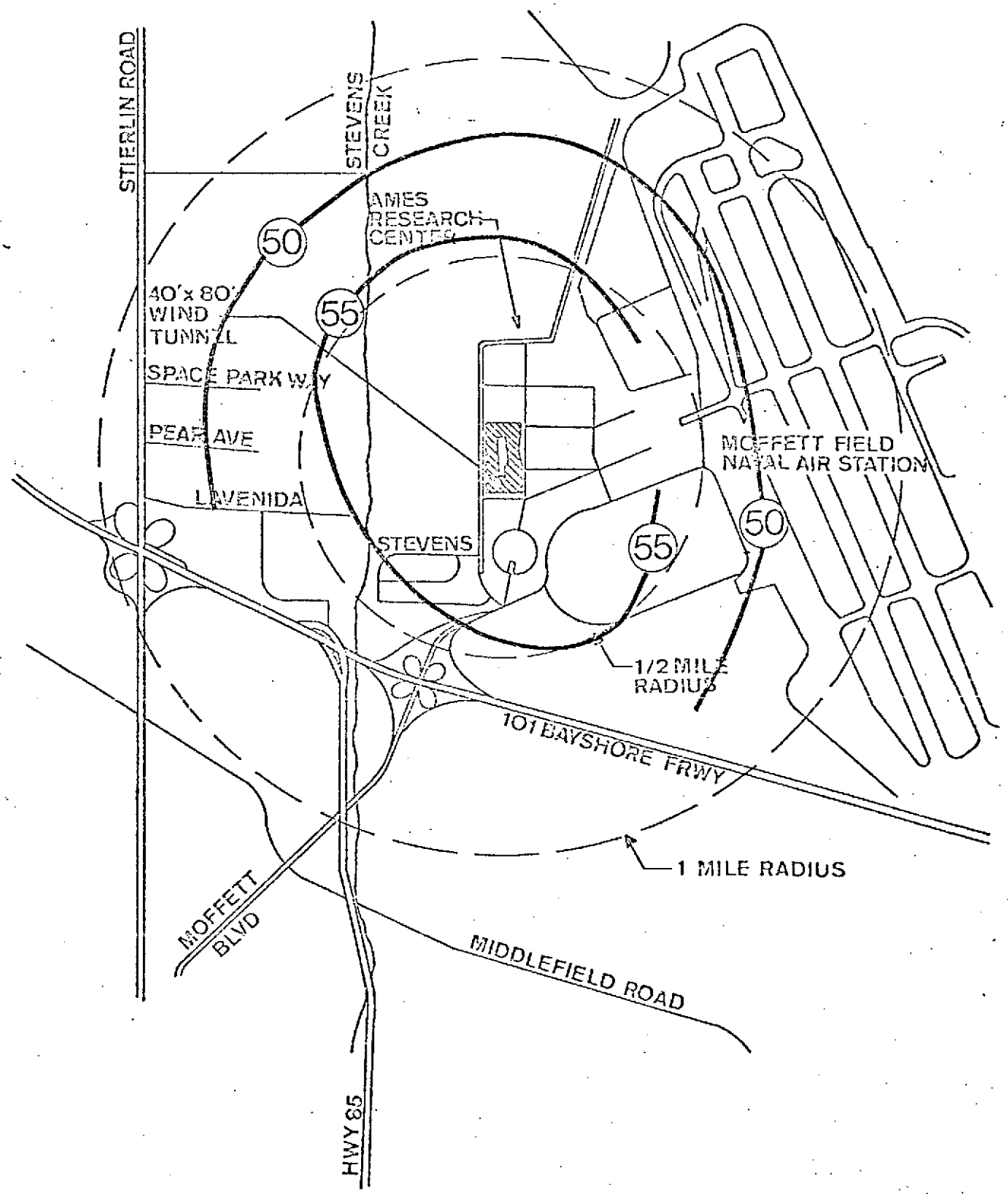

FAR FIELD dBA NOISE CONTOURS, q_u=105

FIGURE 4.53

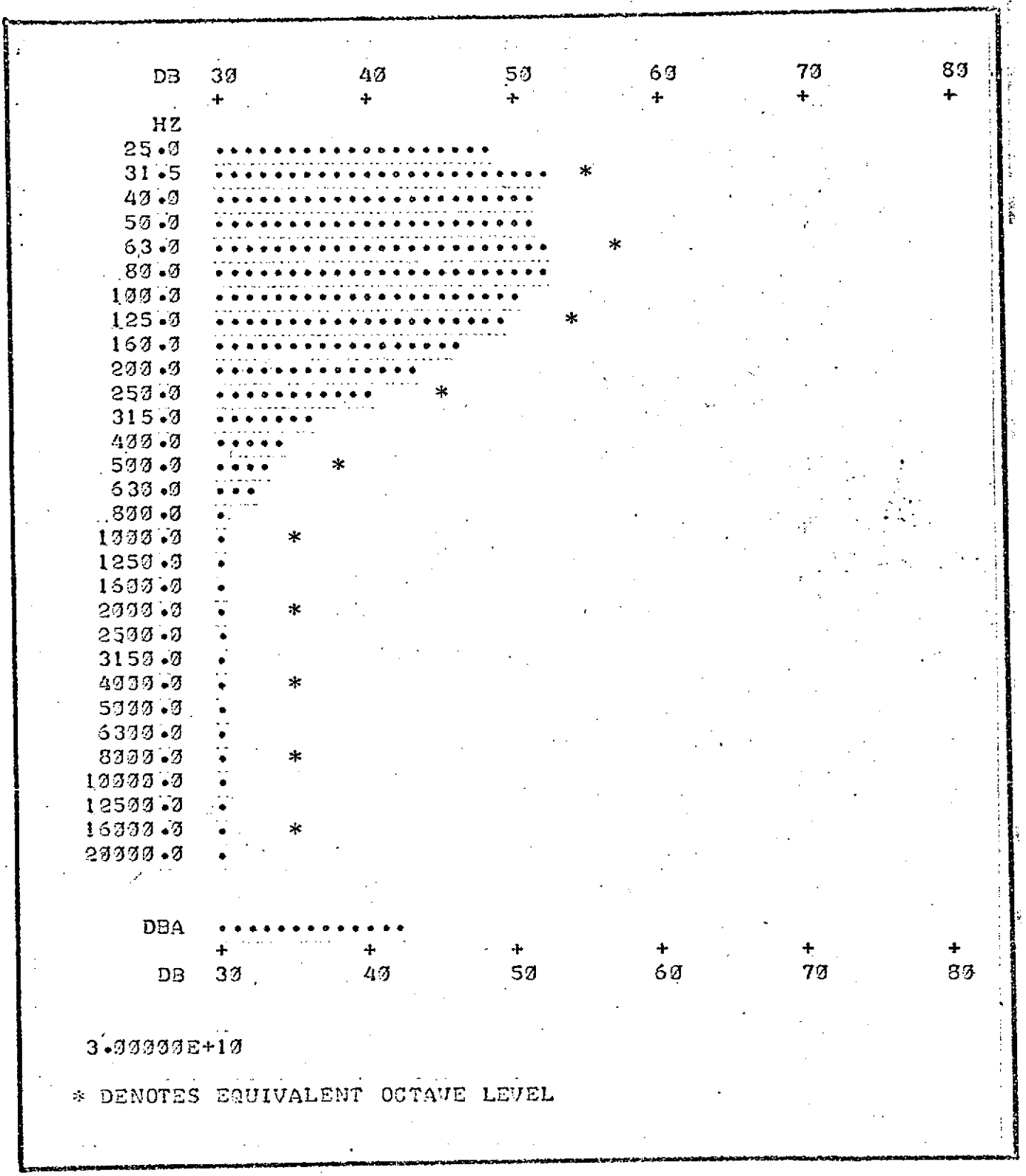

FAR FIELD AMBIENT SPECTRUM POSITION 3 (Fig. 4-53)
RECORDED 12/9/73

Figure 4-54

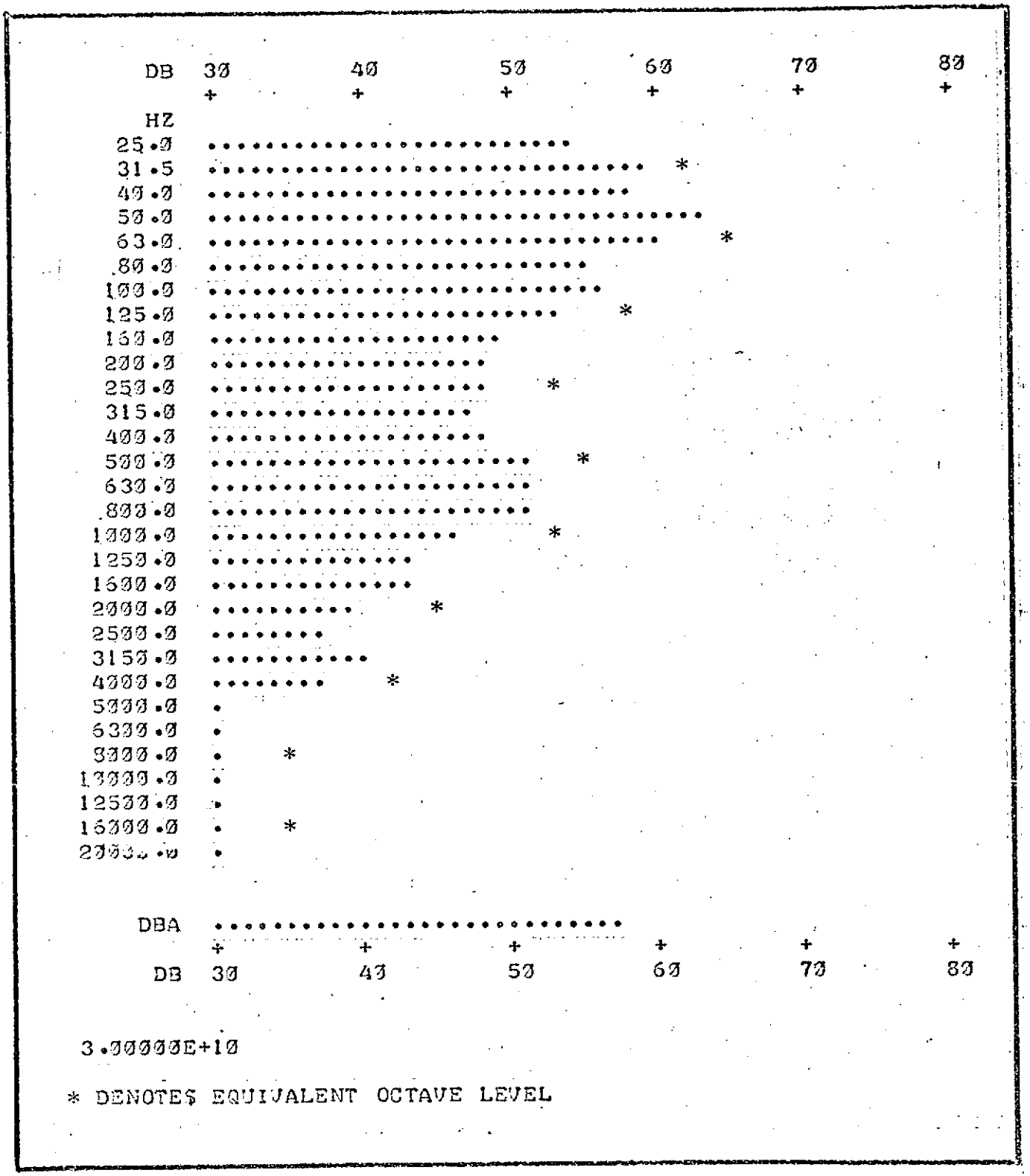

FAR FIELD AMBIENT SPECTRUM, POSITION 3 (Fig. 4-53)
RECORDED 3/13/74

Figure 4-55

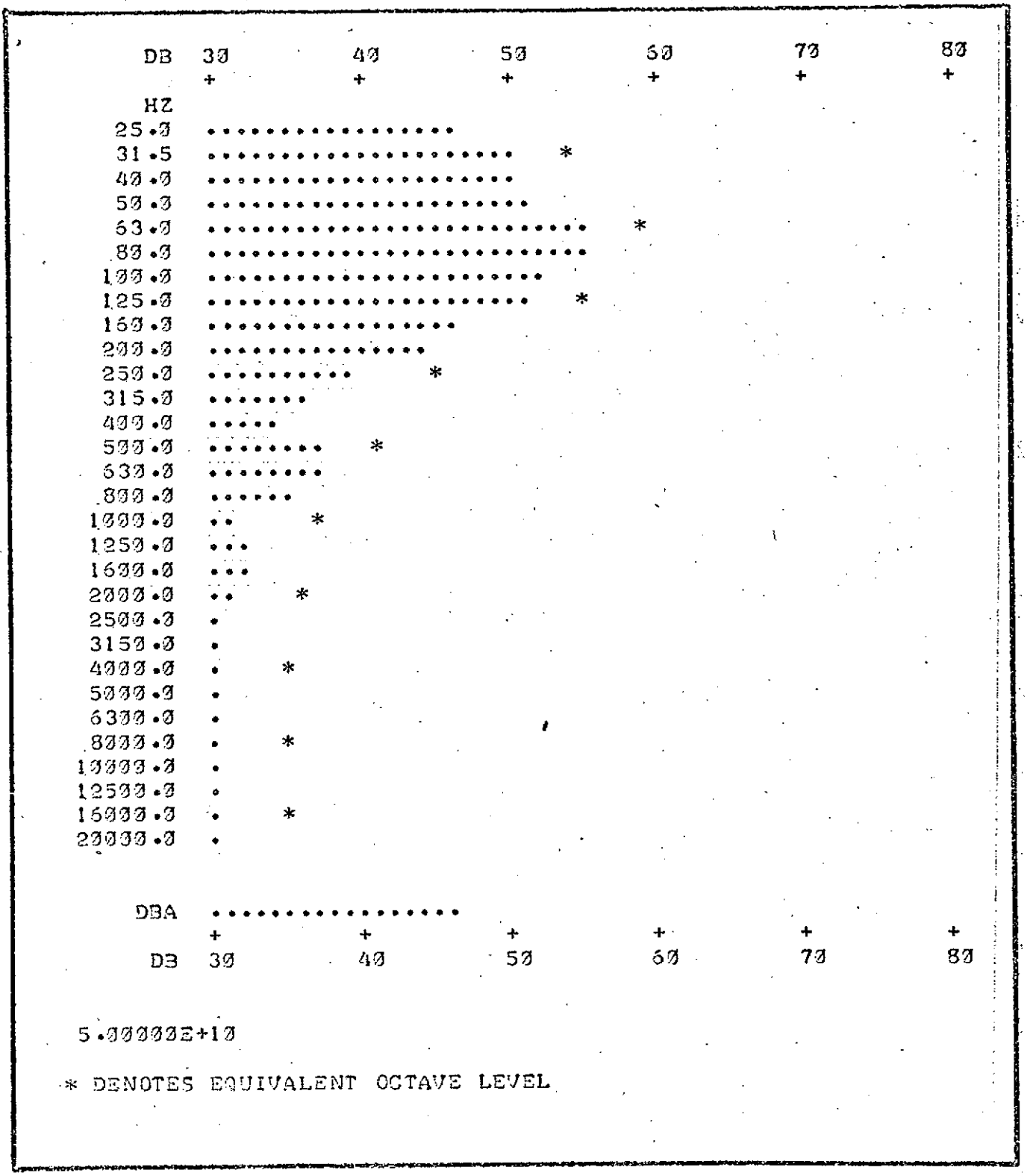

FAR FIELD AMBIENT SPECTRUM, POSITION 5A (Fig. 4-53)
RECORDED 12/8/73

Figure 4-56

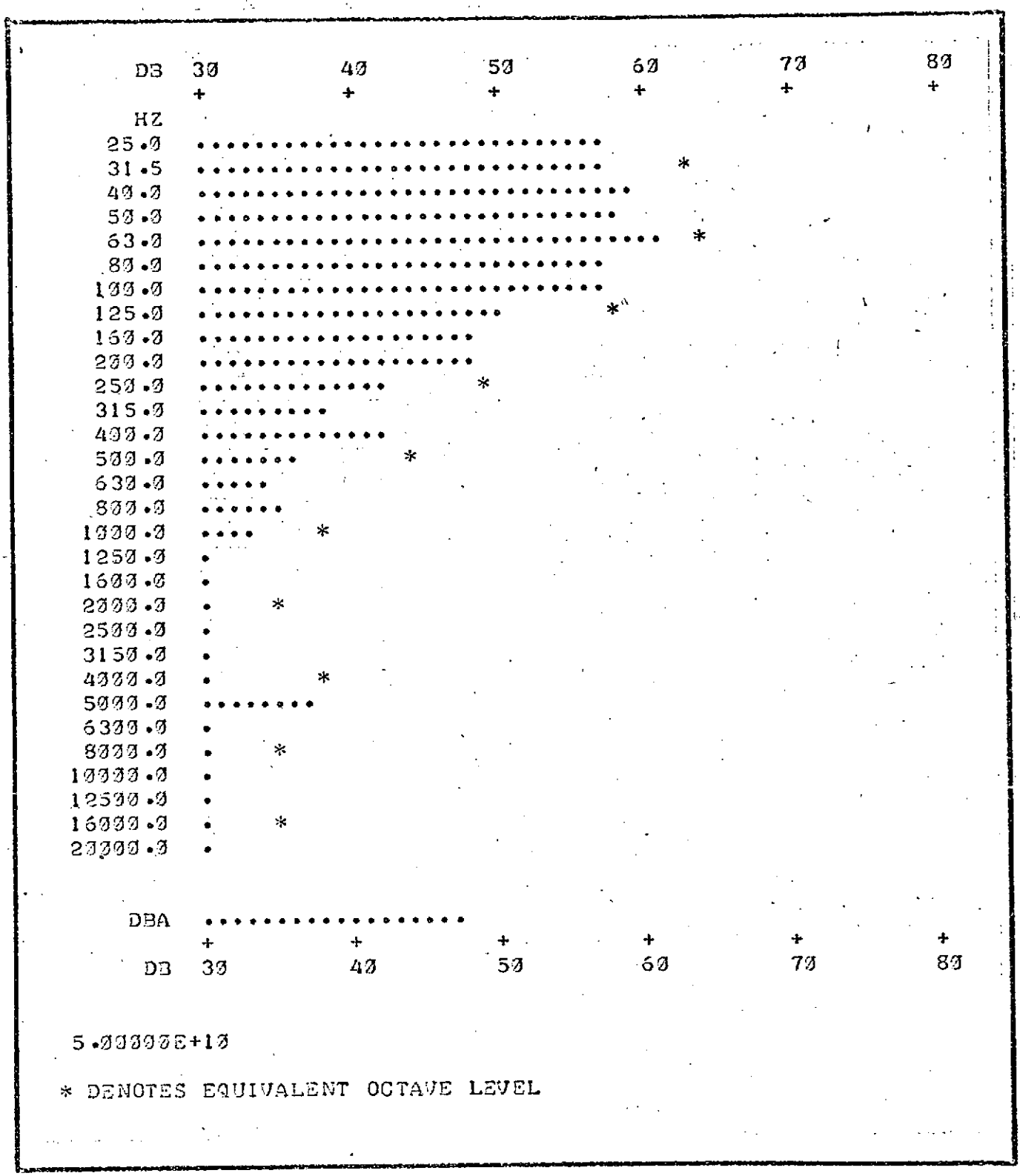

FAR FIELD AMBIENT SPECTRUM, POSITION 5A (Fig. 4-53)
RECORDED 3/13/74

Figure 4-57

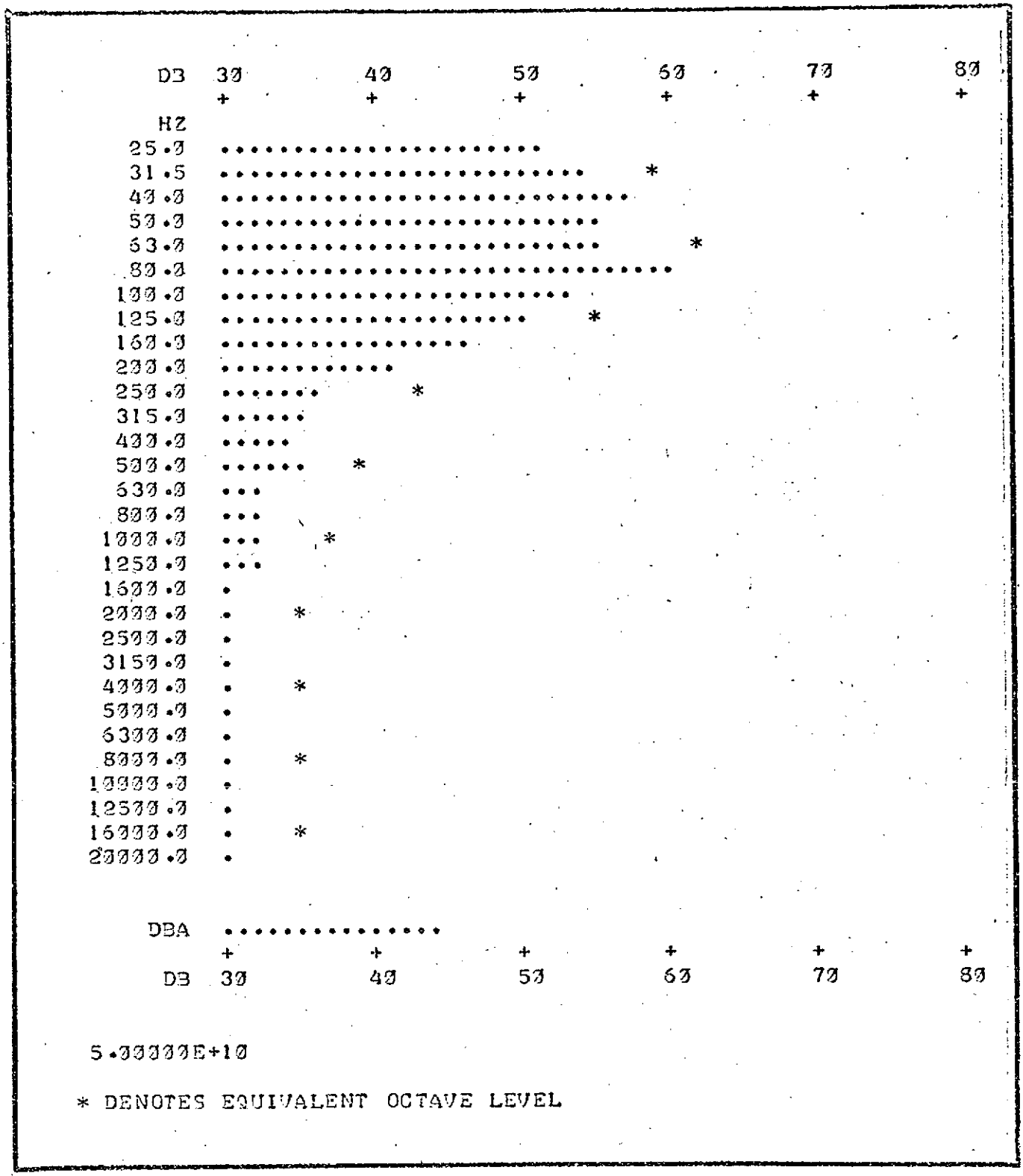

FAR FIELD AMBIENT SPECTRUM, POSITION 5B (Fig. 4-53)
RECORDED 12/8/73

Figure 4-58

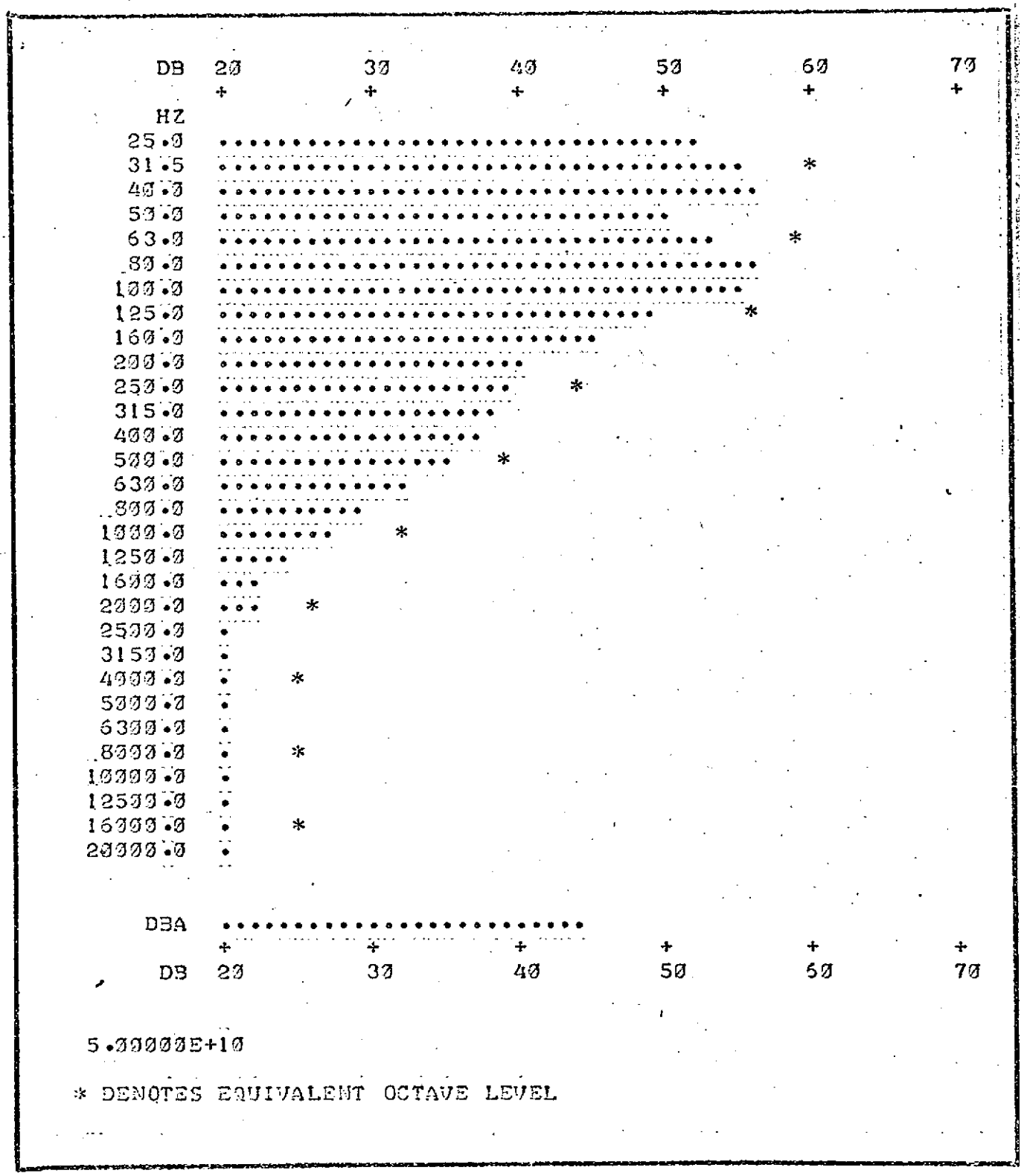

FAR FIELD AMBIENT SPECTRUM, POSITION 5B (Fig. 4-53)
RECORDED 12/9/73

Figure 4-59

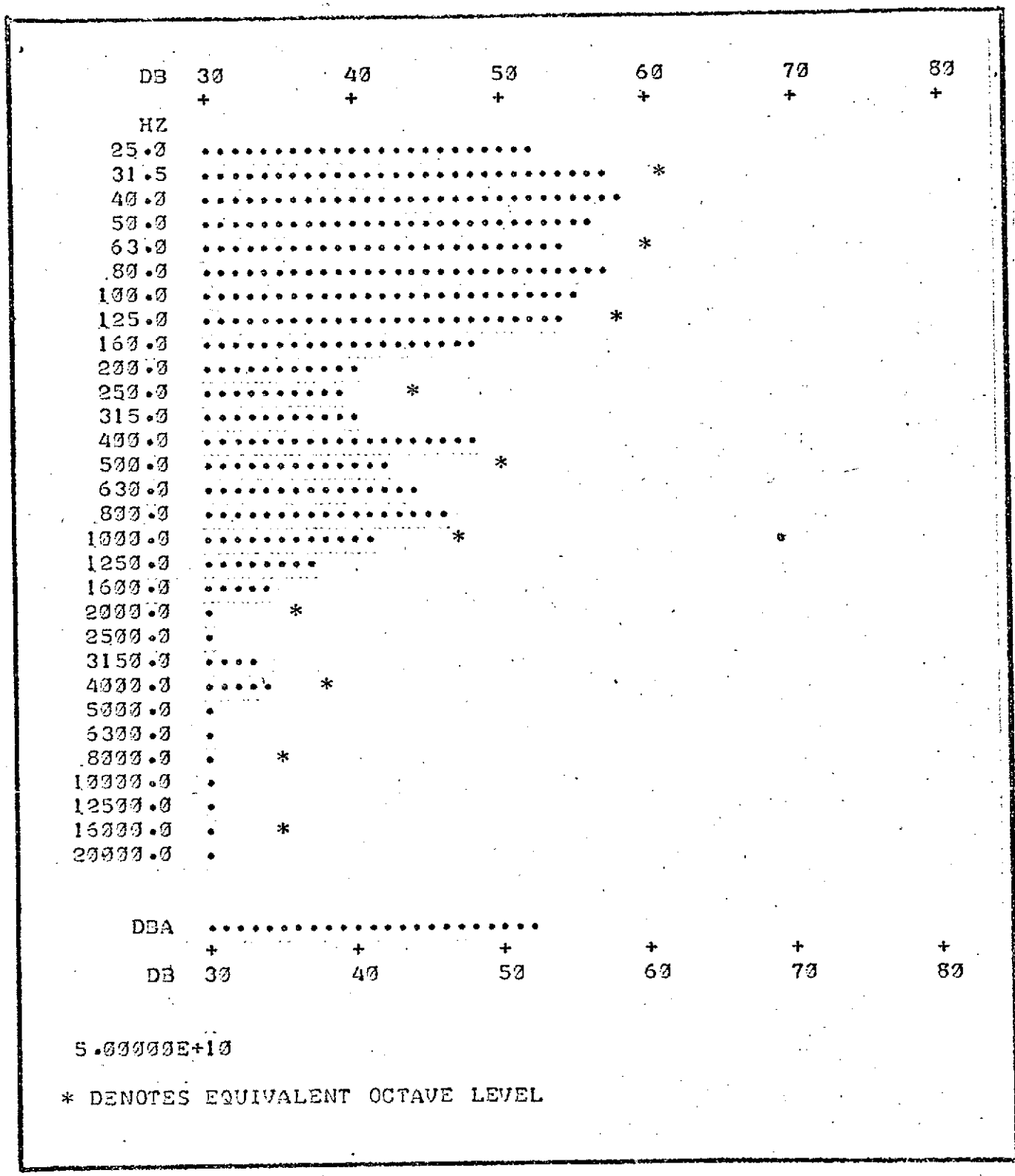

FAR FIELD AMBIENT SPECTRUM, POSITION 5B (Fig. 4-53)
RECORDED 3/13/74

Figure 4-60

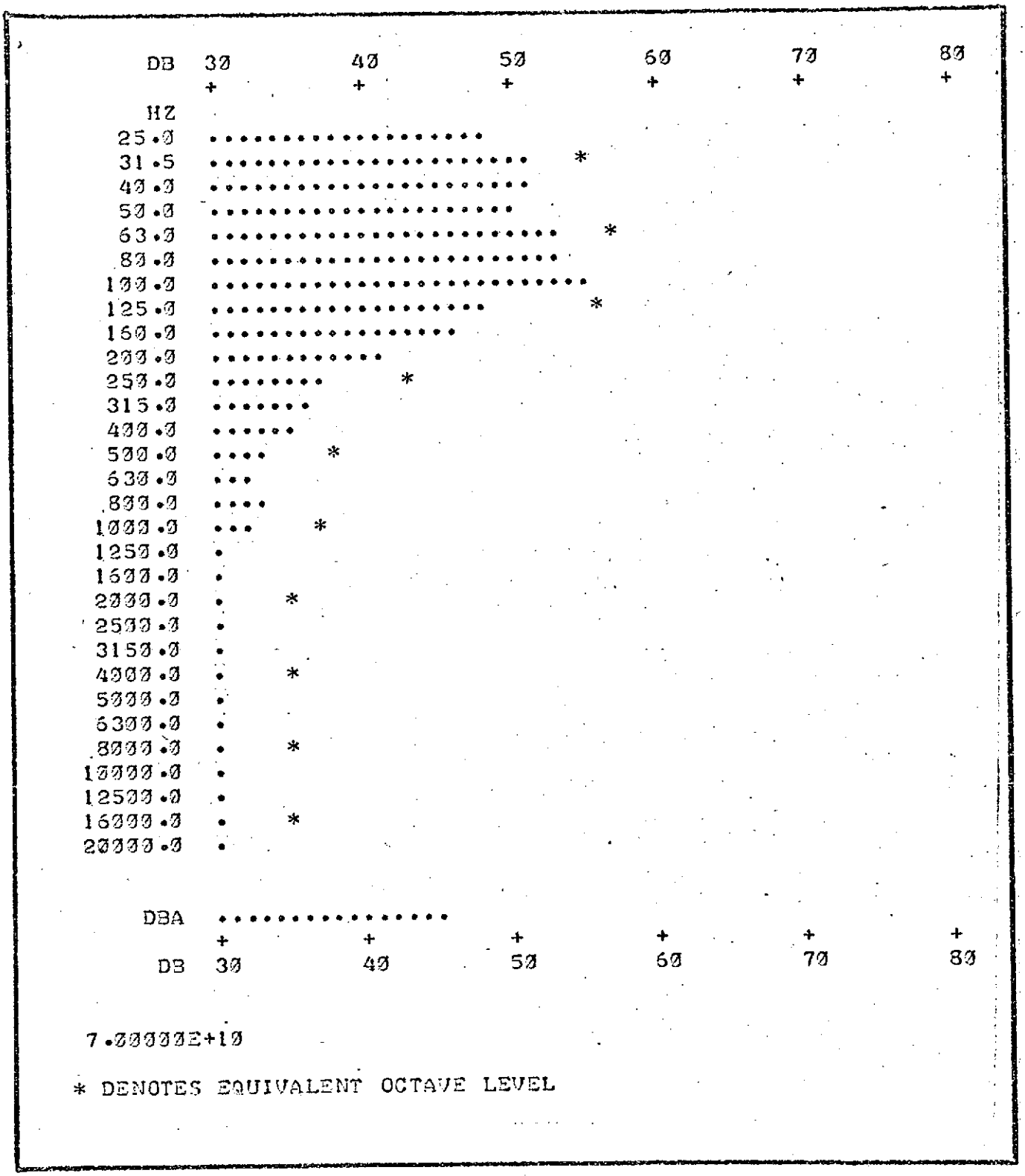

FAR FIELD AMBIENT SPECTRUM, POSITION 7 (Fig. 4-53)
RECORDED 12/8/73

Figure 4-61

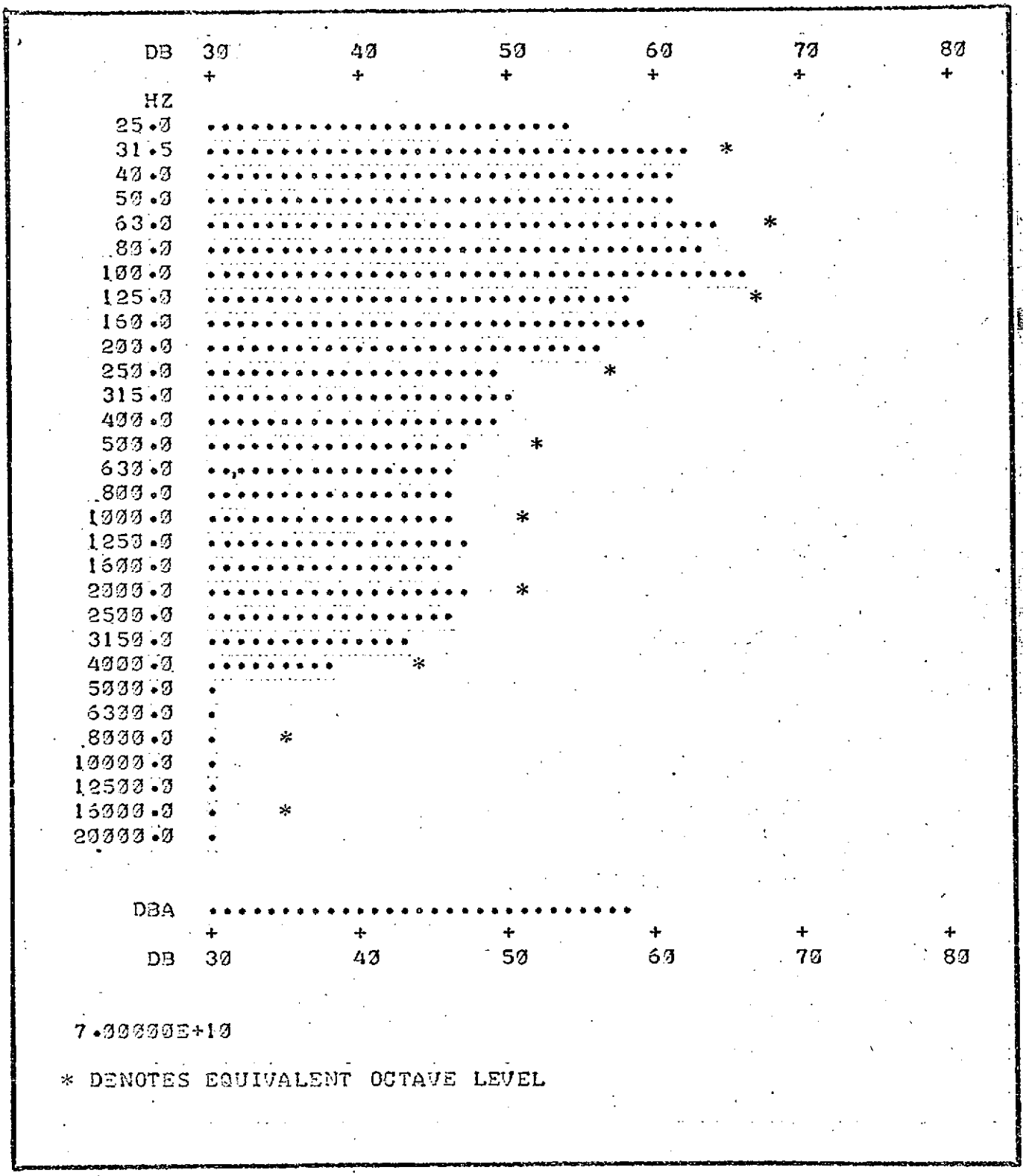

FAR FIELD AMBIENT SPECTRUM, POSITION 7 (Fig. 4-53)
RECORDED 3/13/74

Figure 4-62

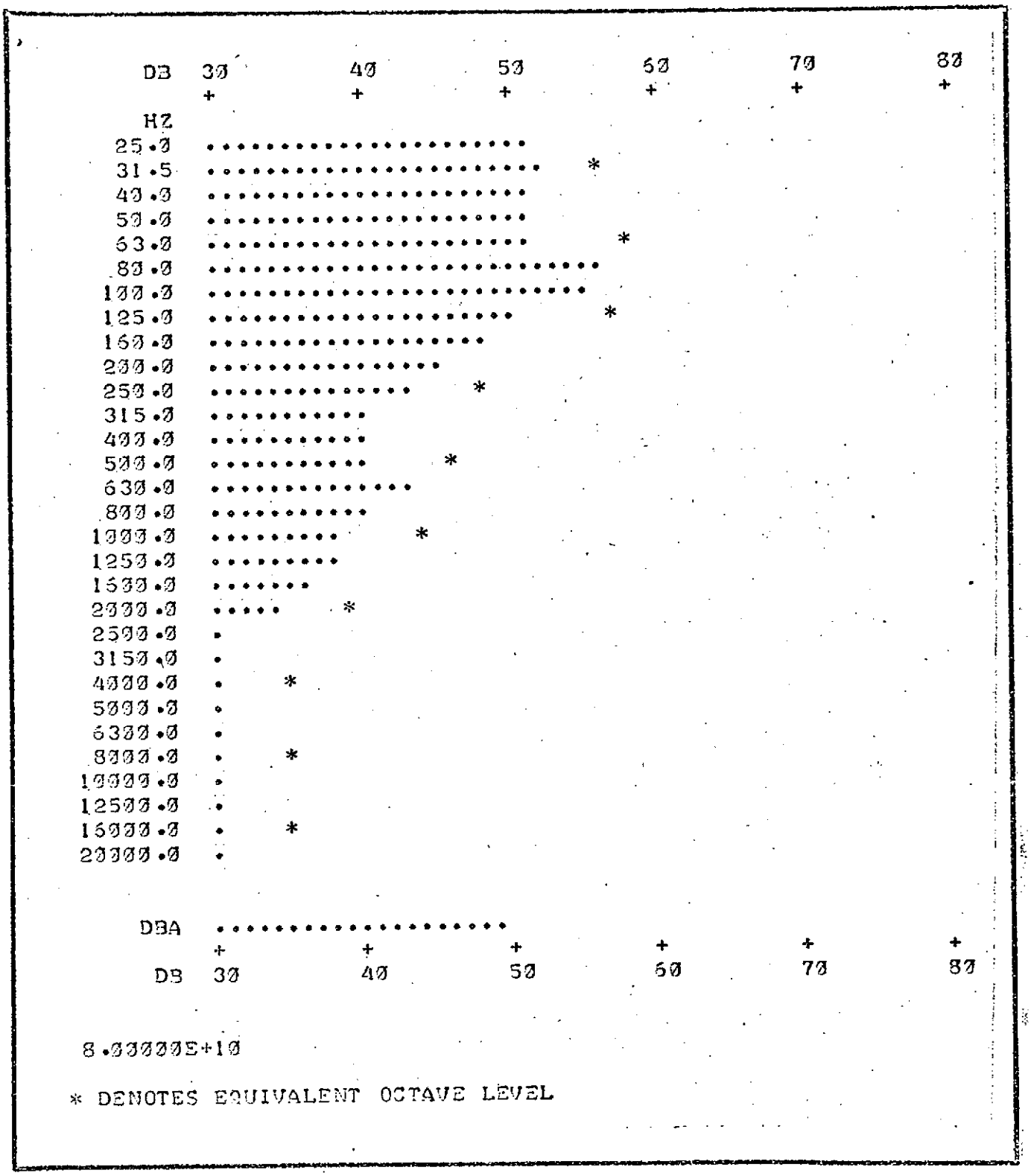

FAR FIELD AMBIENT SPECTRUM, POSITION 8A (Fig. 4-53)
RECORDED 12/8/73

Figure 4-63

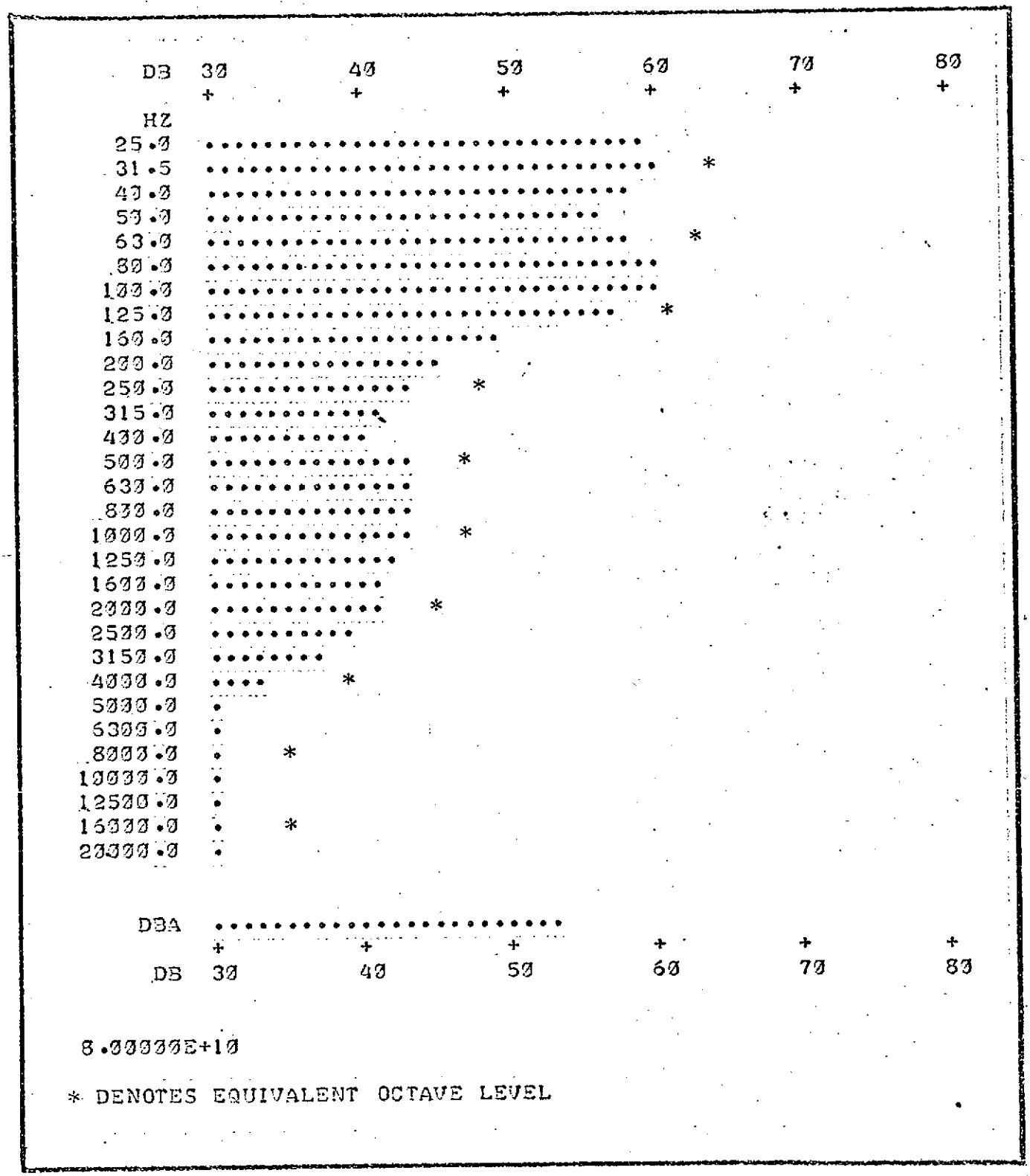

FAR FIELD AMBIENT SPECTRUM, POSITION 8A (Fig. 4-53)
RECORDED 3/13/74

Figure 4-64

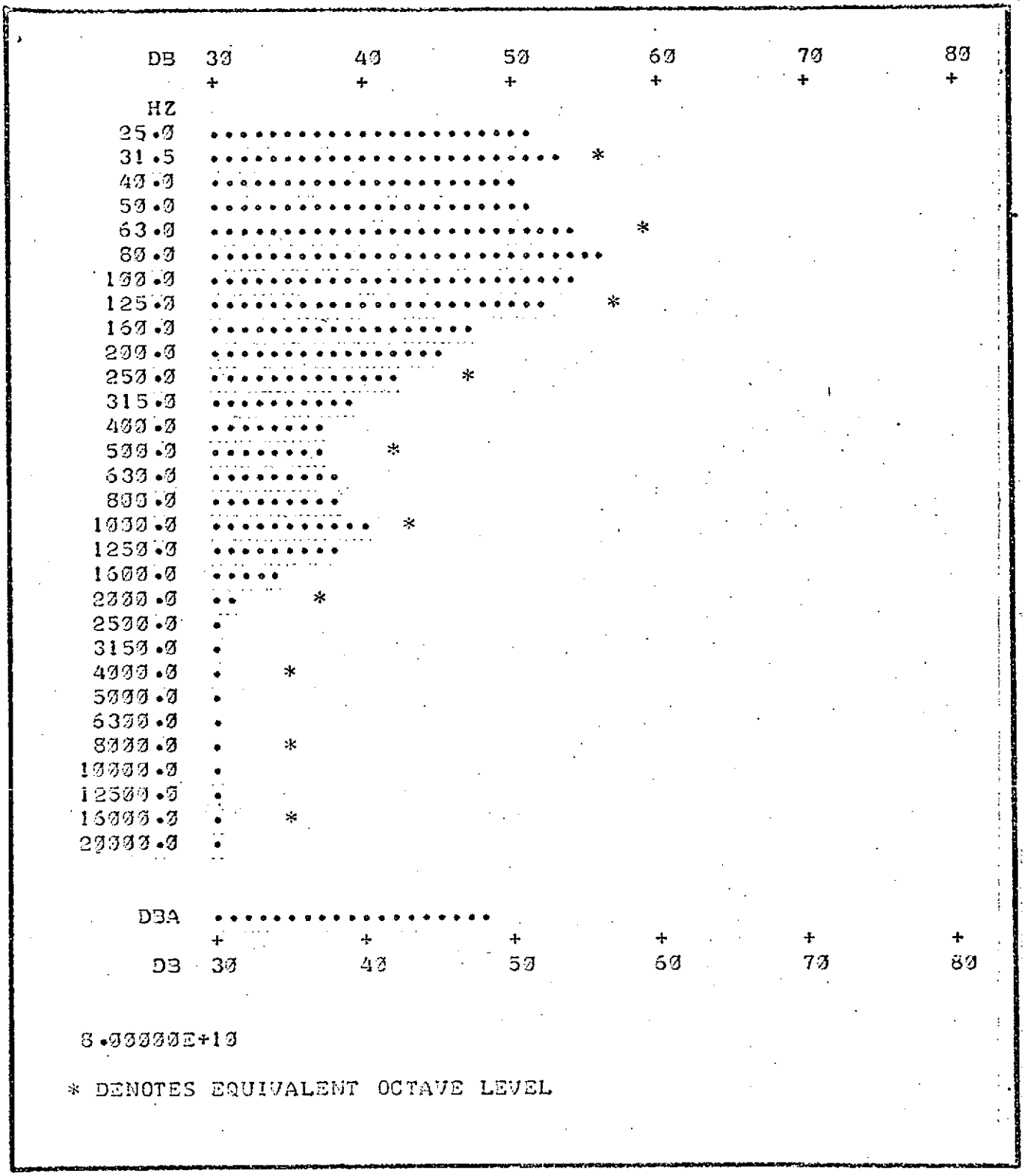

FAR FIELD AMBIENT SPECTRUM, POSITION 8B (Fig. 4-53)
RECORDED 12/9/73

Figure 4-65

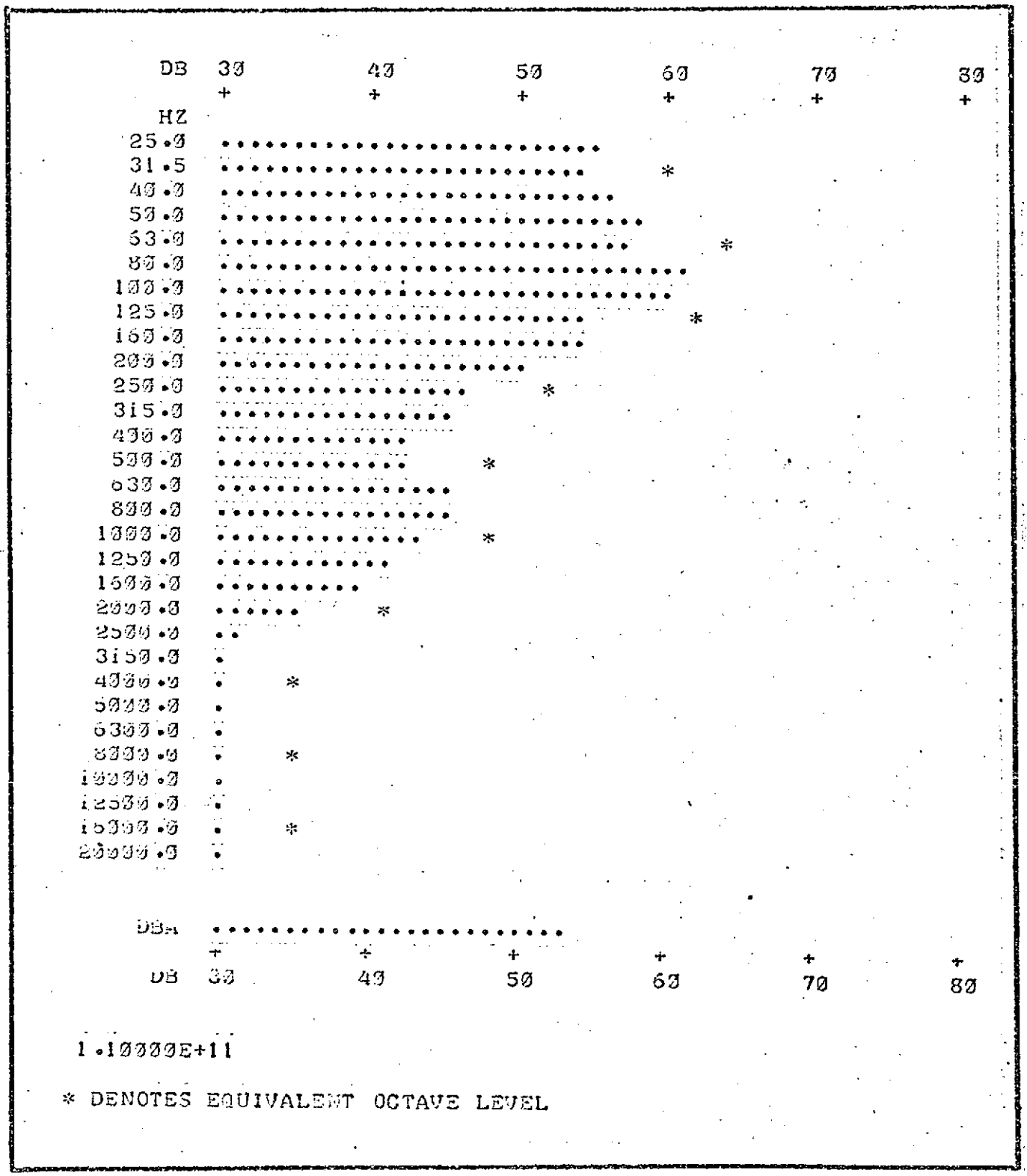

FAR FIELD AMBIENT SPECTRUM, POSITION 11C (Fig. 4-53)
RECORDED 12/9/73

Figure 4-66

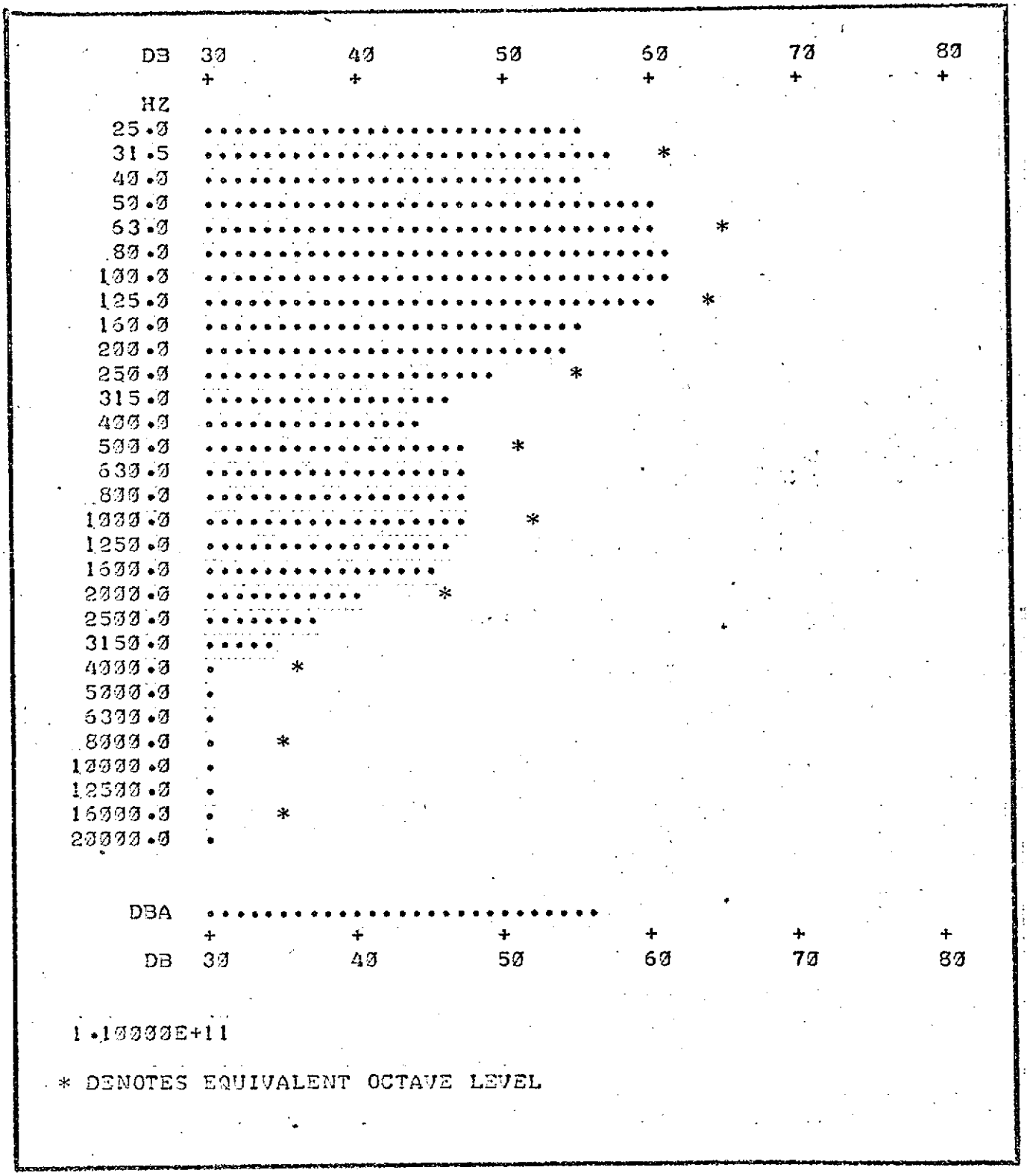

FAR FIELD AMBIENT SPECTRUM, POSITION 11A (Fig. 4-53)
RECORDED 3/13/74

Figure 4-67

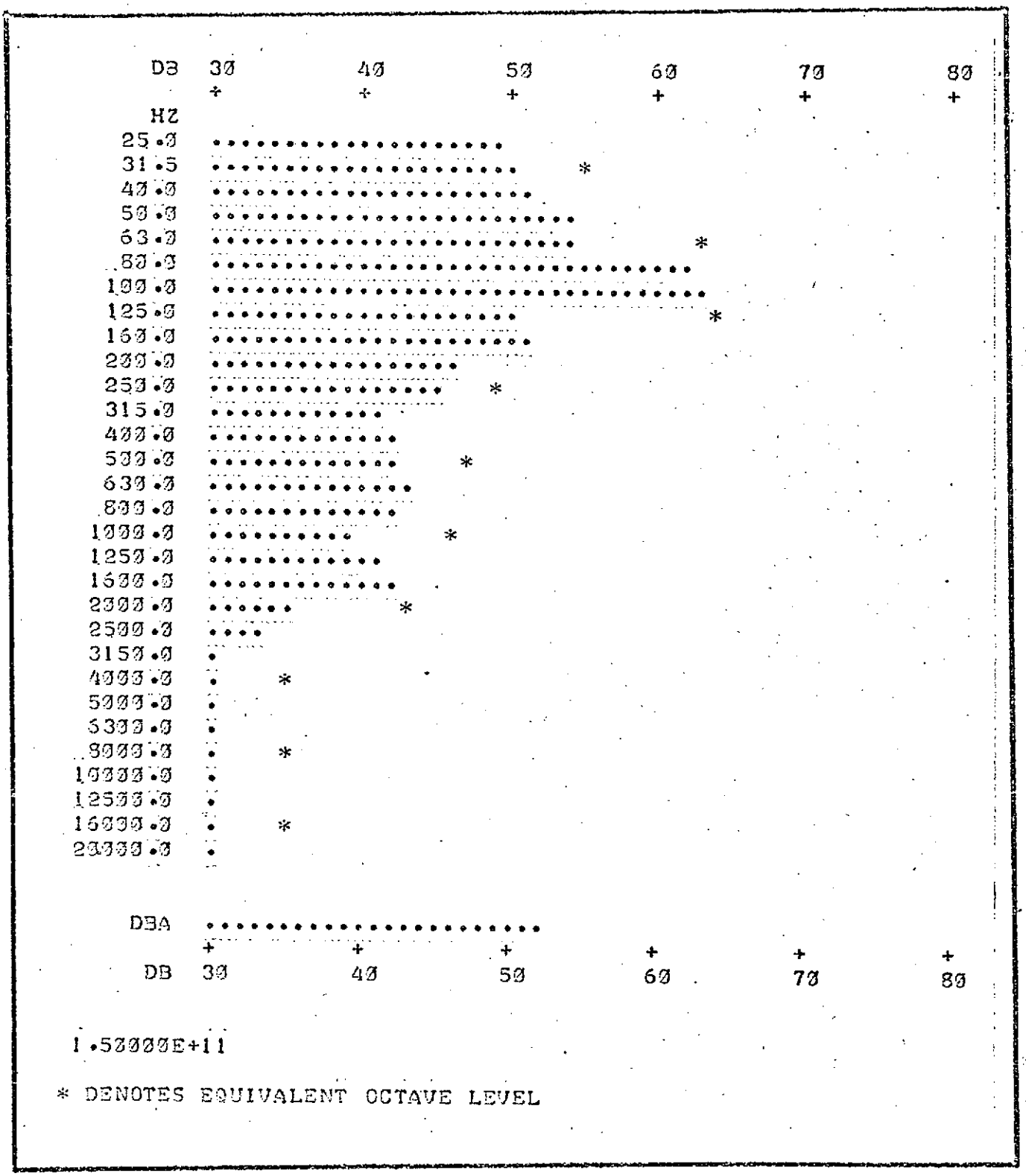

FAR FIELD AMBIENT SPECTRUM, POSITION 11A (Fig. 4-53)
RECORDED 4/13/74

Figure 4-68

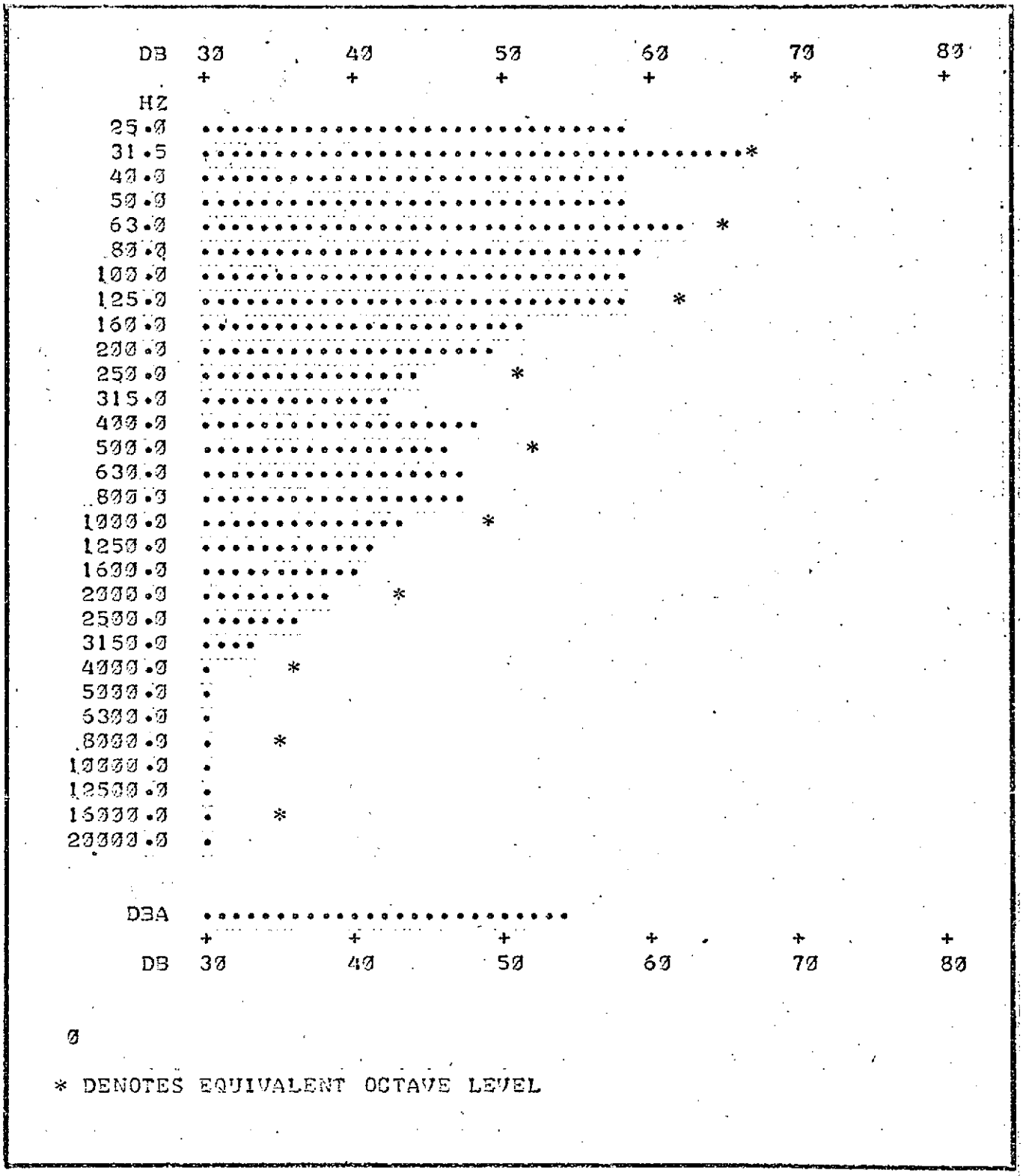

FAR FIELD AMBIENT SPECTRUM, POSITION 11C (Fig. 4-53)
RECORDED 3/13/74

Figure 4-69

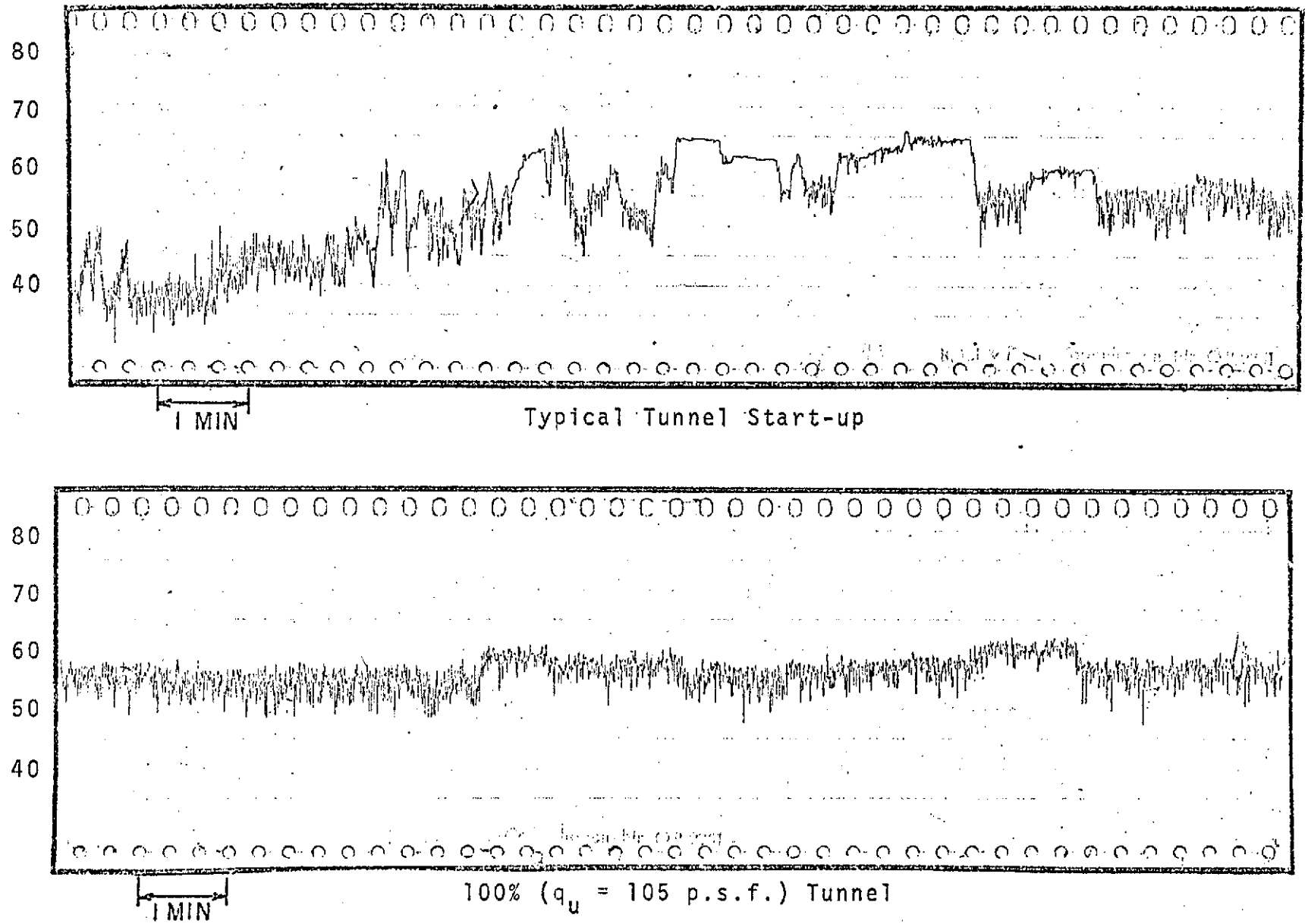

REPRESENTATIVE PERMANENT MONITORING STATION RESULTS

Figure 4-70

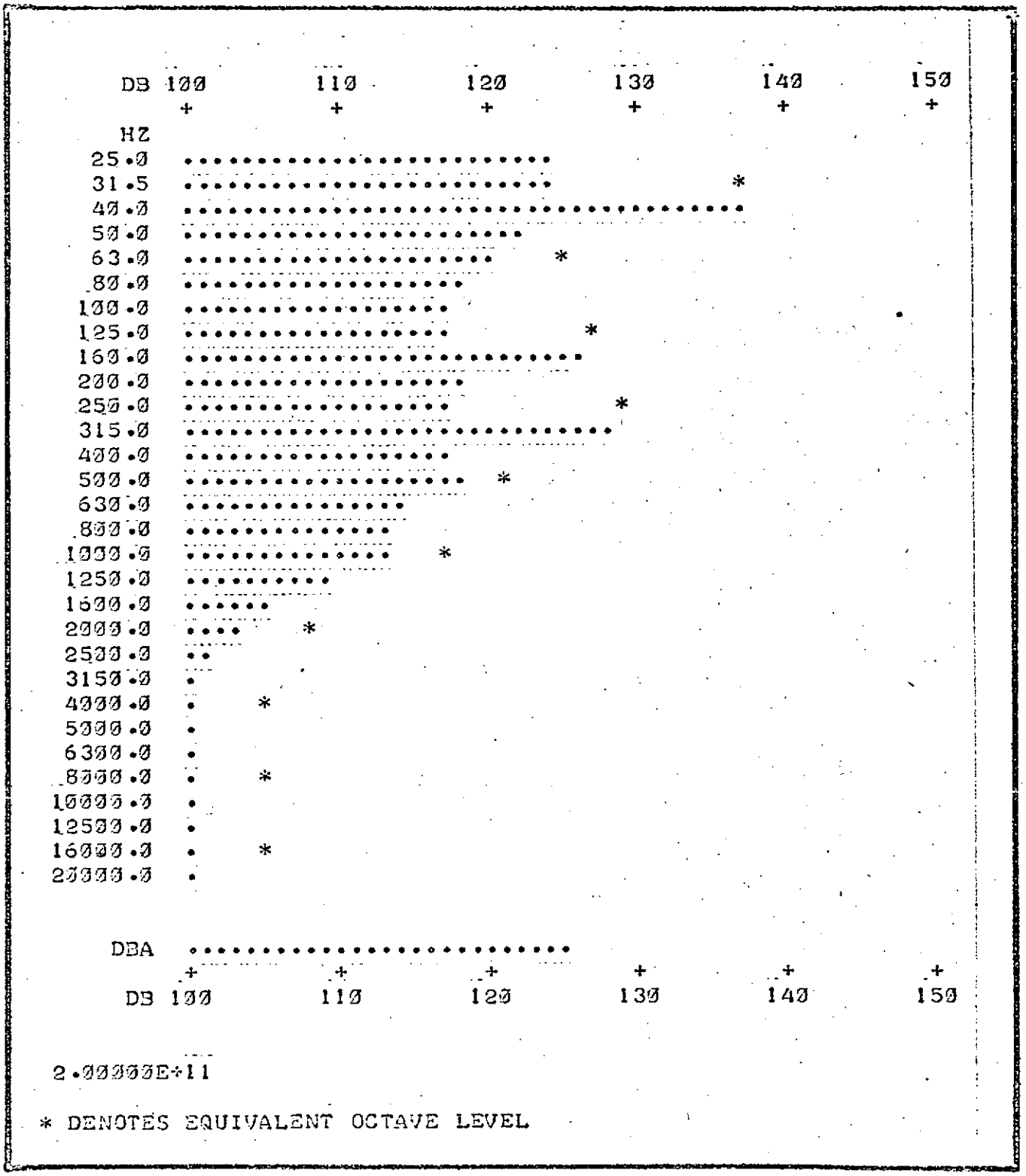

Tunnel Spectrum, Position 1, Test 1, q_u = 60

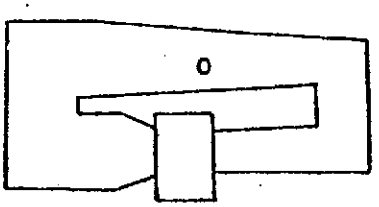

Figure 4-71

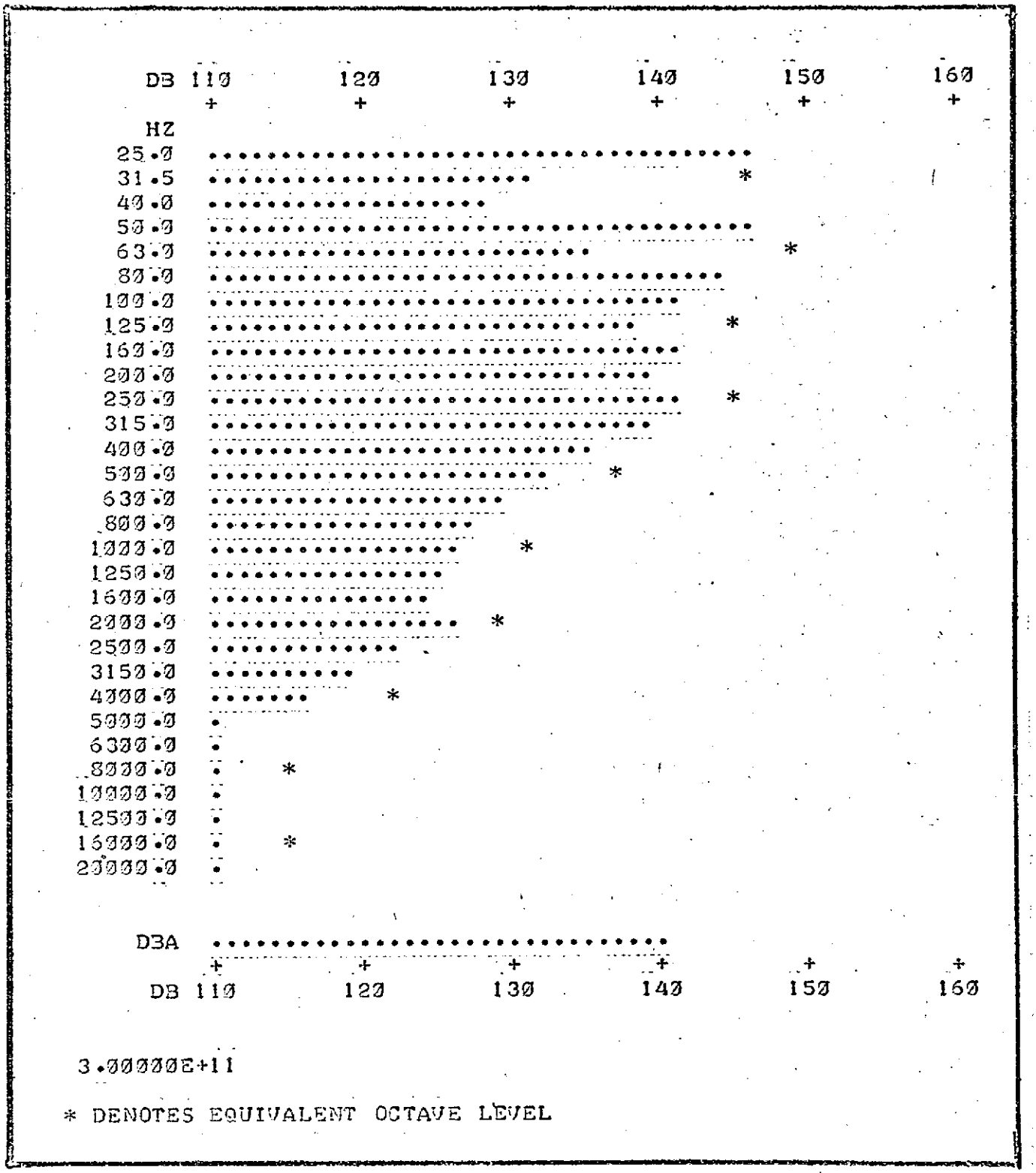

Tunnel Spectrum, Position 1 Test 1, q_u=105

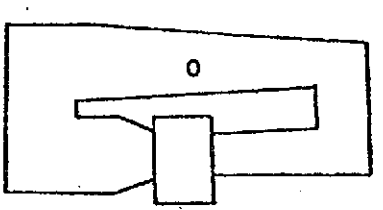

Figure 4-72

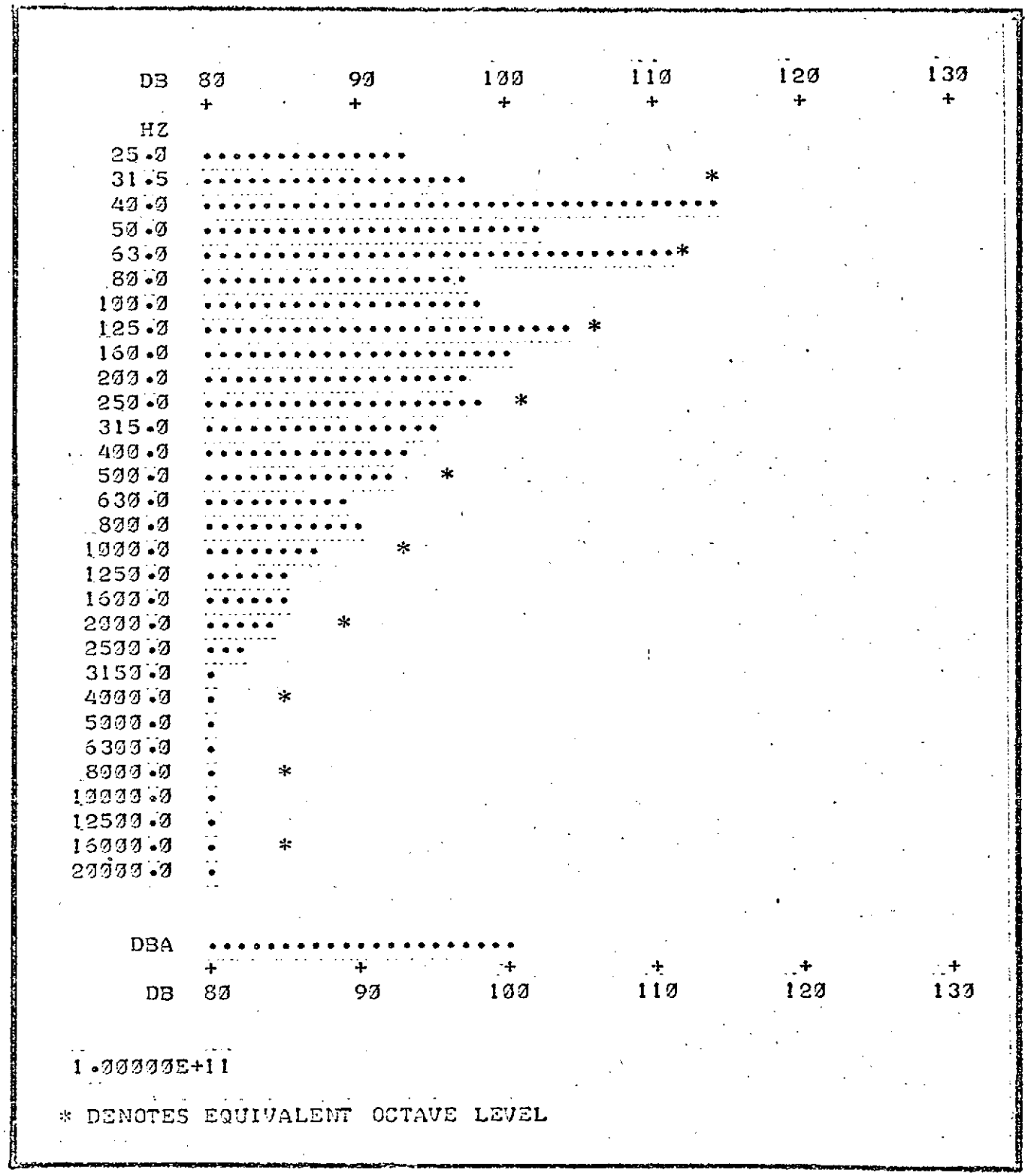

Tunnel Spectrum, Position 2, Test 1, q_u = 60

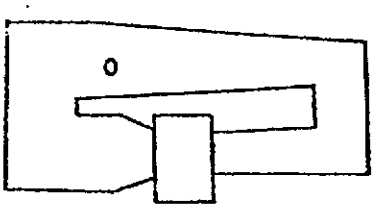

Figure 4-73

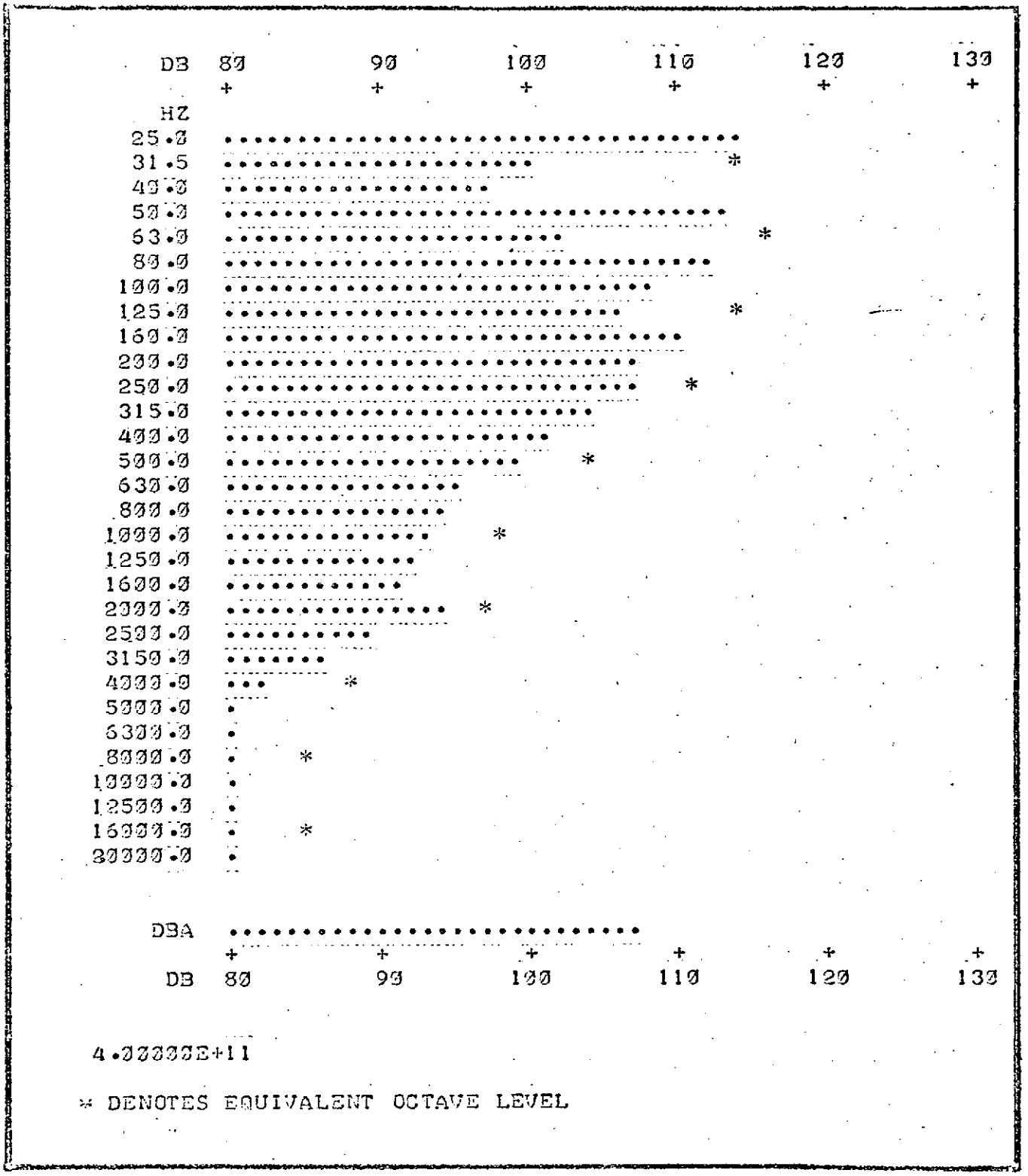

Tunnel Spectrum, Position 2, Test 1, q_u = 105

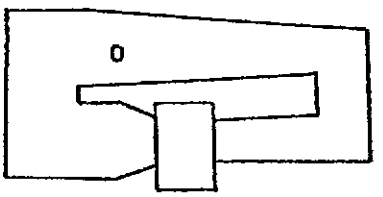

Figure 4-74

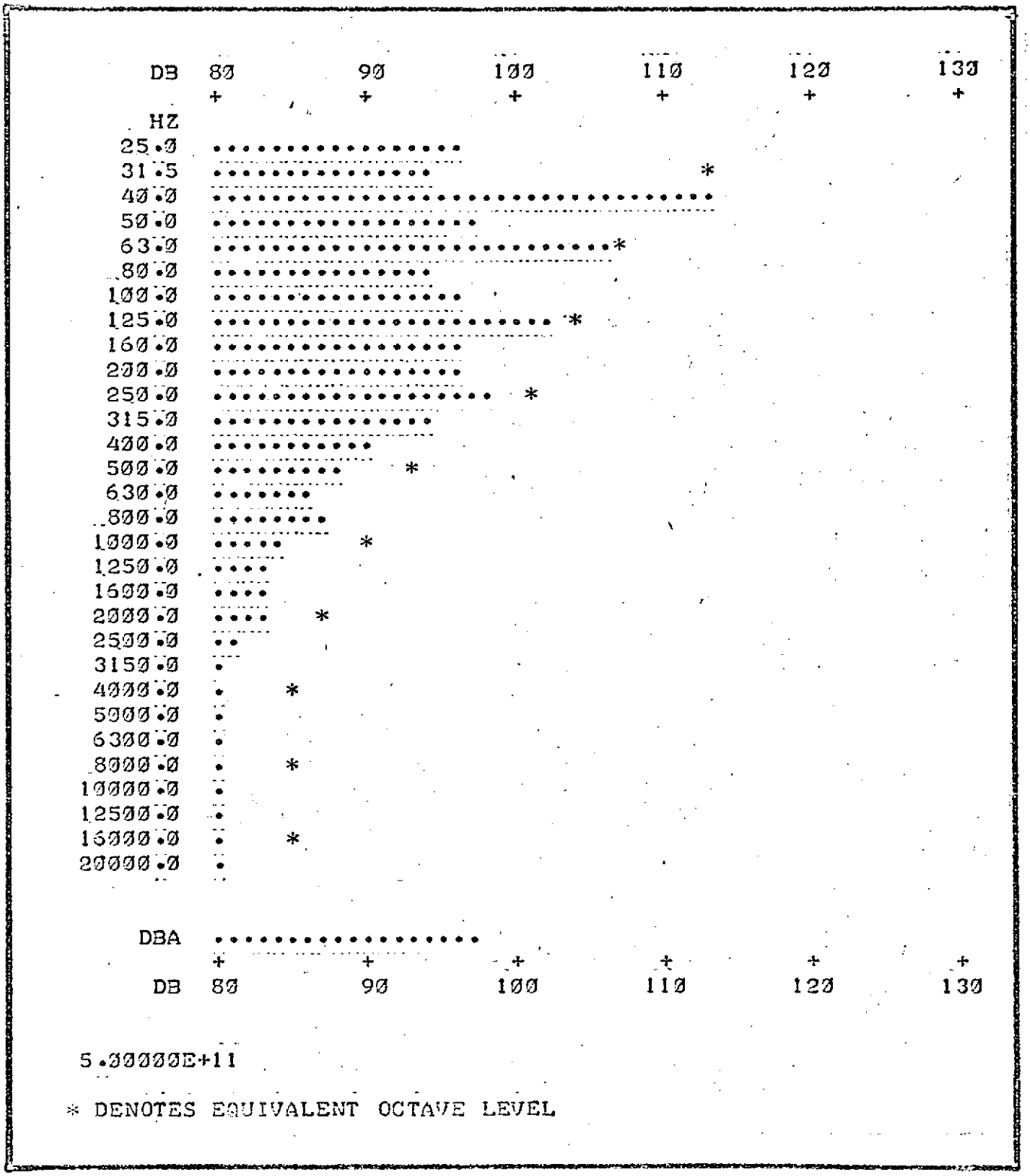

Tunnel Spectrum, Position 2, Test 2, q_u = 60

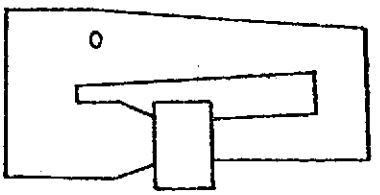

Figure 4-75

```
      DB   80          90          100         110         120         130
           +           +           +           +           +           +
      HZ
    25.0   ••••••••••••••••••••••••••••••••••
    31.5   ••••••••••••••••                    *
    40.0   ••••••••••••••
    50.0   •••••••••••••••••••••••••••••••••••
    63.0   ••••••••••••••••••••••                        *
    80.0   ••••••••••••••••••••••••••••••••••
   100.0   ••••••••••••••••••••••••••
   125.0   ••••••••••••••••••••••••••                   *
   160.0   ••••••••••••••••••••••••••••
   200.0   ••••••••••••••••••••••••••
   250.0   ••••••••••••••••••••••          *
   315.0   ••••••••••••••••••••
   400.0   ••••••••••••••••••
   500.0   ••••••••••••••••        *
   630.0   ••••••••••••
   800.0   ••••••••••
  1000.0   •••••••••     *
  1250.0   •••••••••
  1600.0   •••••••••
  2000.0   ••••••••••   *
  2500.0   •••••••
  3150.0   ••••
  4000.0   •    *
  5000.0   •
  6300.0   •
  8000.0   •   *
 10000.0   •
 12500.0   •
 16000.0   •   *
 20000.0   •

     DBA   •••••••••••••••••••••••••
           +           +           +           +           +           +
      DB   80          90          100         110         120         130

 7.000000E+11

* DENOTES EQUIVALENT OCTAVE LEVEL
```

Tunnel Spectrum, Position 2, Test 2, q_u= 105

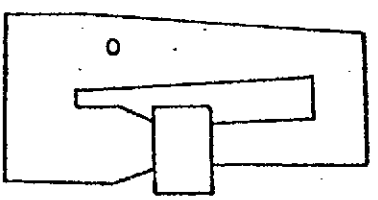

Figure 4-76

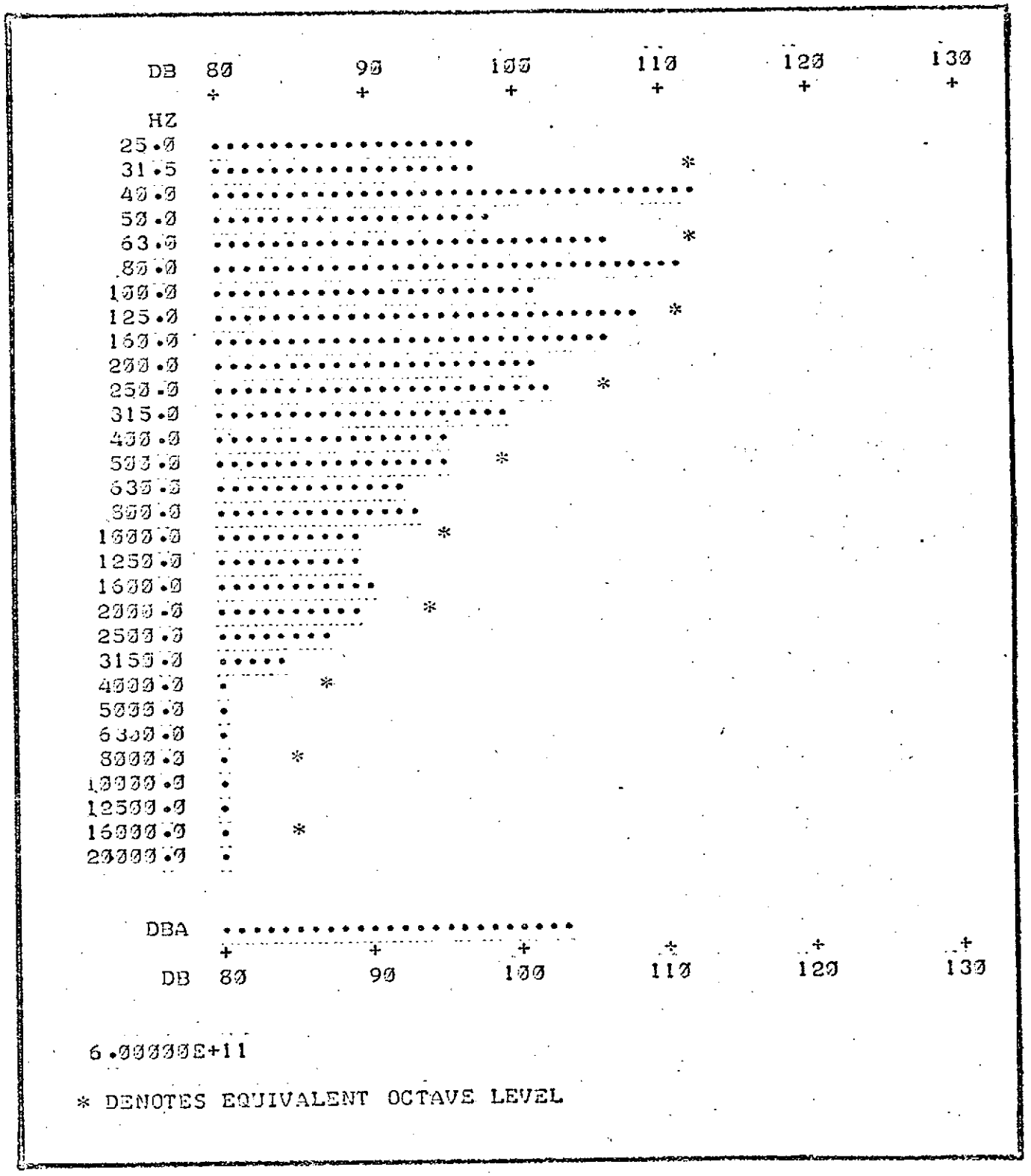

Tunnel Spectrum, Position 5, Test 2, q_u = 60

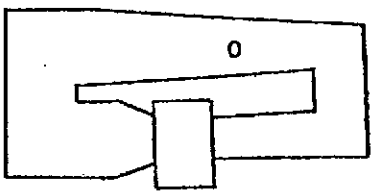

Figure 4-77

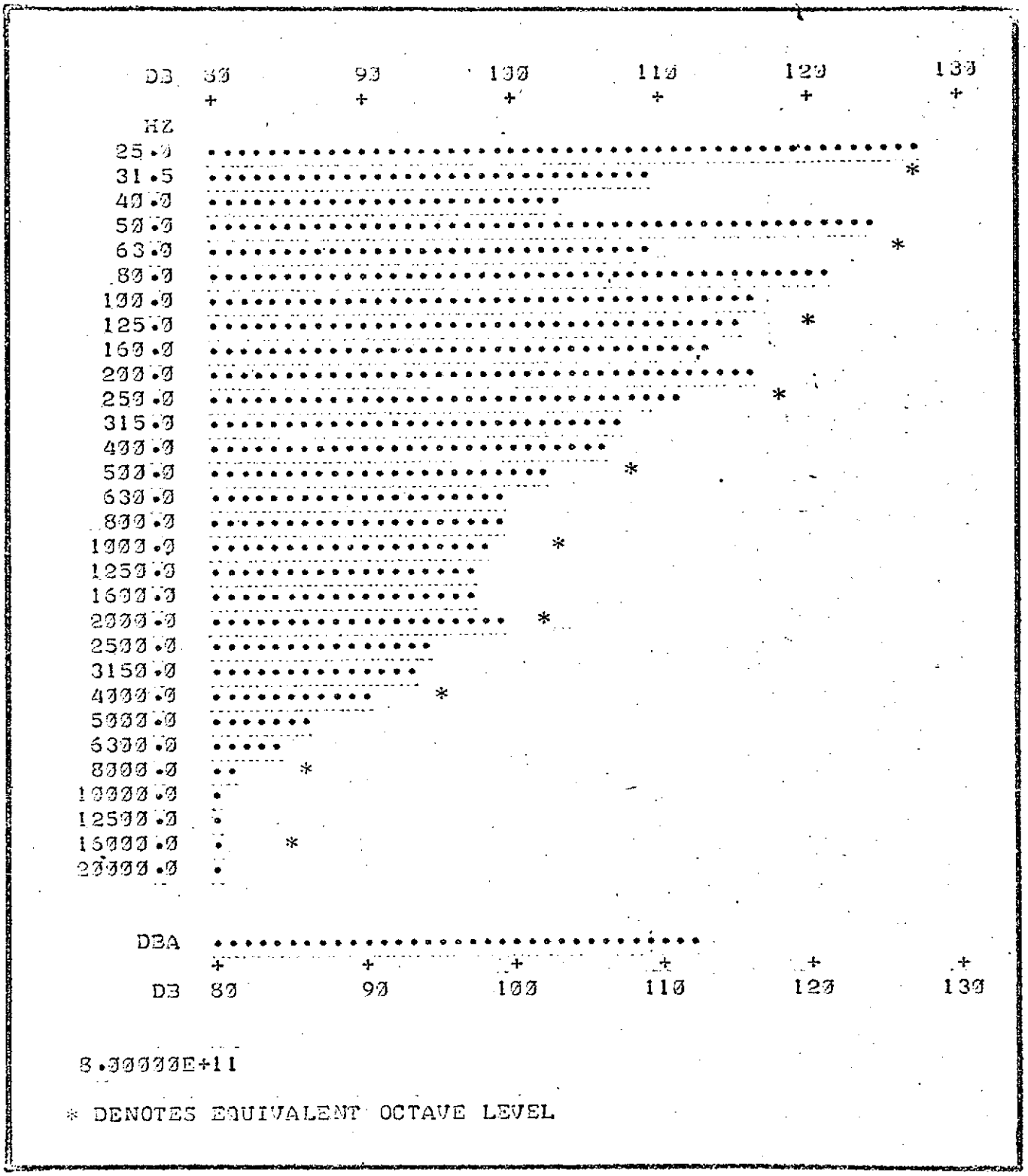

Tunnel Spectrum, Position 5, Test 2, q_u = 105

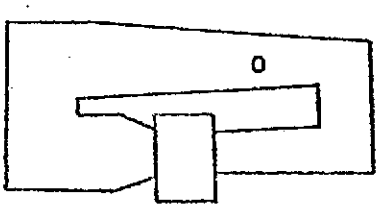

Figure 4.78

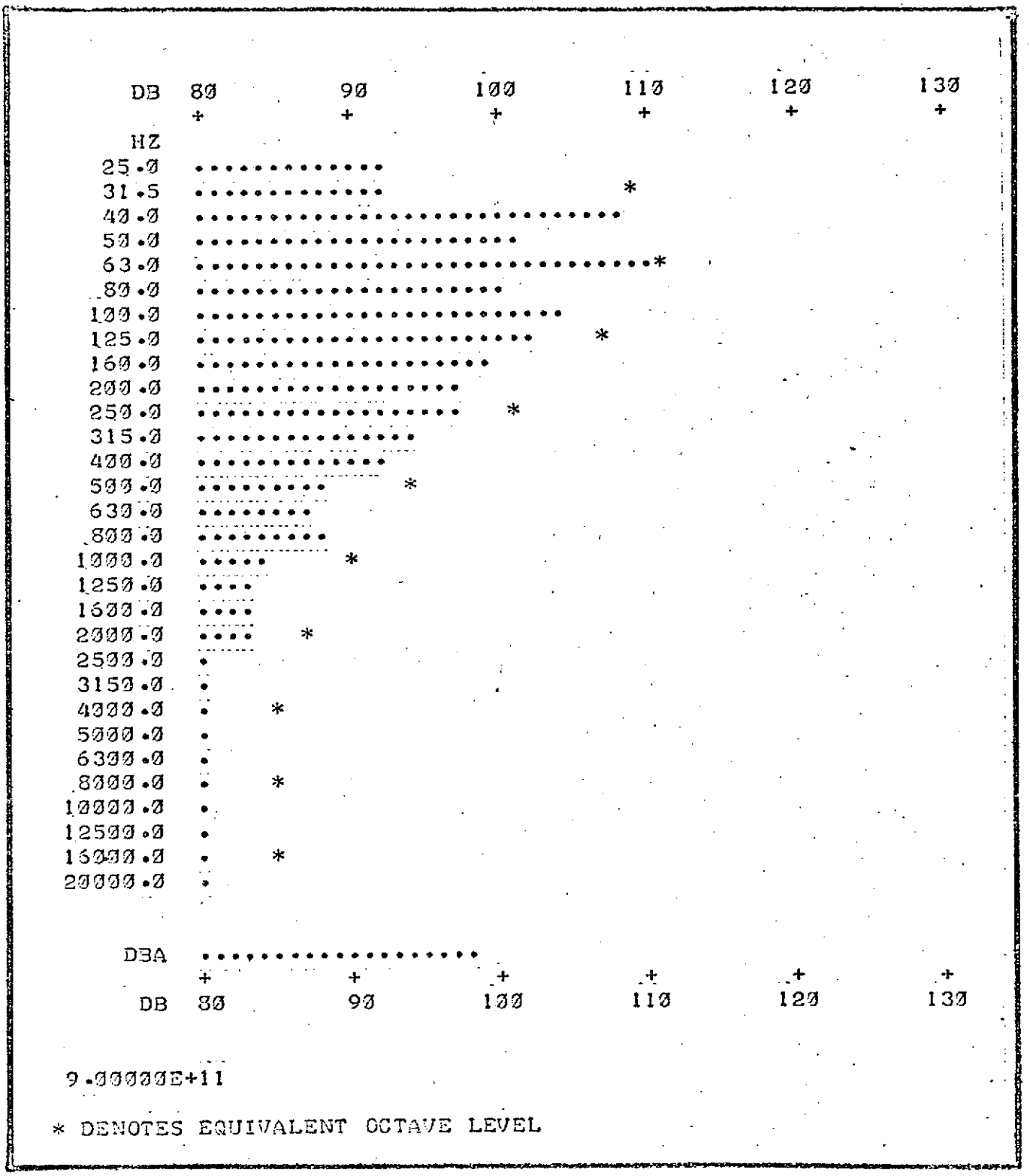

Tunnel Spectrum, Position 2, Test 3, q_u = 60

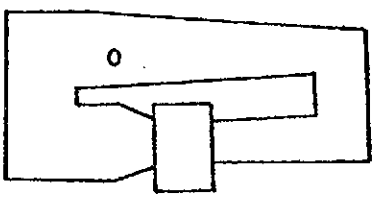

Figure 4-79

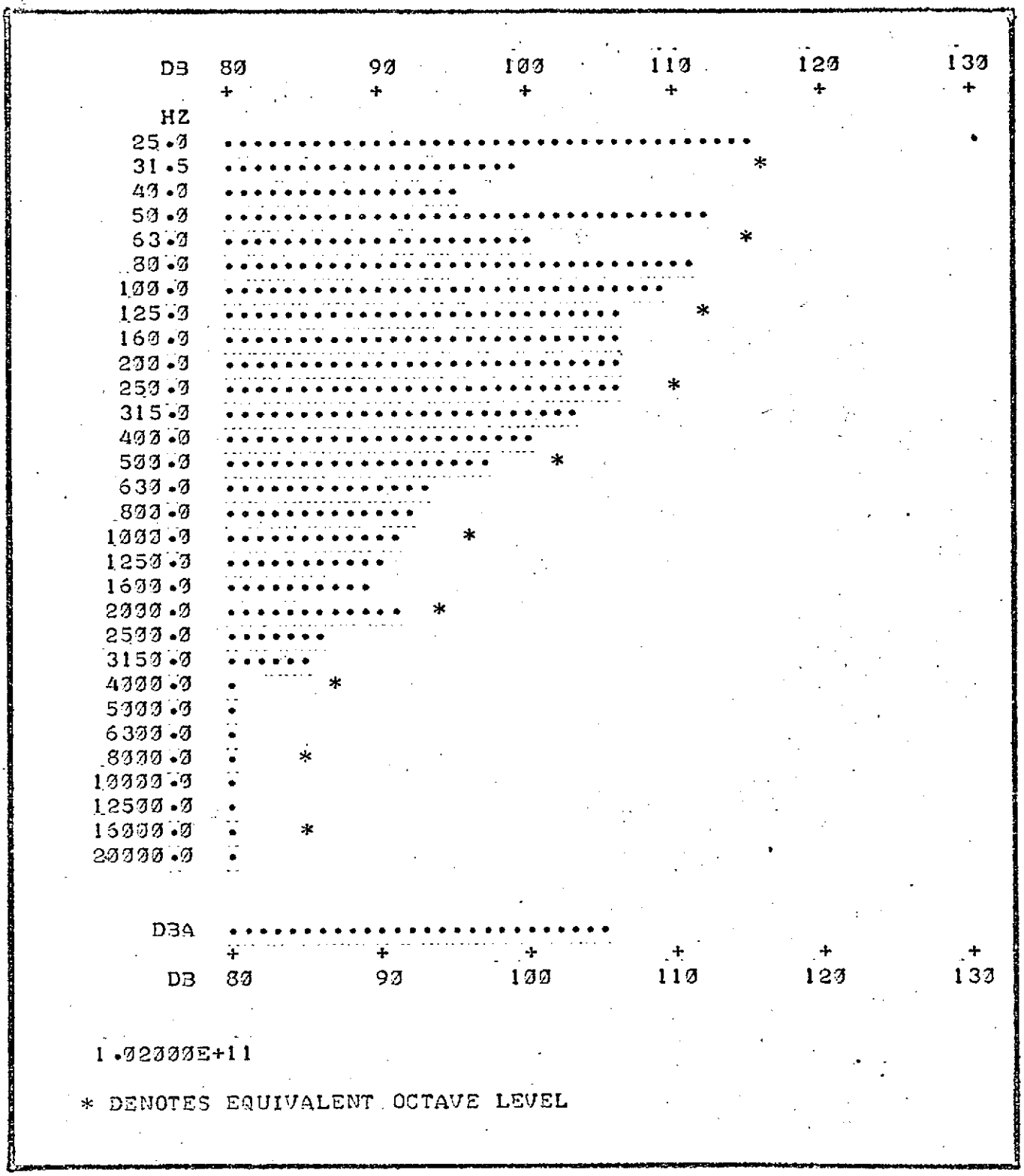

Tunnel Spectrum, Position 2, Test 3, q_u= 105

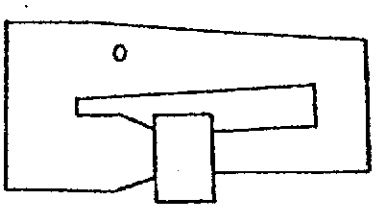

Figure 4.80

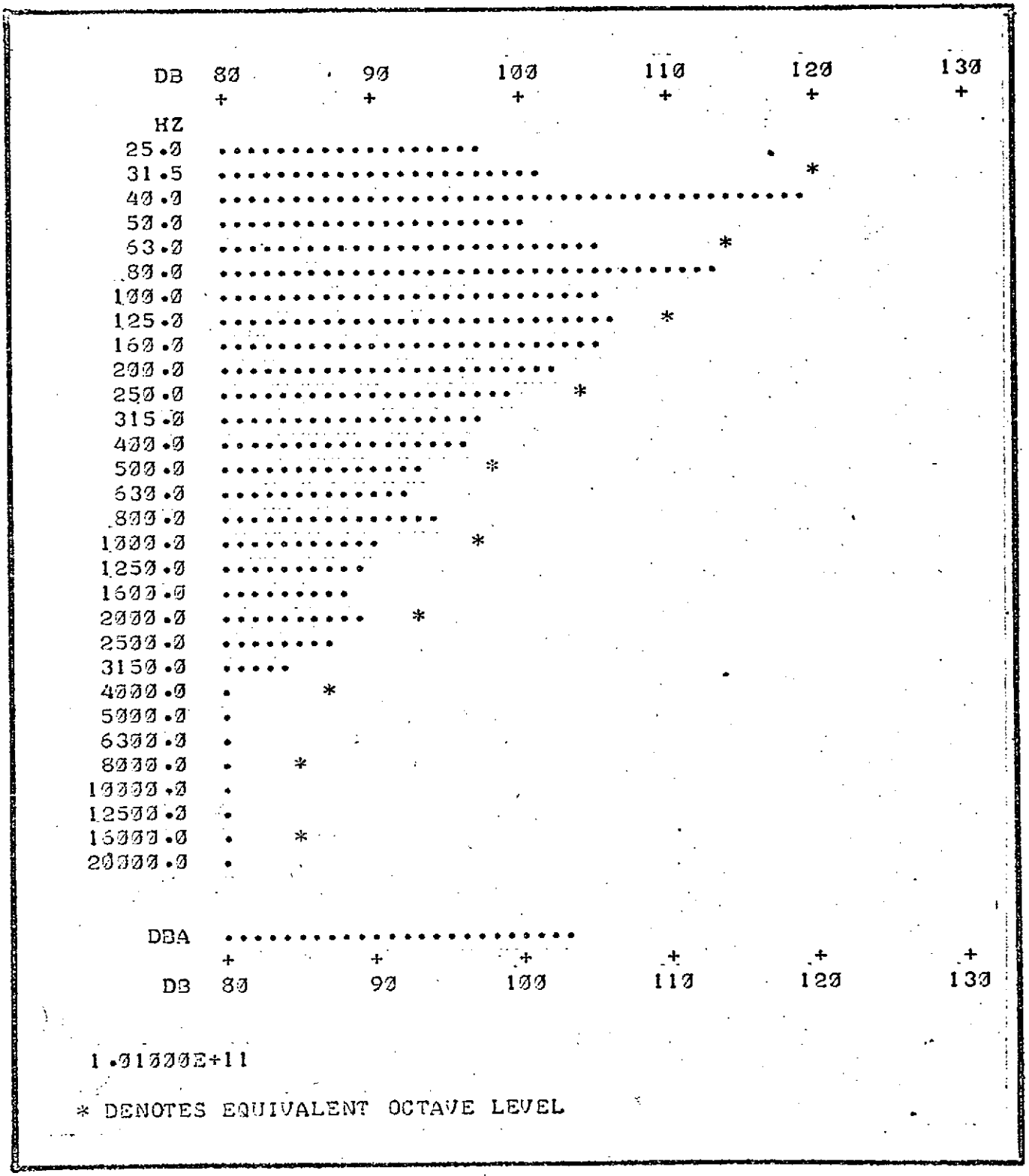

Tunnel Spectrum, Position 5, Test 3, q_u= 60

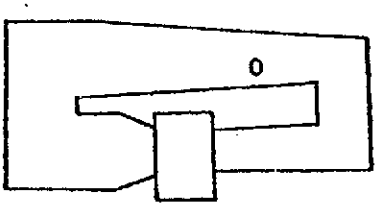

Figure 4.81

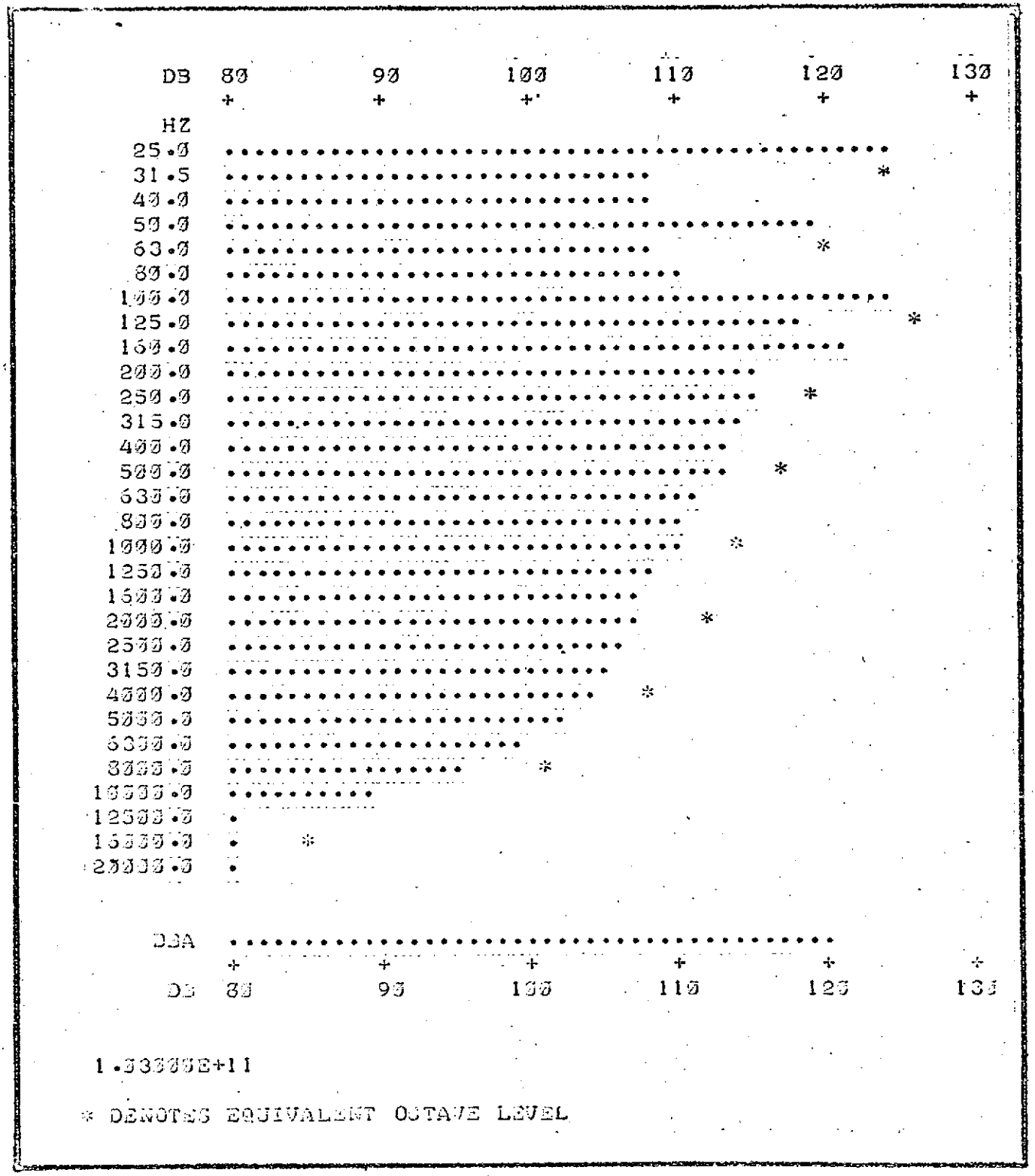

Tunnel Spectrum, Position 5, Test 3, q_u= 105

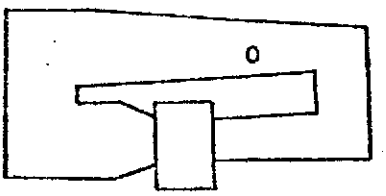

Figure 4.82

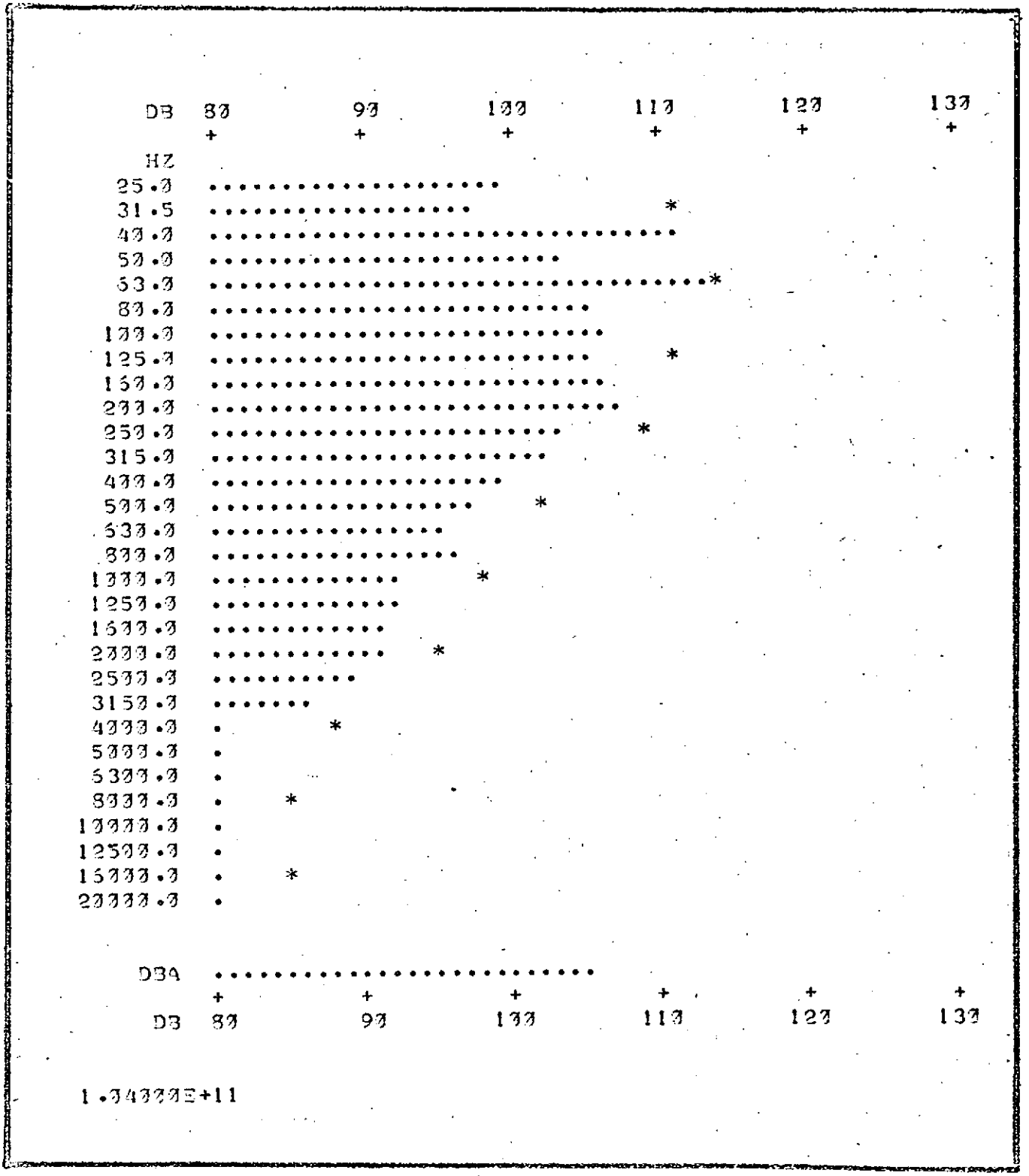

Tunnel Spectrum, Position 2, Test 4, q_u= 60

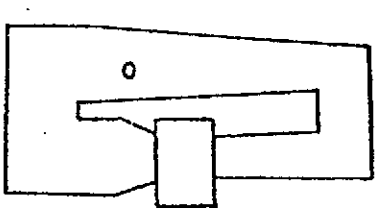

Figure 4.83

```
     DB  80          90          100         110         120         130
         +           +           +           +           +           +
     HZ
   25.0  ..........................................
   31.5  ......................                      *
   40.0  ..................
   50.0  ......................................
   63.0  ......................                  *
   80.0  ................................
  100.0  ..............................
  125.0  ............................          *
  160.0  ..........................
  200.0  ........................
  250.0  ..............................    *
  315.0  ......................
  400.0  ....................
  500.0  ..................      *
  630.0  ..............
  800.0  ............
 1000.0  ..........      *
 1250.0  ..........
 1600.0  ..........
 2000.0  ............  *
 2500.0  ........
 3150.0  ......
 4000.0  .     *
 5000.0  .
 6300.0  .
 8000.0  .   *
10000.0  .
12500.0  .
16000.0  .   *
20000.0  .


     DBA ............................
         +           +           +           +           +           +
      DB 80          90          100         110         120         130


1.070000E+11

* DENOTES EQUIVALENT OCTAVE LEVEL
```

Tunnel Spectrum, Position 2, Test 4, q_u= 105

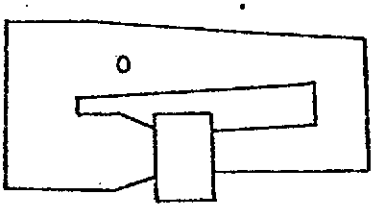

Figure 4.84

```
      DB   70        80        90        100       110       120
           +         +         +         +         +         +
      HZ
    25.0   ..............................
    31.5   ..............                          *
    40.0   ...................................
    50.0   ................
    63.0   ..............................*
    80.0   ............
   100.0   ............
   125.0   ................  *
   160.0   ................
   200.0   ...........
   250.0   ........     *
   315.0   ..........
   400.0   ........
   500.0   ..........  *
   630.0   ........
   800.0   ........
  1000.0   ........    *
  1250.0   ......
  1600.0   ...
  2000.0   ...    *
  2500.0   .
  3150.0   .
  4000.0   .    *
  5000.0   .
  6300.0   .
  8000.0   .    *
 10000.0   .
 12500.0   .
 16000.0   .    *
 20000.0   .

      DBA  ................
           +         +         +         +         +         +
      DB   70        80        90        100       110       120

 1.050000E+11

* DENOTES EQUIVALENT OCTAVE LEVEL
```

Tunnel Spectrum, Position 11, Test 4, q_u= 60

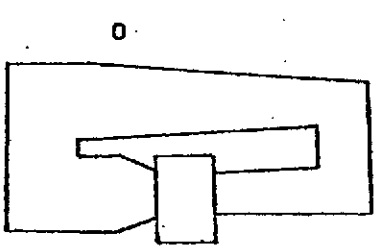

Figure 4-85

```
    DB   70        80        90        100       110       120
         +         +         +         +         +         +
    HZ
  25.0   ..........................................
  31.5   ......................                    *
  40.0   ..............
  50.0   ........................
  63.0   ..................        *
  80.0   ....................
 100.0   ........................
 125.0   ....................      *
 160.0   ........................
 200.0   ................
 250.0   ............    *
 315.0   ...........
 400.0   ...........
 500.0   ...........  *
 630.0   ..........
 800.0   .........
1000.0   ......    *
1250.0   .....
1600.0   ..
2000.0   .   *
2500.0   .
3150.0   .
4000.0   .   *
5000.0   .
6300.0   .
8000.0   .   *
10000.0  .
12500.0  .
16000.0  .   *
20000.0  .

    DBA  ..................
         +         +         +         +         +         +
    DB   70        80        90        100       110       120

1.000000E+11

* DENOTES EQUIVALENT OCTAVE LEVEL
```

Tunnel Spectrum, Position 11, Test 4, q_u = 105

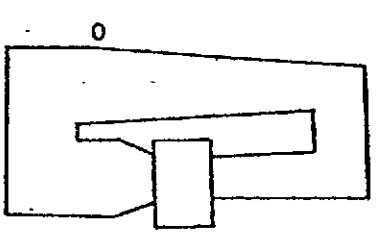

Figure 4-86

```
     DB   80          90          100         110         120         130
          +           +           +           +           +           +
     HZ
   25.0   ..............
   31.5   ..............                      *
   40.0   ..............................
   50.0   ..................
   63.0   ...........................*
   80.0   ..................
  100.0   ..................
  125.0   ........................  *
  160.0   ......................
  200.0   ..................
  250.0   ..................   *
  315.0   ................
  400.0   ..............
  500.0   ............    *
  630.0   ..........
  800.0   ..........
 1000.0   ........     *
 1250.0   ......
 1600.0   .....
 2000.0   ....    *
 2500.0   ...
 3150.0   .
 4000.0   .   *
 5000.0   .
 6300.0   .
 8000.0   .   *
10000.0   .
12500.0   .
16000.0   .   *
20000.0   .

     DBA  ....................
          +           +           +           +           +           +
     DB   80          90          100         110         120         130

1.000000E+11

* DENOTES EQUIVALENT OCTAVE LEVEL
```

Tunnel Spectrum, Position 2, Test 5, q_u= 60

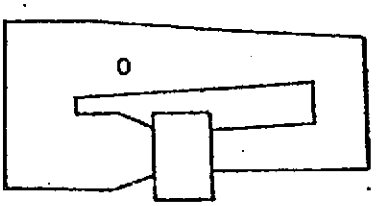

Figure 4.87

```
     DB   80          90          100         110         120         130
          +           +           +           +           +           +
     HZ
   25.0   ..........................................
   31.5   ......................                      *
   40.0   ..................
   50.0   ....................................
   63.0   ......................                  *
   80.0   ..............................
  100.0   ................................
  125.0   ........................            *
  160.0   ..............................
  200.0   ............................
  250.0   ............................  *
  315.0   ........................
  400.0   ......................
  500.0   ..................    *
  630.0   ................
  800.0   ..............
 1000.0   ............    *
 1250.0   ..........
 1600.0   ..........
 2000.0   ............  *
 2500.0   ........
 3150.0   .......
 4000.0   ...     *
 5000.0   .
 6300.0   .
 8000.0   .    *
10000.0   .
12500.0   .
16000.0   .    *
20000.0   .


    DBA   ............................
          +           +           +           +           +           +
     DB   80          90          100         110         120         130


1.09000E+11

* DENOTES EQUIVALENT OCTAVE LEVEL
```

Tunnel Spectrum, Position 2, Test 5, q_u= 105

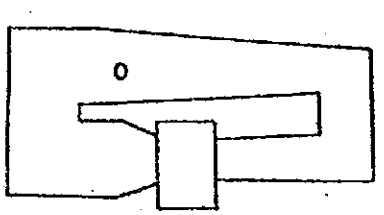

Figure 4.88

```
      DB   80          90          100         110         120         130
           +           +           +           +           +           +
      HZ
    25.0   ............
    31.5   ............                                    *
    40.0   ..................................
    50.0   ...............
    63.0   ........................  *
    80.0   ........................
   100.0   ....................
   125.0   ........................  *
   160.0   ........................
   200.0   ..................
   250.0   ...............    *
   315.0   ..............
   400.0   ............
   500.0   ...........   *
   630.0   .........
   800.0   .........
  1000.0   ......      *
  1250.0   ......
  1600.0   .....
  2000.0   .....   *
  2500.0   ..
  3150.0   .
  4000.0   .    *
  5000.0   .
  6300.0   .
  8000.0   .    *
 10000.0   .
 12500.0   .
 16000.0   .    *
 20000.0   .

      DBA  ..................
           +           +           +           +           +           +
      DB   80          90          100         110         120         130

1.11000E+11

* DENOTES EQUIVALENT OCTAVE LEVEL
```

Tunnel Spectrum, Position 14, Test 5, q_u = 60

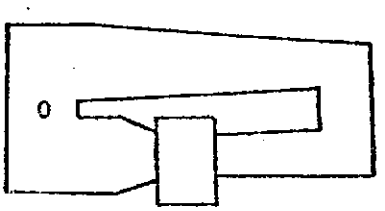

Figure 4.89

```
     DB   80          90          100         110         120         130
          +           +           +           +           +           +
     HZ
   25.0   ..........................................
   31.5   ....................                        *
   40.0   ................
   50.0   ..........................................
   63.0   ........................                    *
   80.0   ....................................
  100.0   ........................
  125.0   ..............................          *
  160.0   ..............................
  200.0   ..............................
  250.0   ............................            *
  315.0   ........................
  400.0   ......................
  500.0   ..................      *
  630.0   ................
  800.0   ..............
 1000.0   ..............    *
 1250.0   ............
 1600.0   ...........
 2000.0   ................ *
 2500.0   .........
 3150.0   ......
 4000.0   ..    *
 5000.0   .
 6300.0   .
 8000.0   .   *
10000.0   .
12500.0   .
16000.0   .   *
20000.0   .

     DBA  ............................
          +           +           +           +           +           +
      DB  80          90          100         110         120         130

1.12000E+11

* DENOTES EQUIVALENT OCTAVE LEVEL
```

Tunnel Spectrum, Position 14, Test 5, q_u = 105

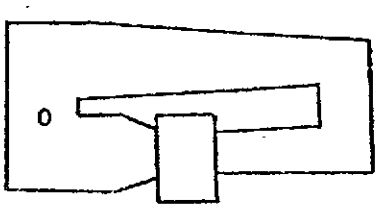

Figure 4-90

```
      DB  60          70          80          90          100         110
          +           +           +           +           +           +
      HZ
    25.0  ....................
    31.5  ........................                        *
    40.0  ..........................................
    50.0  ....................
    63.0  ............................  *
    80.0  ..........................
   100.0  ....................
   125.0  ......................  *
   160.0  ................
   200.0  ..............
   250.0  ..........      *
   315.0  ........
   400.0  ........
   500.0  ........    *
   630.0  .....
   800.0  ......
  1000.0  ...       *
  1250.0  ....
  1600.0  ...
  2000.0  ....      *
  2500.0  .....
  3150.0  .......
  4000.0  ..........      *
  5000.0  ............
  6300.0  ............
  8000.0  .....         *
 10000.0  .
 12500.0  .
 16000.0  .      *
 20000.0  .


     DBA  ....................
          +           +           +           +           +           +
      DB  60          70          80          90          100         110

1.100000E+11

* DENOTES EQUIVALENT OCTAVE LEVEL
```

Tunnel Spectrum, Position 15, Test 5, q_u= 60

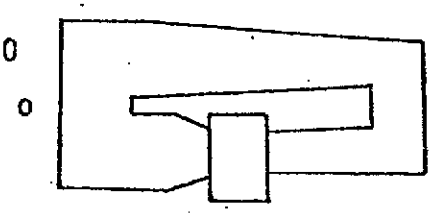

Figure 4.91

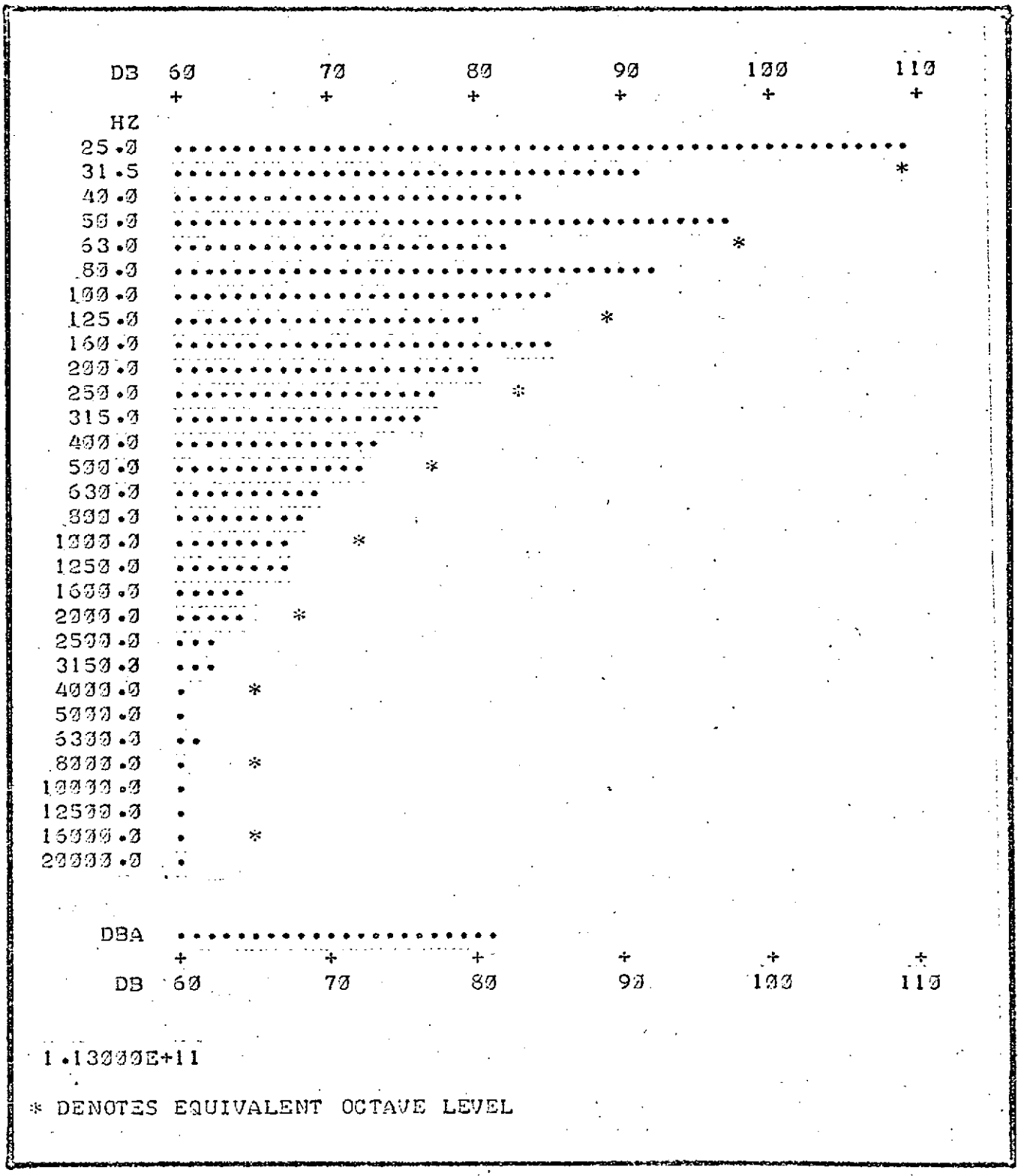

Tunnel Spectrum, Position 15, Test 5, q_u= 105

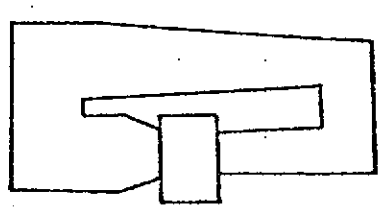

Figure 4.92

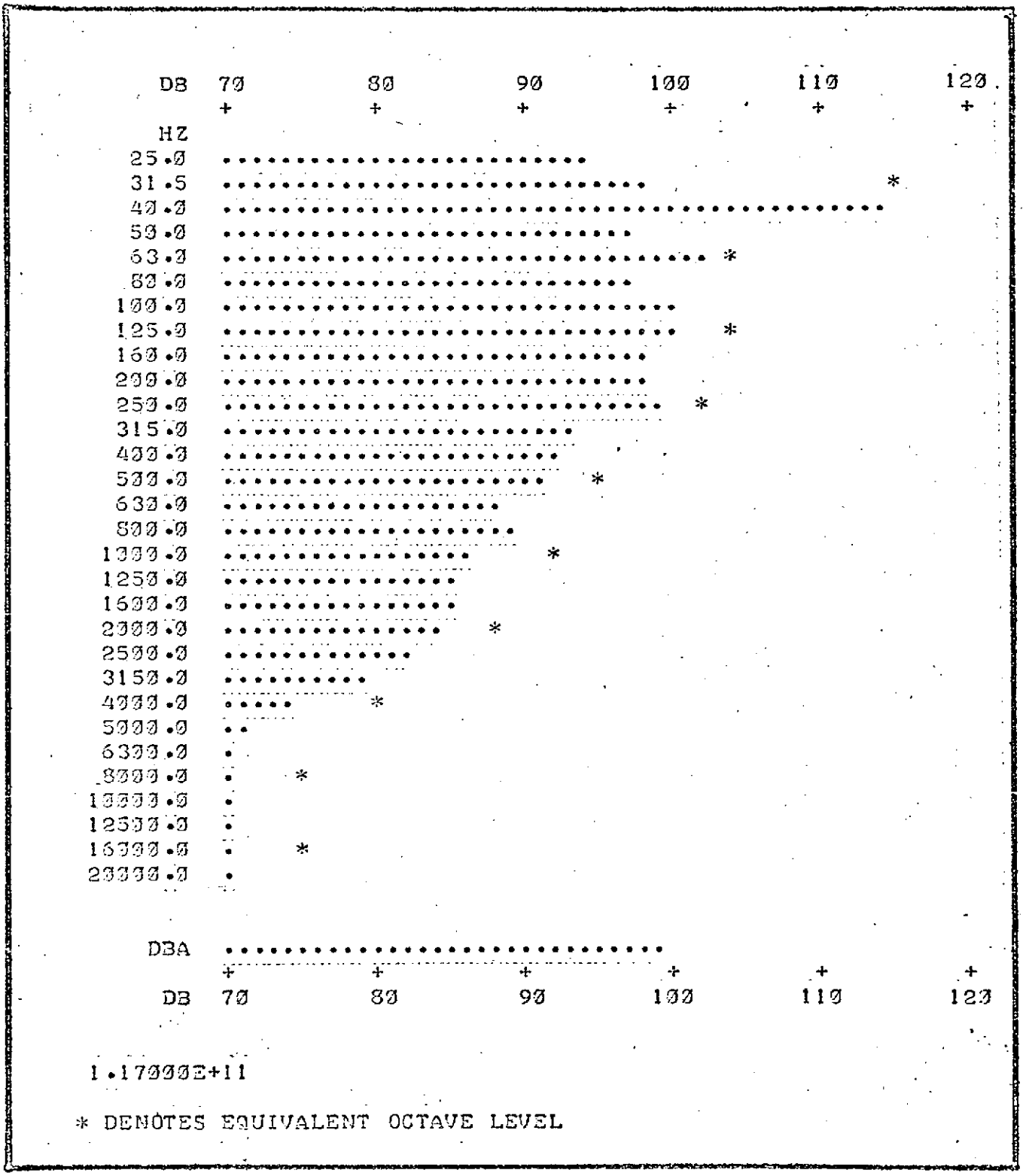

Tunnel Spectrum, Position 2, Test 6, q_u= 60

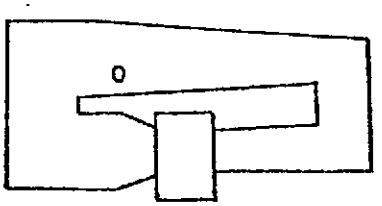

Figure 4.93

```
      DB   80          90          100         110         120         130
           +           +           +           +           +           +
      HZ
    25.0   ....................................
    31.5   ....................                *
    40.0   ..................
    50.0   ..................................
    63.0   ....................              *
    80.0   ........................
   100.0   ........................
   125.0   ........................          *
   160.0   ..............................
   200.0   ..............................
   250.0   ..............................    *
   315.0   ........................
   400.0   ....................
   500.0   ..................      *
   630.0   ................
   800.0   ................
  1000.0   ..............      *
  1250.0   ............
  1600.0   ............
  2000.0   ............  *
  2500.0   ........
  3150.0   ......
  4000.0   .     *
  5000.0   .
  6300.0   .
  8000.0   .   *
 10000.0   .
 12500.0   .
 16000.0   .   *
 20000.0   .

       DBA  ............................
           +           +           +           +           +           +
        DB  80          90          100         110         120         130

 1.140000E+11

* DENOTES EQUIVALENT OCTAVE LEVEL
```

Tunnel Spectrum, Position 2, Test 6, q_u= 110

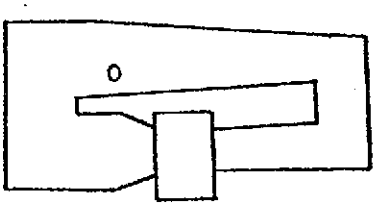

Figure 4.94

```
      DB   80         90         100        110        120        130
           +          +          +          +          +          +
      HZ
    25.0   ..........................................
    31.5   ..................                         *
    40.0   ...............
    50.0   ..................................
    63.0   ....................                       *
    80.0   ...................................
   100.0   ...................................
   125.0   ........................                   *
   160.0   ..............................
   200.0   ............................
   250.0   ..............................  *
   315.0   ........................
   400.0   ......................
   500.0   ..................     *
   630.0   ...............
   800.0   .............
  1000.0   ............      *
  1250.0   ..........
  1600.0   ..........
  2000.0   ............  *
  2500.0   ........
  3150.0   ......
  4000.0   ..    *
  5000.0   .
  6300.0   .
  8000.0   .   *
 10000.0   .
 12500.0   .
 16000.0   .   *
 20000.0   .

      DBA  ............................
           +          +          +          +          +          +
       DB  80         90         100        110        120        130

 1.200000E+11

* DENOTES EQUIVALENT OCTAVE LEVEL
```

Tunnel Spectrum, Position 2, Test 6, q_u= 105

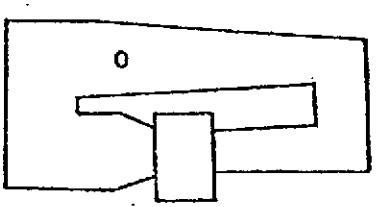

Figure 4-95

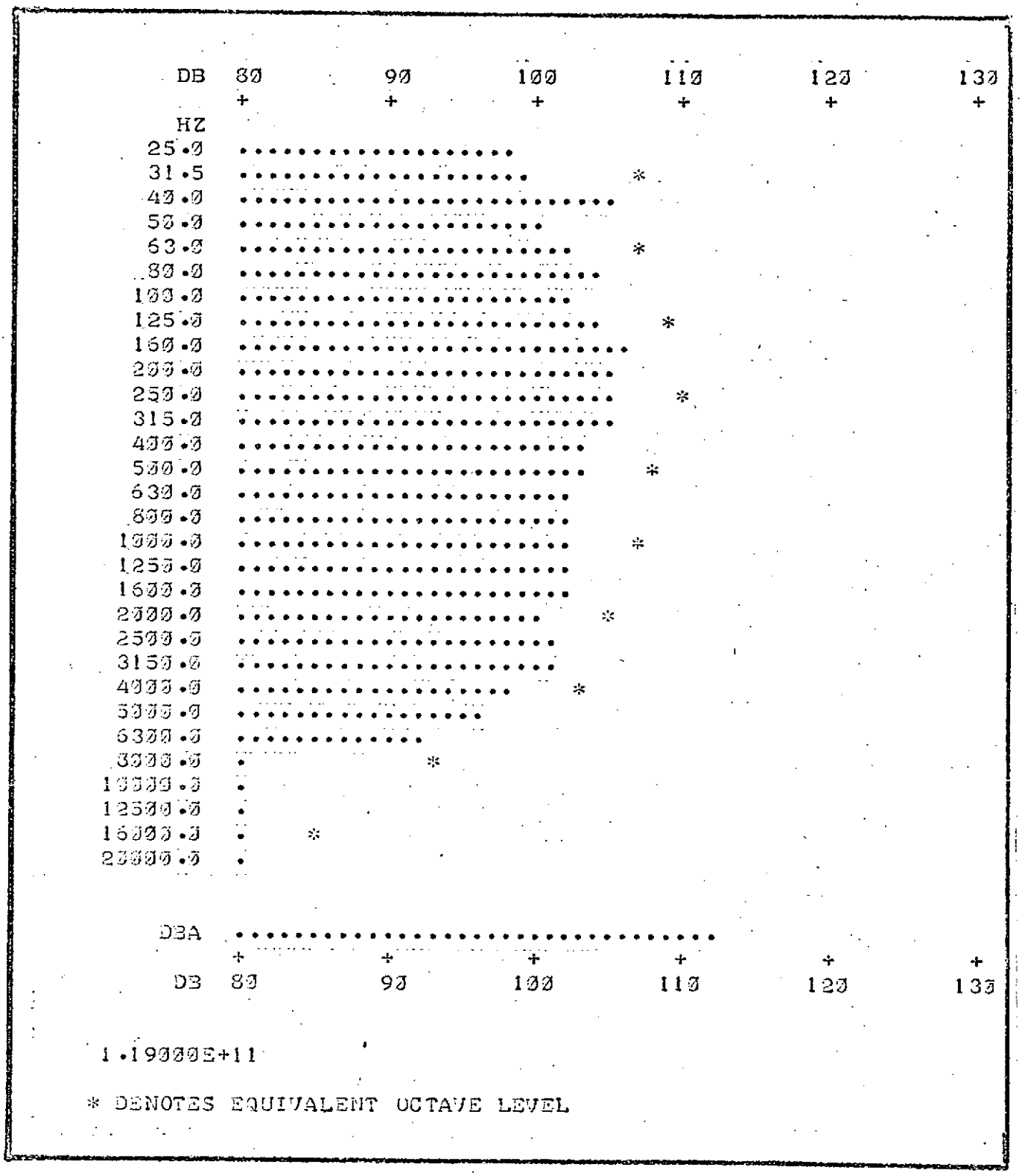

Tunnel Spectrum, Position 18, Test 6, q_u= 60

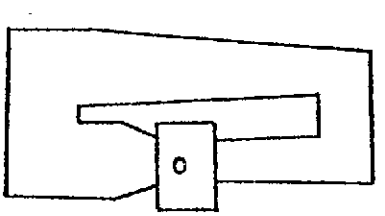

Figure 4-96

```
      DB   80          90          100         110         120         130
           +           +           +           +           +           +
      HZ
    25.0   ..............................
    31.5   ..........................      *
    40.0   ........................
    50.0   ....................................
    63.0   ........................              *
    80.0   ..............................
   100.0   ..................................
   125.0   ....................................    *
   160.0   ..................................
   200.0   ..................................
   250.0   ................................      *
   315.0   ..................................
   400.0   ....................................
   500.0   ..................................      *
   630.0   ................................
   800.0   ..............................
  1000.0   ..............................      *
  1250.0   ..............................
  1600.0   ..............................
  2000.0   ................................    *
  2500.0   ............................
  3150.0   ..........................
  4000.0   ..............................    *
  5000.0   ........................
  6300.0   ..................
  8000.0   ..........          *
 10000.0   .
 12500.0   .
 16000.0   .     *
 20000.0   .

     DBA   ........................................
           +           +           +           +           +           +
      DB   80          90          100         110         120         130

 1.220000E+11

* DENOTES EQUIVALENT OCTAVE LEVEL
```

Tunnel Spectrum, Position 18, Test 6, q_u= 105

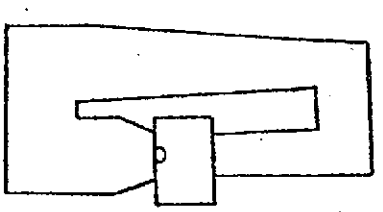

Figure 4-97

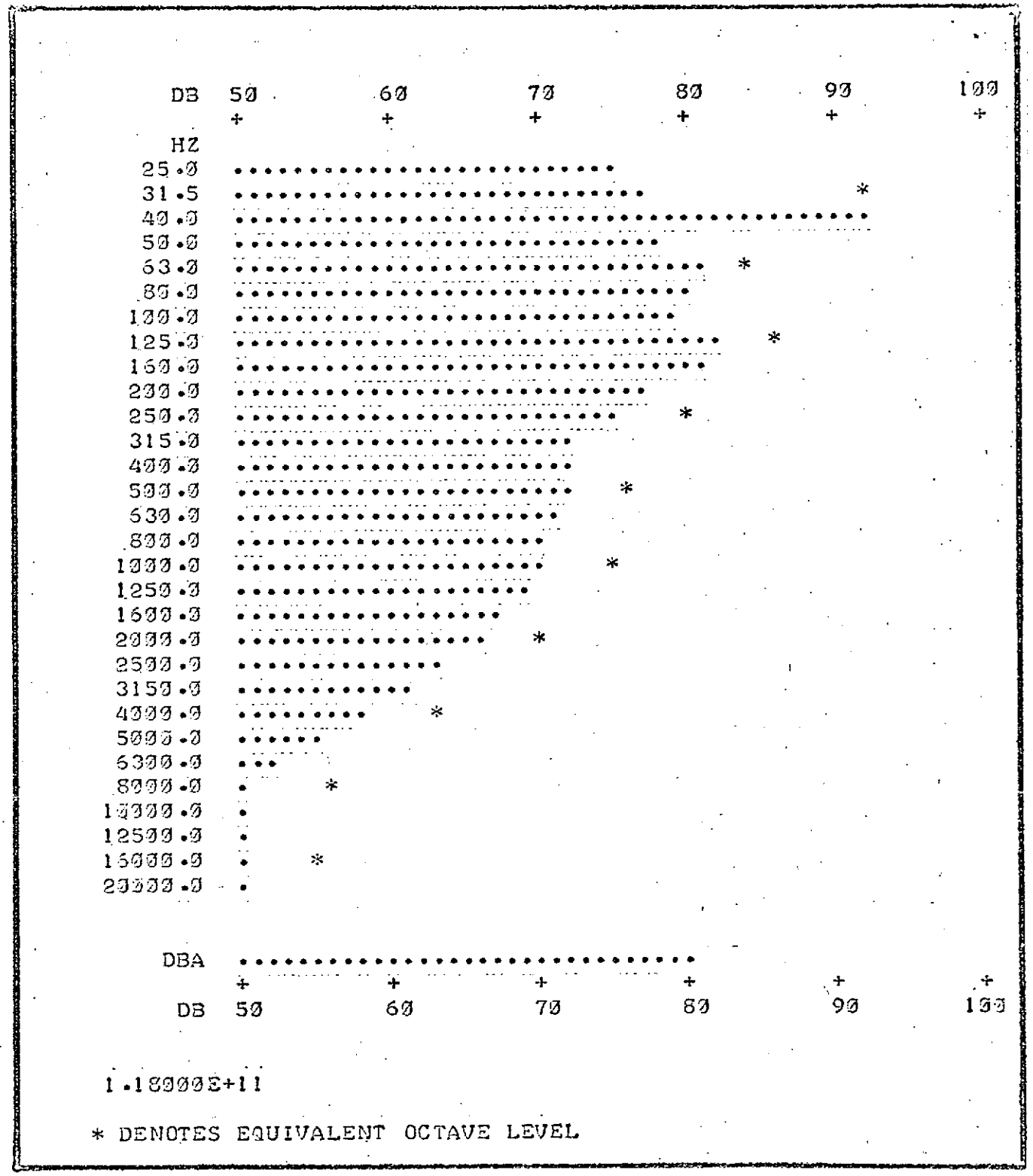

Tunnel Spectrum, Position 17, Test 6, q_u= 60

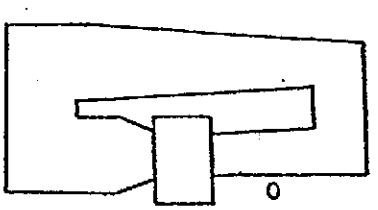

Figure 4-98

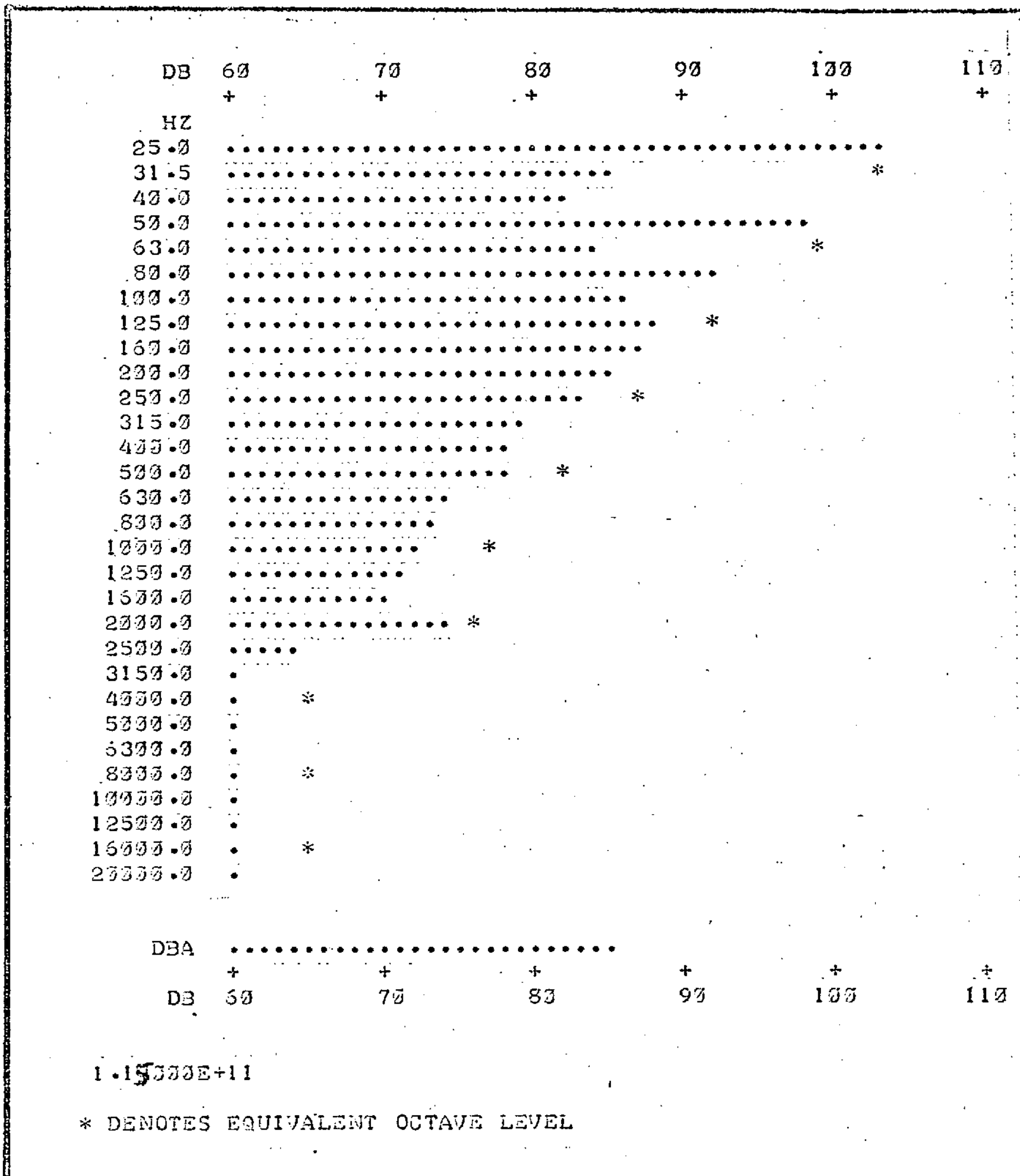

Tunnel Spectrum, Position 17, Test 6, $q_u = 110$

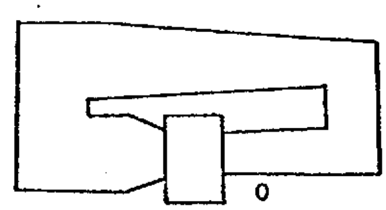

Figure 4-99

```
      DB   60        70        80        90        100       110
           +         +         +         +         +         +
      HZ
    25.0   ••••••••••••••••••••••••••••••••••••••••••••••••••
    31.5   ••••••••••••••••••••••••••                        *
    40.0   ••••••••••••••••••••••
    50.0   ••••••••••••••••••••••••••••••
    63.0   ••••••••••••••••••••••                  *
    80.0   •••••••••••••••••••••••••••••••••••
   100.0   ••••••••••••••••••••••••••••••••••••
   125.0   •••••••••••••••••••••••••••••••                *
   160.0   ••••••••••••••••••••••••
   200.0   ••••••••••••••••••••••••
   250.0   ••••••••••••••••••••••••          *
   315.0   ••••••••••••••••••
   400.0   •••••••••••••••••
   500.0   ••••••••••••••••          *
   630.0   •••••••••••••
   800.0   ••••••••••••
  1000.0   ••••••••••••      *
  1250.0   ••••••••••
  1600.0   •••••••••
  2000.0   ••••••••••••   *
  2500.0   •••••••
  3150.0   ••••
  4000.0   •     *
  5000.0   •
  6300.0   •
  8000.0   •     *
 10000.0   •
 12500.0   •
 16000.0   •     *
 20000.0   •

      DBA  ••••••••••••••••••••••••••
           +         +         +         +         +         +
      DB   60        70        80        90        100       110

 1.21000E+11

* DENOTES EQUIVALENT OCTAVE LEVEL
```

Tunnel Spectrum, Position 17, Test 6, q_u= 105

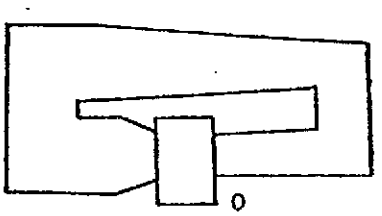

Figure 4-100

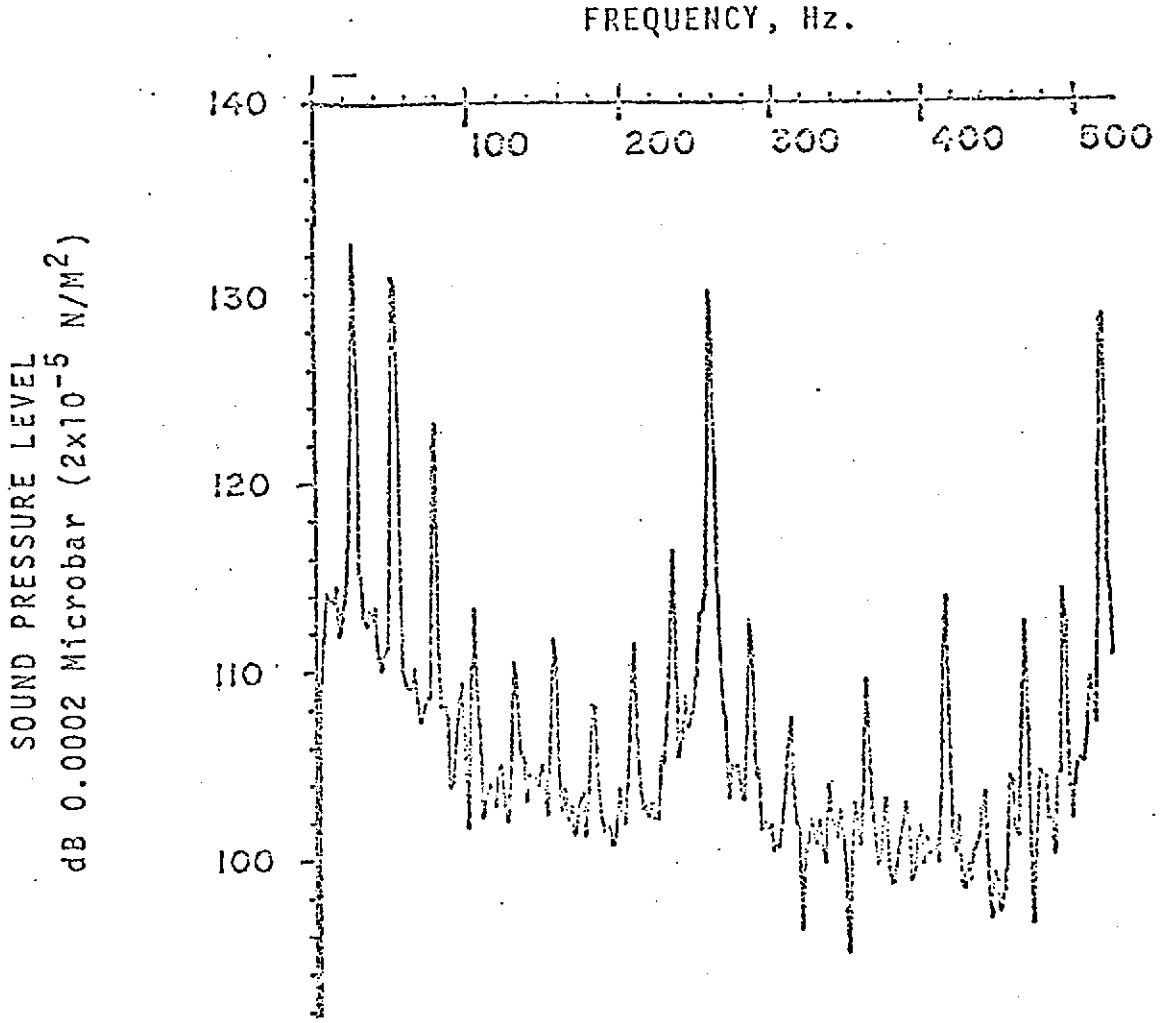

TEST SERIES No. 1
Blade Tip Noise

q_u = 110 p.s.f.

FIGURE 4-101

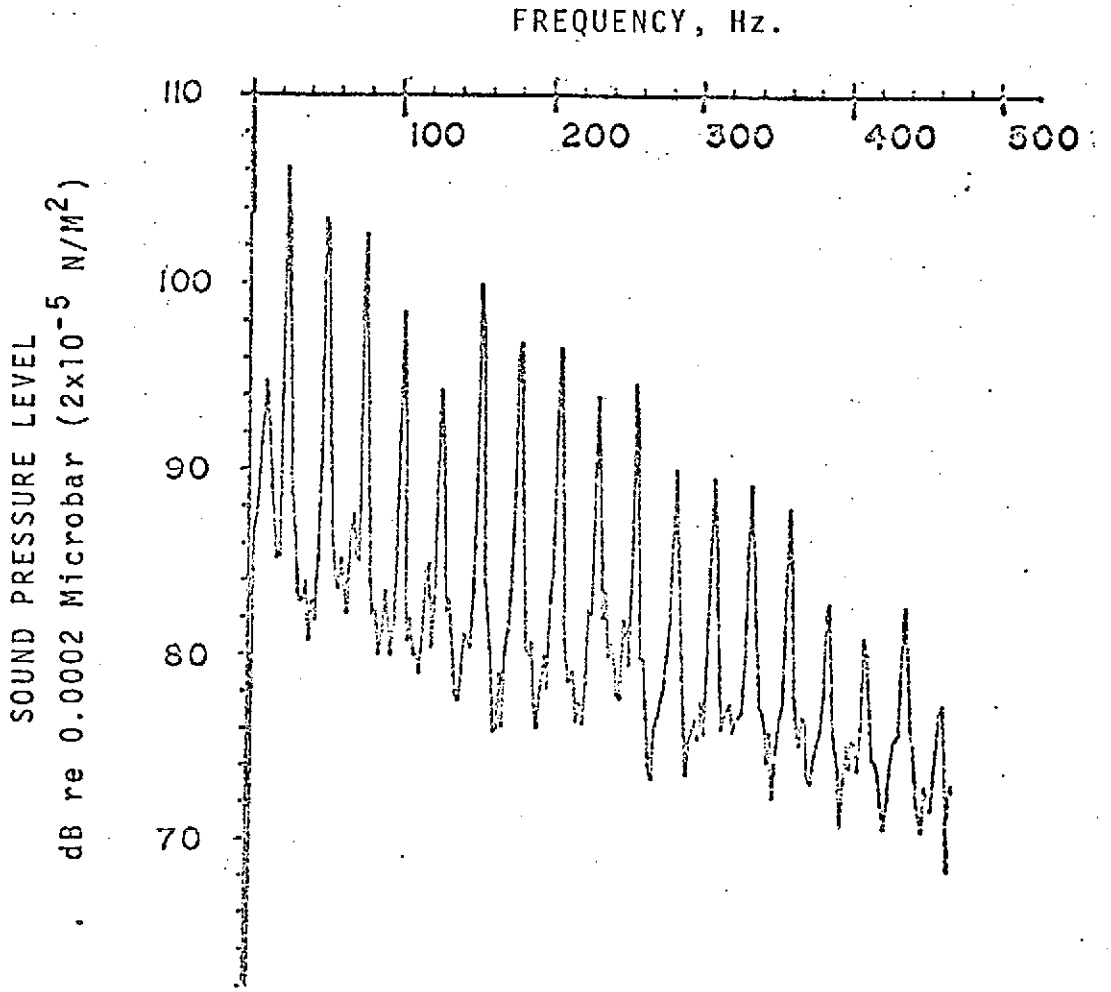

TEST SERIES No. 1
Standard Microphone Noise

$q_u \approx 110$ p.s.f.

FIGURE 4-102

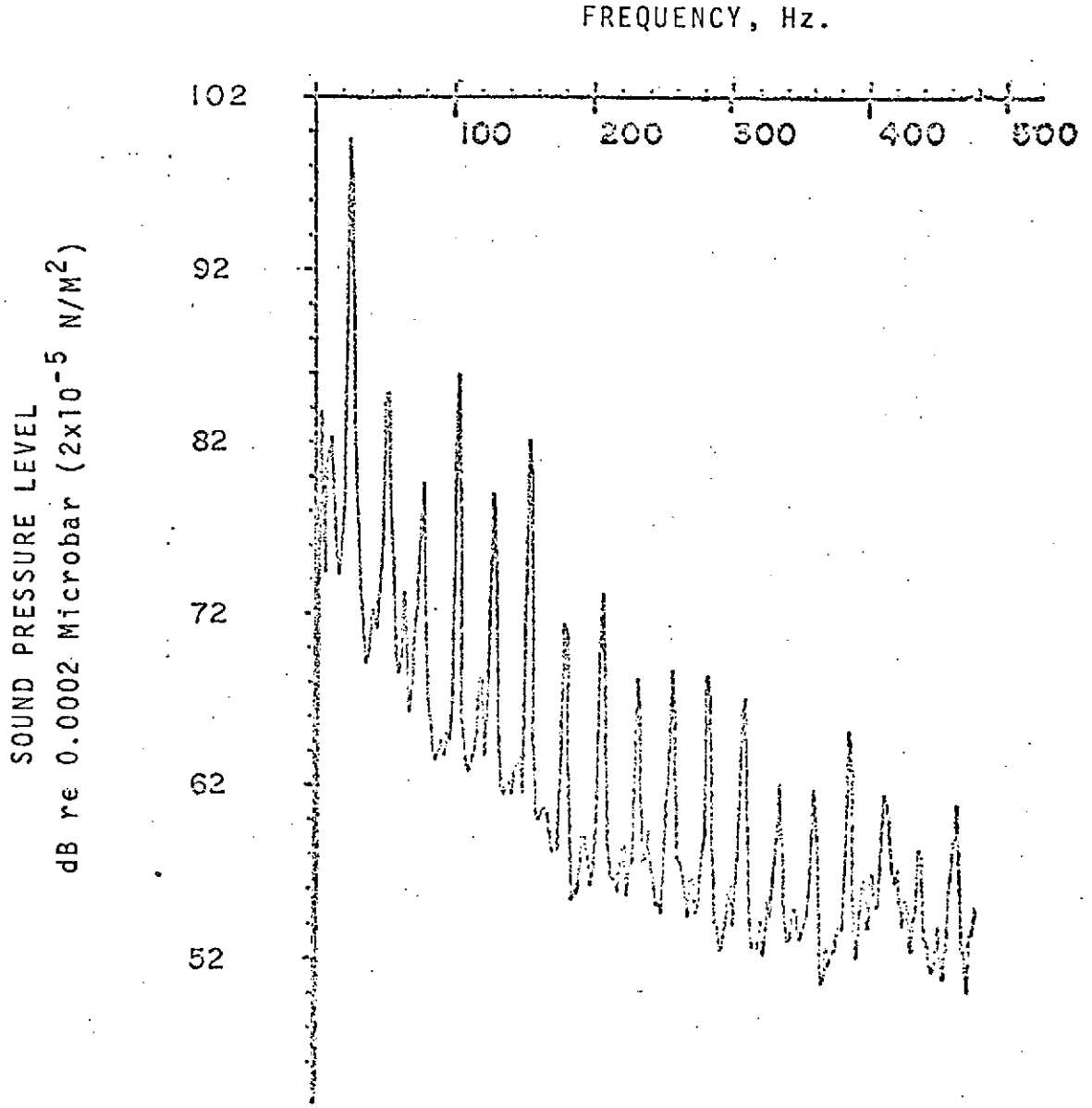

TEST SERIES No. 4
Microphone Outside Tunnel (TP11)

q_u - 110 p.s.f.

FIGURE 4-103

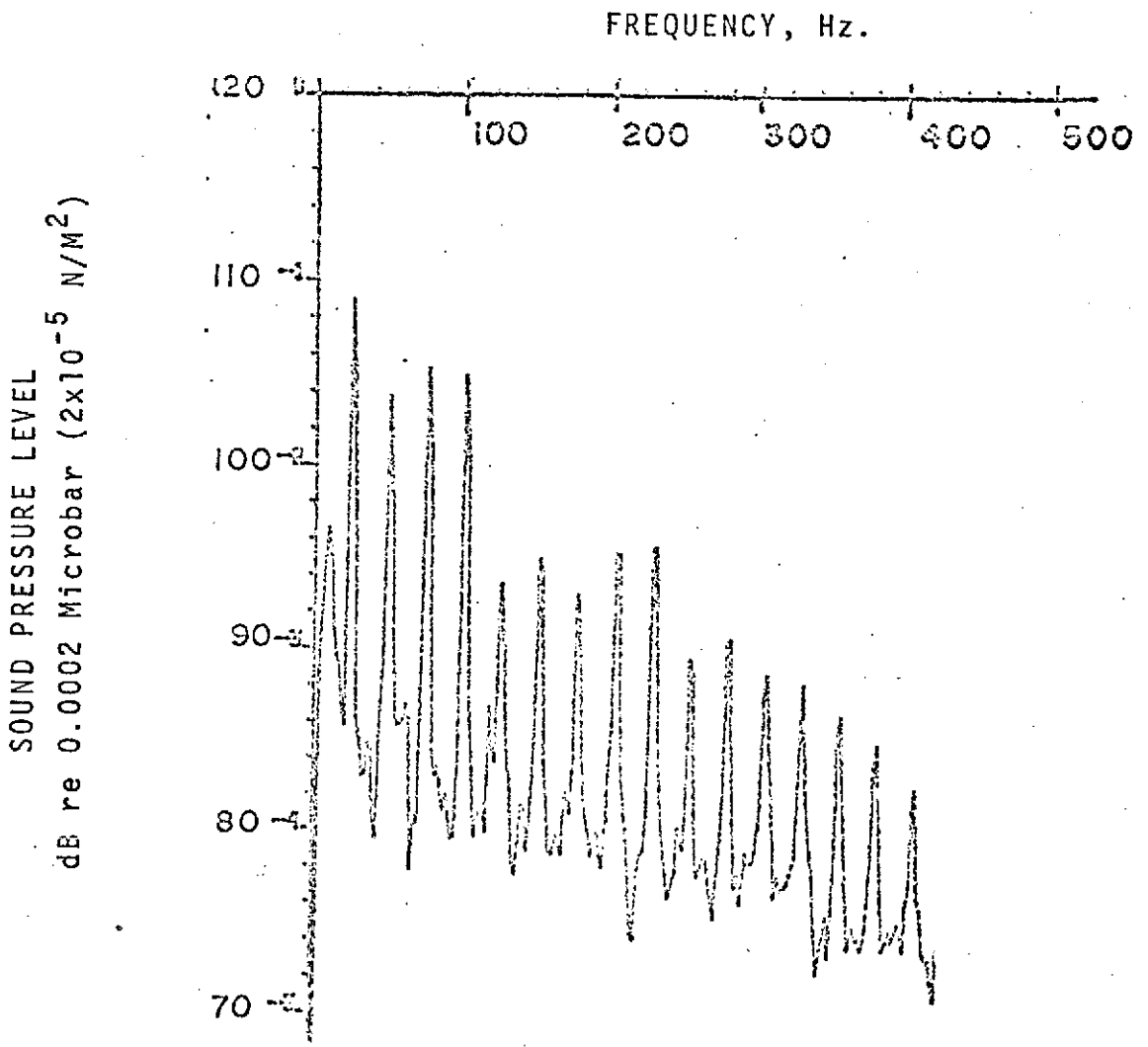

TEST SERIES No. 5
Position No. 14 Noise (Through Tunnel Vanes)

q_u - 105 p.s.f.

FIGURE 4-104

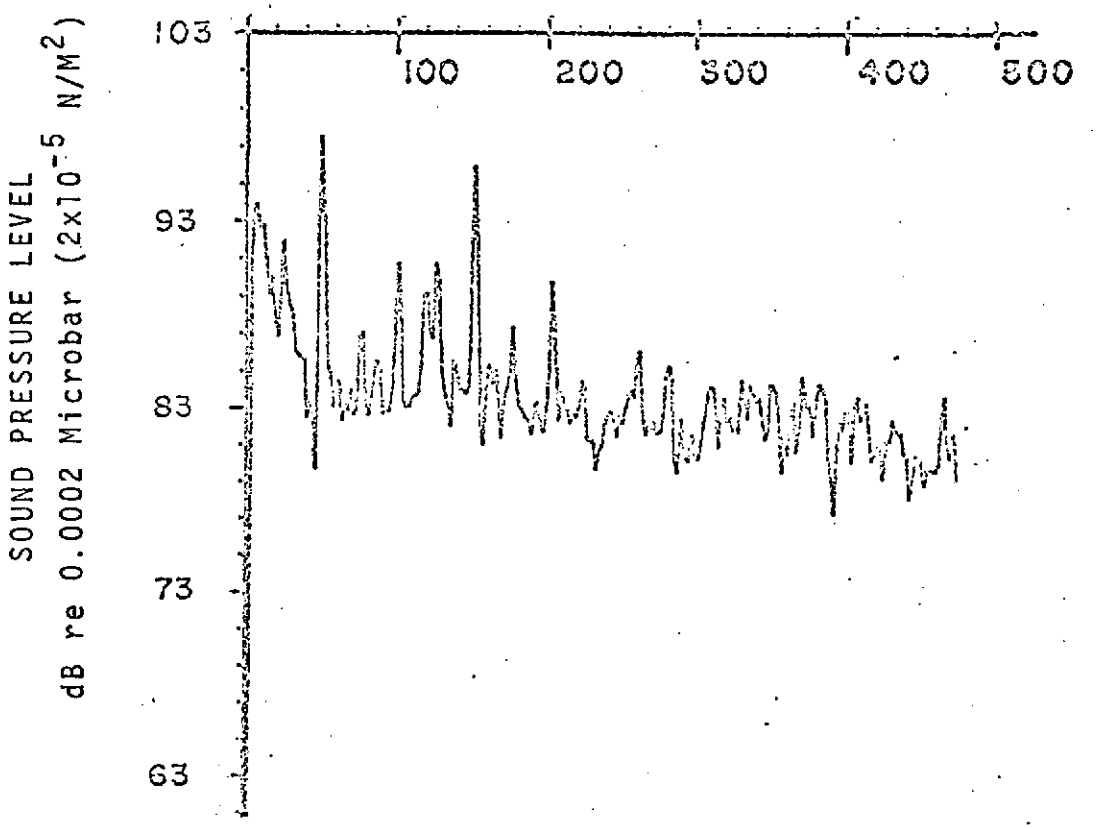

TEST SERIES No. 6
Test Section Noise Pos. 8

q_u = 105 p.s.f.

FIGURE 4-105

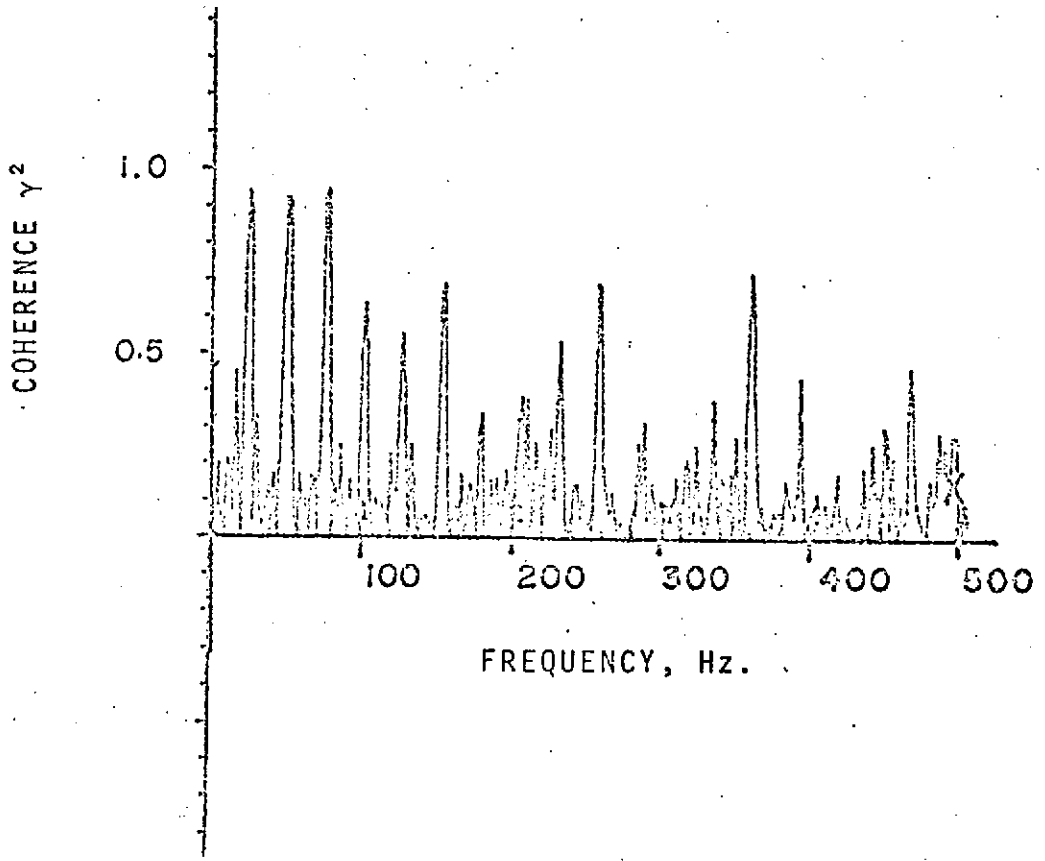

TEST SERIES No. 1
Coherence, Blade Tip Noise vs Standard Mic

FIGURE 4-106

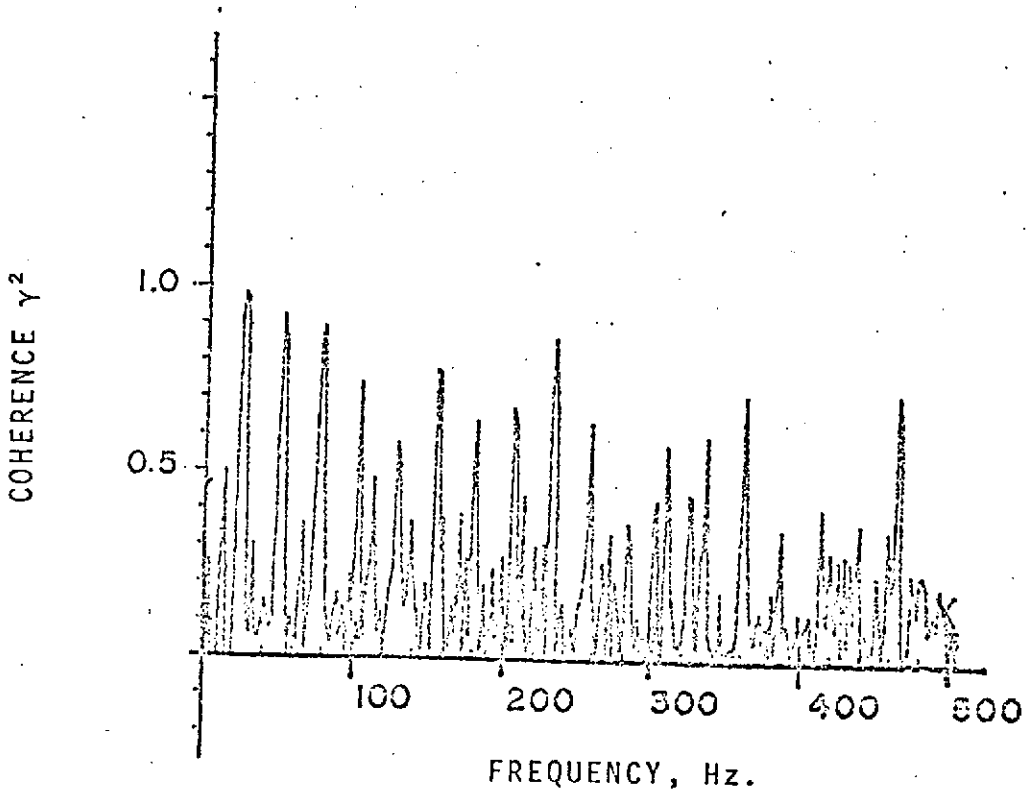

TEST SERIES No. 1
Coherence Blade Tip Noise vs Strut Vib.

q_u - 110 p.s.f.

FIGURE 4-107

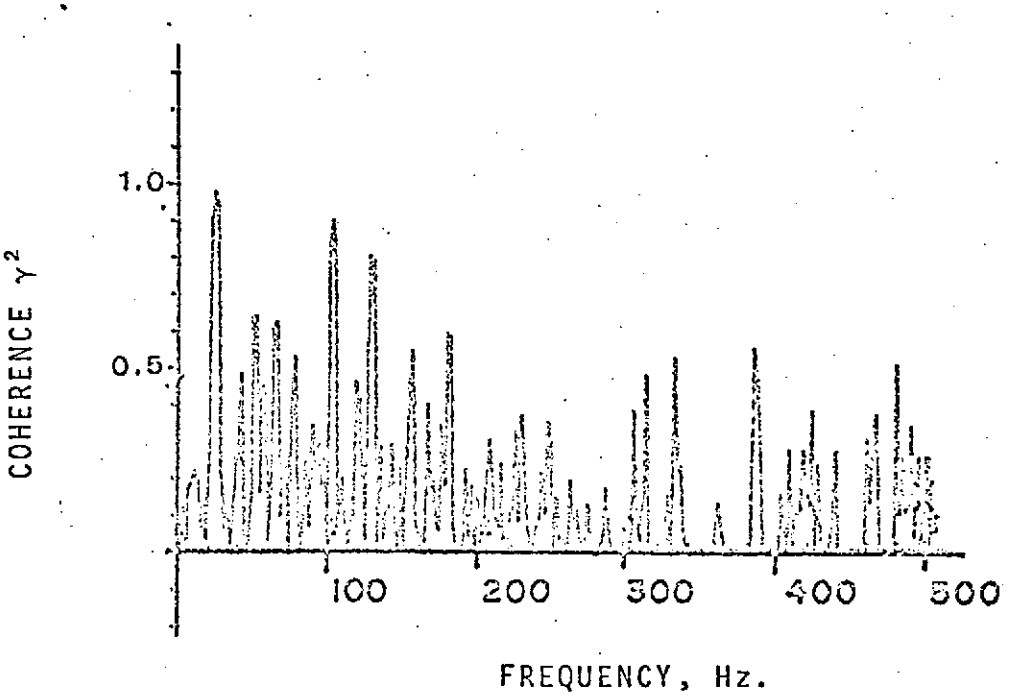

TEST SERIES No. 4
Coherence, Standard Mic. vs. Outside Mic.

FIGURE 4-108

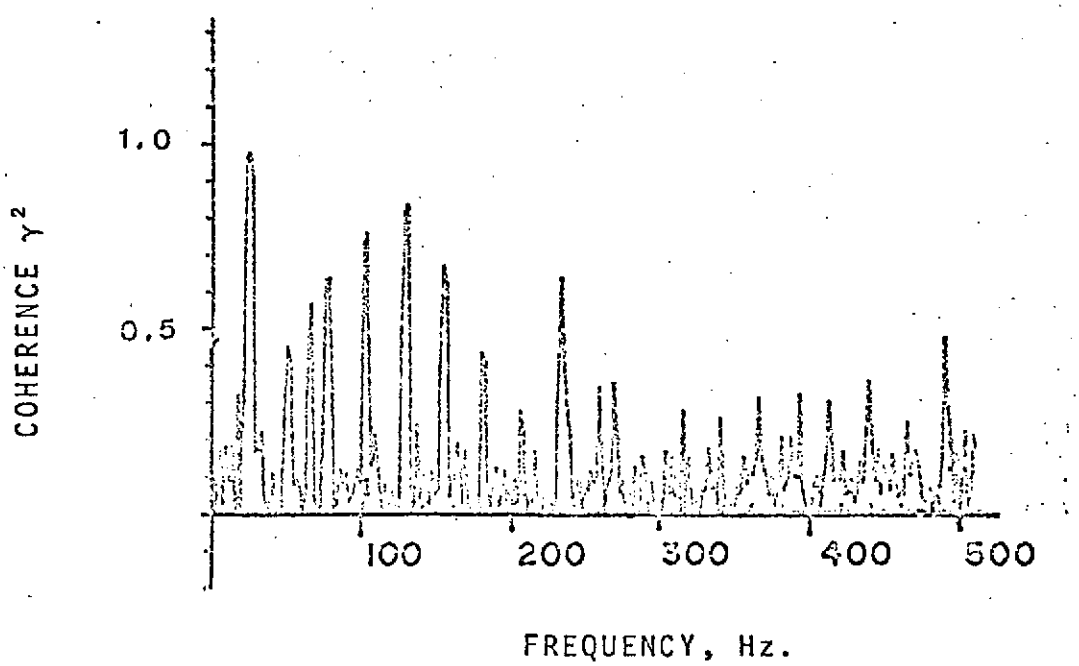

TEST SERIES No. 4
Coherence, Standard Mic. vs Wall Acceleration

FIGURE 4-109

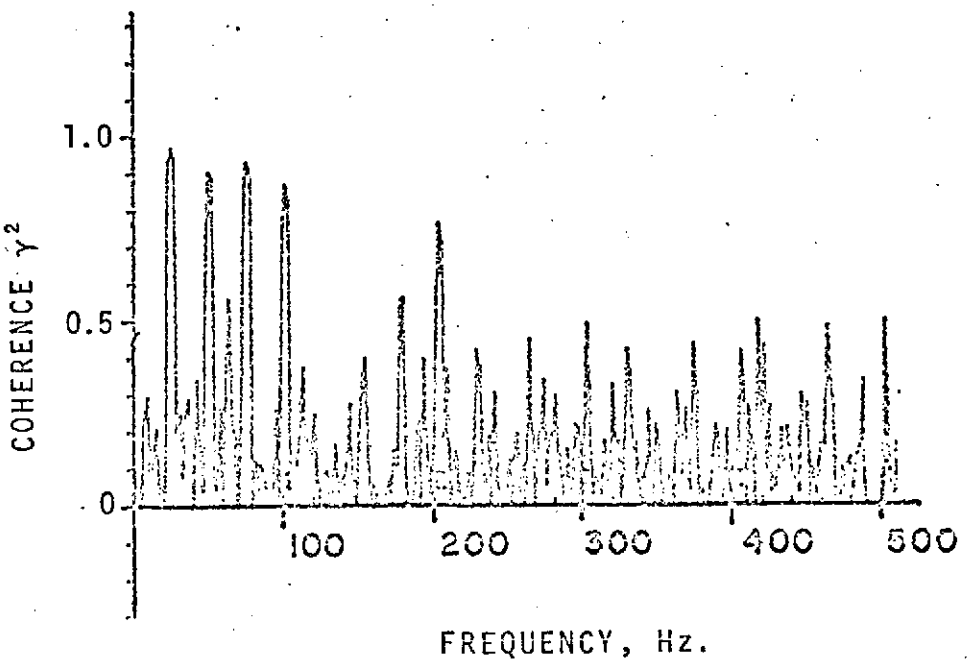

TEST SERIES No. 5
Coherence, Standard Mic. vs. Position 14

FIGURE 4-110

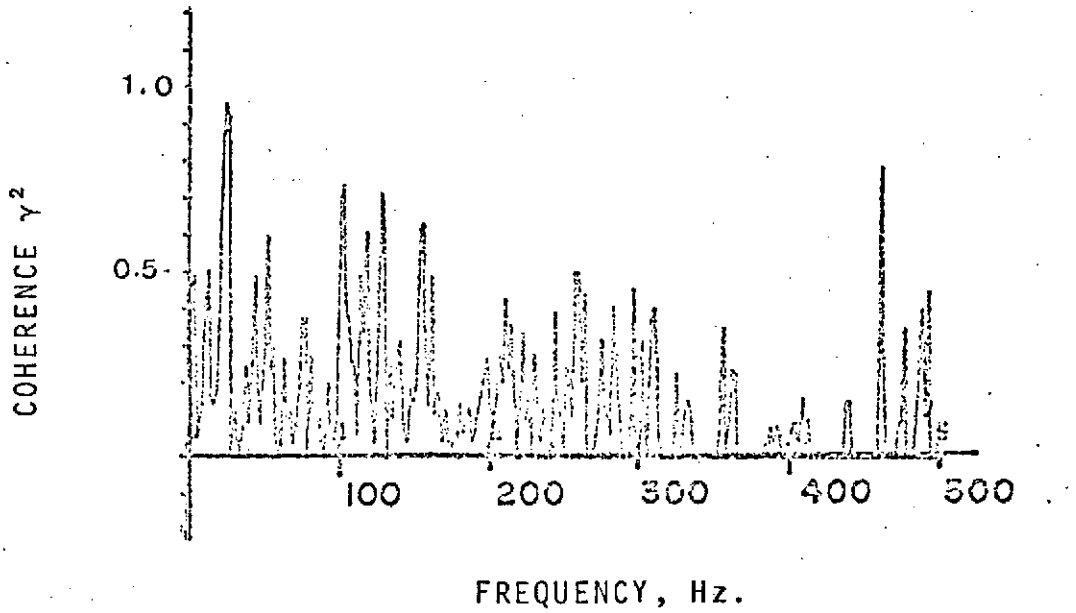

TEST SERIES No. 4
Coherence, Wall Acceleration vs. Microphone Outside

q_u = 110 p.s.f.

FIGURE 4-111

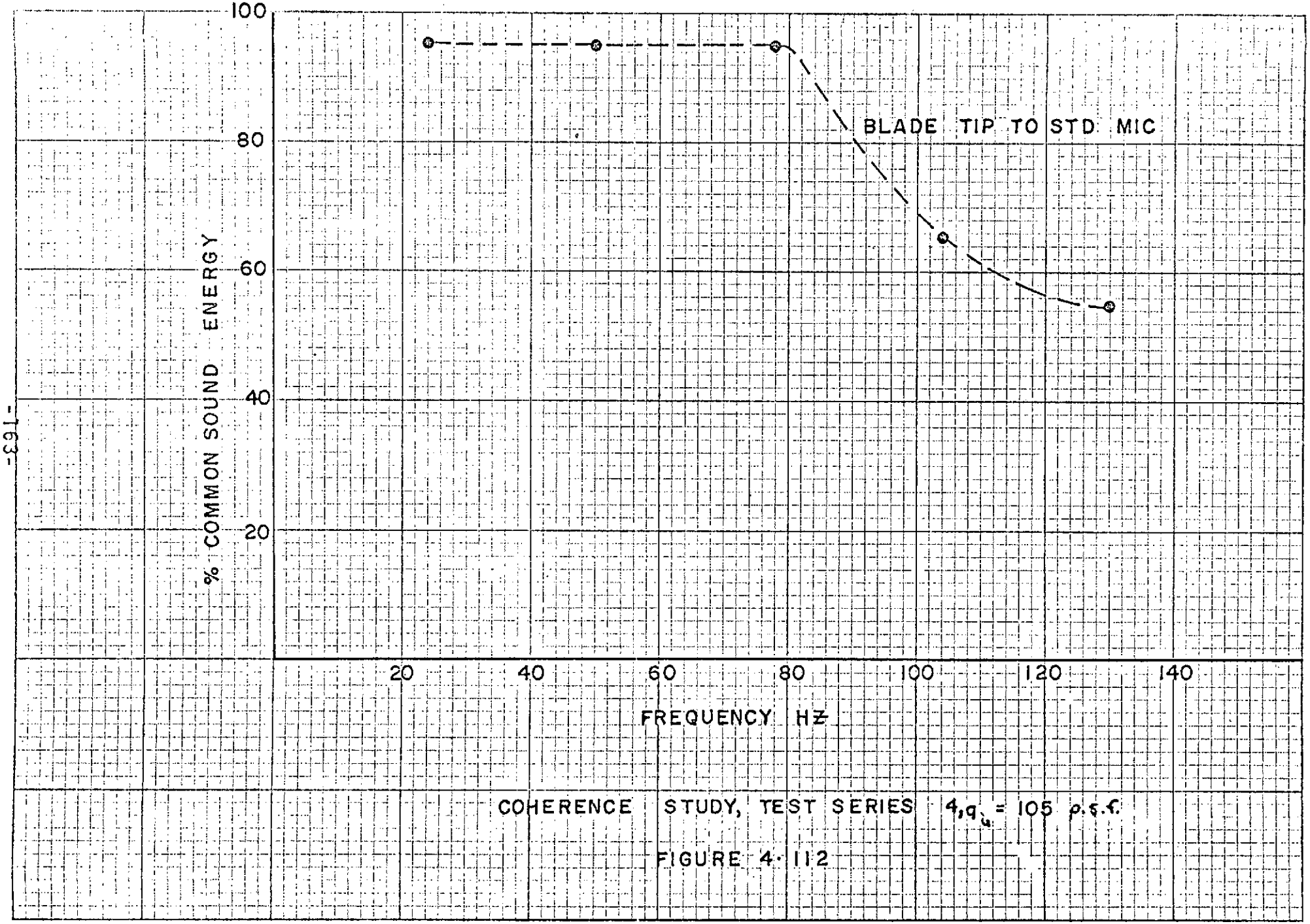

COHERENCE STUDY, TEST SERIES 4, q_a = 105 p.s.f.

FIGURE 4·112

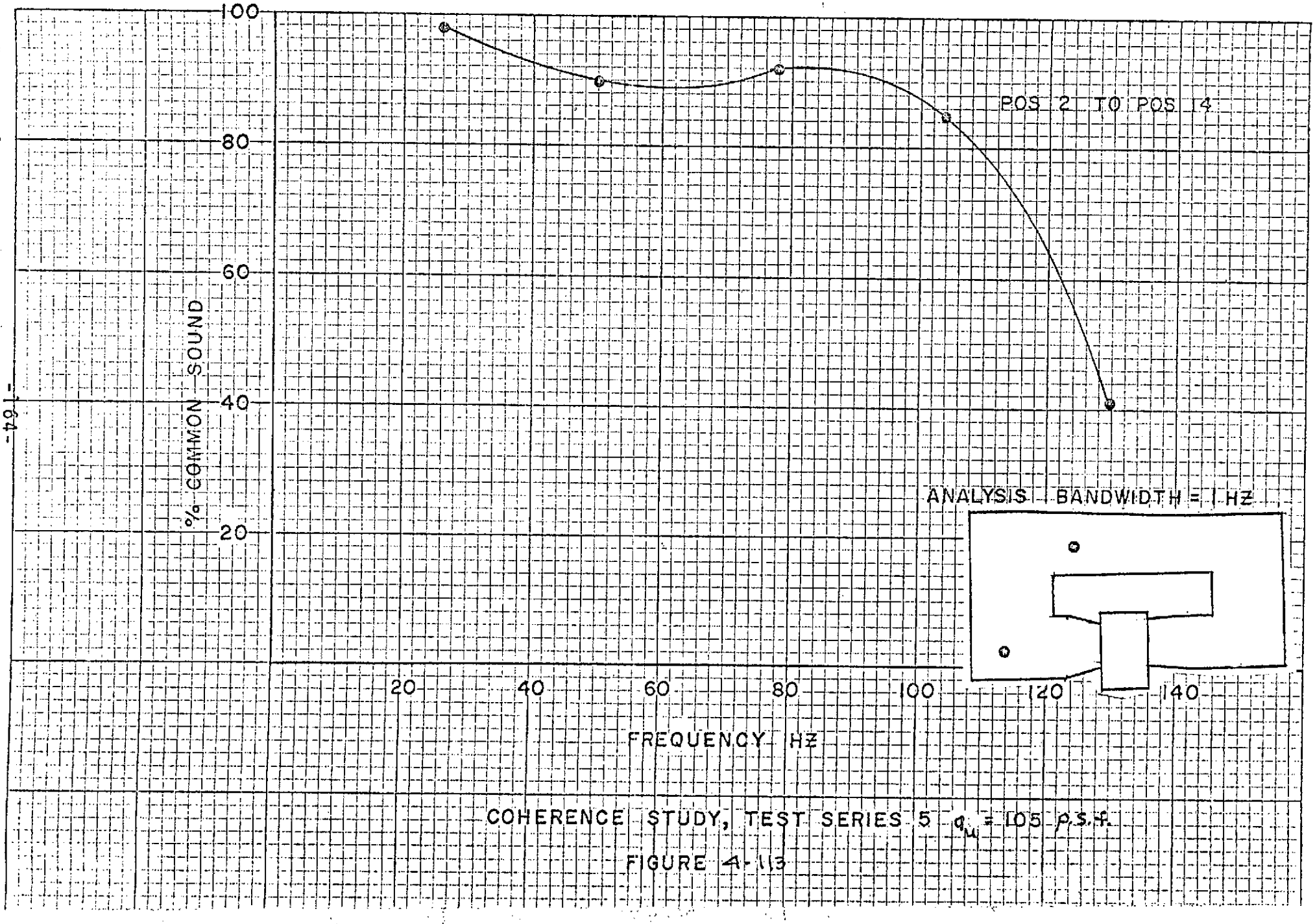

COHERENCE STUDY, TEST SERIES 5 q_u = 105 P.S.F.

FIGURE A-113

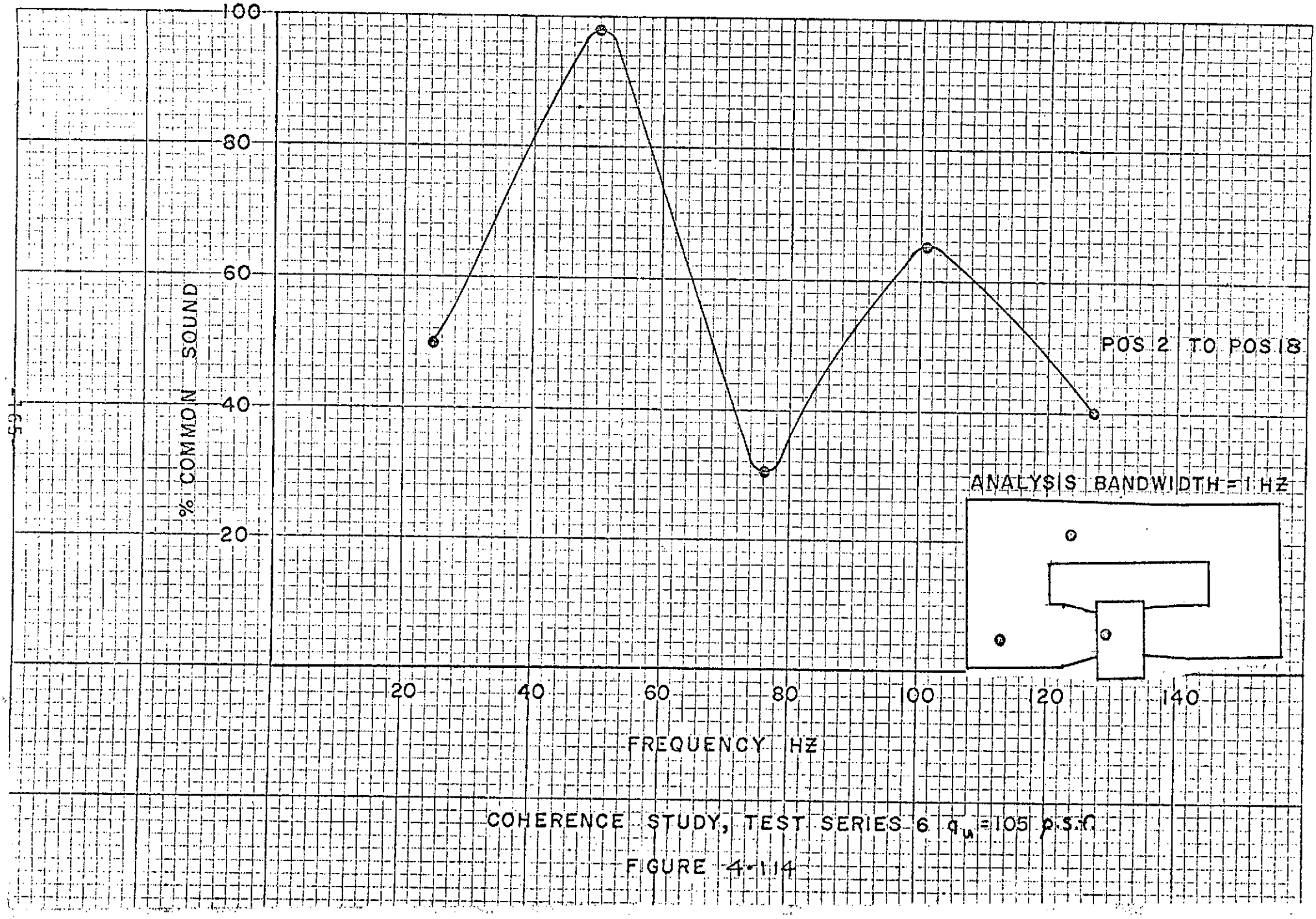

COHERENCE STUDY, TEST SERIES 6 q_u = 105 p.s.f.

FIGURE 4-114

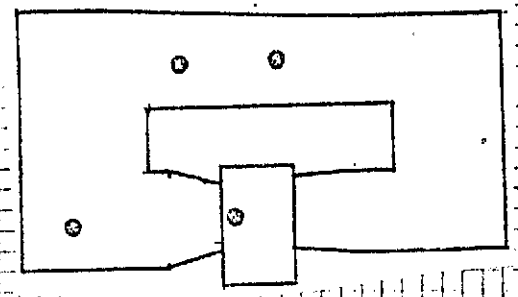

GUIDE VANES START

F = 1.38 Hz

PLANE OF FAN BLADES

SOUND—PRESSURE—LEVEL—DIFFERENCE—db RE 0.0002 MICROBAR (2 X 10-5 N/M2

60

40

20

20

40

100 200 300 400 500 600 700

DISTANCE FROM PLANE OF FAN, FEET

SOUND PRESSURE LEVEL DIFFERENCE AROUND TUNNEL

q_u = 105 p.s.f.

FIGURE A-115

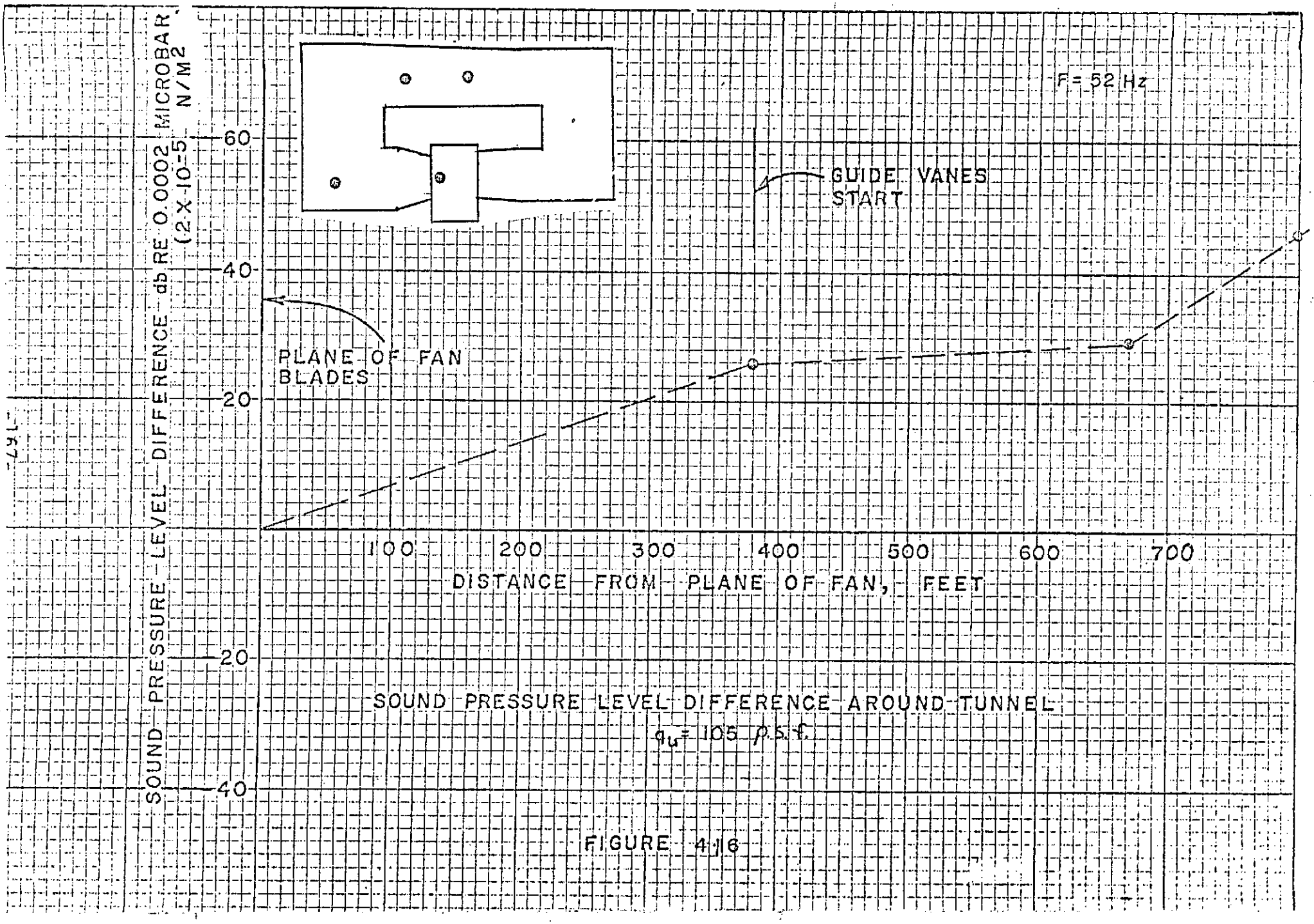

FIGURE 4.16

KEUFFEL & ESSER CO.

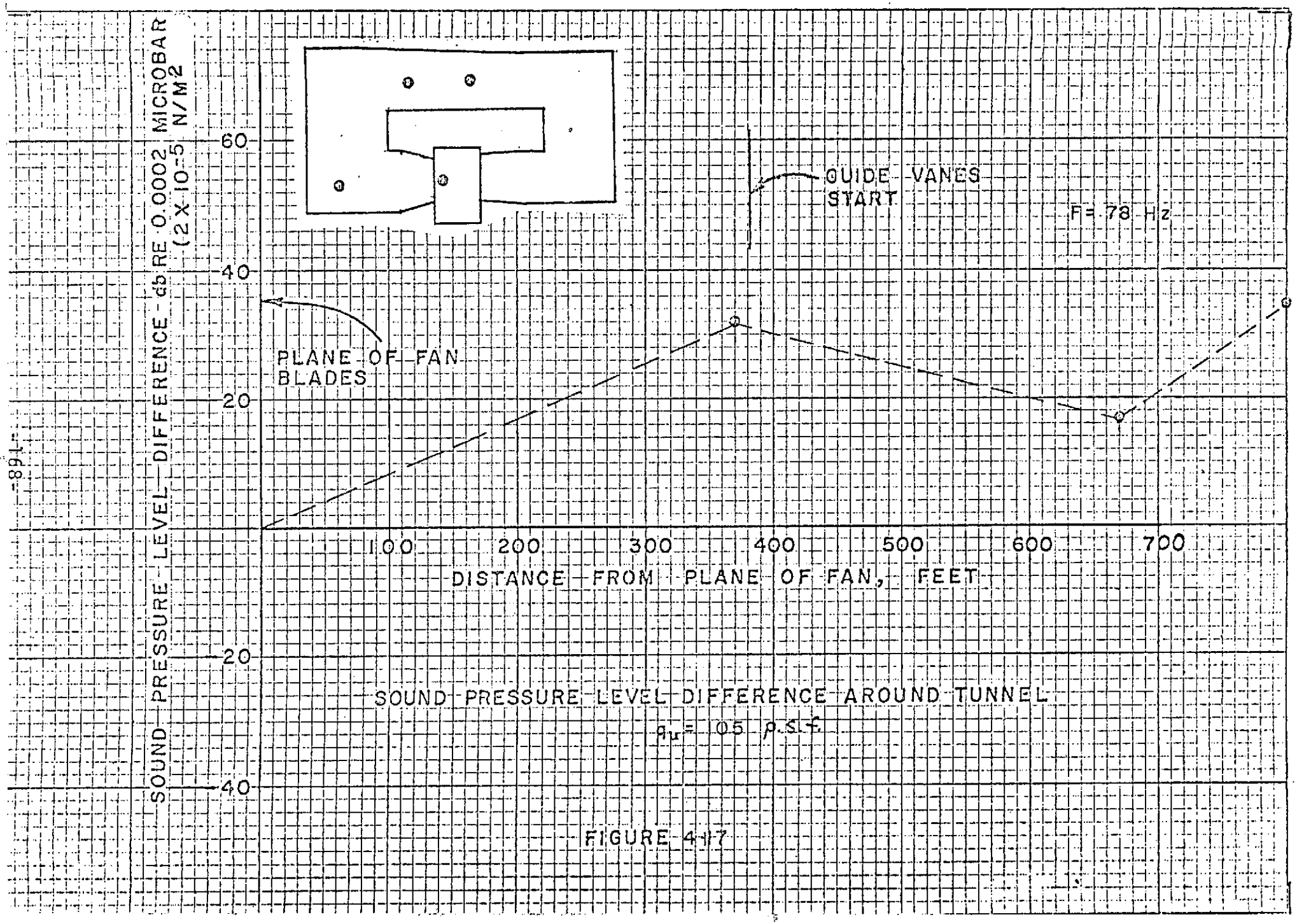

FIGURE 4-17

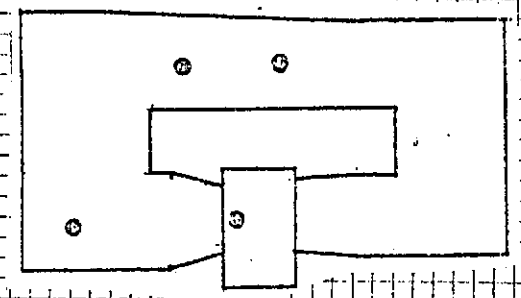

GUIDE VANES START

PLANE OF FAN BLADES

SOUND PRESSURE LEVEL DIFFERENCE db RE 0.0002 MICROBAR (2 X 10-5)

60
40
20

100 200 300 400 500 600 700

DISTANCE FROM PLANE OF FAN, FEET

20
40

SOUND PRESSURE LEVEL DIFFERENCE AROUND TUNNEL

q_u = 105 p.s.f.

FIGURE 4.118

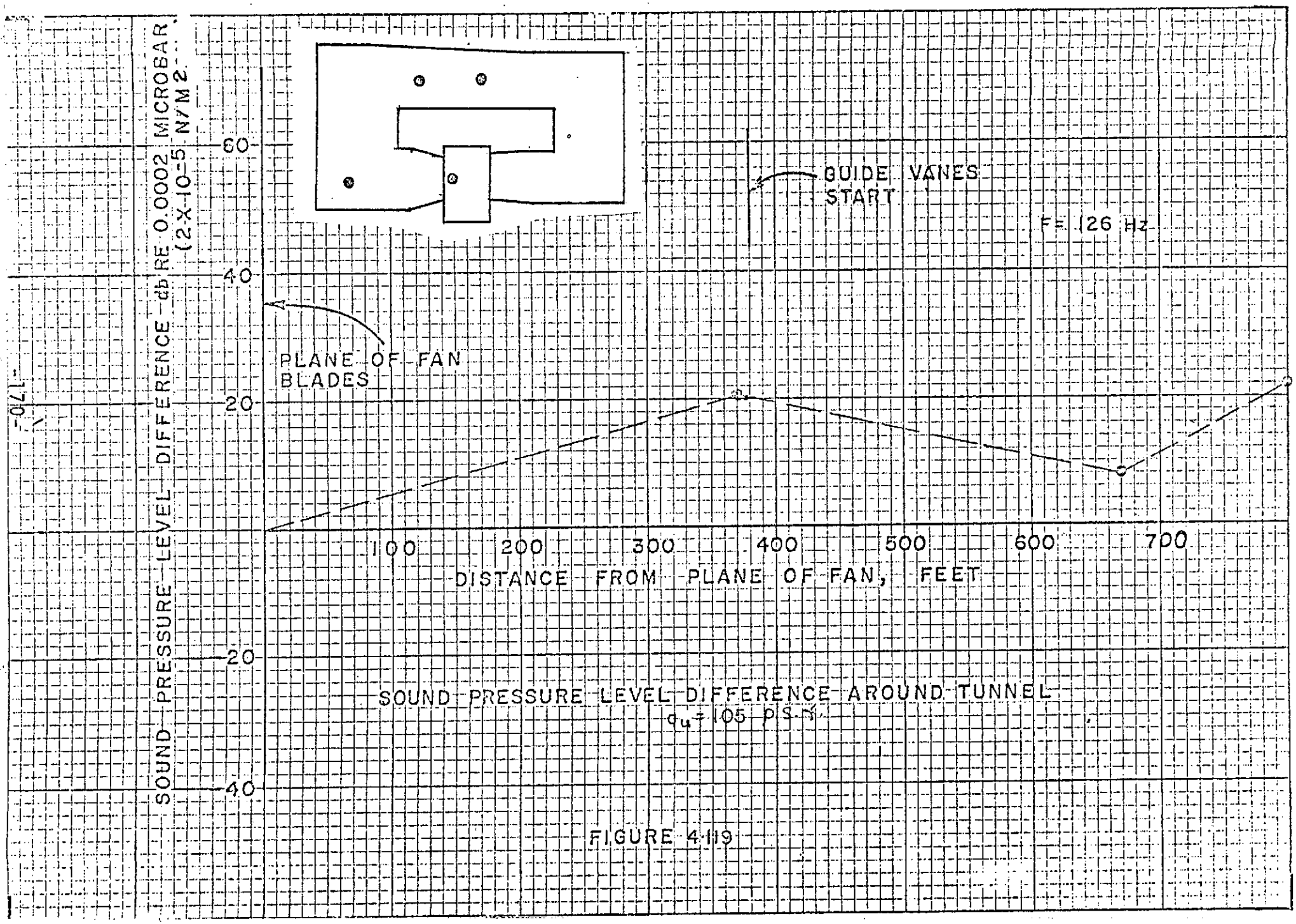
SOUND PRESSURE LEVEL DIFFERENCE -db RE 0.0002 MICROBAR (2-X-10-5 N/M2
60
40
20
PLANE OF FAN BLADES
GUIDE VANES START
F= 126 Hz
100
200
300
400
500
600
700
DISTANCE FROM PLANE OF FAN, FEET
20
40
SOUND PRESSURE LEVEL DIFFERENCE AROUND TUNNEL
q_d = 105 P.S.F.

FIGURE 4-119

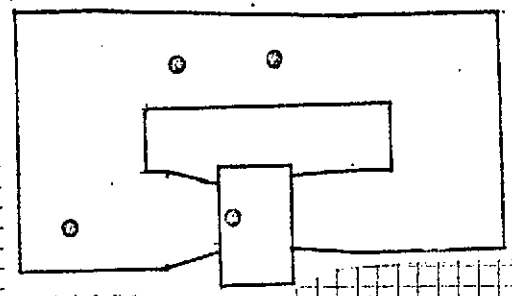

GUIDE VANES START

PLANE OF FAN BLADES

SOUND PRESSURE LEVEL DIFFERENCE - db RE 0.0002 MICROBAR (2 X 10-5 N/M2

60
40
20
20
40

100 200 300 400 500 600 700

DISTANCE FROM PLANE OF FAN, FEET

q_u = 105 P.S.F.

SOUND PRESSURE LEVEL DIFFERENCE AROUND TUNNEL

FIGURE 4-20

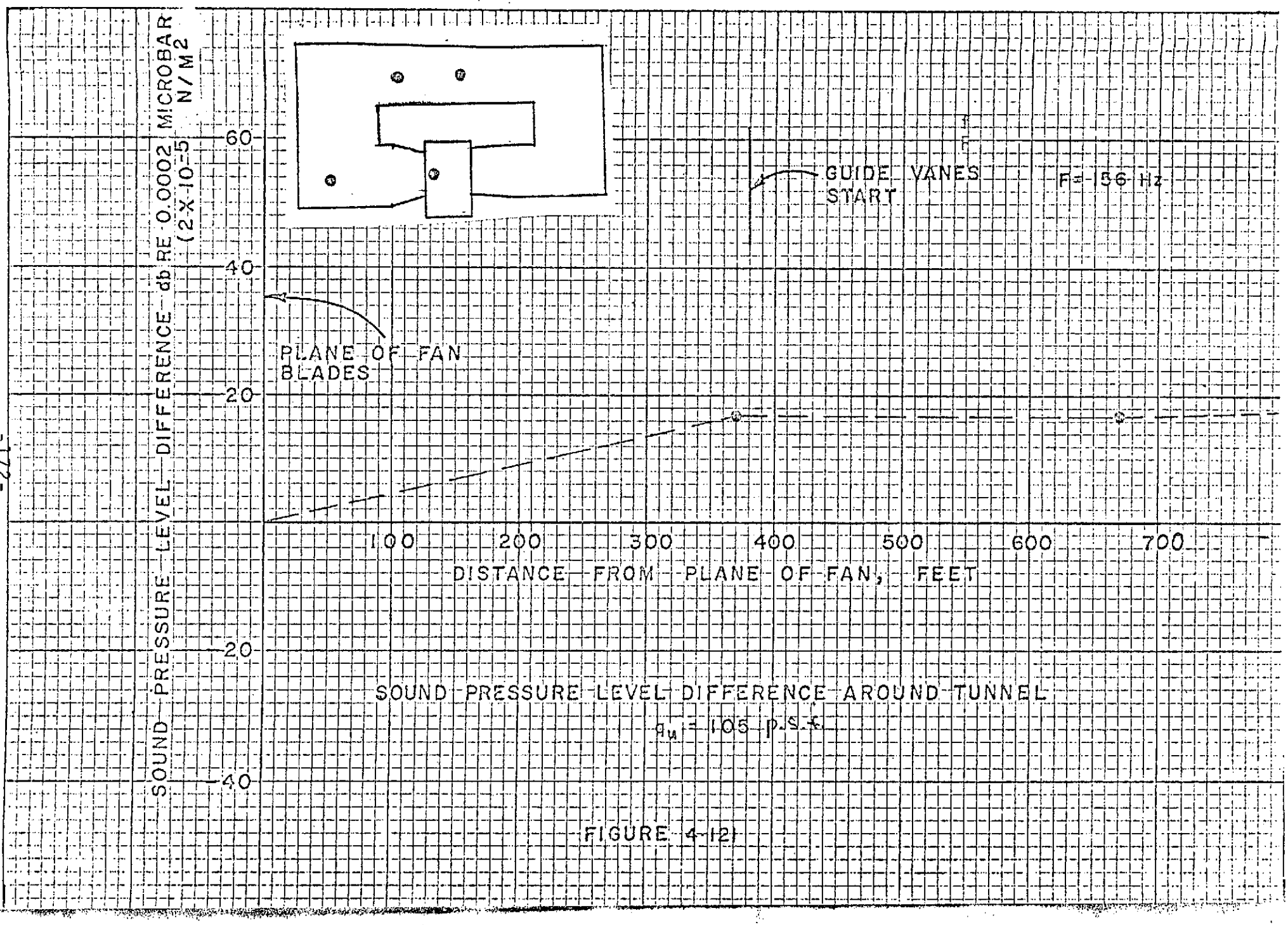
SOUND PRESSURE LEVEL DIFFERENCE—db RE 0.0002 MICROBAR (2 X 10⁻⁵ N/M²)
60
40
20
20
40
GUIDE VANES START
F = 156 Hz
PLANE OF FAN BLADES
100
200
300
400
500
600
700
DISTANCE FROM PLANE OF FAN, FEET
SOUND PRESSURE LEVEL DIFFERENCE AROUND TUNNEL
q_M = 105 p.s.f.

FIGURE 4-12

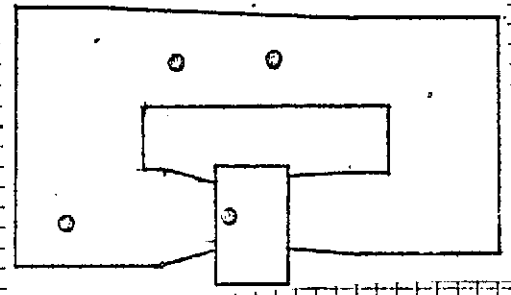

F = 182 Hz

GUIDE VANES START

PLANE OF FAN BLADES

SOUND PRESSURE LEVEL—DIFFERENCE—db RE 0.0002 MICROBAR (2 × 10⁻⁵ N/M2)

60
40
20
20
40

100 200 300 400 500 600 700

DISTANCE FROM PLANE OF FAN, FEET

SOUND PRESSURE LEVEL DIFFERENCE AROUND TUNNEL

$q_u = 105$ P.S.F.

FIGURE 4-122

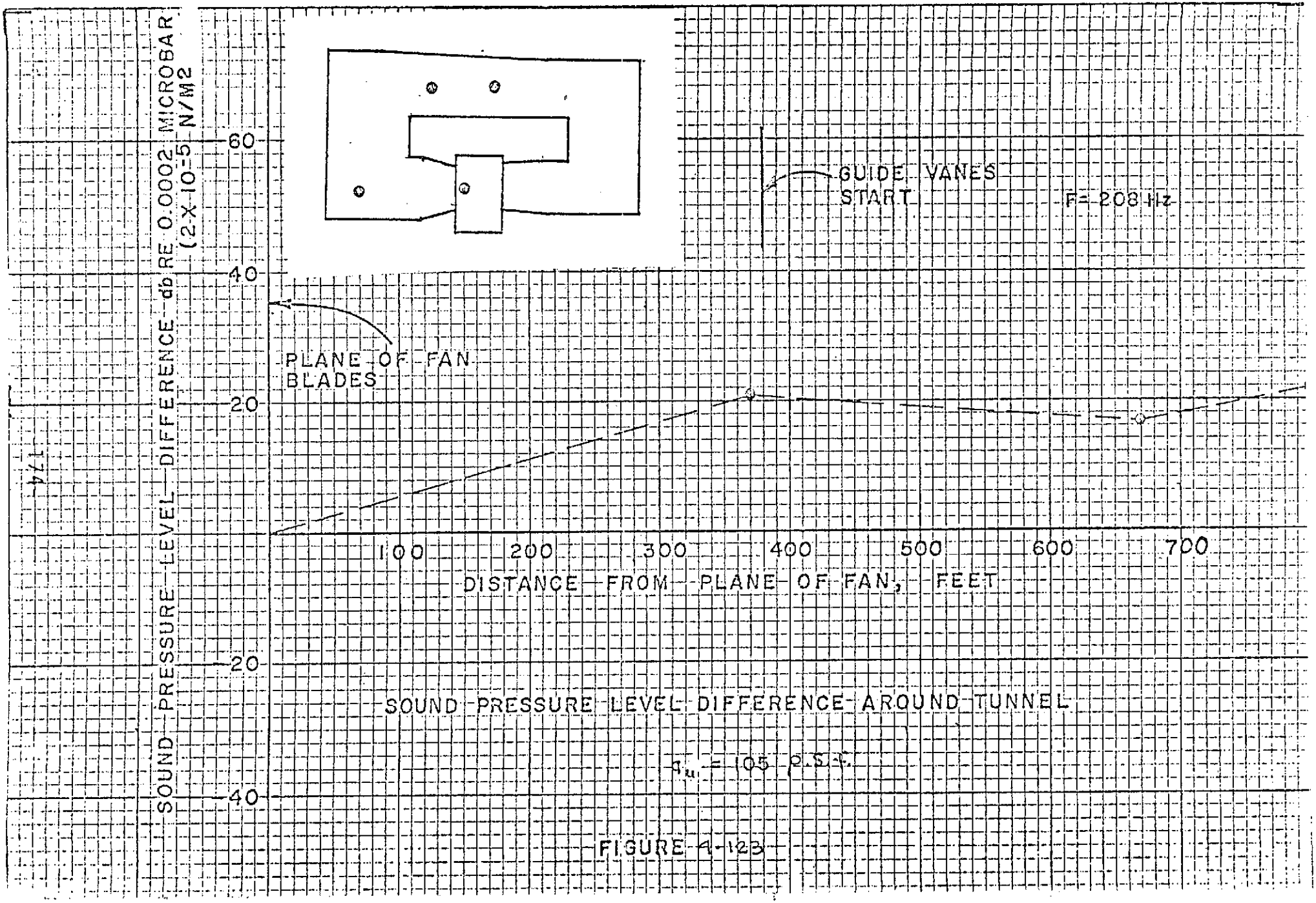
SOUND PRESSURE LEVEL DIFFERENCE - db RE 0.0002 MICROBAR (2 X 10-5 N/M2
60
40
20
20
40
GUIDE VANES START
F= 208 Hz
PLANE OF FAN BLADES
100
200
300
400
500
600
700
DISTANCE FROM PLANE OF FAN, FEET
SOUND PRESSURE LEVEL DIFFERENCE AROUND TUNNEL
τ_u = 105 p.s.f.

FIGURE A-123

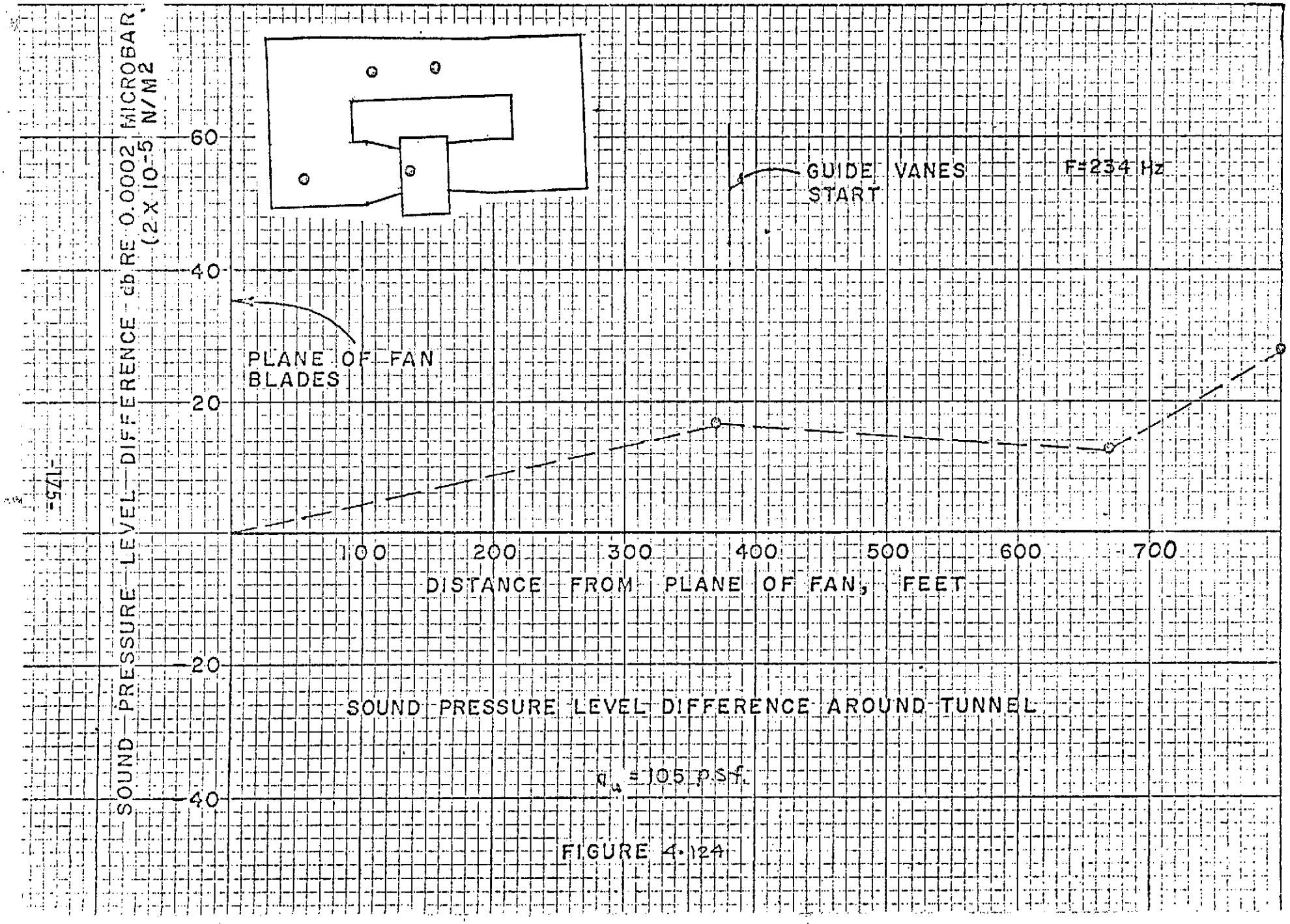

FIGURE 4-124

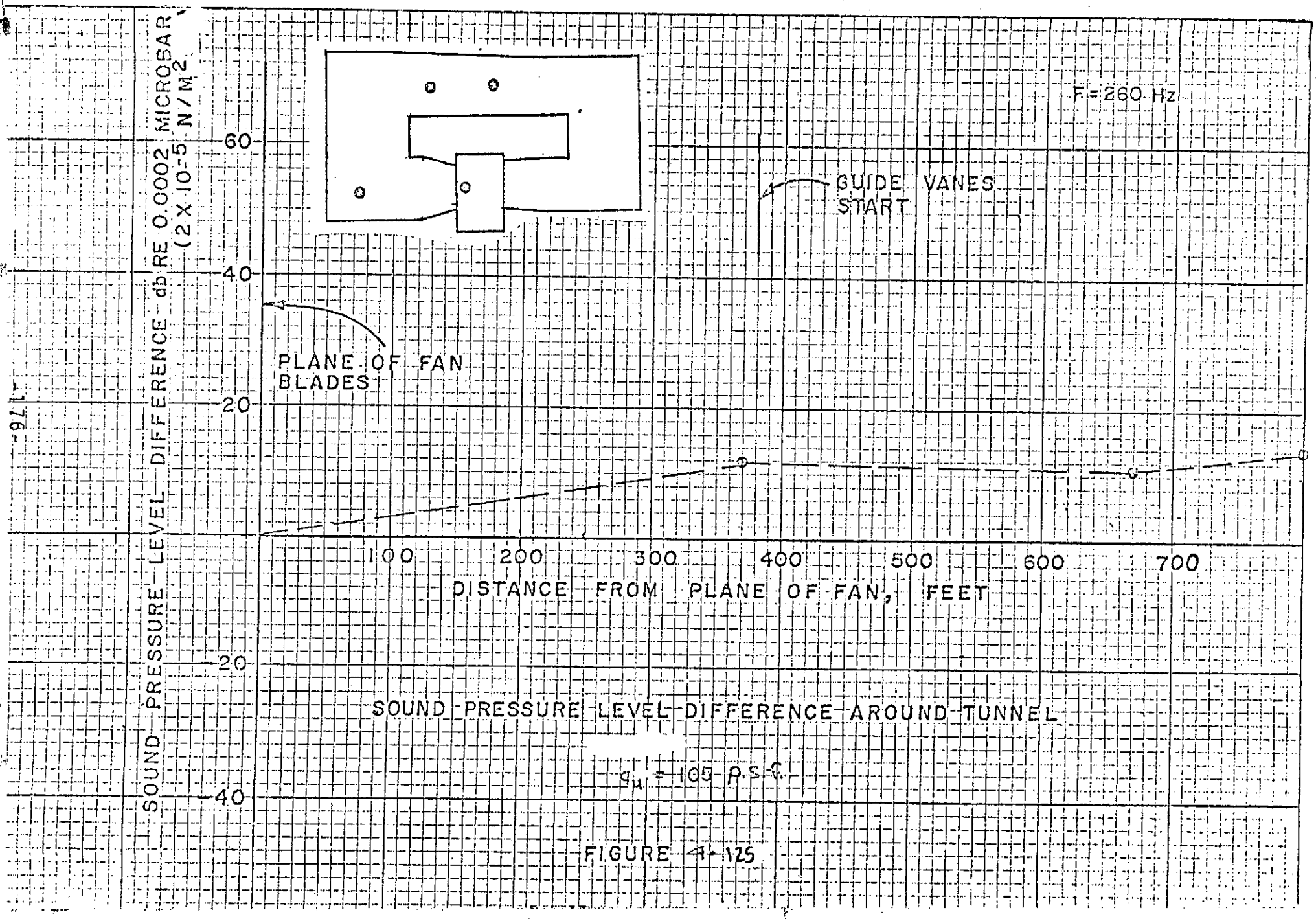

FIGURE A-125

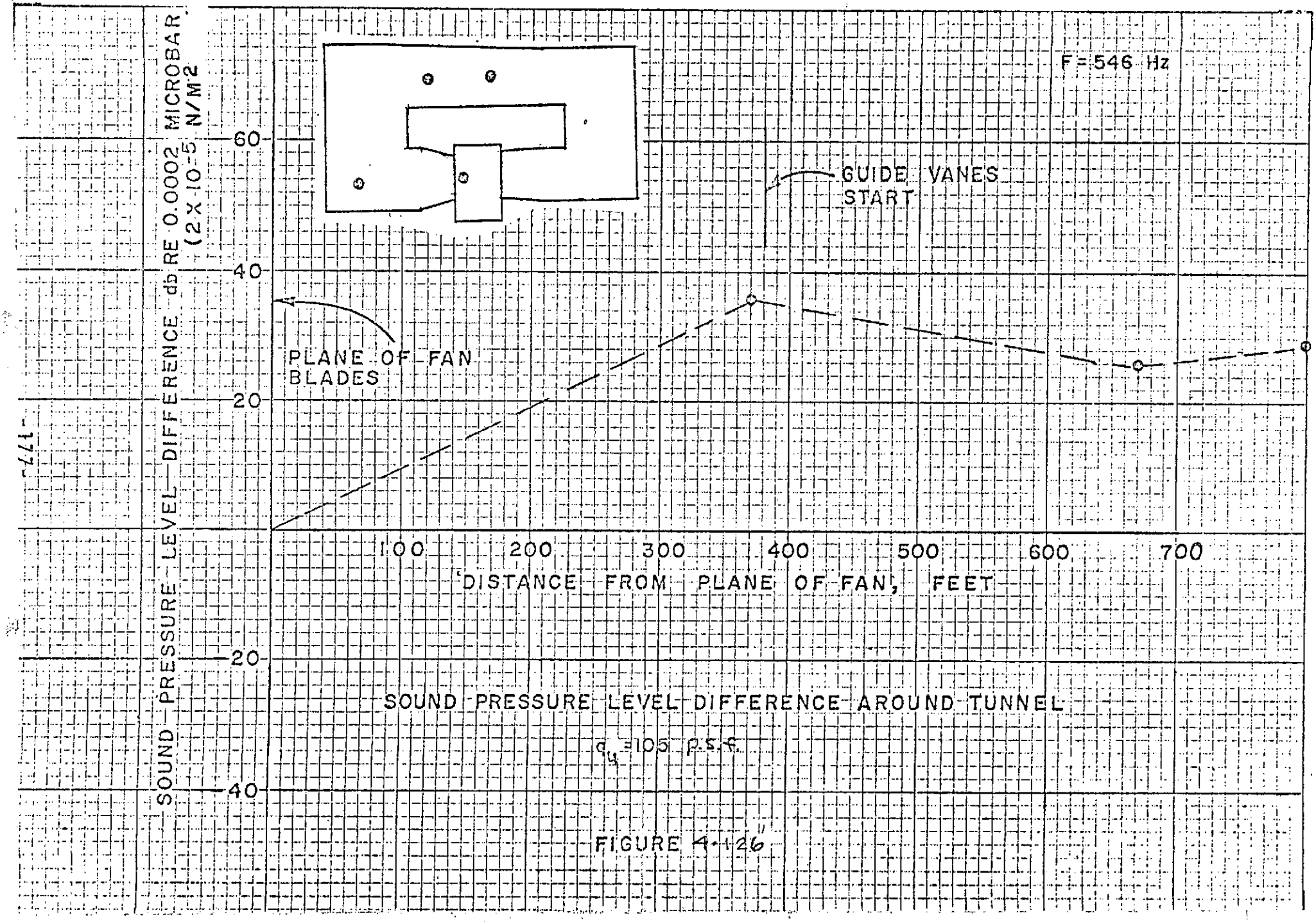

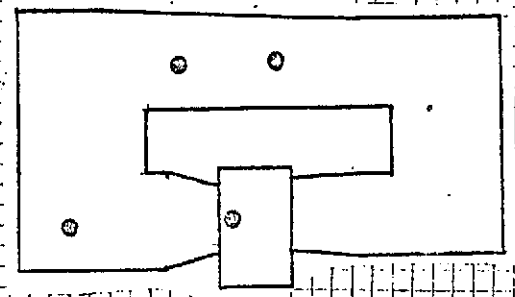

F=338 Hz

GUIDE VANES START

PLANE OF FAN BLADES

SOUND PRESSURE LEVEL DIFFERENCE - db RE 0.0002 MICROBAR (2 X 10-5 N/M2

60
40
20

100 200 300 400 500 600 700

DISTANCE FROM PLANE OF FAN, FEET

SOUND PRESSURE LEVEL DIFFERENCE AROUND TUNNEL

q_4 = 105 p.s.f.

20
40

FIGURE 4-127

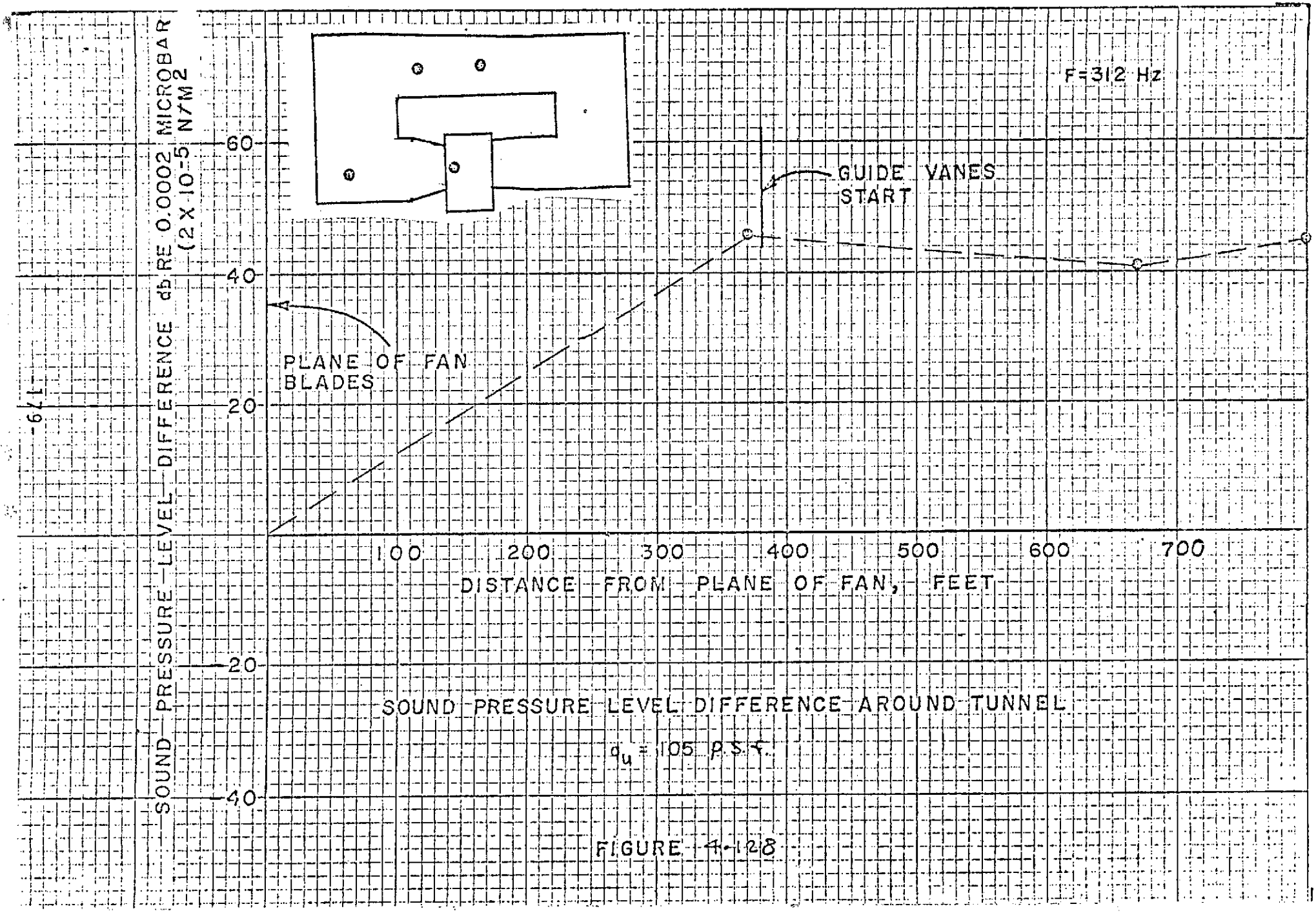

FIGURE 4-128

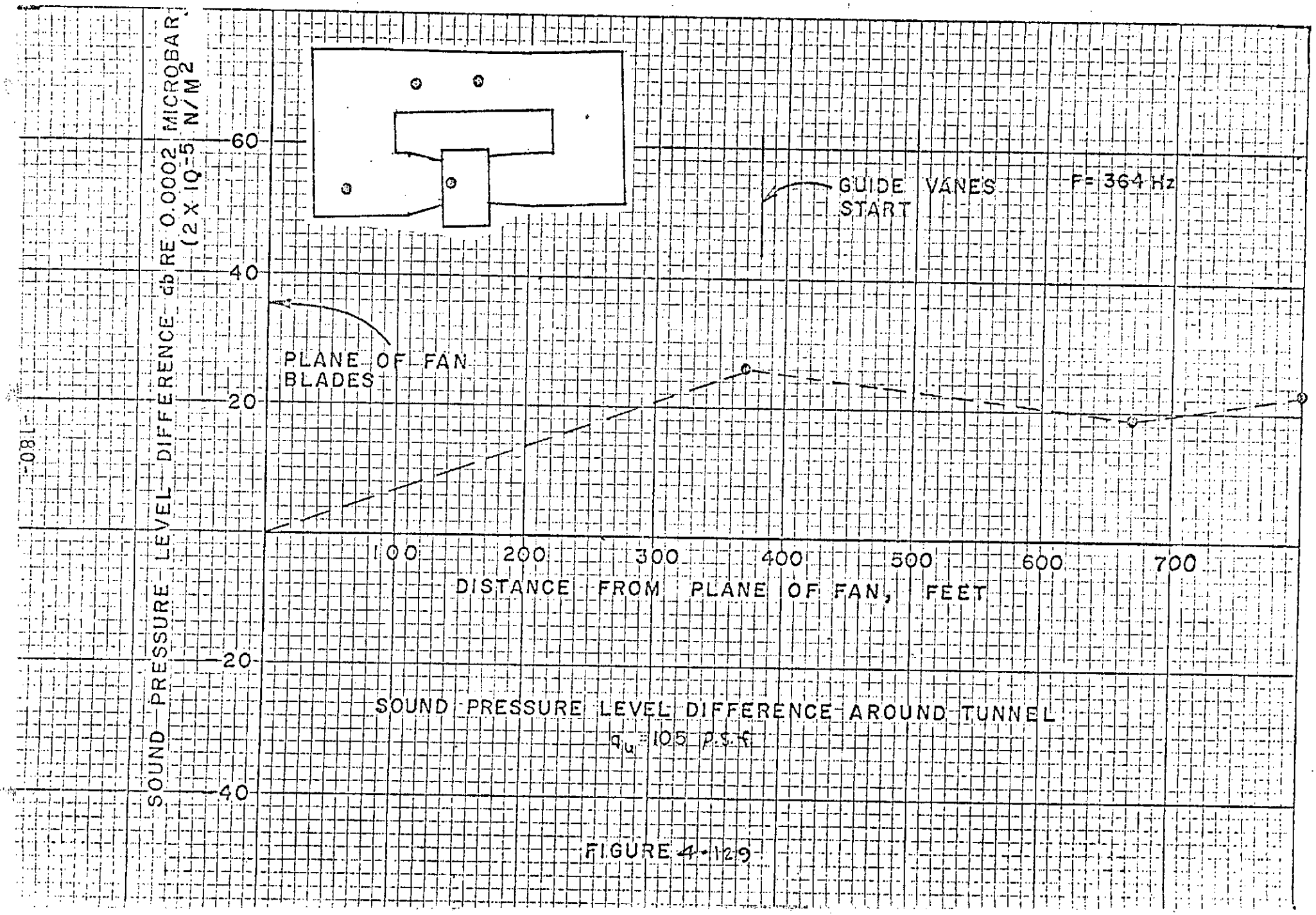

FIGURE 4-129

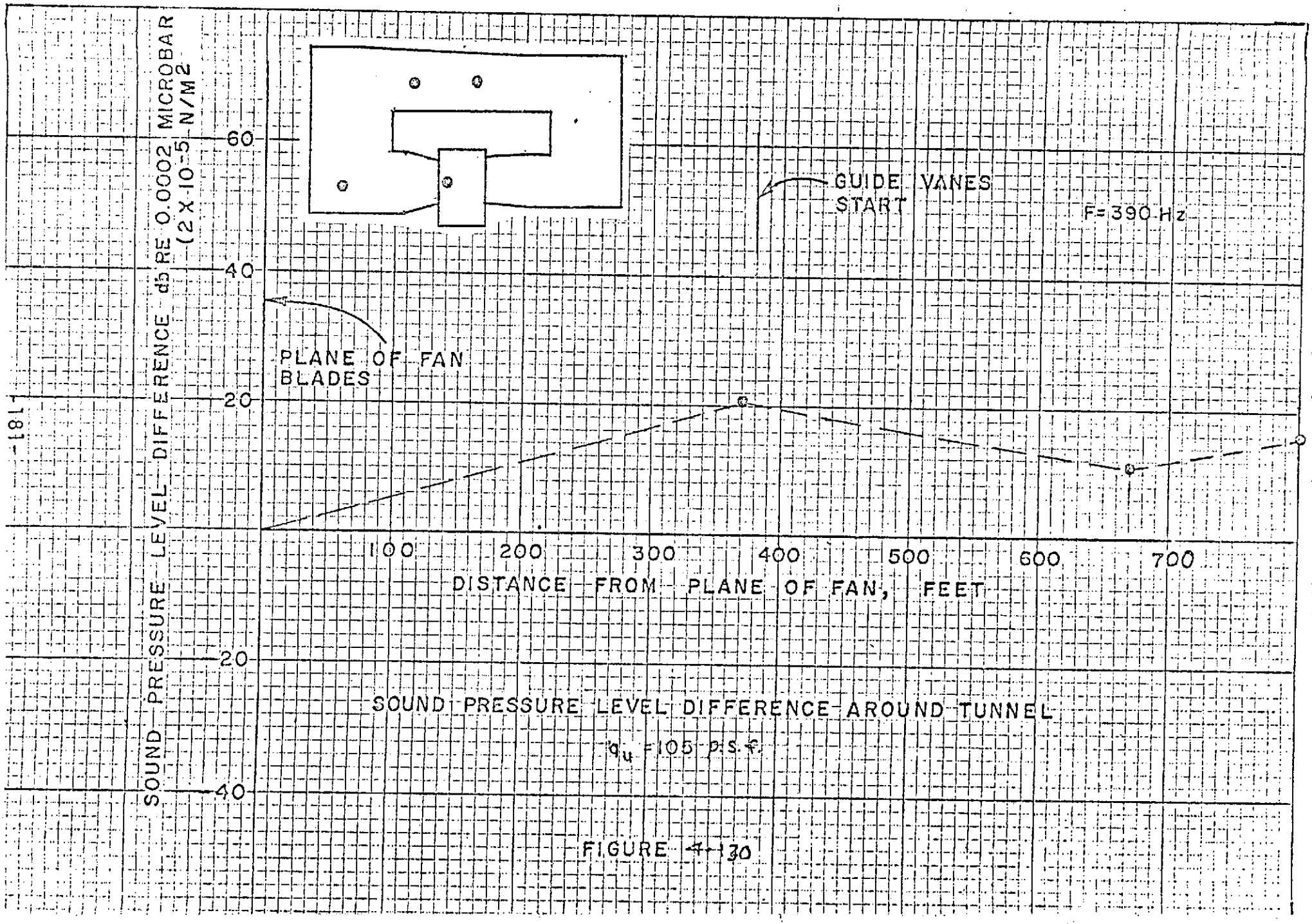

FIGURE 4-130

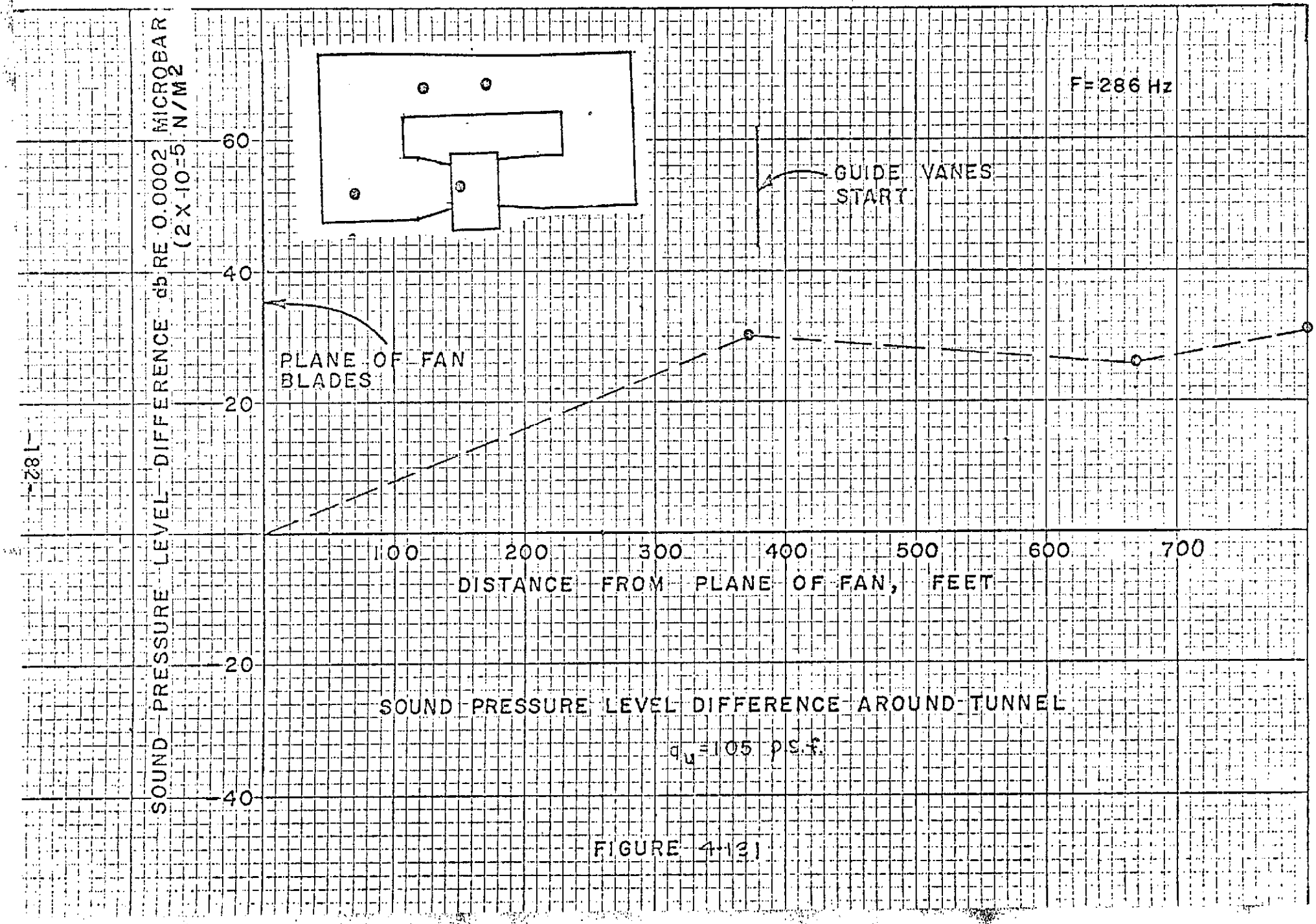

FIGURE 4-131

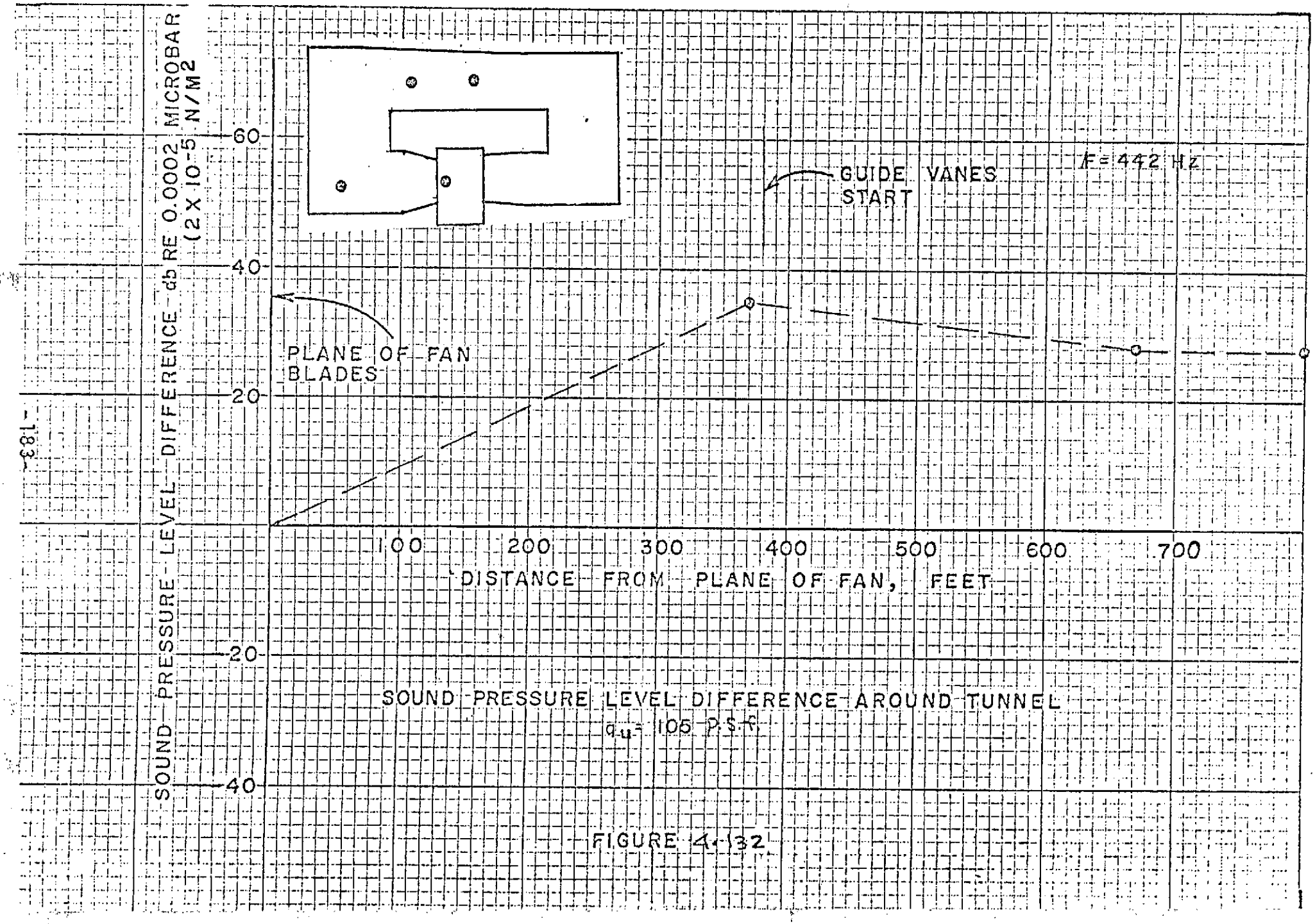

FIGURE 4-132

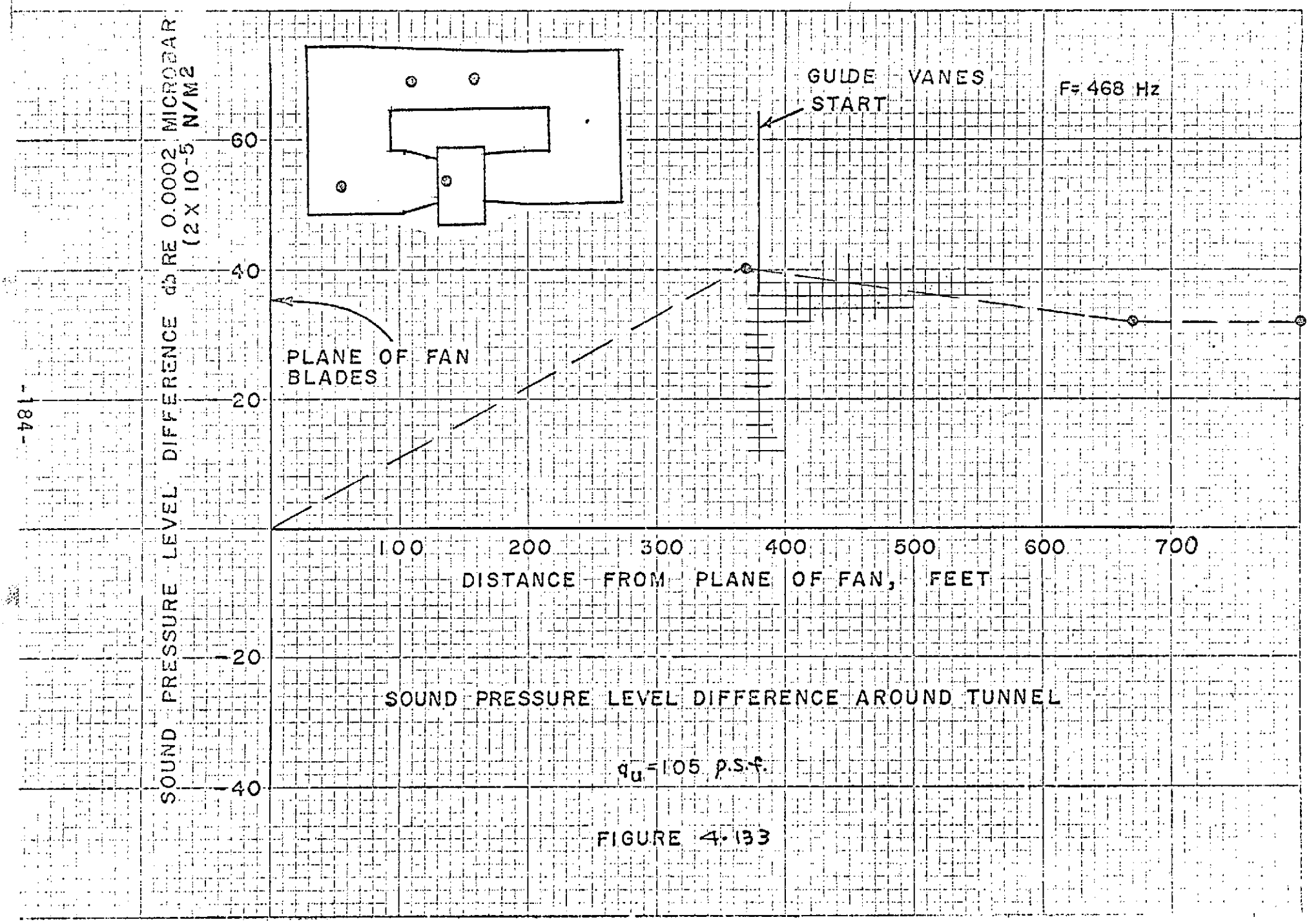

FIGURE 4.133

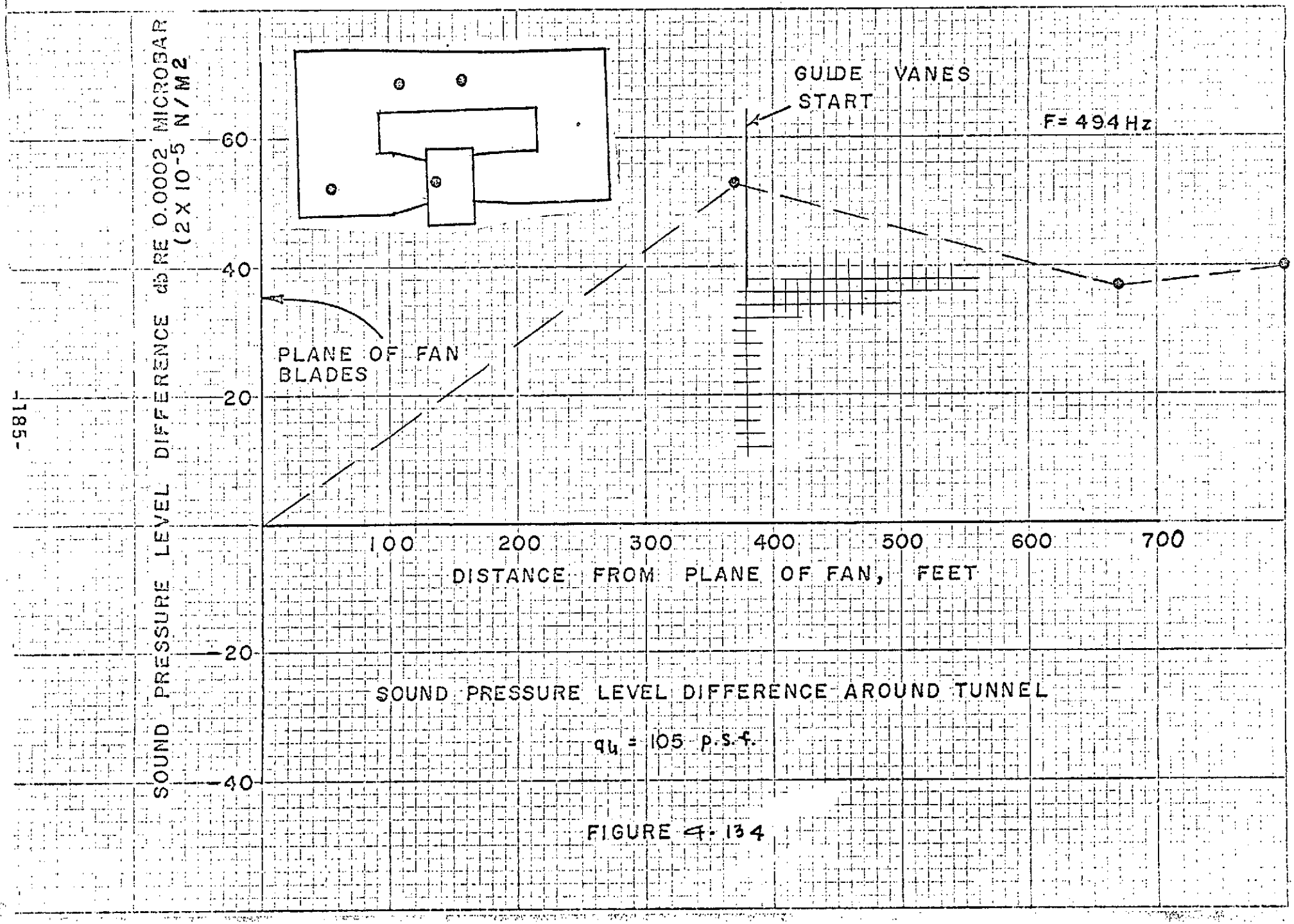
SOUND PRESSURE LEVEL DIFFERENCE db RE 0.0002 MICROBAR (2 X 10-5 N/M2
60
40
20
20
40
GUIDE VANES START
F = 494 Hz
PLANE OF FAN BLADES
100
200
300
400
500
600
700
DISTANCE FROM PLANE OF FAN, FEET
SOUND PRESSURE LEVEL DIFFERENCE AROUND TUNNEL
q_u = 105 p.s.f.

FIGURE 4-134

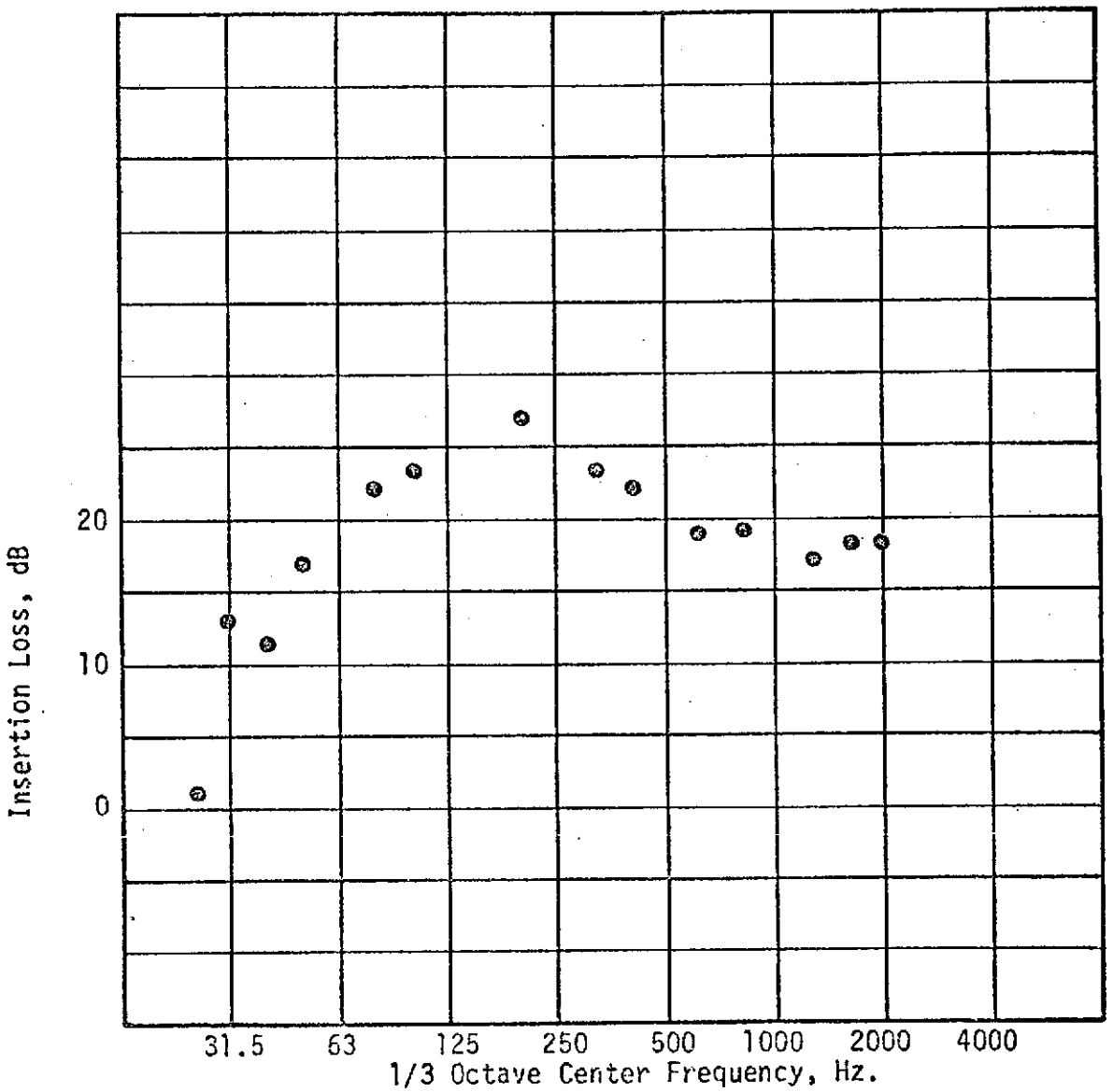

FIELD INSERTION LOSS
MEASURED AT BENT 74

q_u = 60 p.s.f.

Figure 4.135

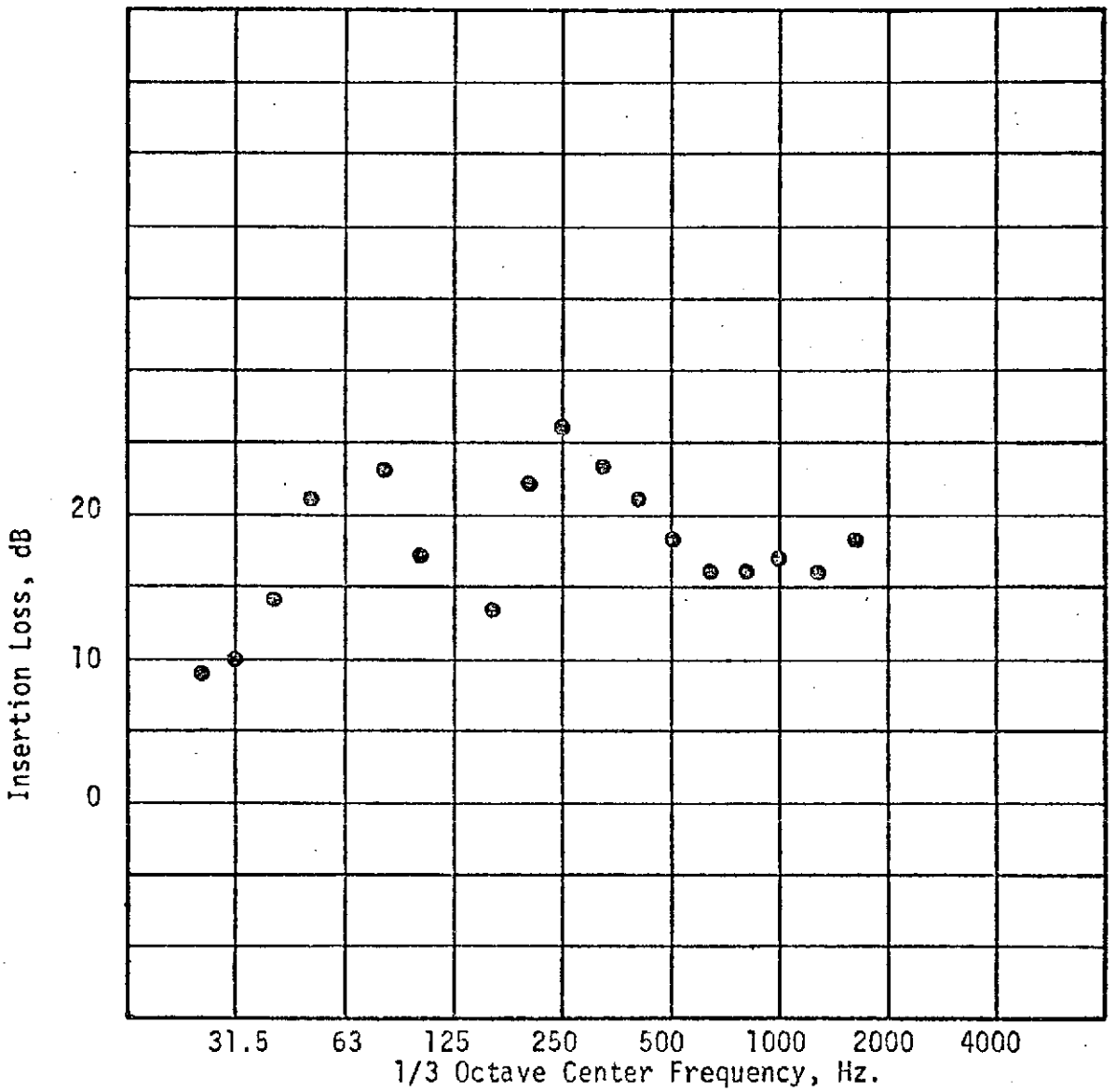

FIELD INSERTION LOSS
MEASURED AT BENT 74

q_u = 105 p.s.f.

Figure 4-136

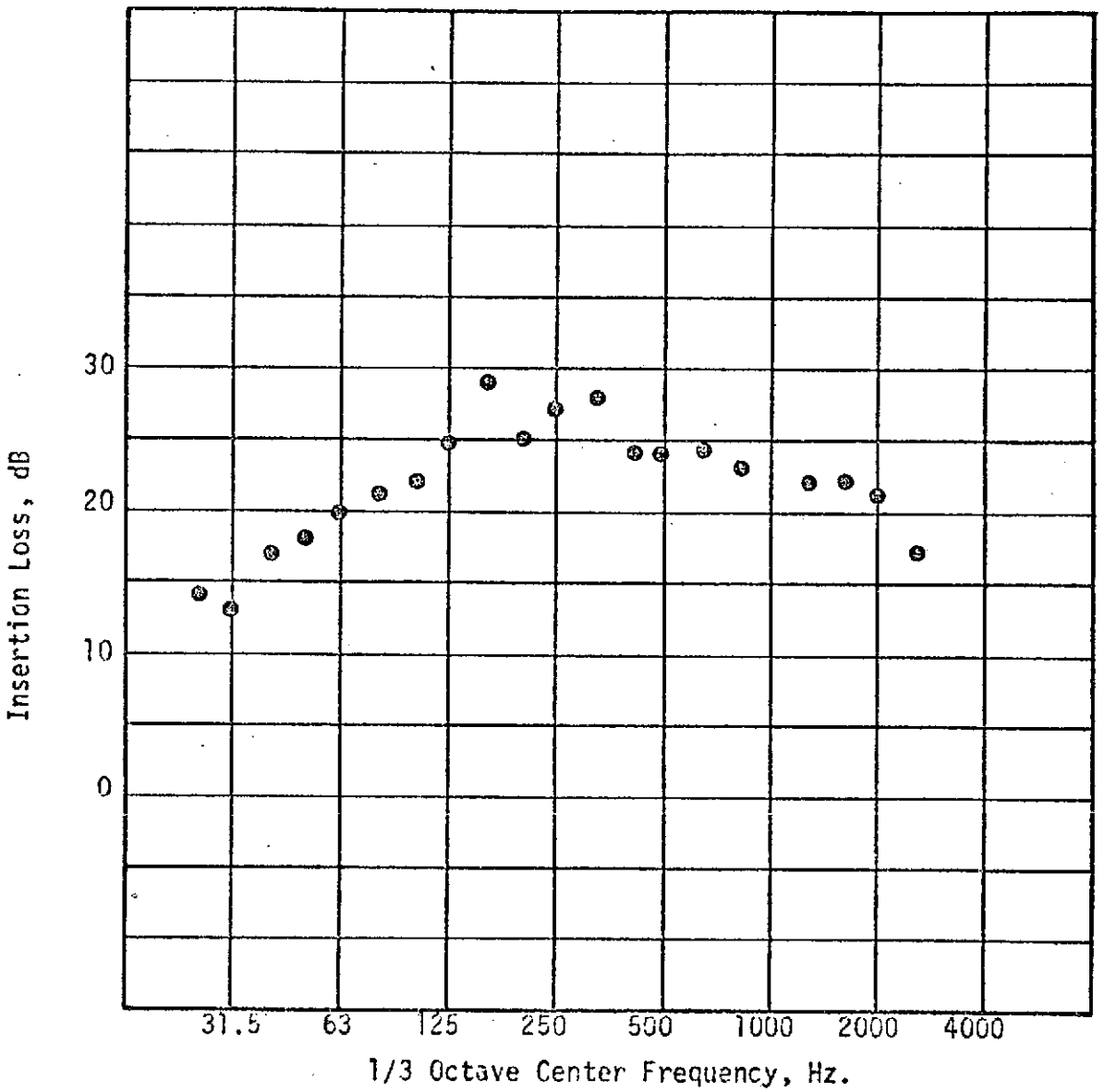

FIELD INSERTION LOSS
MEASURED AT BENT 91
q_u = 60 p.s.f.

Figure 4-137

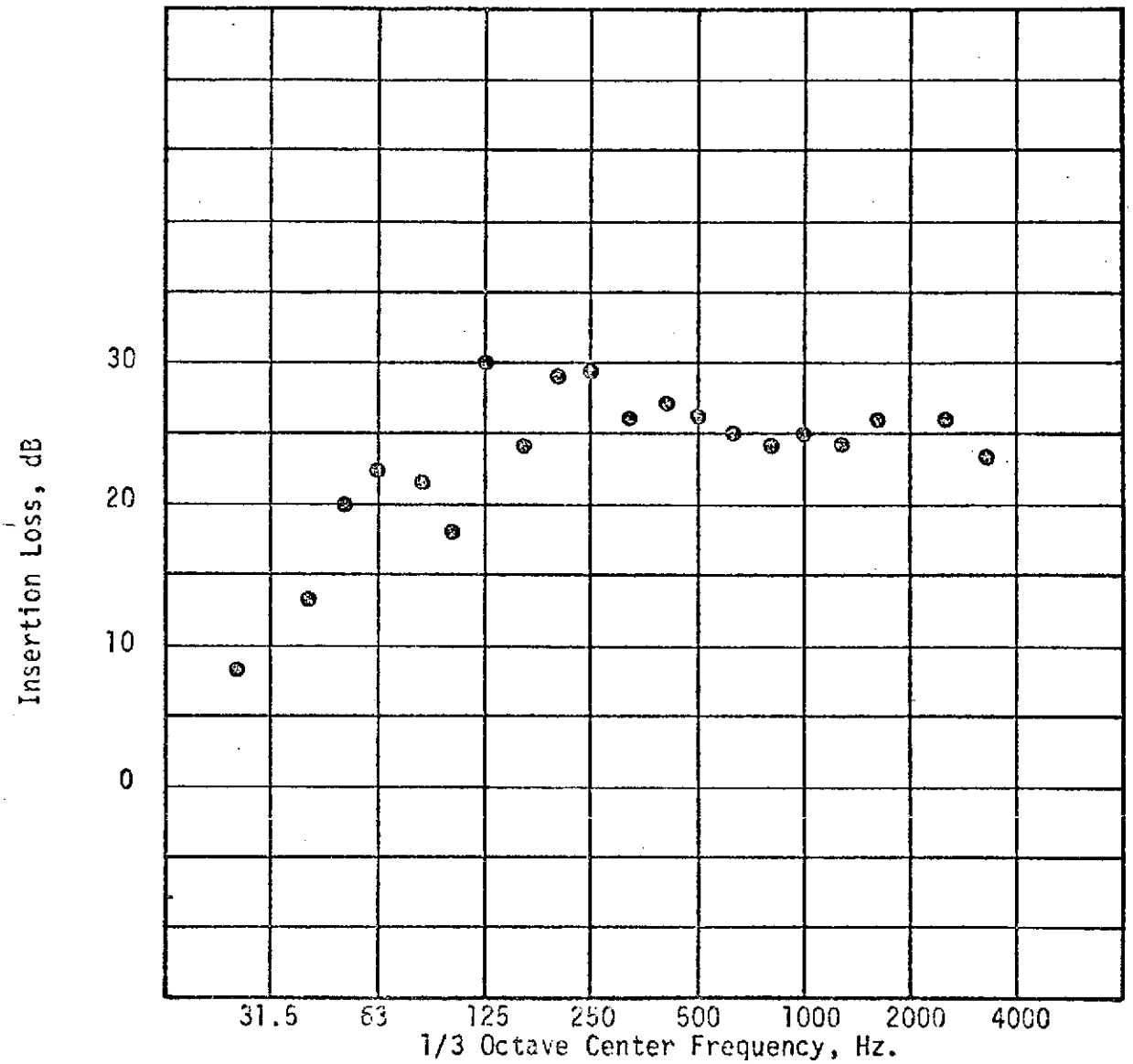

FIELD INSERTION LOSS
MEASURED AT BENT 91

q_u = 105 p.s.f.

Figure 4-138

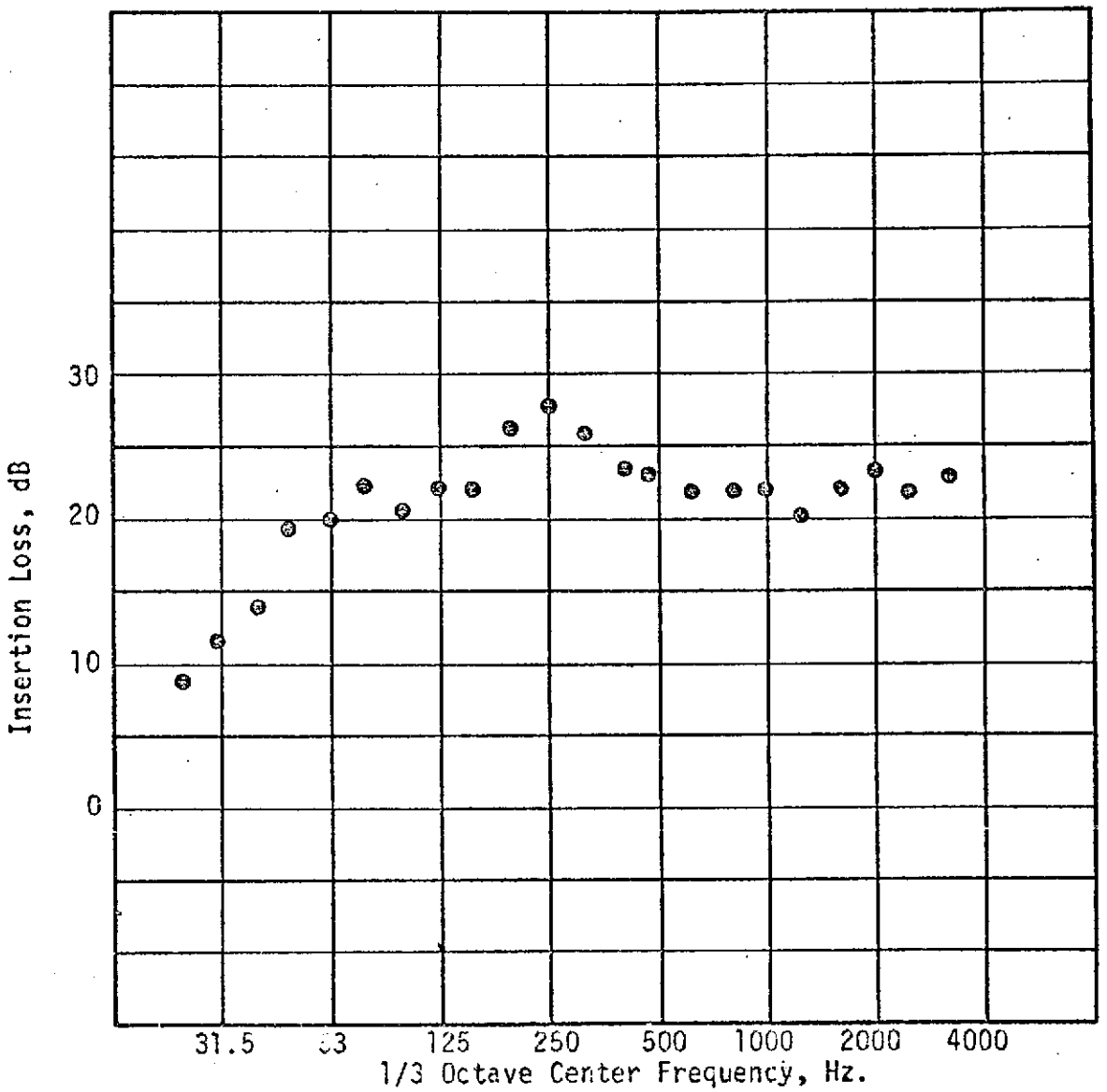

AVERAGE FIELD INSERTION LOSS (F.I.L)
OF TUNNEL WALL

Figure 4-139

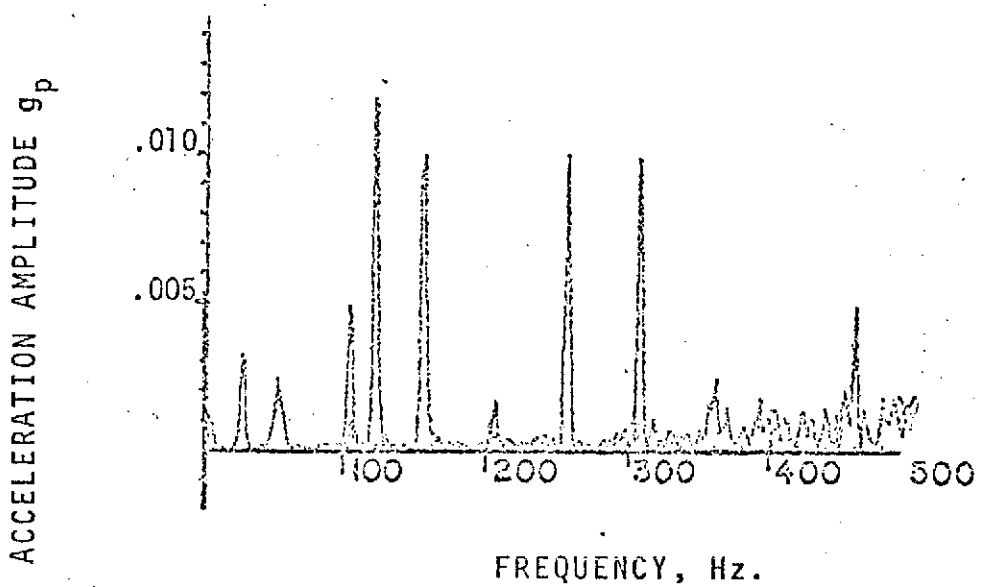

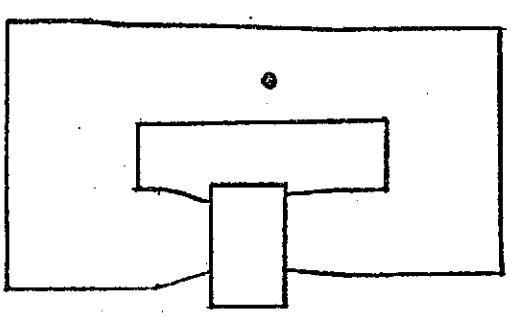

VIBRATION SPECTRUM
TEST POINT 3

q_u - 60 p.s.f.

FIGURE 4-140

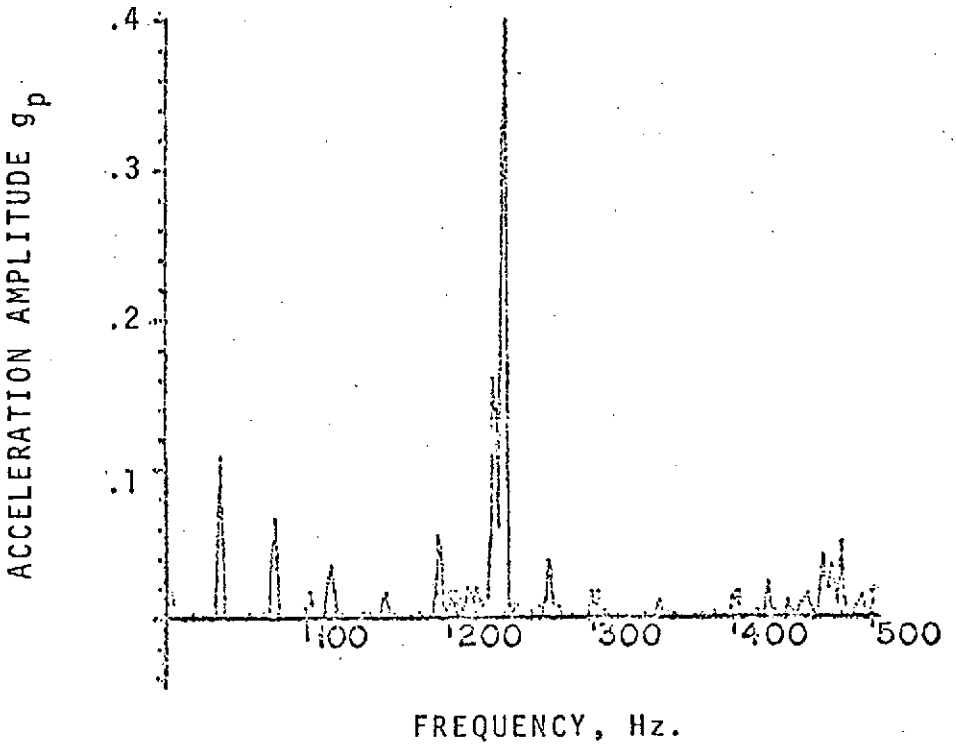

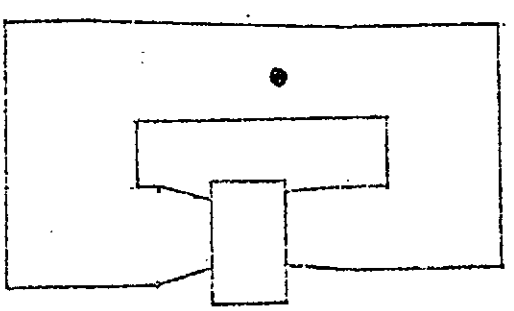

VIBRATION SPECTRUM
TEST POINT 4

q_u = 60 p.s.f.

FIGURE 4-141

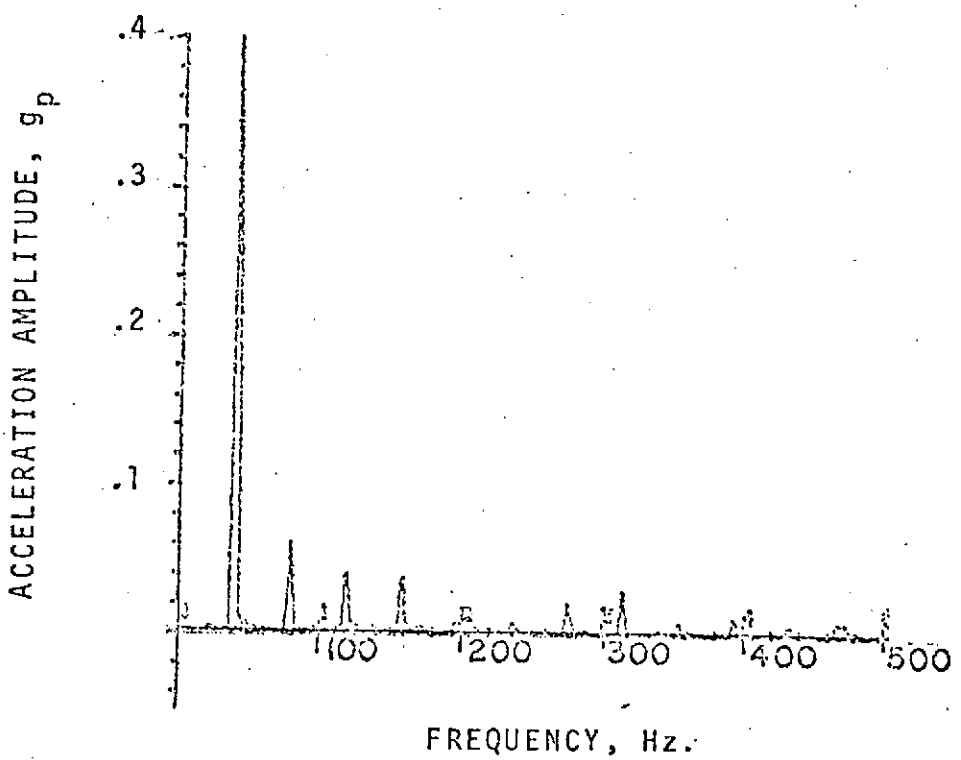

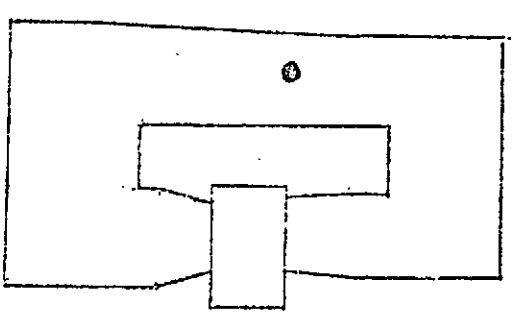

VIBRATION SPECTRUM
TEST POINT 3

q_u - 105 p.s.f.

FIGURE 4-142

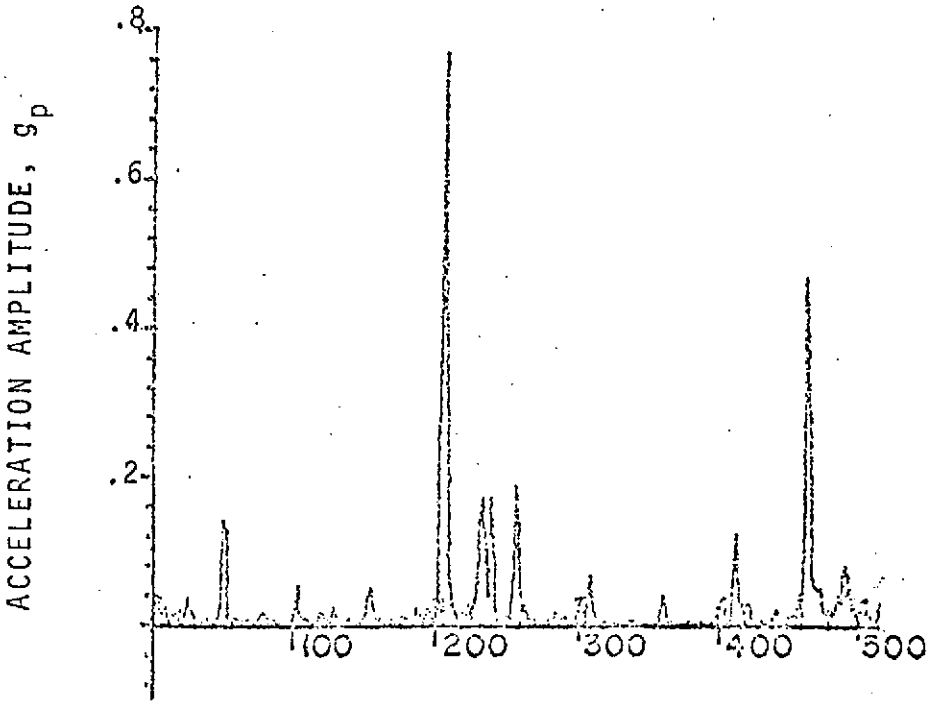

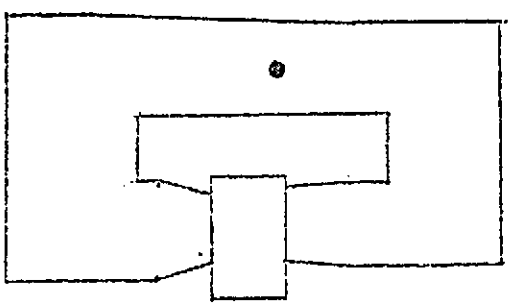

VIBRATION SPECTRUM
TEST POINT 4

q_u = 105 p.s.f.

FIGURE 4-143

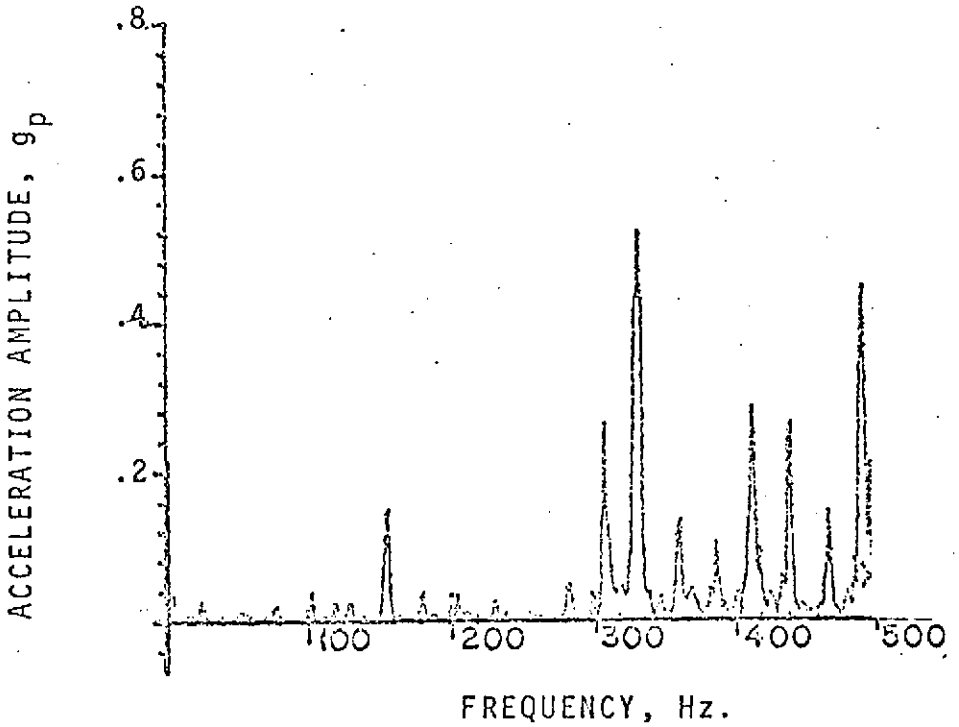

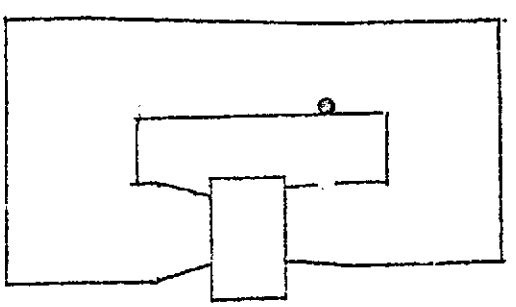

VIBRATION SPECTRUM
TEST POINT 7

q_u = 60 p.s.f.

FIGURE 4-144

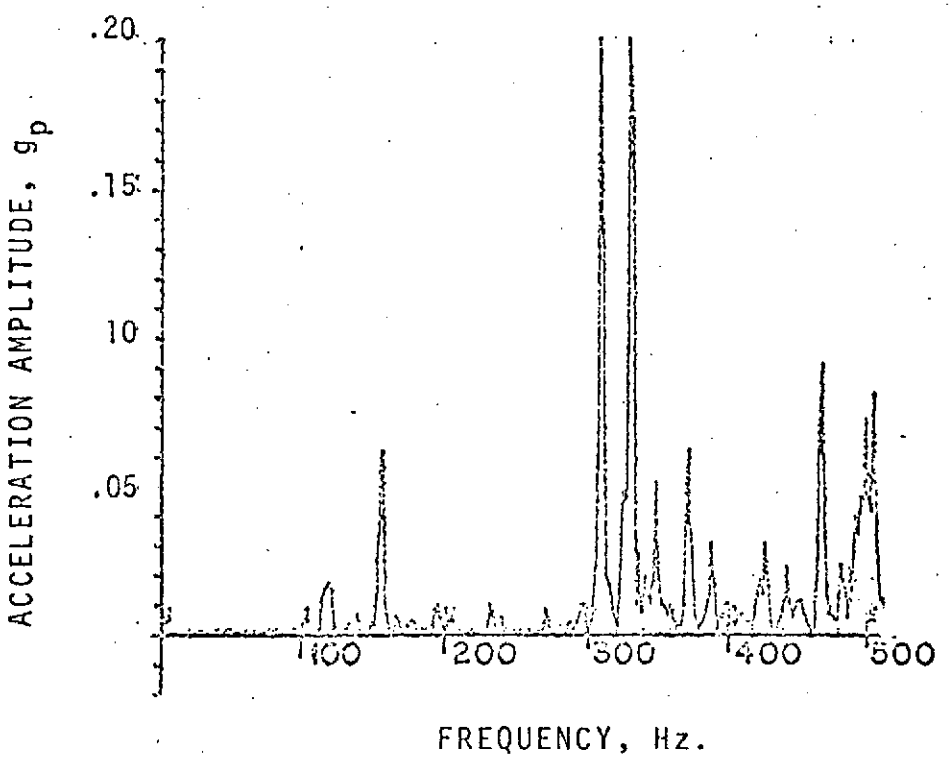

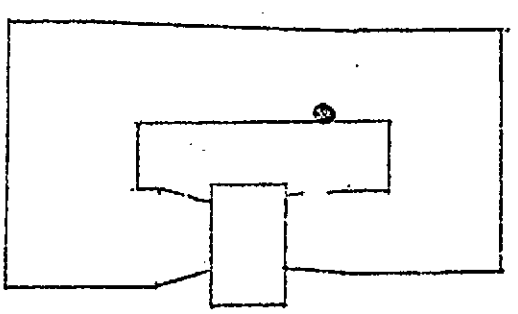

VIBRATION SPECTRUM
TEST POINT 6

q_u = 60 p.s.f.

FIGURE 4-145

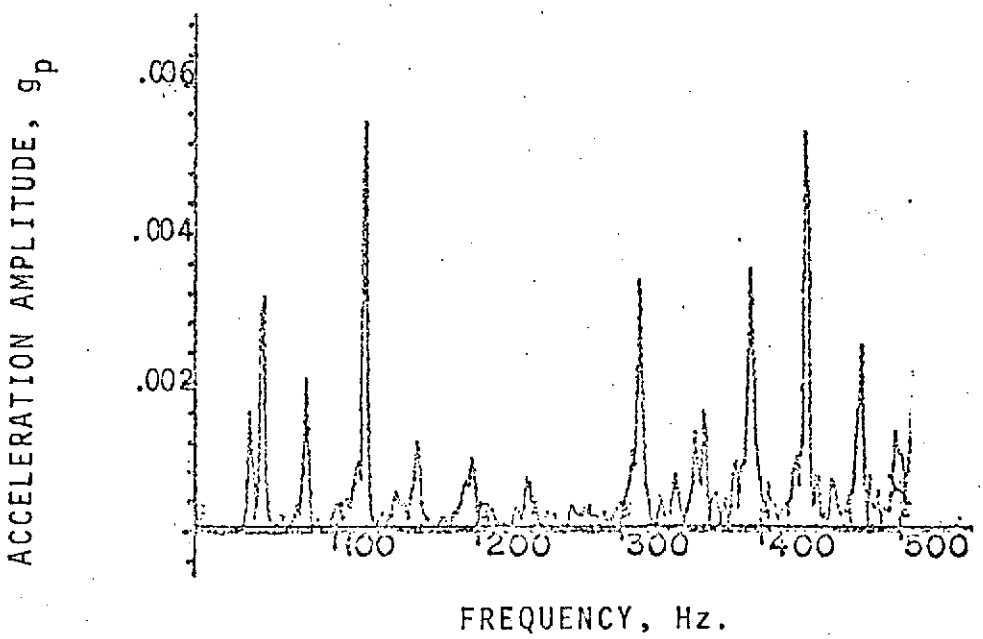

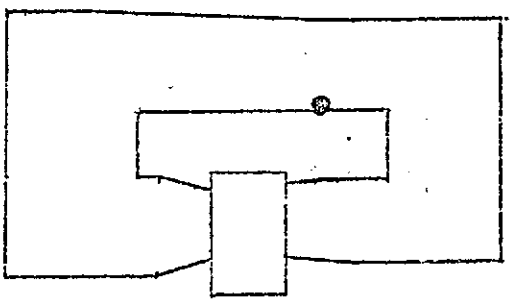

VIBRATION SPECTRUM
TEST POINT 7

q_u = 100 p.s.f.

FIGURE 4-146

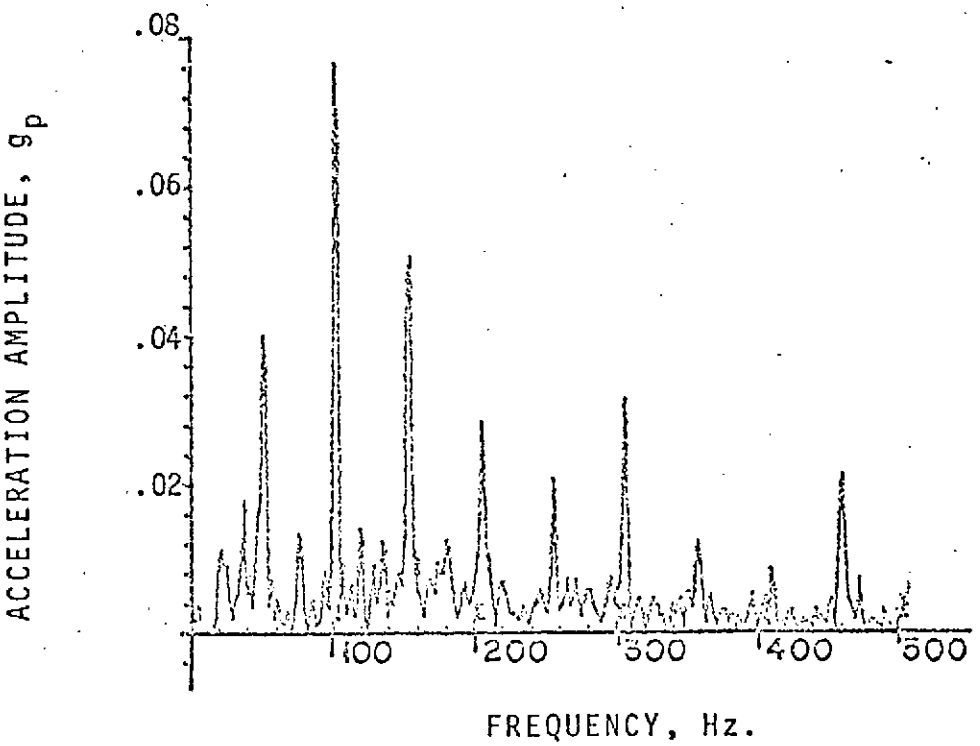

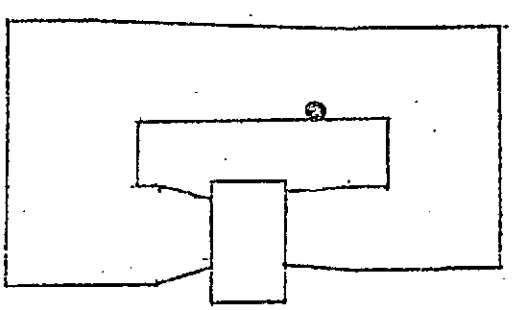

VIBRATION SPECTRUM
TEST POINT 6

q_u = 105 p.s.f.

FIGURE 4-147

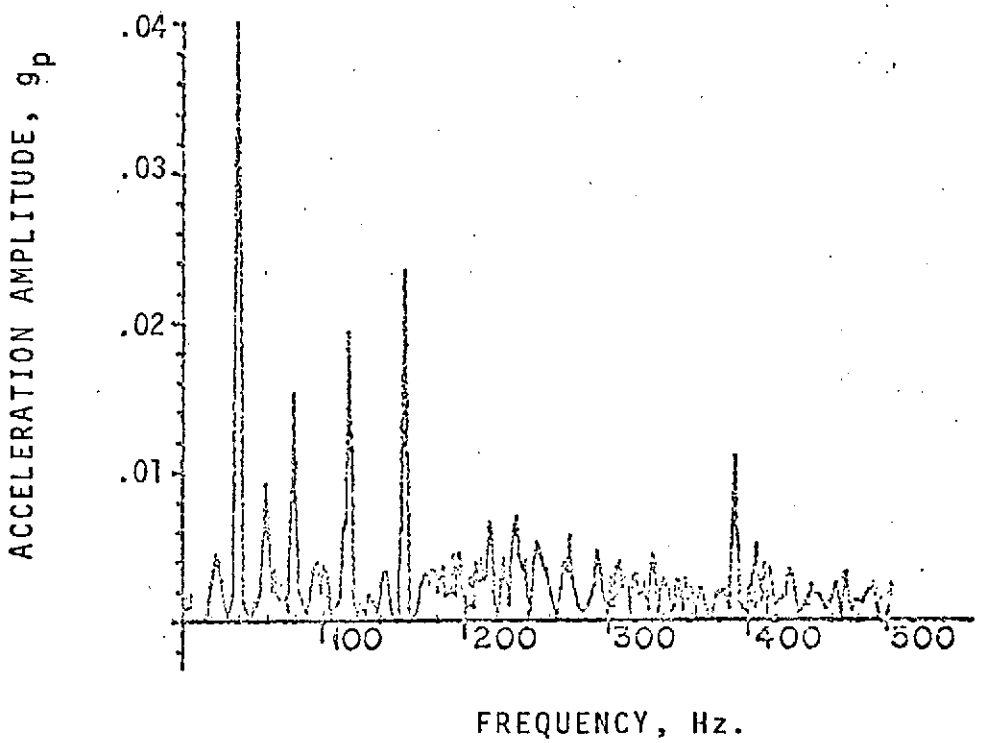

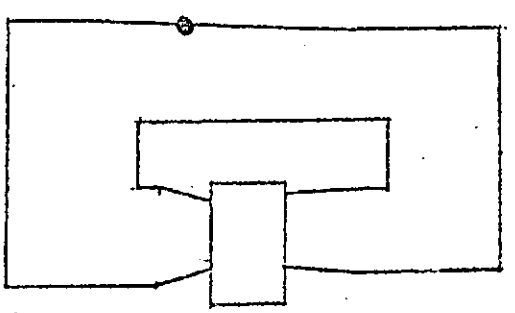

VIBRATION SPECTRUM
TEST POINT 8

q_u = 60 p.s.f.

FIGURE 4-148

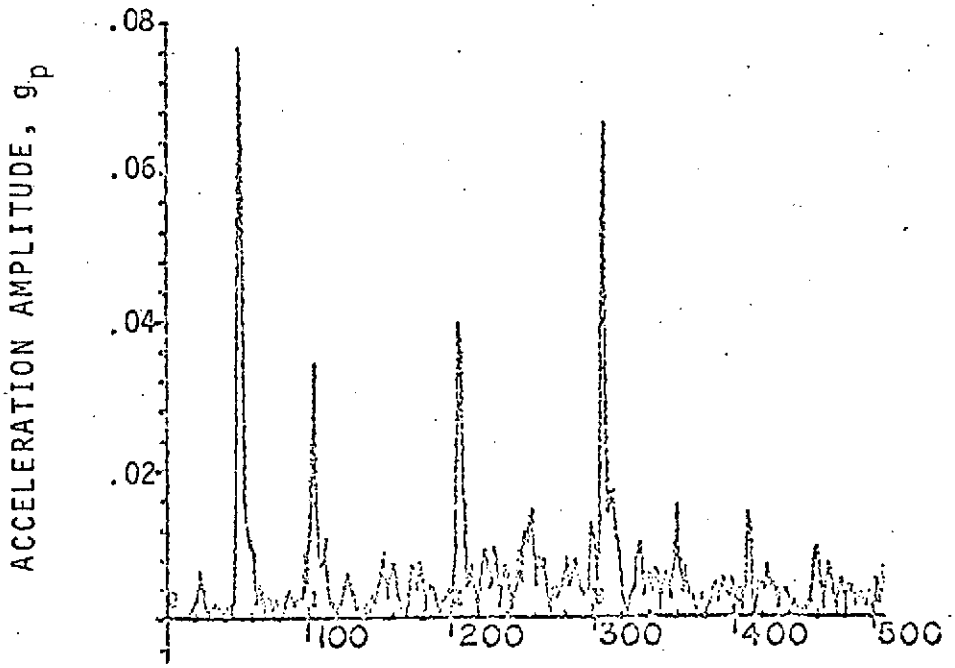

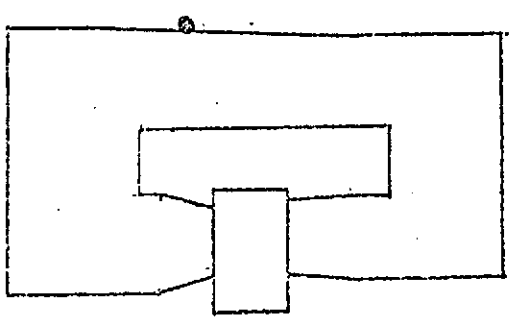

VIBRATION SPECTRUM
TEST POINT 8

q_u = 105 p.s.f.

FIGURE 4-149

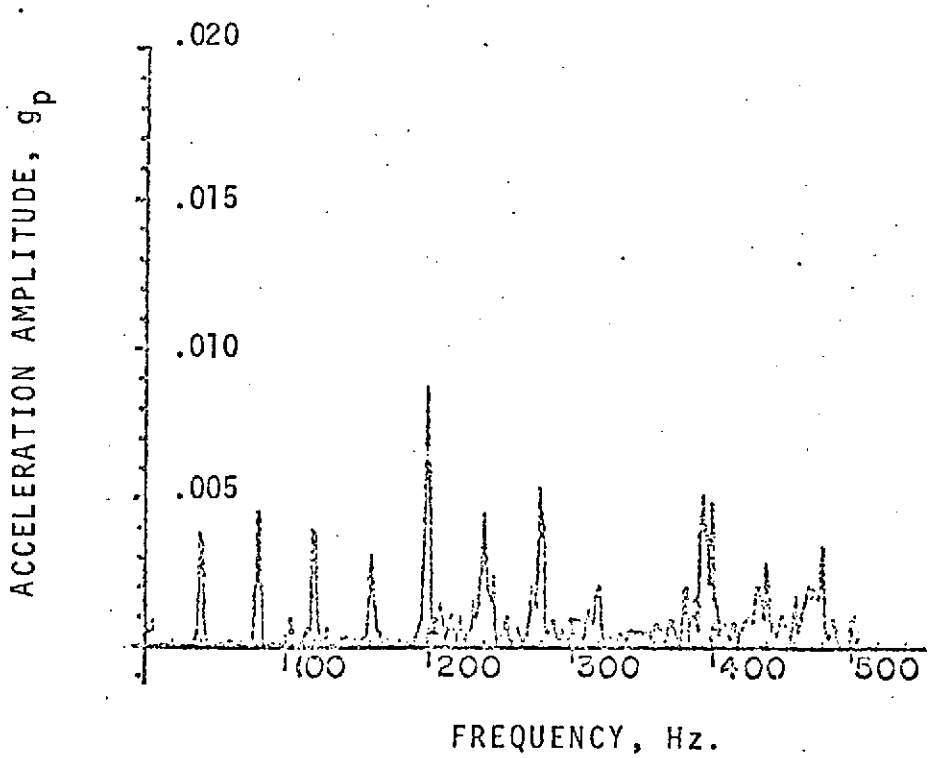

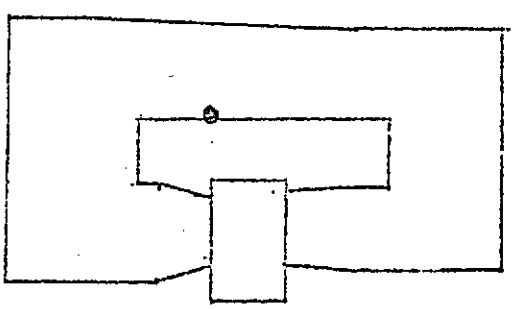

VIBRATION SPECTRUM
TEST POINT 13

q_u = 60 p.s.f.

FIGURE 4-150

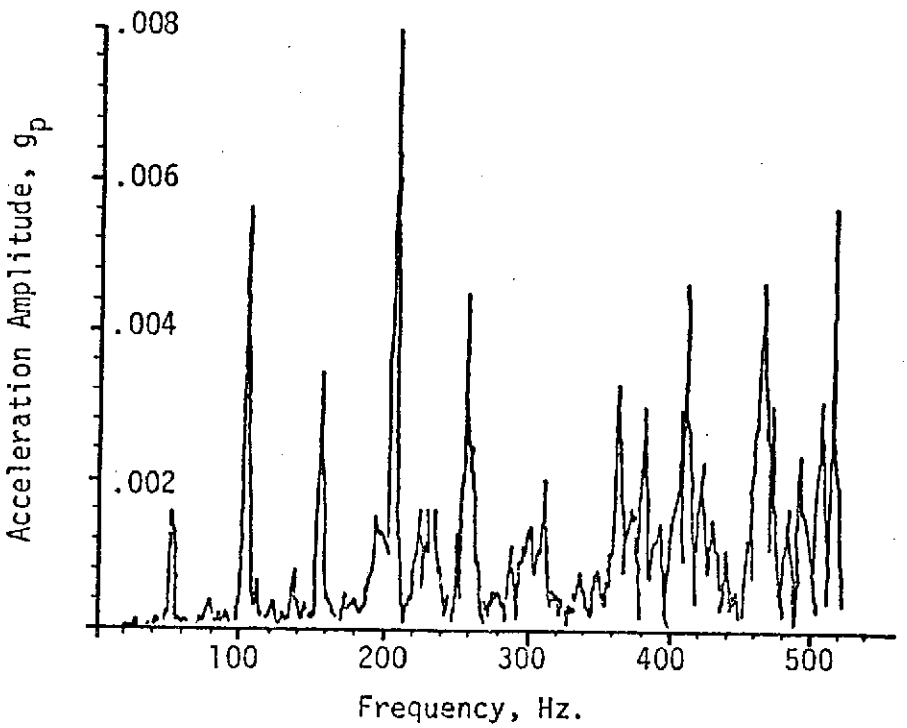

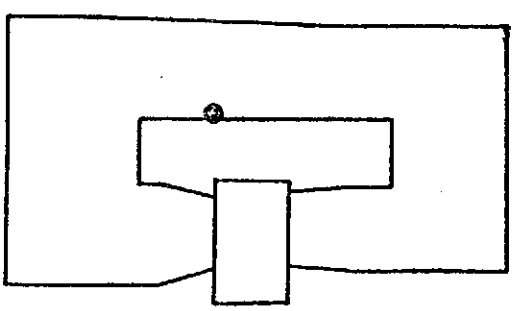

VIBRATION SPECTRUM
TEST POINT 13
q_u = 105 p.s.f.

FIGURE 4-151

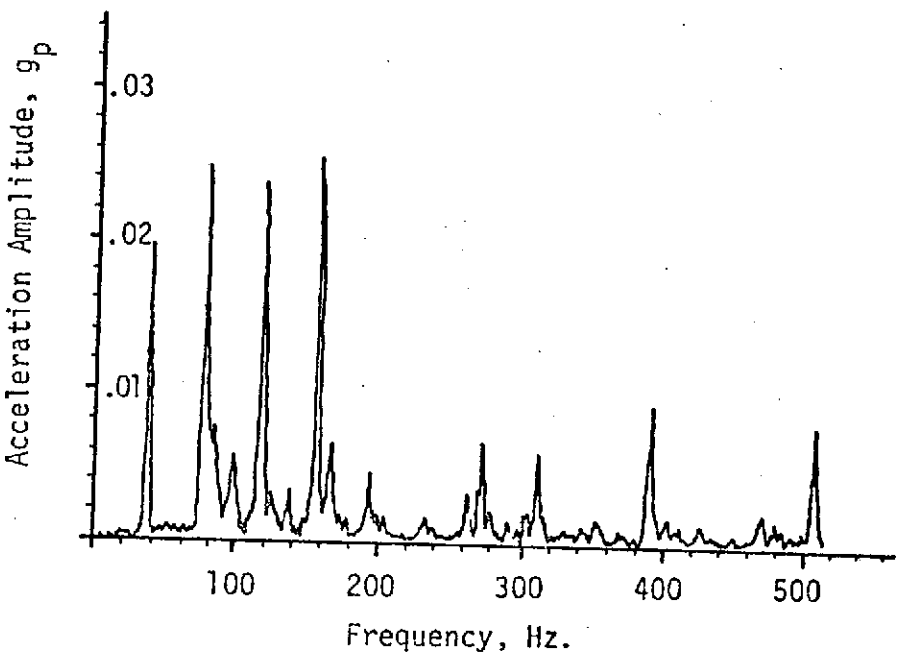

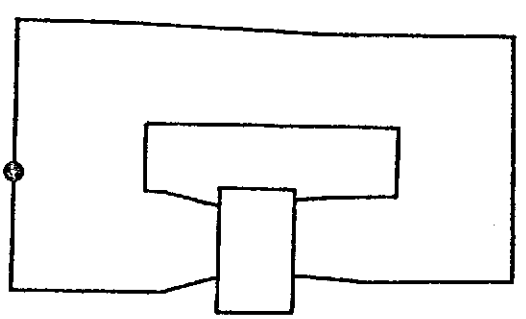

VIBRATION SPECTRUM
TEST POINT 16
q_u = 60 p.s.f.

FIGURE 4-152

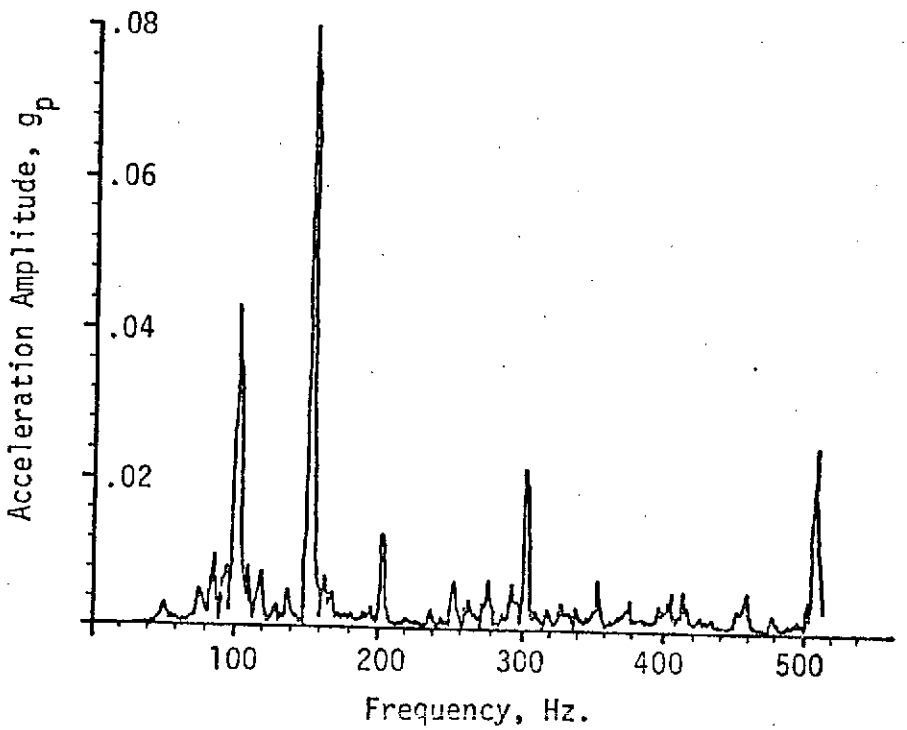

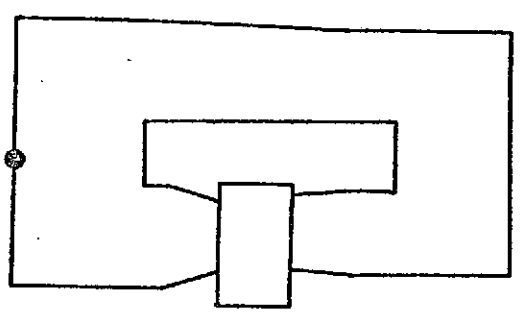

VIBRATION SPECTRUM
TEST POINT 16
q_u = 105 p.s.f.

FIGURE 4-153

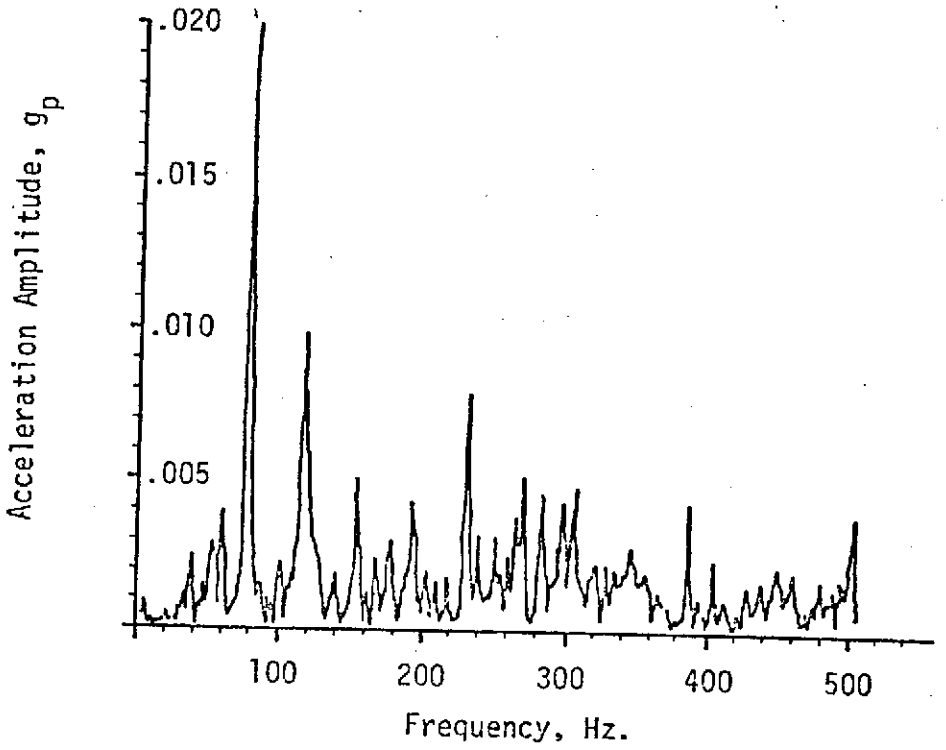

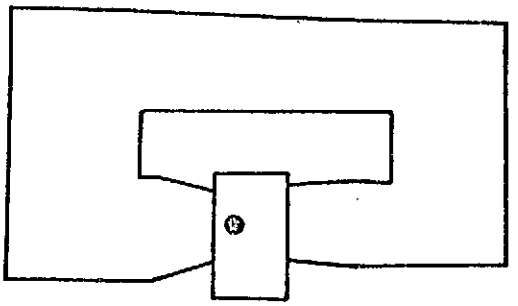

VIBRATION SPECTRUM
TEST POINT 19
q_u = 60 p.s.f.

FIGURE 4-154

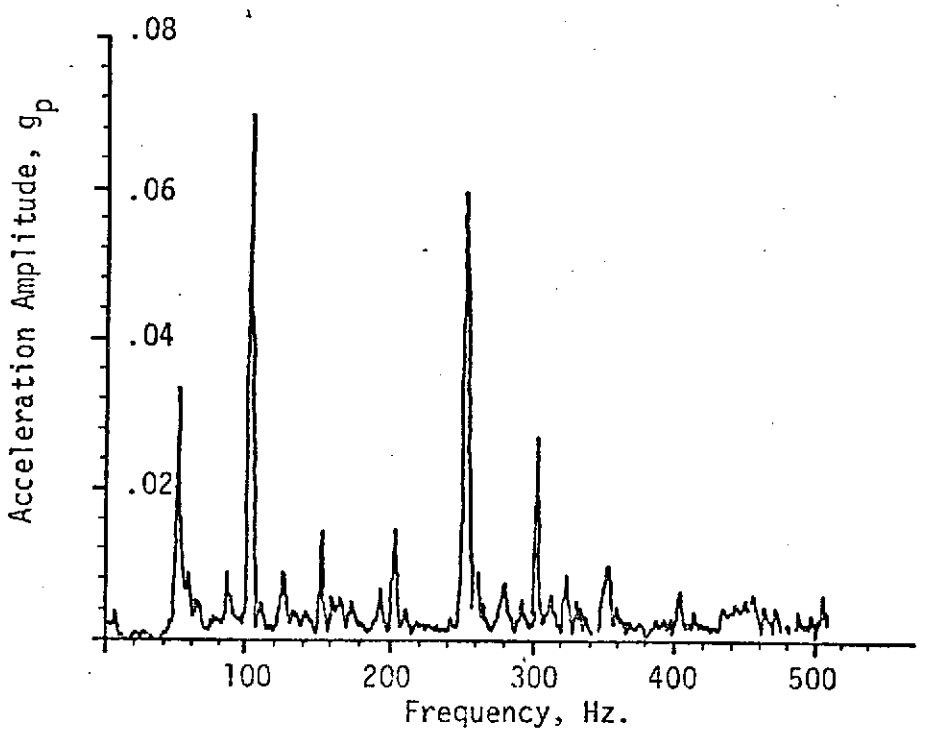

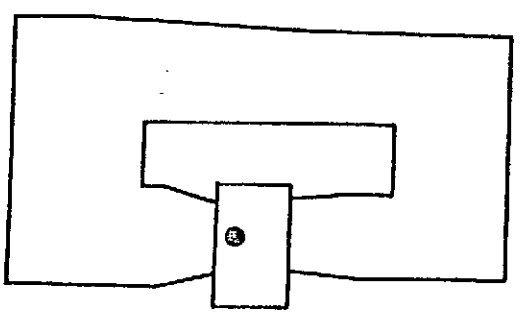

VIBRATION SPECTRUM
TEST POINT 19
q_u = 105 P.S.F.

FIGURE 4-155

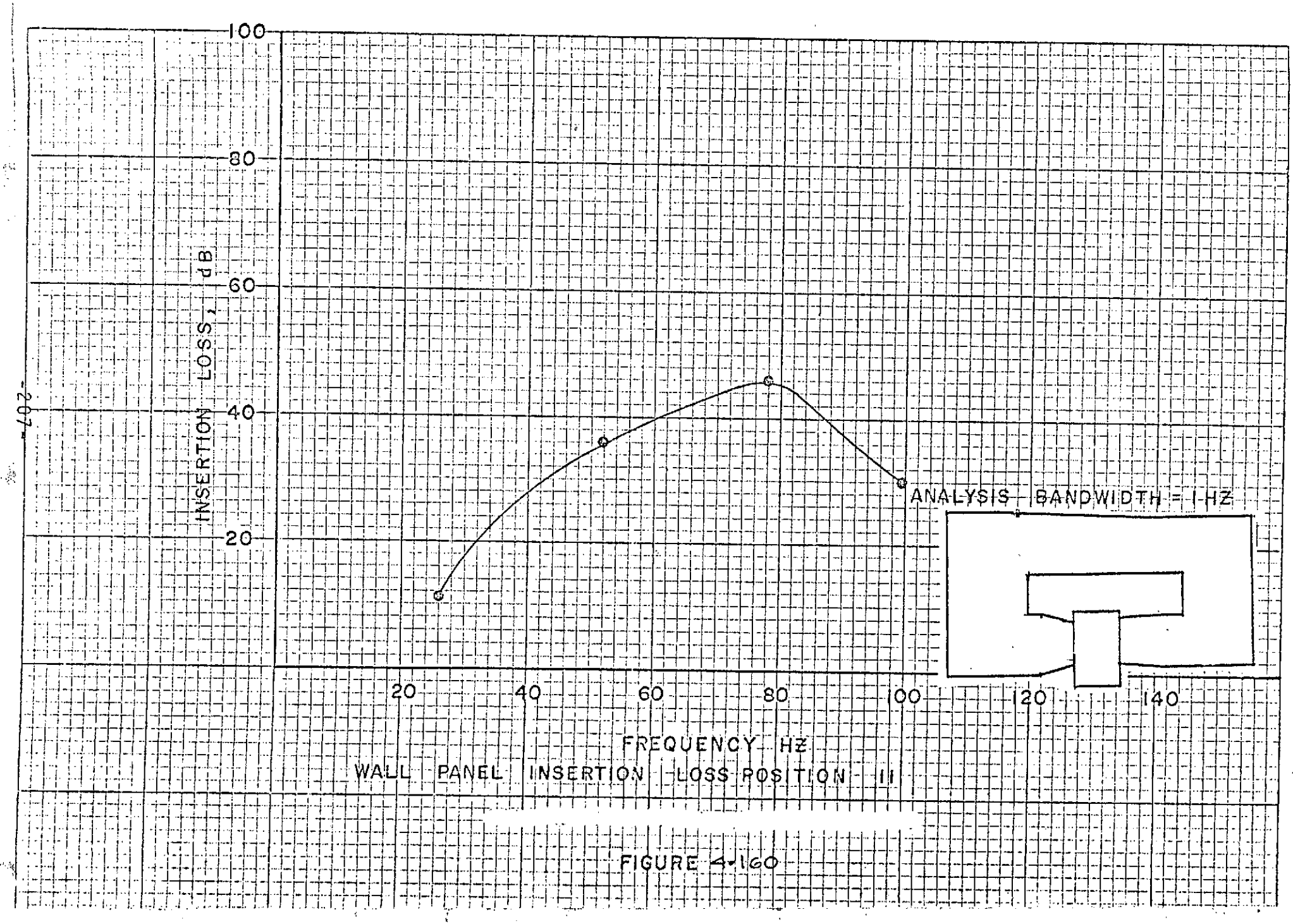

WALL PANEL INSERTION LOSS POSITION II

FIGURE 4-160

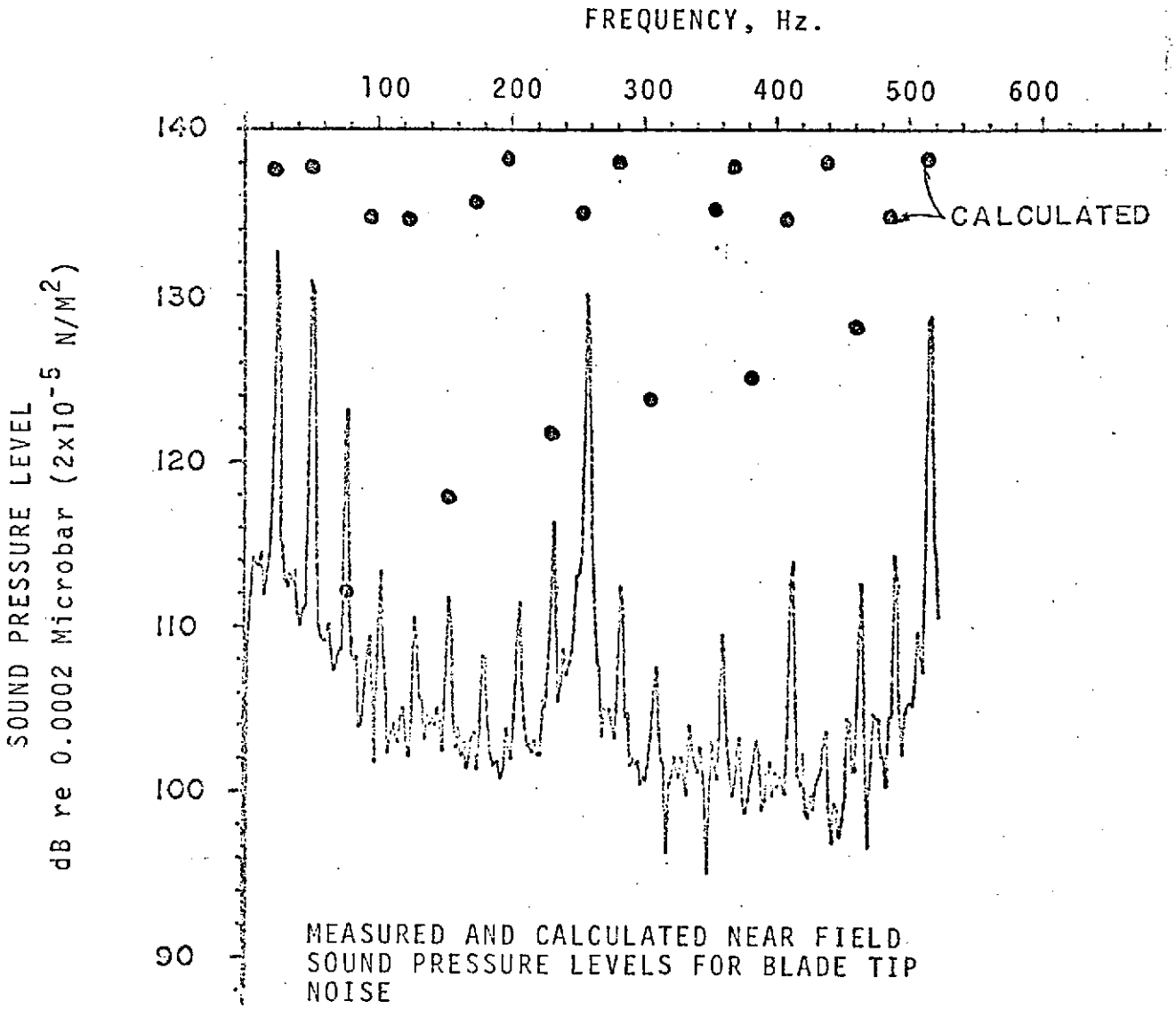

MEASURED AND CALCULATED NEAR FIELD SOUND PRESSURE LEVELS FOR BLADE TIP NOISE

TEST SERIES No. 1
Blade Tip Noise

q_u = 110 p.s.f.

FIGURE 5-1

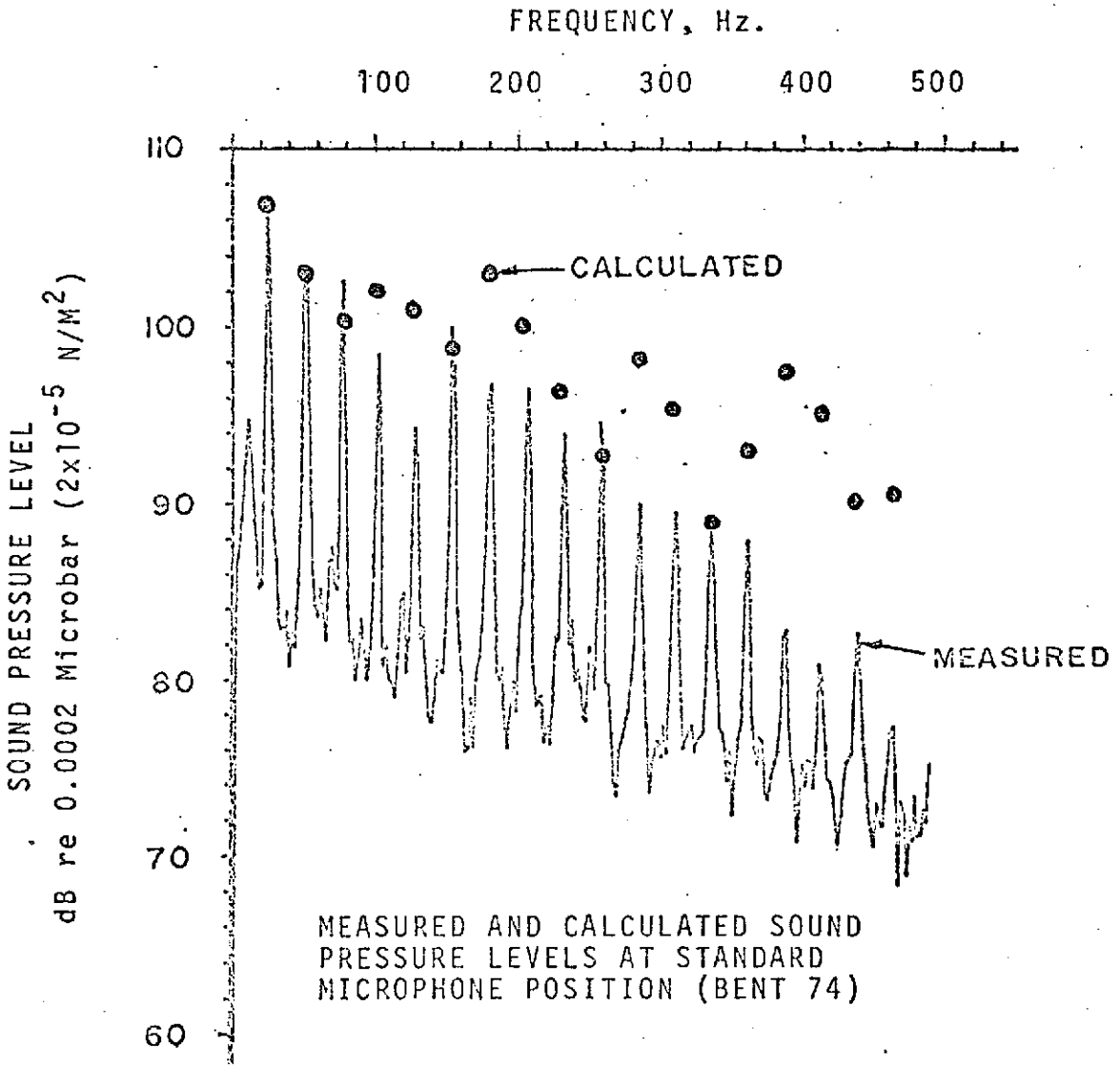

MEASURED AND CALCULATED SOUND PRESSURE LEVELS AT STANDARD MICROPHONE POSITION (BENT 74)

TEST SERIES No. 1
Standard Microphone Noise

q_u = 110 p.s.f.

FIGURE 5-2

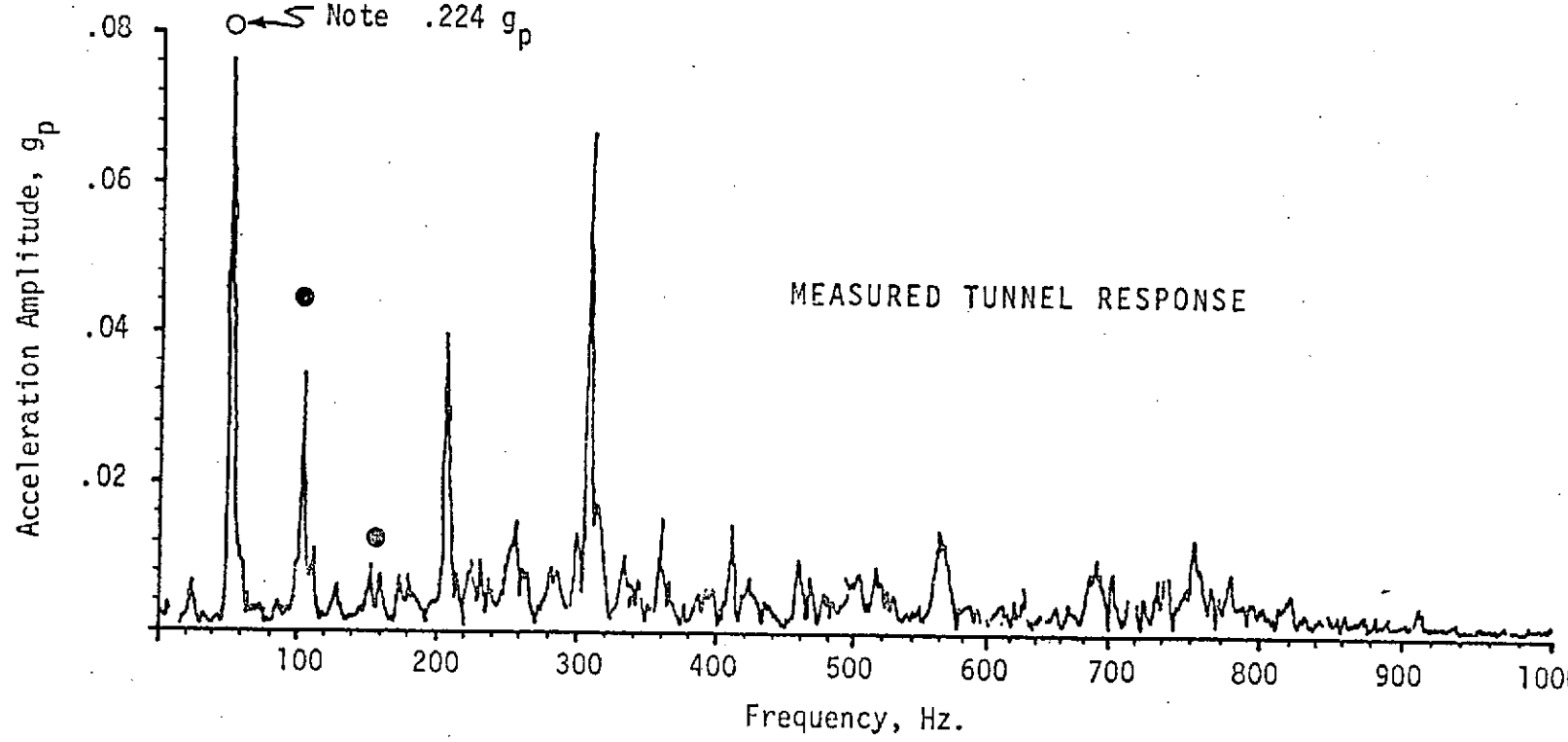

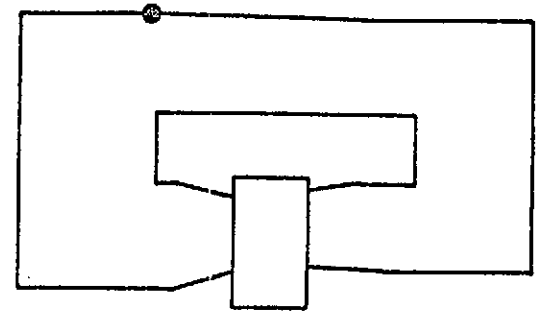

MEASURED AND CALCULATED TUNNEL RESPONSE AT BENT 74
VIBRATION SPECTRUM, TEST POINT 8
q_u = 110 p.s.f.

FIGURE 5-3

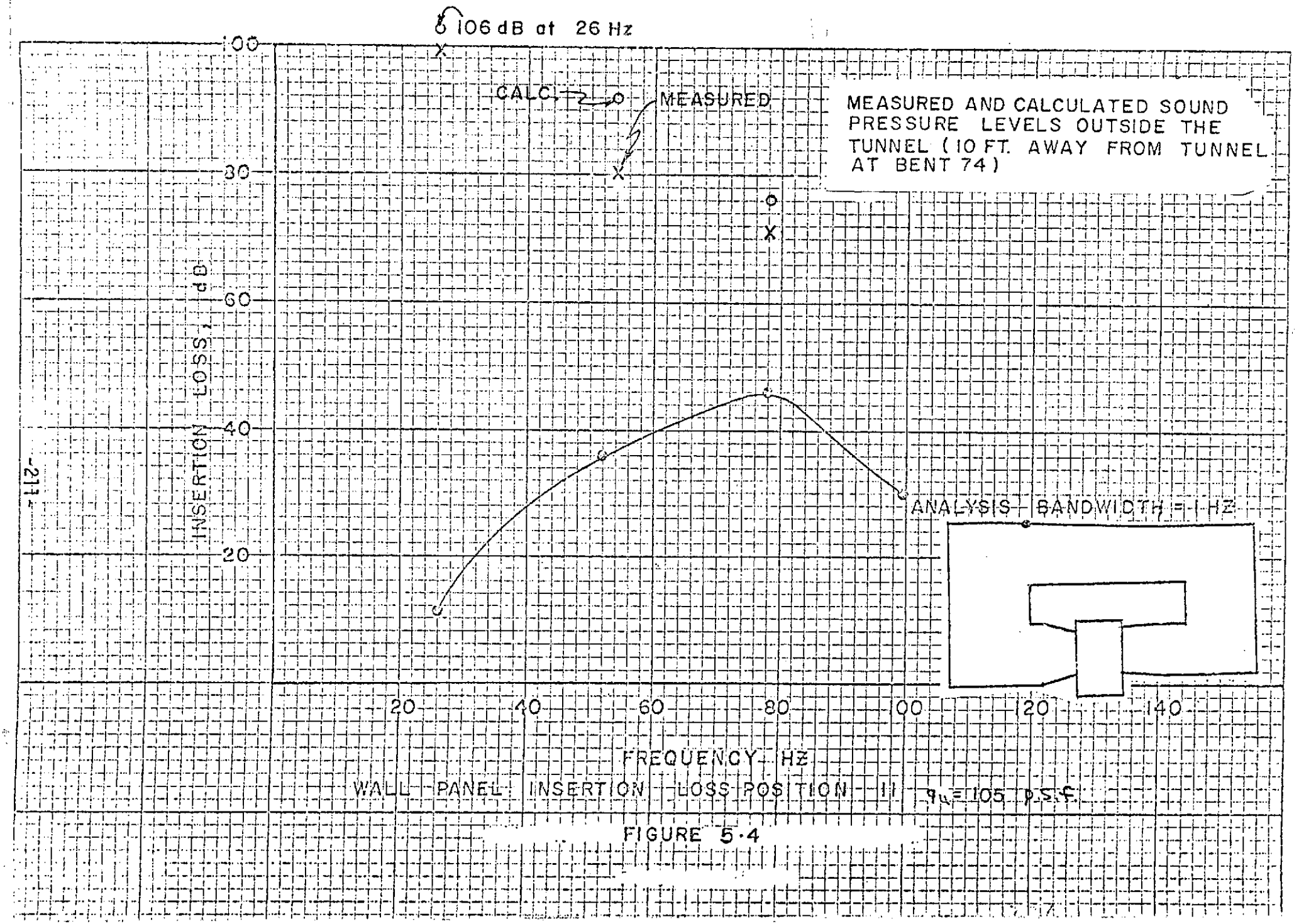

FIGURE 5·4

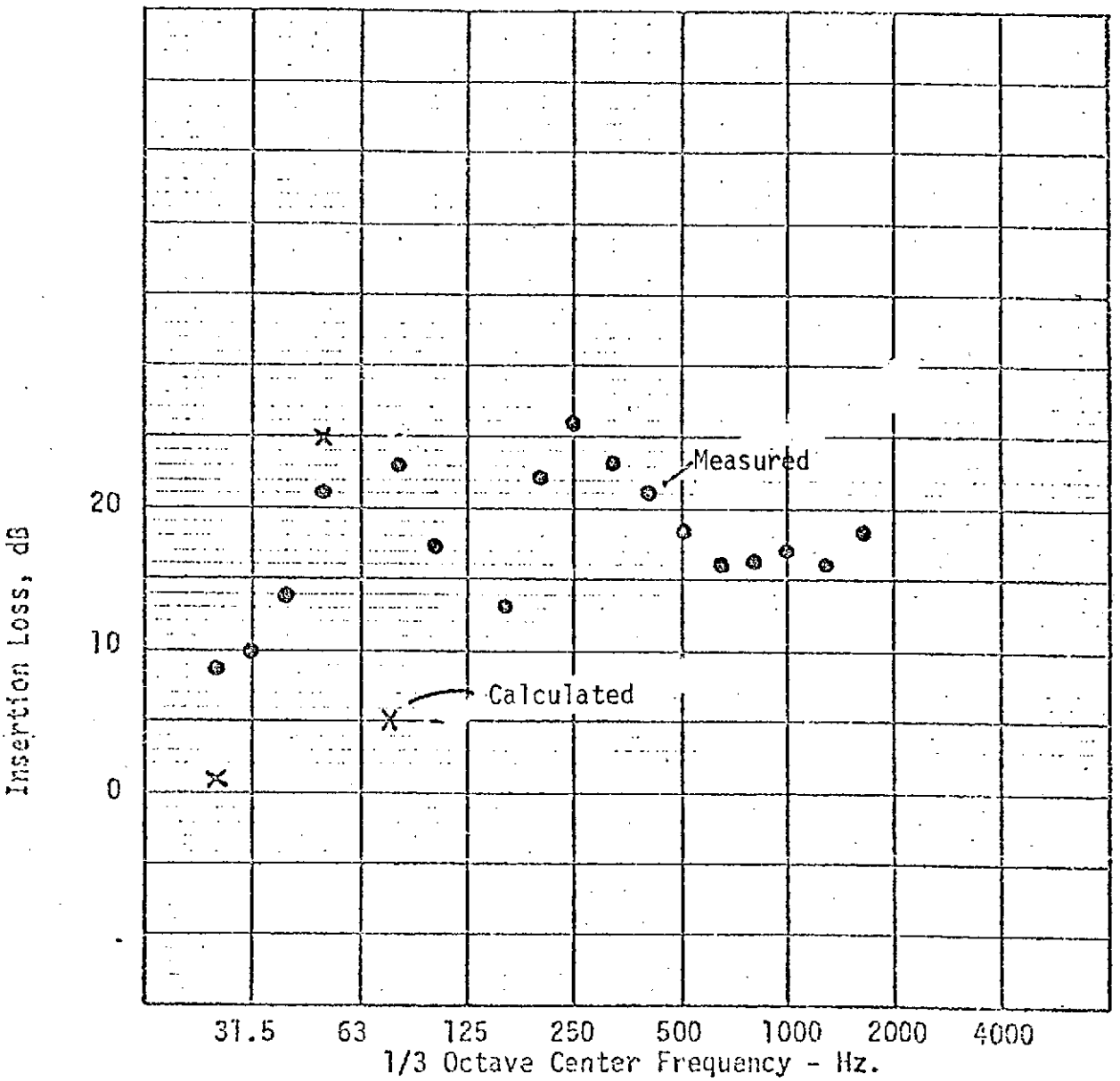

MEASURED AND CALCULATED FIELD INSERTION LOSS

BENT 74

q_u = 105 p.s.f.

Figure 5-5

TABLE 4.1

TUNNEL MEASUREMENT POSITIONS AND PURPOSE

TEST SERIES	PROBE TYPE	PROBE NUMBER	PROBE LOCATION	PURPOSE
1	Mic	1	6'-'0" downstream mid lower fan at floor level.	Blade tip noise spectrum
	Mic	2	Mid tunnel at bent 74 5' from floor.	Overall fan spectrum and reference spectrum for subsequent tests.
	Accum	4	Stbd nacelle strut - center of strut, axis parallel to air stream.	Strut vibration relative to blade forcing frequency.
	Accum	3	Same as 4 perp. to center of strut.	"
2	Mic	2	Mid tunnel at bent 74 5' from floor.	Reference spectrum.
	Mic	5	Mid tunnel at bent 48 5' from floor.	Fan inlet diffuser tunnel noise.
	Accum	6	Bent 48 sidewall panel.	Structure vibration
	Accum	7	Bent 48 floor panel.	
3	Mic	2	Mid tunnel at bent 74 5' from floor.	Reference spectrum
	Mic	5	Mid tunnel at bent 48 5' from floor.	Fan inlet diffuser tunnel noise
	Accum	8	Wall panel at bent 74	Structural vibration
	Accum	6	Wall panel at bent 48	
4	Mic	2	Mid tunnel at bent 74 5' from floor.	Reference spectrum
	Accum	8	Bent 74 sidewall panel	Structure vibration

TABLE 4.1 CONTINUED

TEST SERIES	PROBE TYPE		PROBE LOCATION	PURPOSE
5	Mic	2	Mid tunnel at bent 74 5' from floor	Reference Spectrum
	Mic	14	Mid tunnel at bent 91 5' from floor	Interior Tunnel noise
	Accum	16	Wall panel at bent 91	Structural vibration
	Mic	15	Exterior to tunnel approx. 10' from sidewall at bent 91	Near field radiation with typical panel vibration determined by 4(c)
6	Mic	2	Mid tunnel at bent 74 5' from floor	Reference spectrum
	Mic	18	Mid tunnel at test section 5' from floor	Interior Tunnel noise
	Accum	19	Floor at test section	Structural vibration
	Mic	17	Ground level under entry diffuser	Near field radiation

TABLE 4.2

IMPACT OF THE TUNNEL UPON THE NEAR FIELD (AMES SITE)

Location	Distance To Source (ft.)	Octave Level dB			Estimated Level dB in Building			Estimated Excess Level dB in Building over PNC 35		
		31.5 Hz.	63 Hz.	125 Hz.	31.5 Hz.	63 Hz.	125 Hz.	31.5 Hz	63 Hz.	125 Hz.
A	600	87	80	79	79	66	59	17	11	9
B	500	90	80	80	82	66	60	20	11	10
C	200	98	95	85	90	81	65	28	26	15
D	750	86	85	78	78	71	58	16	16	8
E	1050	77	75	76	69	61	56	7	6	6
F	600	79	82	80	71	68	60	9	13	10
G	700	84	87	76	77	73	56	15	18	6
H	150	101	95	87	87	81	67	25	26	17

TABLE 4.3

REVERBERATION MEASUREMENT RESULTS

TEST NUMBER	REVERBERATION FOR OCTAVE							
	31.5	63	125	250	500	1K	2K	4K
Lower Tunnel Section								
1						17.6	11.9	2.55
2						16.8	12.4	4.38
3						16.8	15.6	5.64
4						20.2	14.0	5.41
5						18.9	14.1	4.84
6	5.79	11.8	14.7	15.6	17.1	16.5		
7	4.13	13.0	15.8	20.4	16.6	16.6		
Section Directly Below Fans								
8							13.0	4.35
9							13.5	4.56
10				17.6	17.9		9.5	
11				16.0	22.6	17.8	12.2	
12			23.1	19.6	19.1	15.2	13.6	9.6
13			16.8	19.2	18.7	17.3	14.8	7.2
14						19.2	14.5	4.22
15						15.6	16.5	11.9
16						16.7	12.0	7.30
17					16.0	17.9	13.6	14.5
18							16.4	16.2
19					21.2	20.4	13.4	
20							12.2	11.7
21					20.2	18.1	12.9	
22					16.8	14.9	12.3	
23							11.5	13.3

REVERBERATION MEASUREMENT RESULTS
continued

TEST NUMBER	REVERBERATION FOR OCTAVE							
	31.5	63	125	250	500	1K	2K	4K
24					12.4	15.5		
25					16.7	26.2	17.0	3.40
26				16.5	26.0	18.0	15.0	16.6
Average	4.96	12.4	17.6	17.8	18.6	17.8	13.6	8.20
Standard Diviation	1.17	0.84	3.77	1.90	3.40	2.50	1.80	4.66
Measure-ments	2	2	4	7	13	20	23	18

APPENDICES

APPENDIX 1

PANEL RESPONSE AND NOISE RADIATION

INTRODUCTION

A number of factors make it difficult to determine, in a definitive analytical sense, the acoustic transmission properties of a structural element. These properties are a function of the velocity response of the element, which is in turn a function of the element stiffness, unit mass, resonant frequencies, modal damping, and the strength of the coupling between the acoustic field and each structural mode. Because of boundary condition uncertainties and the inability to analytically represent real boundary conditions, it is difficult to calculate even the resonant frequencies of a real panel with accuracy beyond the first few modes. Modal damping is a gray area, and the coupling between the acoustic field and the structure can be analytically estimated only if the structure lies in the far field of the acoustic source.

Attempts have been made to collapse structural response data from the NASA space programs by using unit mass and frequency multiplied by diameter as normalizing parameters (Ref. 1). These results have not been completely satisfactory. The bending stiffness is not included in the normalization. The method of acoustic mobility is another technique which has been used (Ref. 2), but this relies either upon experimental data or the calculation of acceleration response throughout the frequency range of interest. The difficulty of the latter has been noted above.

The acoustic transmission properties of a panel can be generally expressed as shown in Figure 1. We propose to treat the analytical determination of the transmission loss and other acoustical properties of the 40' x 80' wind tunnel structure by considering two panel response regions; that region which is resonant controlled and that which is mass controlled.

The third response region shown in Figure 1, the coincidence region, is really a form of resonance in which the panel transmission loss becomes low by virtue of a wave-matching phenomenon. The wave length of sound in air matches the bending wave length of the panel. Further, we will consider the transite portion of the tunnel and the steel plate portions of the wall which make up the fan section. The test section is not considered to be of major concern because of its armour plate walls and the work room which exists between the armour plate and the outside building wall. Test section walls could be of concern, however, to internal tunnel acoustics.

PANEL RESPONSE

We determine the first few resonant modes of the panels (considered to be orthotropic flat plates, uniformly loaded), from existing software which solves the following equation:

$$\omega^2_{n,m} = \frac{D_1 \pi^4}{\rho}\left(\frac{n^4}{A^4} + \frac{nm^4}{B^4} + \frac{(1+n)\mu n^2 m^2}{A^2 B^2} + \frac{2n(1-\mu)n^2 m^2}{A^2 B^2}\right) \qquad (1)$$

where $D_1 = \frac{Et^3}{12(1-\mu^2)} + \frac{EI}{L}$

$n = D_2/D_1$

E = Youngs Modulus

t = thickness

μ = Poisson's Ratio

I = stiffener modulus

L = stiffener spacing

ρ = mass/unit area

Sub 1 = parameter in direction of stiffeners

Sub 2 = parameter normal to direction of stiffeners

This assumes that $\phi = \text{Sin}\left(\frac{n\pi x}{A}\right) \text{Sin}\left(\frac{m\pi y}{B}\right)$ from which $\Sigma m_i \phi_i^2 = \frac{\rho AB}{4}$ for all values of n and m. For panels to which the EI/L term does not apply, the term is omitted.

Sound pressure levels measured inside the 40' x 80' wind tunnel by Soderman (Ref. 3) indicate a broad band noise with the highest levels below 125 Hz.

At large distances from the noise sources, the acoustic field will be something between a plane wave environment and a reverberant environment. The plane wave environment will be somewhat selective in terms of wave length coupling in exciting the structure, whereas the reverberant field tends to excite many structural modes. For those transite panels well removed from the noise sources, we consider the panel response in any mode to be of the form

$$M_s \ddot{\xi}_s + C_s \dot{\xi}_s + K_s \xi_s = F_s(t), \; S = 1 \text{ to } n \qquad (2)$$

where m_s = generalized mass
C_s = generalized damping
K_s = generalized stiffness
$F_s(t)$ = generalized force
ξ = generalized deflection

The solution to the above equation provides a mean square displacement of

$$\xi_s^2 = \int_0^\infty \frac{PSD_f(\omega)}{|Z_s(\omega)|^2} \, d\omega \qquad (3)$$

where $PSD_f(\omega)$ = power spectral density of the generalized force
$Z(\omega)$ = panel mechanical impedance

The generalized force F(t) over the panel is a summation of the product of forcing pressure per unit area and mode deflection, which we express as

$$F(t) = \int_A P(t,a)\phi(a) \, da$$

The square of this force is

$$\{F(t)\}^2 = \iint_{AA} P(t,a,)P(t,a')\phi(a)\phi(a')\, da\, da'.$$

The product of the first two terms is the spatial correlation of total noise pressure at a and a'. The power spectral density of the generalized force at frequency ω is, from Lee (Ref.4)

$$PSD_f(\omega) = \iint_{AA} p(t,a)p(t,a')\phi(a)\phi(a')\, da\, da' \qquad (4)$$

if $p(t,a)p(t,a')$ is the correlation of noise pressure in a narrow band centered at ω. Normalizing this narrow band correlation function by means of dividing by the mean square pressure at some reference a_o and rewriting the power spectral density of the generalized force gives

$$PSD_f(\omega) = \iint_{AA} PSD_N(\omega)R_\omega\phi(a)\phi(a')\, da\, da' \qquad (5)$$

where $PSD_N(\omega)$ = power spectral density of narrow band noise pressure, centered at ω.

$$R_\omega = \frac{p(t,a)p(t,a')}{\overline{p(t,a_o)}^2} = \text{correlation coefficient (normalized correlation function)}$$

Further, if equation (5) is re-written as

$$PSD(\omega) = PSD_N(\omega)A^2\left[\frac{1}{A^2}\iint_{AA} R_\omega\phi(a)\phi(a')\, da\, da'\right],$$

the term in brackets is non-dimensional and will have values equal to or less than one. This allows us to take advantage of the work of Powell (Refs. 5,6), who calls the square root of the expression in brackets the "joint acceptance", which

can be looked upon as a coupling term between the airborne acoustic forcing function and the structure being forced into motion.

The joint acceptance is not calculable for structure close to the noise source. If structure is located far enough from the source to be considered far field, the joint acceptance is calculable. Two cases arise: one in which $\phi(a) = \phi(a')$ (panel moving as a rigid body), and one in which the panel moves as a flexible body. In the former case, Powell provides the square of the joint acceptance as

$$j^2(\omega) = \left(\frac{\lambda}{\pi b} \operatorname{Sin} \frac{\pi b}{\lambda}\right)^2$$

and for the latter case,

$$j^2(\omega) = \frac{2}{n^2\pi^2} \left(\frac{1}{1-b^2/\lambda^2}\right)^2 \left\{1-(-1)^n \cos\left(\frac{n\pi b}{\lambda}\right)\right\}$$

where λ = structural trace wave length

b = panel span

n = number of one-half waves in sinusoidal panel vibration.

Using Equation (3) and the power spectral relationships that have been developed for the generalized force, we can write the power spectral density of displacement as

$$PSD_\xi(\omega) = \frac{PSD_F(\omega)}{|Z(\omega)|^2} = \frac{1}{|Z(\omega)|^2} \iint_{AA} PSD_F(\omega) R_\omega \phi(a)\phi(a')\, da\, da' \qquad (6)$$

This portion of the analysis is concerned only with Region I of Figure 1 (resonant region), which allows for simplification of equation (3). The damping of the normal modes of the structures of concern in the 40' x 80' wind tunnel is expected to be small, which means that the response will be primarily resonant. Wind tunnel noise measured by Soderman

and others indicate that the power spectral density in the region of expected natural frequencies can be assumed to be relatively constant. We will assume that $j^2(\omega)$ is also constant in these narrow frequency bands. Equation (3) can then be simplified as follows:

$$\overline{\xi_s}^2 = \int_0^\infty \frac{PSD_F(\omega_s)}{|Z_s(\omega)|^2} \doteq A^2 PSD_F(\omega_s) j^2(\omega_s) \int_0^\infty \frac{1}{|Z(\omega_s)|^2} \, d\omega$$

$$\doteq A^2 PSD_F(\omega_s) j^2(\omega_s) \frac{\pi}{2C_s K_s}$$

$$= \frac{A^2 PSD_N(\omega_s) j^2(\omega_s) \pi}{4\delta_s m_s{}^2 \omega_s{}^3} \qquad (7)$$

Since damping has been assumed small, modal coupling will be negligible and

$$\overline{\xi}^2 = \frac{\pi A^2}{4} \sum_{s=1}^{s=n} \frac{PSD_F(\omega_s) j^2(\omega_s)}{\delta_s m^2{}_s \omega^2{}_s} \qquad (8)$$

Equations (7) and (8) can be used to estimate panel response in the resonant region of Figure 1.

While it is true that panels will contain many resonances throughout the frequency spectrum, the fact that the higher resonances become very small, compared to the first few, combined with other reasons previously given, enables the panel response beyond the first few resonances to be best represented by mass law response. The mass law response of a panel is given by

$$\frac{}{a^2} = \frac{2\overline{p}^2}{W^2} \qquad (9)$$

where W = surface density

$\overline{p}^2$ = mean square sound pressure

$\overline{a}^2$ = mean square acceleration.

This equation can be used in one form or another with any consistent set of units, and can be applied in the frequency range beyond the first 4 or 5 resonances and below coincidence, where the coincidence frequency is given by

$$f_c \doteq \frac{500}{h}$$

and h = panel thickness in inches.

PANEL SOUND RADIATION

We determine the sound radiated by a vibrating panel as follows:

1. Assume the panel vibrates normal to its plane with small amplitudes.
2. Assume no reflections.

Then an area element of the panel vibrates with a velocity $Ve^{i\omega t}$, and the velocity potential at some point P due to this vibration is

$$\frac{Ve^{i\omega t}\, e^{-ikr}}{2\pi R}\, dx\, dy$$

where $R = (x^2+y^2+r^2)^{\frac{1}{2}}$

and $K = \omega/c$

For a strip of the plate, width dx which is line source, the velocity potential at P is

$$d\phi = \frac{Ve^{i\omega t}dx}{2\pi} \int_{-\infty}^{\infty} \frac{e^{-ik(x^2+y^2+z^2)^{\frac{1}{2}}}}{(x^2+y^2+z^2)^{\frac{1}{2}}}\, dy$$

$$= \frac{Ve^{i(\omega t-\pi/2)}}{2} H_0^{(2)}\{K(r^2+x^2)^{\frac{1}{2}}\}\, dx$$

or for the entire plate

$$\phi = \frac{Ve^{i(\omega t-\pi/2)}}{2} \int_{-\infty}^{\infty} H_0^{(2)}\{K(r^2+x^2)\}^{\frac{1}{2}}\, dx$$

$$= \frac{Ve^{i\omega t}}{K} e^{-i(Kr+\pi/2)}$$

The sound pressure at P is then

$$\rho_o \left(\frac{\partial\phi}{\partial t}\right) = \left(\rho_o \frac{\omega V}{K}\right) e^{i(\omega t-Kr)} \qquad (10)$$

The real part of 10 is

$$p = \rho_o CV \cos(\omega t-Kr) \qquad (11)$$

where r is the distance from the panel. To determine sound pressure level, we divide p in equation (11) by $P_{ref} = .00002\ N/M^2$ and take appropriate logs of this ratio. We justify this method on the basis that in the low frequency region of resonant response, wave lengths are long, and in the high frequency region of mass response we can use velocity averaged in space and time. From noise levels internal to the tunnel and external to the tunnel, the transmission loss is obtained. The acoustic field set up in the work spaces adjacent to the test section can be determined from the difference between the noise reduction and the internal tunnel noise, where noise reduction is

$$NR = TL - 10 \log \left(\frac{A_T}{\bar{\alpha}A_A}\right) \quad dB$$

and TL = transmission loss

A_T = total transmitting surface area

$\bar{\alpha}$ = average absorption coefficient of the work room

A_A = total absorbing surface area.

REFERENCES

1. Franken, P.A., "Sound Induced Vibrations in Cylindrical vehicles", J.A.S.A. 34, 1962
2. Sutherland, L.C., "Sonic and Vibration Environment for Ground Facilities - A Design Manual", Report to NASA Marshall Space Flight Center, Contract NAS8-11217, March, 1968.
3. Soderman, P.T., "Sound Levels Generated by Ames 40' x 80' Wind Tunnel", March, 1972.
4. Lee, Y.W., "Statistical Theory of Communication", John Wiley & Sons, Inc. 1960.
5. Powell, A., "On Structural Vibrations Excited by Random Noise Pressures", Douglas Aircraft Co., Report S.M. 22795.
6. Crandall, S.D., "Random Vibrations", M.I.T. 1958, Chapter 8.

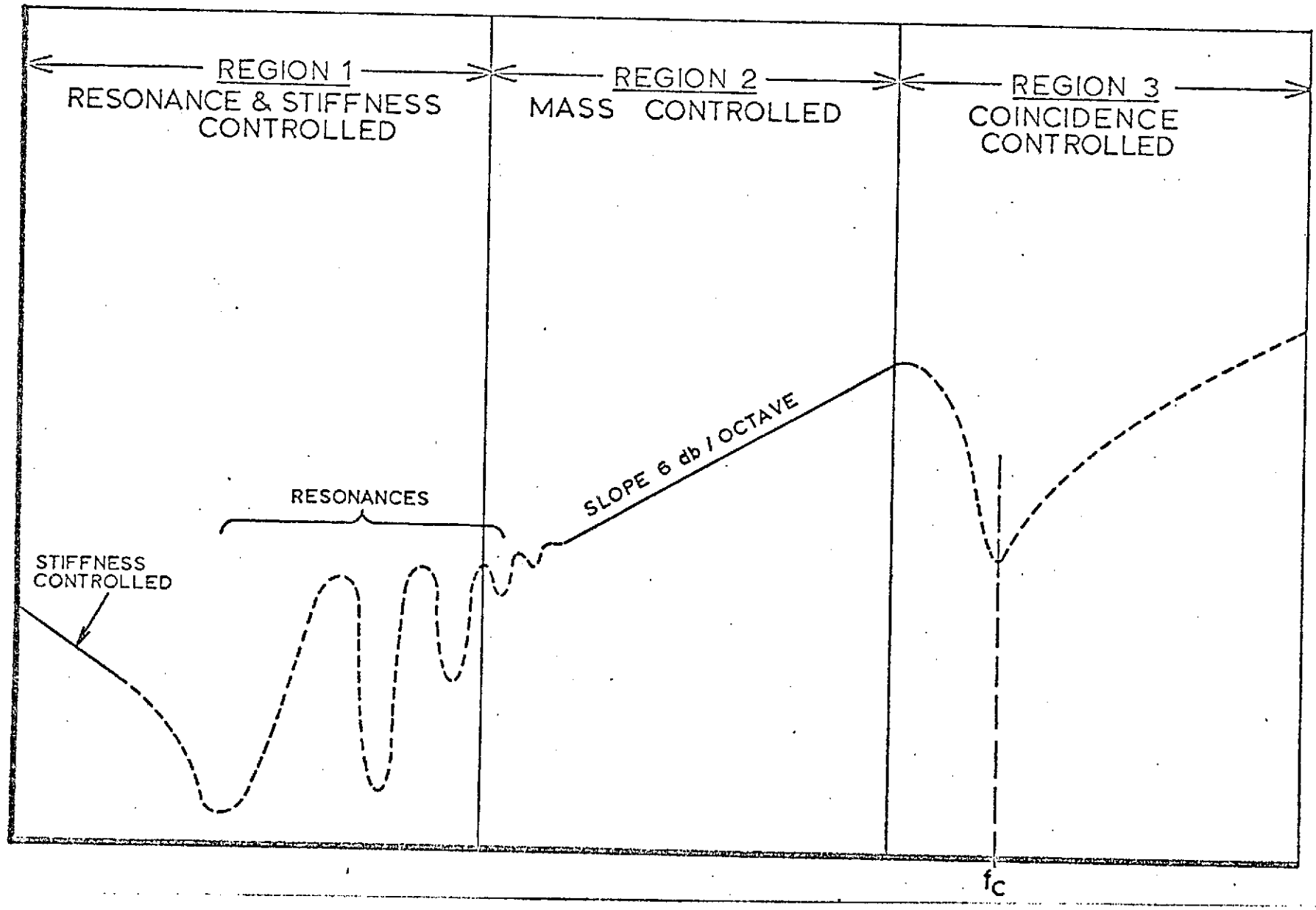

Figure 1 - PANEL RESPONSE TO SOUND

APPENDIX 2

FAN ARRANGEMENT

The free space oscillating pressures generated by propellers can be calculated in close agreement with measured values. It is, therefore, our intent to generate comments about the acoustics of the six-fan arrangement of the 40' x 80' wind tunnel by making calculations appropriate to a single fan, correcting for the enclosure and the remaining five fans, assuming no interaction, and to compare these calculations with measured pressures in the tunnel.

Propeller (fan) noise is composed of three components: a) vortex noise, b) thickness noise, and c) lift noise. In the analysis of fan noise it is convenient to consider each of these components separately.

Typical fan noise spectra show the lowest peak frequency occurring at the fundamental blade passage frequency. Other peaks occur at integral multiples of this frequency. For subsonic tip speeds, the fundamental is the most intense, and as tip speed increases, the intensity of the harmonics generally increase. Consider now each component of fan noise.

Vortex Noise

Vortex noise is due to variations in circulation around an airfoil, and is usually very high frequency noise. This variation in circulation causes vorticity to be shed into the wake, creating an acoustic source. This effect is usually small in comparison to thickness and lift noise.

Thickness Noise

Thickness noise is generated by virtue of a periodic displacement of the air caused by the presence of the fan. Making the usual assumptions, the fan blade can be replaced by a distribution of simple acoustic sources in an infinite wall, which allows the use of Reference 1 to find the velocity potential at any point. The strength of these simple sources is related to the normal velocity distribution on the fan blade so that if this is known for any blade condition the calculations can be made. The normal velocity distribution can be obtained from the pressure distribution over the fan blade and the gradient along the surface.

A given point in the fan disc will have a periodic excitation which can be Fourier analyzed as

$$\frac{\partial \phi}{\partial_n} = \ddot{\xi}_o \left[a_{1B} \operatorname{Sin} (B\omega t+\varepsilon_{1B}) \text{ ---- } + a_{mB} \operatorname{Sin} (mB\omega t+\varepsilon_{mB}) \right. \quad (1)$$

and the velocity of potential due to an element source is then (in the mB harmonic)

$$\phi_{1mB} = \frac{e^{-iKS_\varepsilon}}{2\pi S_\varepsilon} \left(\frac{\partial \phi}{\partial_{\partial N}} dS\right) \quad (2)$$

By introducing the space phase for a general source element in the fan disc (see Figure below), equation *(1)* can be expressed in the form

$$\phi_{imB} = - \ddot{\xi}_{mB} \frac{d_S}{2\pi S_\varepsilon} e^{i(mB\omega t+e_m-mB\Theta-Kr)} \quad (3)$$

and integration over the entire fan disc gives the total velocity potential at any point P as

$$\phi_{mB} = - \int_0^{2\pi R_0} \int_0 \frac{\ddot{\xi}_{mb} e^{i(mB\omega t+e_{mB}-mB\Theta-KS_\varepsilon}}{2\pi S_\varepsilon} dS \quad (4)$$

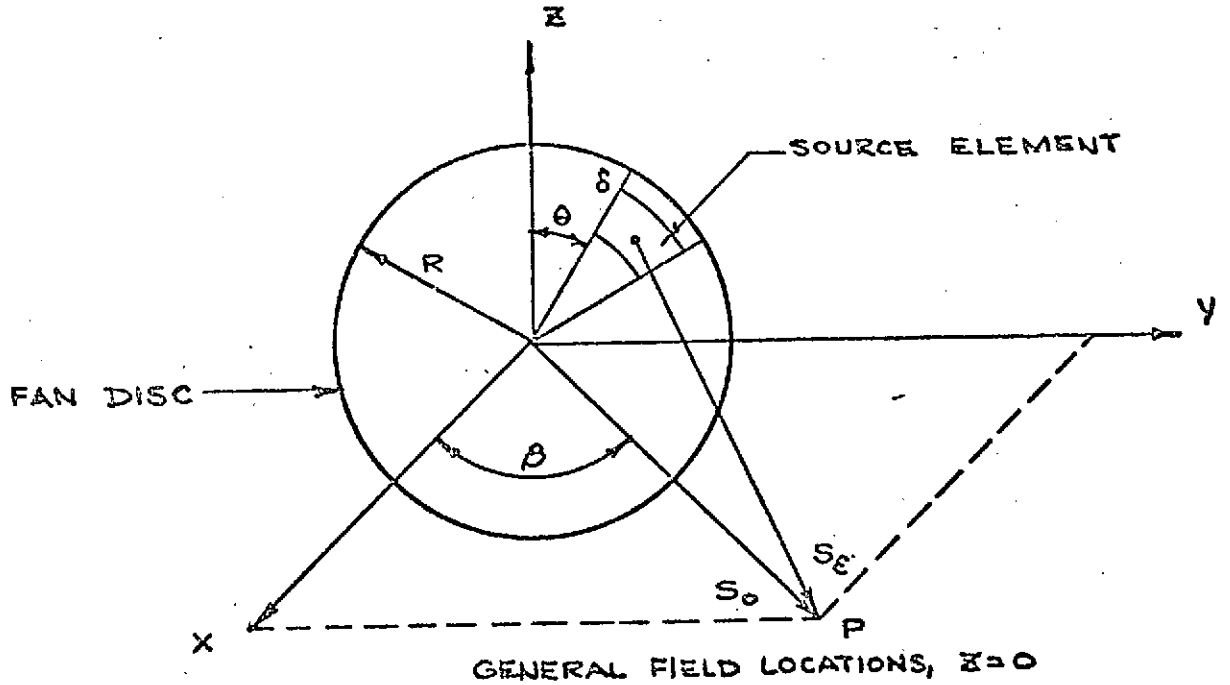

Now,

$$S_\xi = S_o + \delta = S_o + Sin\theta Sin\beta$$

If $\delta << S_o$ (far field), S can be neglected except as it occurs in the exponent, and equation *(4)* can be written

$$\phi_{mB} = (-1)^{mB+1}\ 2\pi \int_o^{R_o} MJ_{mB}(m)\ \ dr$$

Simplifying the Fourier Analysis as

$$P_{mB} = -\rho_o \frac{\partial \phi_{mB}}{\partial t}$$

the amplitude of the oscillating pressure in the mB harmonic is

$$P_{mB} = \left(\frac{\rho C^2}{4\pi}\right)\left(\frac{D}{S_o}\right)(m^2B^2M_R{}^2) \int_0^{R_o} B\left(\frac{b}{R_o}\right)^2 \left(\frac{a}{b}\right) J_{mB}(KR_oSin\beta)\ dr \quad (5)$$

Equation *(5)* will give pressure amplitudes (far field) for the first few harmonics of thickness noise.

Lift Noise

Lift noise is that noise caused by periodic reactions on the air from pressure distributions which rotate along with the fan blades. Lift noise can be calculated in the same general way that thickness noise is calculated; i.e., by replacing the pressure distribution over the fan with a distribution of acoustic doublets, the strength of which are related to the lift distribution. If the fan blade is well loaded, the excitation of an element in the disc can be represented as below.

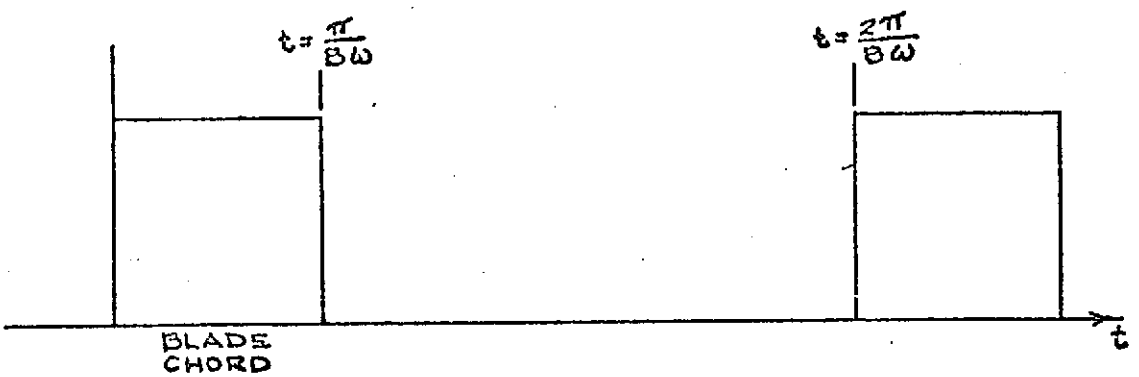

This excitation is periodic and, if Fourier analyzed, can be split into torque and thrust components which take the form

$$F_{x,m} = -\frac{1}{\pi}\frac{dT}{dr} e^{i(\omega t - mB\Theta)} dr\, d\Theta$$

$$F_{y,m} = -\frac{1}{\pi R}\frac{dQ}{dr} \sin\Theta e^{i(\omega t - mB\Theta)} dr\, d\Theta \qquad (6)$$

$$F_{x,m} = -\frac{1}{\pi r}\frac{dQ}{dr} \cos\Theta e^{i(\omega t - mB\Theta)} dr\, d\Theta$$

from which the pressure field is

$$p = \frac{1}{4\pi}\left(F_x \frac{\partial}{\partial x} + F_y \frac{\partial}{\partial y} + F_z \frac{\partial}{\partial z}\right) \frac{e^{-ik\sigma}}{S} \qquad (7)$$

Inserting *(6)* into *(7)* provides total oscillating pressure for any harmonic as a sum of pressures due to torque and thrust. The value of the rmS pressure would be useful because most sound recorders are so calibrated. Harmonic m will contribute to the rmS pressure as

$$P_{rmS} = \frac{\sqrt{2}}{8\pi^2}\left(A^2+B^2\right)^{\frac{1}{2}} \qquad (8)$$

where

$$A = \int_0^{2\pi}\left\{\frac{TX}{S^2}\cos\left(mB\Theta + K\sigma\right) + \left[T\frac{K}{\beta^2}\left(M+\frac{X}{S}\right) - Q\frac{mB}{R^2}\right]\operatorname{Sin}\left(mB\theta+k\sigma\right)\right\}\frac{d\Theta}{dS}$$

$$B = \int_0^{2\pi}\left\{-\frac{TX}{S^2}\operatorname{Sin}\left(mB\Theta+k\sigma\right) + T\left[\frac{K}{\beta^2}\left(M+\frac{X}{S}\right) - Q\frac{mB}{R_o^2}\right]\cos\left(mB\Theta+K\sigma\right)\right\}\frac{d\Theta}{dS}$$

In deriving equation *(8)*, the fan disc has been replaced by an annular ring at which the total thrust and torque has been concentrated. The effective radius of this ring will be a function of the blade load distribution and the harmonic under consideration. To be certain of amplitudes it is best to approximate the real load shape by a series of simple shapes. For a well loaded blade, the assumption of a rectangular load distribution works reasonably well. The expressions for lift noise in the near and far fields then become, respectively,

$$P_{rmS} = \frac{1}{4\pi^2\sqrt{2}} \int_0^{2\pi} \frac{1}{S_\varepsilon} \left(TX + \frac{QY}{R_0} \sin\Theta\right) \left(\frac{iK}{S_\varepsilon} + \frac{1}{S_\varepsilon^2}\right) e^{i(mB\Theta + KS)}\, d\Theta \qquad (9)$$

$$|p| = \frac{\dot{m}\omega_1}{2\pi C S_0} \left| T\frac{x}{S_0} - Q\frac{B_0}{\omega_1 R^2} \right| J_{mB}\left(\frac{K_y R_0}{S_0}\right) \qquad (10)$$

Going from near field to far field depends upon the ratio $\frac{S\varepsilon}{\lambda}$. With a normal propeller, the wave length of the fundamental is about one diameter. The near field therefore extends to about two diameters.

GENERAL OBSERVATIONS

It may be useful to examine a few considerations of a general nature at this time, which are based upon the above theory, our own experience, and the work reported by others. These considerations point to the directions which will be taken at a later time regarding the study of the specific arrangement of fans in the 40' x 80' wind tunnel.

The above theory replaced steady aerodynamic forces on the fan blades with periodic forces which were fixed in the fan disc. Each time a fan blade passes an area element, the air receives a "thump". Fourier analysis of this "thump" provides a steady component and a series of oscillating components. The former translates into fan thrust and the latter into noise.

The greater the number of blades on the fan, the higher is the thump frequency. All harmonics are cancelled except those which are integral multiples of the number of blades. For a given power, a greater number of blades on the fan reduces the noise generated. The amount of noise reduction is a function of the strength of the cancelled harmonics.

In general, less noise reduction is achieved by increasing the number of blades on a fan having high tip speeds than can be realized by increasing the number of blades on a fan having low tip speeds. Therefore, by increasing the number of blades and reducing tip speed a substantial reduction in noise generation will occur. This effect is shown in the figure below, taken from Reference 2.

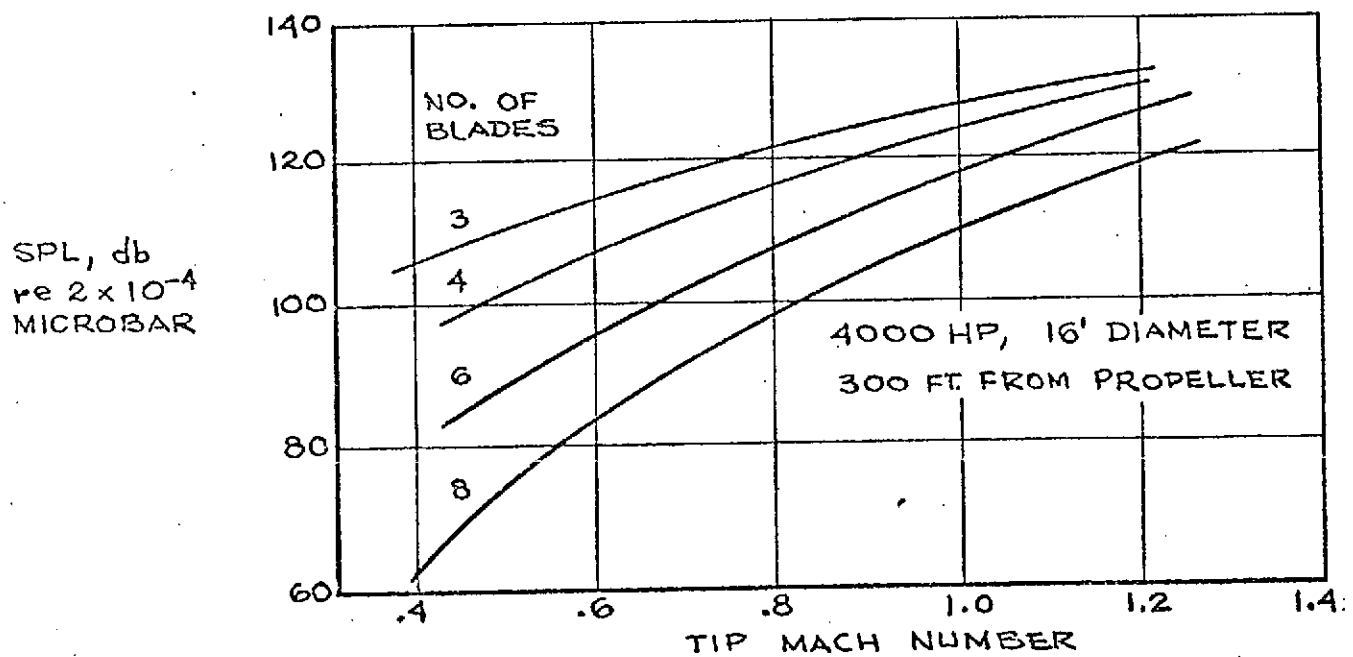

Tip speed influences the amplitude of noise generation by the harmonics, the fundamental harmonic being the loudest for low subsonic tip speeds and the higher harmonics becoming important noise generators as tip speed increases. From what has been said about the acoustic effects of tip speed and blade number, and the know transmission capabilities of structure to low frequency and to high frequency sound, it is apparent that a trade study would be in order for the 40' x 80' wind tunnel configuration. These considerations bear upon individual fan design, and therefore probably do not fall within the scope of this contract which relates to fan arrangement. The relative contribu-

tions of thickness noise and lift noise also fall into this domain.

Tip clearance is a significant parameter. Hubbard shows (reference 27) that in the case of a shrouded propeller with unseparated flow at the shroud surface, the sound pressure does not significantly change with tip clearance provided the clearance ratio does not exceed about 1%. With greater tip clearance and with separated flow at the shroud surface, however, the sound pressures increase rapidly. Hubbard's curve of the effect of tip clearance upon total sound emission of a shrouded propeller is reproduced below.

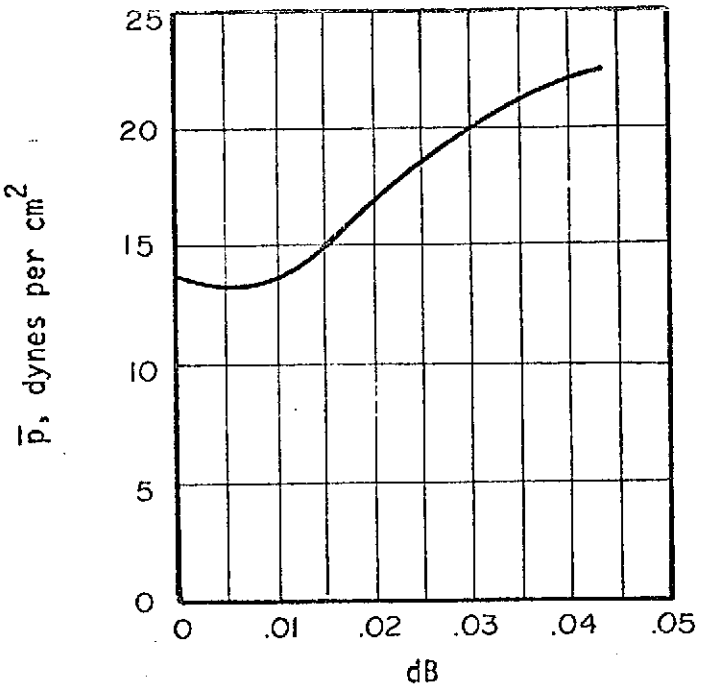

Effect of Tip Clearance Ratio on Total Sound Emission of A Shrouded Propeller

In the case of the 40' x 80' wind tunnel, the walls will have an effect which must be accounted for. Hubbard and Regier report tests (REference 3) made with a flat vertical wall which were about double those observed in free space. Curves are shown below.

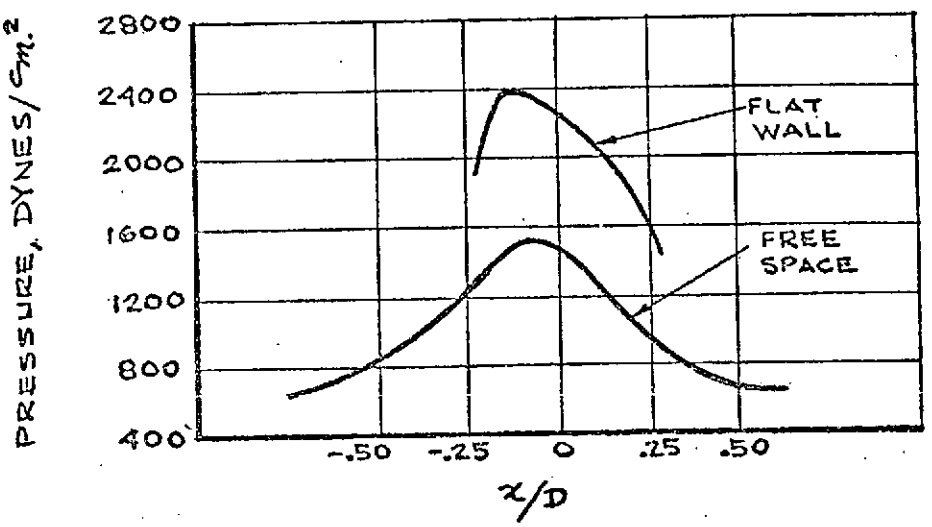

The directivity pattern of propeller noise has bearing upon wind tunnel acoustics. The lift noise, which is the dominant source in low susonic fans and has been represented by a dipole distribution, has the maximum of its directivity pattern about 30° behind the plane of rotation. This area, then, would be proper for acoustical treatment.

In summary, the considerations presented above are expected to describe the magnitude of oscillating pressures in the subsonic fan speed range. The effects of directivity, presence of the tunnel wall, and tip speed have been discussed.

SYMBOLS

a = blade thickness at radius r

b = blade chord at radius r

c = velocity of sound

a_{qn} = Fourier Coefficient

B = number of blades

D = fan diameter $(2R_o)$

m = $KR_o Sin\beta$

M = $\frac{a_{mB}\xi_o}{2\pi\ell}\ Re^{i(mB\omega t+e_{mB}-K\ell)}$

M_R = Rotational tip mach number

F_{im} = periodic forces acting on the air over an element in the "m" harmonic.

R_o = effective fan radius

S = $[(x-x_1)^2+\beta^2(y-y_1)^2+(Z-Z_1)^2]^{\frac{1}{2}}$

S_o = distance from center of disc to field point

S_ε = distance from source to field point

dS = element of area

t = time

$\frac{dQ}{dr}$ = torque gradient

$\frac{dT}{dr}$ = thrust gradient

$\frac{\partial Q}{\partial n}$ = velocity normal to plane

ϕ = velocity potential

$\dot{\xi}_o$ = parameter proportional to V and shape dependent

ω = angular blade velocity

$J_{mB}(M)$ = Bessel Function, order mB, argument M

ρ_o = density

$$\beta = (1-M_x^2)^{\frac{1}{2}}$$

$$\lambda = (1-M_x^2 \sin^2\theta)^{\frac{1}{2}}$$

$$\sigma = \frac{M(x-x_1)+S}{2}$$

$$K = 2\pi/\lambda = \frac{2\pi f}{C} = \frac{mB\omega}{C}.$$

REFERENCES

1. Rayleigh, "The Theory of Sound", Vol. 2

2. Richards, E. J., "Propeller Noise Measurements, Private Communication".

3. Hubbard & Regier, "Free Space Oscillating Pressures Near Propellers", NACA Report 996.

APPENDIX 3

USE OF CORRELATION METHODS TO IDENTIFY NOISE SOURCES

A procedure for identifying sources of noise seems to be ready-made within ancient statistical theory. The modern set has made its contribution, however, through the development of the fast Fourier algorithm and the computer. These two developments have made it possible to apply the old statistical theory to practical problems in our discipline.

Our general interest is to have a technique which will determine the total sound pressure level associated with a given source in an uncontrolled acoustic environment. These "given" sources are associated with the fan drive system (blade tip noise, strut interaction noise, etc.), hence we cannot use the method of deactivating all sources except the one of interest; no drive system - no noise.

The Personian correlation coefficient provides a measure of association between two variables x and y by

$$R^2 = \frac{\overline{xy}^2}{\overline{xy}}$$

We can adapt this coefficient to time series signals, random or periodic, and define a "coherence" function as

$$\gamma^2 = \frac{|\overline{\phi xy}^2|}{\phi_{xx}\,\phi_{yy}}$$

where ϕ_{xy} = cross power spectrum between x and y
ϕ_{xx} = power spectrum of x
ϕ_{yy} = power spectrum of y
and γ^2 = coherence function (the modern effect).

x and y are really two time series functions x(t) and y(t) which may be considered a system input and output. Power spectra are used because they are a convenient way to express the properties of periodic and random signals, parti-

cularly of random signals. The power spectrum is the average power contained in a unit frequency bandwidth. The usual units for power spectra are watts per Hz. This is commonly perverted to $\overline{dB^2}$ per Hz., $\overline{psi^2}$/Hz., g^2/Hz., etc., with little loss of meaning.

The power spectra are computed as follows:

$$\phi_{xx} = S_x S_x^*$$
$$\phi_{yy} = S_y S_y^*$$
$$\phi_{xy} = S_x S_y^*$$

where S_x and S_y are the Fourier transforms of the signals $x(t)$ and $y(t)$, and the starred quantities are the respective complex conjugates. Here enter the modern contributions: the fast Fourier transform algorithm and the computer.

Now, if there should be other sources than x, say z, the response at y is

$$S_y = HS_x + S_z$$

where H = frequency response between x and y (a transfer function). Therefore

$$\phi_{yy} = (HH^*S_xS_x^* + H^*S_zS_x + HS_xS_z^* + S_zS_z^*)$$
$$= (|H|^2\phi_{xx} + H^*\phi_{zx} + \phi_{zz} + H\phi_{xz})$$

If the other source z, which can be called noise because we don't really want it, is uncorrelated with x, the cross-spectral terms ϕ_{zx} and ϕ_{xz} become zero (in the limit), and

$$\phi_{yy} = |H|^2\phi_{xx} + \phi_{zz}.$$

The cross-spectral density term becomes

$$\phi_{xy} = (HS_x + S_z)S_x^*$$
$$= H\phi_{xx} + \phi_{zx}$$

Thinking about limits again (and uncorrelated sources)

$$\phi_{xy} = H\phi_{xx}$$

and

$$\gamma^2 = \frac{|H|^2\phi_{xx}}{|H|^2\phi_{xx} + \phi_{zz}} = \frac{|H|^2\phi_{xx}}{\phi_{yy}}$$

The above numerator represents the power at y due to a source at x, and the denominator is the total power at y. Therefore, if ϕ_{yy} is multiplied by the coherence function, the power at y due to the source at x is obtained.

APPENDIX 4

LIFT NOISE

NTIS Report N73-31945, Reference (11), predicts the harmonic lift noise produced by a propeller in free field as

$$L_N = 124.57 + 10 \log_{10} \left| \frac{C_N}{P_R} \right|^2 \qquad (1)$$

Where L_N = Harmonic Level, dB re 2×10^{-5} N/m²

P_R = 1 psf

$|C_N|^2$ = |Discrete Tone Phasor|²

$$\simeq \left(\frac{N M_E T}{4\pi R r SF^2} \right)^2 \left[4 \left\{ \cos \psi = h_D \left(\frac{SF}{M_E} \right) \right\}^2 J_n^2(nq) + \sum_{\lambda=K_1}^{K_2} g^2(\lambda) J^2_{n-\lambda}(nq) \left\{ \cos \psi - h_D \left(\frac{SF}{M_E} \right) \left(\frac{n-\lambda}{n} \right) \right\}^2 \right]$$

Where K_1 = Max [n(1-q) - 0.5,1], (integer result)

K_2 = n(1+q) + 0.5 (integer result)

$q = |M_E \sin \psi / SF|$

n = NB

M_E = Helical Mach number at radius R

$M_E^2 \simeq M^2 + (M_o \cos\alpha)^2$

M = Rotational Mach Number = $\Omega R / C_o$

Ω = Rotational Speed

R = Radial Centroid for equivalent point load

$g(\lambda)$ = Represents the loading law function

$\simeq 24.4 \, |\lambda|^{-2.5} / \, [1 + (30/\lambda)^2]^{0.5}$

T = Total thrust for rotor

h_D = Drag/thrust ratio

$\simeq$ (Q/R)/T where Q is the total torque on the rotor

r = Distance from rotor hub at "retarded time"- the time the sound is generated, not the time when the sound is heard.

ψ = Directivity angle re. rotor inlet axis at retarded time.

SF = Doppler-shift factor, $1-M_o \cos \xi$

M_o = Aircraft Mach Number

ξ = Angle between flight path and line to the observer at retarded time.

$J_n(nq)$ = Bessel function, argument nq, order n

N = Harmonic Order

Notice that the above formula was written for a moving aircraft with its own associated Mach number. It is easily converted to a stationary propeller by setting $M_o = 0$.

This free field harmonic level must be corrected for tunnel wall reflections, as well as the additional sound power generated by the other five fans. Therefore,

$$L_{N_{TUNNEL}} = L_N + \Delta L_1 + \Delta L_2 \qquad (2)$$

where ΔL_1 = tunnel enclosure correction

ΔL_2 = additional fans correction

A tunnel enclosure correction based upon the Sabine equation (Ref.12) did not appear applicable to the tunnel situation principally because the model components of the drive system would not allow approximately equal Q for all modes, and hence precluded a good approximation to a diffuse field. Indeed, calculations of sound pressure level at the standard microphone position (bent 74) verified this thought.

The alternative used was an evaluation of reverberation based upon the coherence function between the blade tip noise and the tunnel position of interest. This coherence function defines the amount of acoustic pressure at the tunnel position that is caused by direct radiation from the fans. Low coherence implies pressure arriving from other sources, which in this case means reverberant sources. This is a measured quantity and, if applied to the calculated level (L_N), it can be used to help define the far field sound pressure levels in the tunnel. It should be noted here that for purposes of prediction in a design situation, the coherence function can be independently calculated since it is a function of power spectral density ratios, and the power spectra of sound sources can be estimated. The measured coherence was used in this report because the objective was to provide an analytic means of calculating tunnel far field levels which could be correlated with measured levels. Therefore, the parameters involved in the calculation should be real parameters.

To use the coherence function to determine the enclosure correction (or reverberation effect) the spectral value of coherence is multiplied by source sound pressures and added to the calculated direct radiation. The tunnel enclosure correction can be expressed mathematically as follows:

$$P_T = \frac{P_N}{C^2_{TN}}$$

Where P_T = Total acoustic pressure at position of interest inside tunnel

C^2_{TN} = Coherence function between position of interest and blade tip noise

P_N = Calculated acoustic pressure at the same position due to direct radiation from propeller

$= [\text{antilog}_{10}\ (L_N\ /20)]\ [2.9 \times 10^{-9}\ \text{lbs./in}^{-2}]$

Therefore $L_T = L_N - 20 \log_{10} C^2_{TN}$

Where $L_T = 20 \log_{10}[P_T/2.9 \times 10^{-9}\ \text{lbs./in.}^2]$

$L_N = 20 \log_{10}[P_N/2.9 \times 10^{-9}\ \text{lbs./in.}^2]$

Reference (9) gives the increase of the sound pressure level due to the fan shroud as 4 dB.

The total tunnel enclosure correction is then given by:

$$\Delta L_1 = -20 \log_{10}(C^2_{TN}) + 4\ \text{dB}$$

A reasonable correction for the five additional fans is to assume incoherent sources and thereby multiply the sound power of one fan by 6 to obtain the power generated by all six fans. The noise at the position calculated is produced not only by the direct sound radiation, but also by reflections off the surfaces of the tunnel. Therefore, any phase cancellation that might exist from the direct radiation of the six fans is obscured by the reflections from the tunnel walls. The resultant pressure from the direct and reflected waves of each fan thereby acts as if it came from six incoherent sources.

$$\Delta L_2 = 10 \log 6 = 8 \text{ dB}$$

$$\text{Therefore } L_{N_{TUNNEL}} = L_N - 20 \log_{10} (C_{TN}^2) + 4 \text{ dB} + 8 \text{ dB}$$

$$= L_N - 20 \log_{10} (C_{TN}^2) + 12 \text{ dB}$$